Voorspelling van golfoverslag over golfbrekers en zeeweringen met behulp van neurale netwerken

Neural Network Prediction of Wave Overtopping at Coastal Structures

Hadewych Verhaeghe

Promotor: prof. dr. ir. J. De Rouck
Proefschrift ingediend tot het behalen van de graad van
Doctor in de Toegepaste Wetenschappen: Bouwkunde

Vakgroep Civiele Techniek
Voorzitter: prof. dr. ir. P. Verdonck
Faculteit Ingenieurswetenschappen
Academiejaar 2004 - 2005

UNIVERSITEIT GENT

ISBN 90-8578-018-7
NUR 956
Wettelijk Depot: D/2005/10.500/18

Cover Design: Robbrecht en Daem Architecten

Promotor

Prof. dr. ir. Julien De Rouck

Onderzoeksinstelling

Afdeling Weg- en Waterbouwkunde
Vakgroep Civiele Techniek
Faculteit Ingenieurswetenschappen
Universiteit Gent
Technologiepark 904
B-9052 Zwijnaarde

Tel.: +32 9 264 5489
Fax: +32 9 264 5837
Website: http://awww.ugent.be

Doctoraatsbeurs gefinancierd door

Het Fonds voor Wetenschappelijk Onderzoek (FWO) - Vlaanderen

Copyright © Hadewych Verhaeghe

THANKS TO …

my supervisor prof. dr. ir. Julien De Rouck
who gave me the opportunity to prepare this thesis at the department, who supervised and guided me with his great knowledge and critical view through these 4 years of research, and who provided me with 4 years of pleasant working … thanks Julien!

dr. ir. Jentsje W. van der Meer
who was a kind of second supervisor for me during the time I made this thesis, who was most closely involved during the set-up of the CLASH database and who imparted me so many things, whose everlasting interest was a big help for me, and thanks to whom I had many very nice moments during my stay in The Netherlands … thanks Jentsje!

my colleagues at the department
for the cooperation in a nice atmosphere, and especially for their individual support during the last months of hard work … thanks Amélie, Anny, Bart, Cathy, Etienne, Hans, Herman, Herwin, Jan, Jimmy, Leen, Ludo, Nathalie, Peter, Philippe, Sam, Stefaan, Tingqui, Tom and Wouter!

ir. Gosse Jan Steendam
with whom I worked together on the CLASH database, having a nice cooperation during this period

prof. dr. Josep R. Medina
for his useful hints on the neural network development

all partners of the CLASH project
for the close collaboration making possible this thesis and for the fine cooperation during the three years of CLASH

dr. ir. Gerbrant Van Vledder and ir. David Hurdle from Alkyon
for their help and explanation with the SWAN -calculations

prof. dr. ir. Johan Suykens
who taught me the secrets of neural network modelling, for the interesting discussions and for his useful hints on the neural network modelling

friend and colleague Herman
for reading the texts again and correcting them, and for the extra support during the last most difficult weeks of hard work

my sister Sigrid
for reading all texts again

my family and my close friends
for their understanding and support throughout the years

special thanks to
my parents Yves Verhaeghe and Bea Lampaert
for the opportunity they gave me to continue my studies, for their everlasting support throughout the years and for always being there for me

and finally, thanks to
my boyfriend Benjamin, for being there for me ... again and again
… thank you Benjamin!

Hadewych, May 2005

INDEX

LIST OF SYMBOLS

SUMMARY (in Dutch)

CHAPTER 1
INTRODUCTION

CHAPTER 2
LITERATURE SURVEY ON WAVE OVERTOPPING

CHAPTER 3
SET-UP OF A DATABASE ON WAVE OVERTOPPING

CHAPTER 4
DEVELOPMENT OF A NEURAL PREDICTION METHOD FOR WAVE OVERTOPPING

CHAPTER 5
GENERAL CONCLUSIONS AND
RECOMMENDATIONS FOR FURTHER RESEARCH

LIST OF SYMBOLS

A_c	=	armour crest freeboard of a structure	[m]
B	=	width of the berm of a structure, measured horizontally	[m]
B_h	=	width of the horizontally schematised berm of a structure	[m]
B_t	=	width of the toe of a structure	[m]
C_r	=	mean reflection coefficient	[%]
	=	$\sqrt{m_{0,r}} / \sqrt{m_{0,i}}$	
CF	=	complexity factor of a structure section	[-]
D(f,θ)	=	directional spreading function, defined as: $S_\eta(f,\theta) = S_\eta(f) \,.\, D(f,\theta)$ with $\int_0^{2\pi} D(f,\theta)\, d\theta = 1$	[°]
D_n	=	nominal diameter of concrete armour unit	[m]
D_{n50}	=	nominal diameter of rock	[m]
f	=	frequency	[Hz]
f_p	=	spectral peak frequency	[Hz]
	=	frequency at which $S_\eta(f)$ is a maximum	
g	=	acceleration due to gravity (= 9,81)	[m/s²]
G_c	=	crest width of a structure	[m]
h	=	water depth at the toe of a structure	[m]
	=	water depth just in front of the toe of a structure	
h_b	=	water depth on the berm of a structure (negative value if berm above swl)	[m]
h_{deep}	=	water depth at deep water	[m]
h_t	=	water depth on the toe of a structure	[m]
H	=	wave height	[m]
$H_{1/x}$	=	mean of the highest $1/x^{th}$ of the wave heights derived from time domain analysis	[m]
$H_{x\%}$	=	wave height exceeded by x% of all wave heights	[m]
H_s	=	significant wave height	[m]
$H_{1/3}$	=	significant wave height derived from time domain analysis = H_s	[m]

H_{max}	=	wave height of the highest individual wave in a record	[m]
H_{m0}	=	estimate of significant wave height from spectral analysis	[m]
	=	$4\sqrt{m_0}$	
$H_{m0\ deep}$	=	estimate of significant wave height from spectral analysis at deep water	[m]
$H_{m0\ toe}$	=	estimate of significant wave height from spectral analysis at the toe of a structure	[m]
H_{rms}	=	root-mean-square wave height = $\sqrt{\sum_{i=1}^{N} \frac{H_i^2}{N}}$, with H_i the individual wave heights from time series	[m]
k	=	angular wave number (= 2π/L)	[rad/m]
L	=	wave length	[m]
L_0	=	deep water wave length based on $T_{m-1,0} = gT^2_{m-1,0}/2\pi$	[m]
L_{0m}	=	deep water wave length based on $T_m = gT^2_m/2\pi$	[m]
L_{0p}	=	deep water wave length based on $T_p = gT^2_p/2\pi$	[m]
m	=	measure of the slope of a foreshore	[-]
	=	1 (unit vertically) : m (units horizontally)	
m_n	=	n^{th} moment of spectral density	[m^2/s^n]
	=	$\int_{f_1}^{f_2} f^n \, S_\eta(f)\, df$	
		lower integration limit = f_1 = min(1/3.f_p, 0.05 full scale)	
		upper integration limit = f_2 = 3.f_p	
$m_{n,x}$	=	n^{th} moment of spectral density for x	[m^2/s^n]
		x may be:	
		i for incident spectrum	
		r for reflected spectrum	
N_{ow}	=	number of overtopping waves	[-]
N_w	=	number of incident waves	[-]
p(x)	=	probability density function	
P(x)	=	probability distribution function	
P_V	=	$P(\underline{V} \geq V)$ = probability of the overtopping volume $\underline{V}$ being larger or equal to V	[-]
P_{ow}	=	probability of overtopping per wave	
	=	N_{ow}/N_w or	[-]
	=	$(N_{ow}/N_w).100$	[%]
q	=	mean overtopping discharge per meter structure width	[$m^3/s/m$]
R_c	=	crest freeboard of a structure	[m]
	=	height of 'wave return point' of a structure in relation to swl	

RF	=	reliabilityfactor of overtopping test = 1, 2, 3 or 4	[-]
Ru	=	run-up level, vertical measured in relation to swl	[m]
$Ru_{2\%}$	=	run-up level exceeded by 2% of the incident waves	[m]
s	=	wave steepness = H/L	[-]
s_0	=	wave steepness with L_0 based on $T_{m-1,0} = H_{m0}/L_0 = 2\pi H_{m0}/(gT^2_{m-1,0})$	[-]
s_{0p}	=	wave steepness with L_0 based on $T_p = H_{m0}/L_{0p} = 2\pi H_{m0}/(gT^2_p)$	[-]
s_{0m}	=	wave steepness with L_0 based on $T_m = H_{m0}/L_{0m} = 2\pi H_{m0}/(gT^2_m)$	[-]
swl	=	still water level	
$S_\eta(f)$	=	spectral density	[m²/Hz]
$S_{\eta,i}(f)$	=	incident spectral density	[m²/Hz]
$S_{\eta,r}(f)$	=	reflected spectral density	[m²/Hz]
$S_\eta(f, \theta)$	=	directional spectral density	[(m²/Hz)/°]
t	=	time variable	[s]
T	=	wave period = 1/f	[s]
T_m	=	mean wave period derived either from time domain analysis or from spectral analysis	[s]
T_p	=	peak wave period derived from spectral analysis = $1/f_p$	[s]
$T_{H1/x}$	=	mean of the wave periods of the highest $1/x^{th}$ of wave heights	[s]
T_s	=	significant wave period	[s]
$T_{H1/3}$	=	significant wave period derived from time domain analysis = T_s	[s]
T_{max}	=	wave period of the highest individual wave in a record	[s]
$T_{mi,j}$	=	mean wave period calculated from spectral moments, e.g.:	[s]
$T_{m0,1}$	=	mean wave period derived from spectral analysis = m_0/m_1	[s]
$T_{m0,2}$	=	mean wave period derived from spectral analysis = $\sqrt{m_0 / m_2}$	[s]
$T_{m-1,0}$	=	mean wave period derived from spectral analysis = m_{-1}/m_0	[s]
T_R	=	record length	[s]
V	=	volume of overtopping wave per unit crest width	[m^3/m]
α	=	slope angle	[°]
α_B	=	angle that sloping berm makes with a horizontal	[°]
α_d	=	angle that structure part below the berm makes with a horizontal	[°]
α_{excl}	=	mean angle that structure makes with a horizontal, excluding the berm	[°]

α_{incl}	=	mean angle that structure makes with a horizontal, including the berm	[°]
α_u	=	angle that structure part above the berm makes with a horizontal	[°]
β	=	angle of wave attack with respect to the normal on a structure	[°]
$\eta(t)$	=	surface elevation with respect to swl	[m]
γ_f	=	factor accounting for the roughness and permeability of or on the slope of a structure	[-]
ξ_0	=	breaker parameter	[-]
	=	$\frac{\tan\alpha}{\sqrt{s_0}}$	
ξ_{0m}	=	breaker parameter based on s_{0m}	[-]
ξ_{0p}	=	breaker parameter based on s_{0p}	[-]
$\mu_{(x)}$	=	mean of measured parameter x with normal distribution	[..]
$\sigma_{(x)}$	=	standard deviation of measured parameter x with normal distribution	[..]
ω	=	angular frequency = $2\pi f$	[rad/s]

SUMMARY (in Dutch)

VOORSPELLING VAN GOLFOVERSLAG OVER GOLFBREKERS EN ZEEWERINGEN MET BEHULP VAN NEURALE NETWERKEN

1 Inleiding

1.1 Situatieschets

Golfbrekers en zeeweringen worden ontworpen om (vaak dichtbevolkte) kustgebieden te beschermen tegen de krachten van de zee. De kruinhoogte van deze structuren speelt een overheersende rol in het ontwerp ervan. Klimaatsveranderingen hebben een rijzing van de zeespiegel tot gevolg, gepaard gaande met hevigere stormen (Carter et al., 1988), wat het belang van een goed ontwerp benadrukt. Het zeewater dat over de kruin van een structuur landinwaarts getransporteerd wordt, wordt 'golfoverslag' genoemd, en is een kritieke ontwerpfactor in deze context.

Het ontwerp van golfbrekers en zeeweringen moet leiden tot een 'aanvaardbare' hoeveelheid golfoverslag. Welke hoeveelheid golfoverslag aanvaardbaar is, hangt af van socio-economische factoren. Structuren met hoge kruinen worden liefst vermeden aangezien deze het zicht belemmeren, waar het uitgestrekte zicht op zee precies een belangrijke toeristische trekpleister is. Nochtans moet de kruinhoogte van golfbrekers en zeeweringen voldoende hoog zijn zodat veiligheid gegarandeerd wordt voor mensen en voertuigen op en achter de structuur, en zodat structurele schade vermeden wordt. Ook het behoud van de eventuele economische functie van de structuur onder slechte weersomstandigheden kan meespelen in het ontwerp.

Niettemin is er een tekort aan betrouwbare en robuuste voorspellingsmethodes voor golfoverslag. De meest gebruikte modellen voor hedendaags ontwerp van golfbrekers en zeeweringen betreffen empirische modellen, ontwikkeld op basis van fysische modelproeven. Een nadeel van deze modellen is dat een voorspelling enkel mogelijk is binnen bepaalde parametergrenzen (bepaald door de metingen

waarop het model gebaseerd is). Bovendien is het moeilijk om tot betrouwbare overslagvoorspellingen te komen voor structuren die niet aan een standaard ontwerp voldoen.
Tenslotte bestaat het vermoeden dat huidige voorspellingsmethodes voor golfoverslag onderhevig zijn aan model- en schaaleffecten, die resulteren in een verschil tussen prototype en model respons. Dit vermoeden vindt zijn oorsprong in het Europese project OPTICREST (De Rouck et al., 2001). In dit project werd bevonden dat de golfoploop overschreden door 2% van de golven, $Ru_{2\%}$, op een ruwe helling tijdens prototype stormen ongeveer 20% hoger is dan opgemeten tijdens vergelijkbare modelproeven.

1.2 Definitie van golfoverslag

'Golfoverslag' of kort 'overslag' wordt gedefinieerd als zeewater dat over de kruin van een structuur landinwaarts stroomt (figuur 1). Golfoverslag is gerelateerd aan golfoploop: golfoverslag treedt op wanneer de oplopende golf de kruin van de structuur bereikt en erover vloeit. Naast dit zogenaamde 'green water' valt ook 'spray' onder de noemer van golfoverslag. Spray betreft kleine hoeveelheden golfoverslag onder de vorm van fijne druppeltjes water die onder eigen momentum en/of door de wind achter de kruin van de structuur terecht komen.
Onderzoek naar golfoverslag in laboratoria beschouwt zelden het effect van wind op (spray) overslag. Voor kleine hoeveelheden overslag kan dit windeffect een aanzienlijke (relatieve) bijdrage leveren.

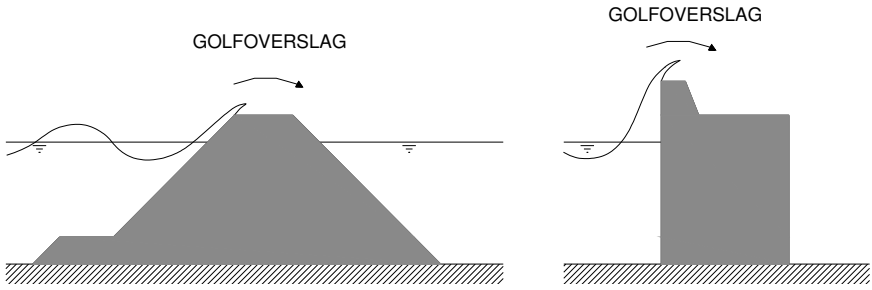

Figuur 1 Definitie van golfoverslag

Er kan onderscheid gemaakt worden tussen twee benaderingen van het fenomeen overslag. De eerste benadering beschouwt het volume zeewater per golf die overslaat. De tweede en meest voorkomende benadering beschouwt een gemiddeld overslagdebiet over een zekere tijd en per meter breedte van de structuur, i.e. q in $m^3/s/m$ of in l/s/m. De bevinding dat golfoverslag zeer onregelmatig verdeeld is in tijd, ruimte en volume (ten gevolge van het

onregelmatige karakter van de golven) ligt aan de oorsprong van deze tweede benadering. Men spreekt dikwijls over een tijdsvenster van ongeveer 1000 golven om tot een 'reproduceerbaar' overslagdebiet te komen.
Ook in dit proefschrift worden gemiddelde overslagdebieten bestudeerd: er wordt een neurale voorspellingsmethode voor gemiddelde overslagdebieten over een willekeurige structuur ontwikkeld.

1.3 Het Europese project CLASH

De intentie van het door de Europese Commissie gefinancierde 'CLASH' project (Crest Level Assessment of coastal Structures by full scale monitoring, neural network prediction and Hazard analysis on permissible wave overtopping) was een verdieping van de bestaande kennis over het fenomeen overslag. Twee bevindingen lagen aan de basis van het project:

- het ontbreken van algemeen toepasbare voorspellingsmethodes voor golfoverslag om kruinhoogtes van golfbrekers en zeeweringen te ontwerpen, en
- de bevinding dat de golfoploop $Ru_{2\%}$ op ruwe hellingen in kleinschalige proeven lager is vergeleken met prototype metingen.

Het CLASH project, onder contract nummer EVK3-CT-2001-00058, liep van januari 2002 tot december 2004 (www.clash-eu.org). Het onderzoek beschreven in dit proefschrift werd gedeeltelijk uitgevoerd binnen CLASH. Voor gedetailleerde informatie over het CLASH project wordt verwezen naar De Rouck et al. (2005). Het project had 3 belangrijke doelstellingen:

1) het probleem van de vermoedelijke model- en schaaleffecten voor golfoverslag oplossen,
2) een algemeen toepasbare voorspellingsmethode voor golfoverslag ontwikkelen, gebaseerd op een grote hoeveelheid bestaande overslagmetingen verzameld in één grote databank, en
3) richtlijnen definiëren voor toelaatbare overslaggrenzen.

In het kader van de eerste CLASH doelstelling werd golfoverslag over 3 bestaande golfbrekers/zeeweringen gemeten:

- een stortsteengolfbreker in Zeebrugge (België), waarbij de deklaag is opgebouwd uit antifer kubussen,
- een stortsteengolfbreker in Ostia (Italië), waarbij de deklaag is opgebouwd uit rotsblokken, en
- een verticale wand in Samphire Hoe (Verenigd Koninkrijk), waarbij rotsblokken een bescherming van de teen voorzien.

De opgemeten prototype stormen werden op kleine schaal gereproduceerd in verschillende laboratoria. Finaal werden ook numerieke berekeningen aangewend om het probleem van de model- en schaaleffecten op te lossen.
Het onderzoek bevestigde het vermoeden dat model- en schaaleffecten onder specifieke omstandigheden kleinschalige overslagmetingen beïnvloeden, en resulteerde in een 'CLASH schaalprocedure' die deze effecten onder specifieke omstandigheden kwantificeert. Het overeenkomstige CLASH rapport (Kortenhaus et al., 2005) geeft gedetailleerde informatie over de bekomen resultaten.

De tweede CLASH doelstelling vereiste in een eerste fase het opstellen van een uitgebreide databank met overslaggegevens. Het opstellen van deze databank is een onderdeel van dit proefschrift en is beschreven in punt 3 (en in het overeenkomstig CLASH rapport, Van der Meer et al., 2005b).
Er werden zoveel mogelijk bestaande overslagproeven opgespoord. Na grondig nazicht werden deze aan de hand van een beperkt aantal parameters in een databank verzameld. Additioneel werden binnen CLASH zogenaamde 'white spot' -proeven uitgevoerd, i.e. extra fysische modelproeven om ontbrekende kennis in de databank aan te vullen.
In een tweede fase werd een algemeen toepasbare voorspellingsmethode voor golfoverslag ontwikkeld, gebaseerd op de CLASH databank. Hiervoor werd de gesofisticeerde techniek van neurale netwerken gebruikt, resulterend in een CLASH voorspellingsmethode voor golfoverslag op kleine schaal (Pozueta et al., 2004a en 2004b). Onafhankelijk van het CLASH project, maar binnen het kader van dit proefschrift, werd een vergelijkbare voorspellingsmethode opgesteld. Het fundamentele verschil tussen beide voorspellingsmethodes bestaat erin dat in dit proefschrift een opeenvolging van 2 neurale netwerken voorgesteld wordt, terwijl de CLASH methode slechts uit één netwerk bestaat. In dit proefschrift wordt aangetoond dat het gebruik van 2 opeenvolgende netwerken een significante meerwaarde heeft in vergelijking met het gebruik van slechts één netwerk: grote overpredicties ten gevolge van het niet kunnen voorspellen van geen of weinig overslag door één enkel model worden vermeden. Aangezien beide methodes ongeveer tegelijkertijd ontwikkeld werden, valt een gedetailleerde vergelijking van beide methodes buiten het kader van dit proefschrift.

De derde en laatste CLASH doelstelling bestond erin om toelaatbare overslaggrenzen te bepalen/verfijnen, om de veiligheid van mensen en voertuigen aanwezig op of achter een golfbreker/zeewering te garanderen, en daarnaast ook structurele veiligheid te voorzien. De impact van golfoverslag op het sociale en economische leven in dichtbevolkte kustgebieden werd ook bestudeerd. Voor gedetailleerde informatie wordt verwezen naar twee CLASH rapporten: Bouma et al. (2004) en Allsop (2005).

1.4 Doelstellingen

De doelstellingen van dit proefschrift kunnen als volgt worden samengevat:

- het uitvoeren van een literatuurstudie naar bestaande overslagmodellen, met als specifiek doel het opsporen van de invloedsfactoren betreffende het fenomeen golfoverslag
- het verzamelen van zoveel mogelijk bestaande overslagmetingen waarbij alle gegevens nagezien worden op consistentie om op die manier tot een homogene verzameling gegevens te komen
- het opstellen van een databank met overslaggegevens waarbij elke verzamelde meting beschreven wordt aan de hand van parameters die een beschrijving geven van de overslagmeting zelf, van de betreffende structuur, van de golfkarakteristieken en tenslotte van de betrouwbaarheid van de beschrijving van de meting aan de hand van deze parameterwaarden
- het ontwikkelen van een algemeen toepasbaar voorspellingsmodel voor golfoverslag door het trainen van een neuraal netwerk op basis van de opgestelde databank met overslaggegevens
- het valideren van het ontworpen voorspellingsmodel op basis van beschikbare prototype metingen in combinatie met de beschikbare CLASH schaalprocedure enerzijds en op basis van kunstmatige datasets waarvan het overslaggedrag gekend is anderzijds

2 Bestaande overslagmodellen met hun invloedsparameters

In het verleden werd reeds heel wat onderzoek verricht naar het fenomeen golfoverslag. Saville (1955) is een van de eerste onderzoekers die fysische modelproeven met regelmatige golven uitvoert waarbij overslag gemeten wordt. Vanaf dan wordt golfoverslag intensiever bestudeerd, met een waaier aan modellen als resultaat, ontworpen om golfoverslag over verschillende structuren te voorspellen. De eerste decennia worden enkel proeven met regelmatige golven uitgevoerd, doch later worden proeven met onregelmatige golven een standaard procedure. Het eerste bekende model ter voorspelling van golfoverslag is het model van Owen (1980). Ook vandaag nog wordt dit model gebruikt bij het ontwerp van hellende structuren.

Focussend op het voorspellen van gemiddelde overslagdebieten, kunnen verschillende types modellen onderscheiden worden. Empirische modellen (= regressiemodellen) gebaseerd op fysische modelproeven met overslagmetingen, kunnen onderscheiden worden van numerieke modellen. Numerieke modellen simuleren overslaggebeurtenissen in een numerieke golfgoot, maar staan nog in hun kinderschoenen vergeleken met de eerste groep modellen.

Binnen de groep van de empirische modellen kan onderscheid gemaakt worden tussen eenvoudige regressiemodellen, overlaat-modellen, modellen gebaseerd op golfoploop en grafische modellen.
De eenvoudige regressiemodellen beschrijven typisch een verband tussen een zeker dimensieloos overslagdebiet en een zekere dimensieloze kruinhoogte, waarbij modelparameters geschat worden op basis van overslagmetingen in het laboratorium. Deze modellen liggen ook heden nog steeds aan de basis van het ontwerp van golfbrekers en zeeweringen.
De overlaat-modellen en modellen gebaseerd op golfoploop hebben een meer fysische achtergrond dan de eenvoudige regressiemodellen. Kikkawa (1968) introduceerde de analogie met een overlaat bij het beschrijven van golfoverslag. De modellen gebaseerd op golfoploop vertrekken van metingen van golfoploop om overslagdebieten te voorspellen.
In grafische modellen presenteren onderzoekers hun resultaten grafisch, met als resultaat ontwerpdiagrammen voor golfoverslag. De modellen van Goda (1985) zijn een bekend voorbeeld.

Onderzoek naar golfoverslag concentreerde zich tot op heden steeds op één bepaald type structuur. Modellen voor verticale muren onderscheiden zich van modellen voor hellende (ruwe of gladde) structuren. Daarnaast zijn ook modellen ontwikkeld voor samengestelde structuren, bv. een verticale wand met een stortsteenbescherming ervoor.
In dit proefschrift worden alle mogelijke structuren geïntegreerd in één overslagmodel, dat ontwikkeld wordt met behulp van neurale netwerken. Het is duidelijk dat het algemeen toepasbaar zijn van het ontwikkelde model een groot voordeel oplevert tegenover de klassieke modellen die slechts geldig zijn voor één type structuur.

Zonder hier in detail in te gaan op de verschillende modellen, kan vermeld worden dat huidige modellen slechts gebruik maken van een beperkt aantal golfparameters en structurele parameters. Dit wordt deels verklaard door het feit dat elk model opgesteld is voor slechts één type structuur. Wanneer verschillende overslagmodellen voor allerlei structuren naast elkaar bestudeerd worden, ziet men dat overslag bepaald wordt door een waaier aan parameters.
Veel onderzoekers stellen daarenboven correctiefactoren op om toe te voegen aan bestaande overslagmodellen. Deze factoren houden rekening met extra overslaginvloeden die niet beschouwd worden in het originele model.

Het specifieke doel van de studie van overslagmodellen in dit proefschrift is om de parameters te identificeren die een invloed hebben op het fenomeen golfoverslag, ongeacht het type structuur. Tabel 1 vat de gevonden invloedsfactoren (en overeenkomstige parameters) samen. Wanneer een invloedsfactor enkel verschijnt

door middel van een correctiefactor, is de corresponderende factor weergegeven tussen haakjes. Voor de invloedsfactoren die tot op heden nog niet gekwantificeerd zijn, is geen parameter weergegeven.

Tabel 1 Invloedsfactoren en overeenkomstige parameters voor overslag over golfbrekers en zeeweringen, aanwezig in bestaande overslagmodellen

Invloedsfactoren	**Parameters**
Golfkarakteristieken	
• golfhoogte op diep water/aan de teen van de structuur	H_s of H_{m0} [m]
• golfperiode op diep water/aan de teen van de structuur	T_p, T_m, $T_{1/3}$ of $T_{m-1,0}$ [s]
• golfrichting	β [°]
• kortkruinige golven	(γ_β)
Structurele karakteristieken	
• helling van de vooroever	1:m
• helling van de structuur	α [°]
• kruinbreedte	G_c [m]
• hoogte van kruin t.o.v. swl	R_c [m]
• hoogte van kruin deklaag t.o.v. swl	A_c [m]
• ruwheid/doorlatendheid van de structuur (inclusief verschillende types deklaag)	(γ_f)
• karakteristieken van de berm	h_b [m], B [m] en α_b [°], (of in γ_b)
• waterdiepte aan de teen van de structuur	h [m]
• waterdiepte op de berm voor een verticale muur	d [m]
• plaatsing van de deklaagelementen	-
• aanwezigheid van een parapet	-
• dimensies van een muurtje bovenaan een structuur	(γ_v)
• specifieke geometrie van een verticale muur (vb. porositeit, neus,…)	(γ of γ_s)
Omgevingskarakteristieken	
• wind	U [m/s]

De verworven kennis betreffende de invloedsparameters voor golfoverslag is direct bruikbaar voor het opstellen van de databank met overslaggegevens: iedere overslagproef wordt in de databank beschreven aan de hand van een beperkt aantal parameters.

3 Opstellen van een databank met overslaggegevens

3.1 Inleiding

In dit hoofdstuk wordt het opstellen van de CLASH databank met overslaggegevens besproken. De databank (Van der Meer et al., 2005a) is beschikbaar op de bijgevoegde CD-ROM.
De databank werd opgesteld in 2 fasen. Een eerste voorlopige databank, samengesteld uit 6500 overslagproeven daterend van voor 2003, werd in augustus 2003 binnen CLASH als tussentijds resultaat uitgegeven, zie Verhaeghe et al. (2003a and 2003b). In een tweede fase, van augustus 2003 tot december 2004, werd deze voorlopige databank uitgebreid en geoptimaliseerd tot een finale databank, bestaande uit 10532 proeven afkomstig uit 163 verschillende proevenreeksen.

De gegevens verzameld gedurende de eerste fase werden in de tweede fase aangevuld met volgende extra proeven:

1) de prototype metingen uitgevoerd binnen het CLASH project, te Ostia (Italië), Samphire Hoe (Verenigd Koninkrijk) en Zeebrugge (België)
2) de kleinschalige reproducties van de opgemeten CLASH prototype stormen
3) de extra fysische modelproeven uitgevoerd binnen CLASH om ontbrekende kennis in de voorlopige databank aan te vullen (zogenaamde 'white spot' proeven), om zo tot een meer homogene databank te komen
4) extra verzamelde proeven van over de hele wereld, afkomstig van zowel nieuwe gevonden referenties van overslagproeven uitgevoerd in het verleden als van recent onderzoek naar golfoverslag

De optimalisatie van de voorlopige databank betreft enerzijds kleine aanpassingen aan de definities van bepaalde parameters, en anderzijds nieuwe waarden toegekend aan de factor γ_f (zie punt 3.3). De γ_f -waarden opgenomen in de voorlopige databank betreffen voornamelijk geschatte waarden, waar de waarden opgenomen in de definitieve databank waarden zijn resulterend uit het recente CLASH onderzoek naar een van de white spots, namelijk 'invloed van ruwheid en doorlatendheid op golfoverslag'.

Het uiteindelijke nut van de databank is tweeledig:

- De databank geeft een summier overzicht van de vele betrouwbare overslagproeven die ooit uitgevoerd werden, onafhankelijk van plaats of tijd. Voor onderzoekers betreft het een schat aan gegevens die zeer bruikbaar is voor verder onderzoek, zowel naar golfoverslag als in gerelateerde onderzoeksdomeinen.

- Het fundamentele doel van de databank is deze aan te wenden voor het ontwikkelen van een algemeen toepasbaar voorspellingsmodel voor golfoverslag. Naast de CLASH voorspellingsmethode (Pozueta et al., 2004a and 2004b) werd in dit proefschrift, onafhankelijk van het CLASH project, een tweeledig neuraal netwerk opgesteld (zie punt 4).

3.2 Werkwijze

Gedurende de laatste 30 jaar werd intensief modelonderzoek naar golfoverslag verricht, resulterend in een grote hoeveelheid informatie betreffende dit onderwerp, doch verspreid over universiteiten en onderzoeksinstellingen over de hele wereld. Daarom werd in eerste instantie getracht zoveel mogelijk van deze gegevens samen te brengen. Ongeveer 75% van de uiteindelijk verzamelde gegevens betreft openbaar onderzoek, versus 25% vertrouwelijke onderzoek. Voor vertrouwelijke gegevens was het soms nodig om de betrokken onderzoeksinstelling te bezoeken.
Om een homogene databank te bekomen was het belangrijk om zoveel mogelijk informatie te verzamelen over de betreffende proeven. In die context werd niet alleen informatie over de structuur, de golven en de gemeten overslag verzameld, maar ook over de testfaciliteit, de verwerking van de gegevens en de precisie waarmee tewerk gegaan werd.

De verzamelde gegevens werden vervolgens aan de hand van een beperkt aantal parameters in de databank ingevoerd. Alle proeven werden opgenomen in de databank op de schaal waarop ze uitgevoerd werden.
De parameters dienden zodanig gekozen dat een zo volledig mogelijk overzicht van de overslagproef werd verkregen. De verworven kennis betreffende de invloedsparameters voor golfoverslag (zie tabel 1) was hier onmiddellijk bruikbaar.
Uiteindelijk werd iedere proef ingevoerd in de databank aan de hand van 31 parameters. Er kan onderscheid gemaakt worden tussen 11 hydraulische parameters, 17 structurele parameters en 3 algemene parameters. In volgende secties worden de 31 parameters afzonderlijk besproken.
Het dient vermeld dat, met het oog op het verder gebruik van de databank op zich, zoveel mogelijk informatie werd verzameld in de databank, i.e. meer informatie dan strikt gezien nodig is voor het ontwikkelen van een neurale voorspellingsmethode.

3.3 Bepalen van de hydraulische parameters

De golfkarakteristieken en de gemeten golfoverslag worden in de databank beschreven aan de hand van volgende hydraulische parameters:

1	$H_{m0\ deep}$ [m]	Significante golfhoogte uit spectraalanalyse = $4\sqrt{m_0}$, bepaald op diep water
2	$T_{p\ deep}$ [s]	Piekperiode van golven uit spectraalanalyse, bepaald op diep water
3	$T_{m\ deep}$ [s]	Gemiddelde golfperiode uit spectraalanalyse = $\sqrt{m_0/m_2}$ of uit analyse in het tijdsdomein ('zero-downcrossing'), bepaald op diep water
4	$T_{m-1,0\ deep}$ [s]	Gemiddelde golfperiode uit spectraalanalyse = m_{-1}/m_0 , bepaald op diep water
5	β [°]	Hoek van golfaanval ten opzichte van de normaal op de structuur
6	$H_{m0\ toe}$ [m]	Significante golfhoogte uit spectraalanalyse = $4\sqrt{m_0}$, bepaald aan de teen van de structuur
7	$T_{p\ toe}$ [s]	Piekperiode van golven uit spectraalanalyse, bepaald aan de teen van de structuur
8	$T_{m\ toe}$ [s]	Gemiddelde golfperiode uit spectraalanalyse = $\sqrt{m_0/m_2}$ of uit analyse in het tijdsdomein ('zero-downcrossing'), bepaald aan de teen van de structuur
9	$T_{m-1,0\ toe}$ [s]	Gemiddelde golfperiode uit spectraalanalyse = m_{-1}/m_0 , bepaald aan de teen van de structuur
10	q [m^3/s/m]	Gemiddeld overslagdebiet (volume per seconde) per meter breedte
11	P_{ow} [%]	Percentage van de golven dat resulteert in overslag = $(N_{ow}/N_w).100$

Dikwijls was (waren) in het overeenkomstige rapport van de proef een (meerdere) van deze hydraulische parameters niet beschikbaar. De reden hiervoor is dat de betreffende parameter(s) niet gemeten of niet genoteerd werd(en) tijdens het uitvoeren van de proef. Bij het ontbreken van parameters werd indien mogelijk een schatting van de betreffende parameter gemaakt. Hiervoor werd enerzijds beroep gedaan op extra berekeningen, en anderzijds op door vroeger onderzoek gefundeerde aannames.
Er kan onderscheid gemaakt worden tussen volgende berekeningen/schattingen:

1) *Berekening van de golfkarakteristieken aan de teen van de structuur met het numerieke model SWAN (Booij et al., 1999)*
   Voor een deel van de verzamelde overslagproeven waren enkel de golfkarakteristieken op diep water beschikbaar. In dergelijke gevallen werden de golfkarakteristieken aan de teen van de structuur berekend met het numerieke model SWAN, waarbij wordt uitgegaan van de beschikbare golfkarakteristieken op diep water en de vooroever.

Aangezien de meerderheid van de beschikbare proeven in de databank tweedimensionale proeven betreft (uitgevoerd in een golfgoot), werd de 'one-dimensional' mode van SWAN gebruikt, waarbij tweedimensionale berekeningen uitgevoerd worden.

2) *Schatting van ontbrekende golfkarakteristieken op basis van door vroeger onderzoek gefundeerde aannames*
Longuet-Higgins (1952) toonde aan dat golfhoogtes van golven op diep water een Rayleigh distributie aannemen. Dit leidt tot de mogelijkheid om karakteristieke golfhoogtes van elkaar af te leiden. Zo geldt op diep water:

$$H_{m0} = 4\sqrt{m_0} = H_{1/3} \quad (1)$$

Golfperiodes op diep water zijn niet Rayleigh verdeeld, doch er werden een aantal empirische verbanden tussen karakteristieke golfperiodes op diep water opgesteld. Een voorbeeld hiervan is het verband tussen T_p en $T_{m-1,0}$, geldig voor enkelpiekige spectra (TAW, 2002):

$$T_p \approx 1.1\ T_{m-1,0} \quad (2)$$

3) *Bepaling van $H_{m0\ toe}$ uit $H_{s\ toe}$ in ondiep water aan de hand van het model voorgesteld door Battjes en Groenendijk (2000)*
Aangezien de distributie van golfhoogtes in ondiep water afwijkt van de Rayleigh distributie, kunnen de verbanden afgeleid voor diep water niet gebruikt worden in ondiep water. Battjes en Groenendijk (2000) stelden een model op voor golfhoogtes in ondiep water, opgebouwd uit 2 Weibull distributies. De parameters werden gekalibreerd aan de hand van fysische modelproeven, en uitgedrukt in termen van locale golfenergie (m_0), waterdiepte (h) en bodemhelling (1:m).
Bij het ontbreken van de waarde van $H_{m0\ toe}$ voor een bepaalde proef, laat het model toe om uitgaande van de gekende golfhoogte $H_{s\ toe}$, de helling van de vooroever 1:m en de waterdiepte aan de teen van de constructie h, de gewenste waarde van $H_{m0\ toe}$ te berekenen.

In sommige gevallen was het niet mogelijk om een betrouwbare schatting van een ontbrekende parameter te maken. In dergelijke gevallen werd de voorkeur gegeven aan een lege plaats in de databank. Een voorbeeld is de waarde van de parameter P_{ow} : aangezien het hier een proefresultaat betreft, is het niet mogelijk om deze parameter te schatten.

Er wordt in de databank rekening gehouden met het benaderende karakter van de hierboven beschreven berekeningen en schattingen in de waarde van de

betrouwbaarheidsfactor RF toegekend aan een proef (zie verder punt 3.4). Om de berekende en geschatte waarden bovendien te kunnen onderscheiden van gemeten waarden, worden kleuren gebruikt:

- SWAN resultaten zijn gemarkeerd in blauw
- geschatte parameters zijn gemarkeerd in rood
- berekende parameters volgens Battjes en Groenendijk (2000) zijn gemarkeerd in groen

3.4 Bepalen van de structurele parameters

De 17 structurele parameters in de databank beschrijven de sectie die beproefd wordt en zijn zodanig gekozen dat een groot aantal verschillende secties kan beschreven worden:

1	h_{deep} [m]	Waterdiepte op diep water
2	m [-]	Maat voor de helling van de vooroever = 1 (eenheid verticaal) : m (eenheden horizontaal)
3	h [m]	Waterdiepte vlak voor de structuur
4	h_t [m]	Waterdiepte op de teen van de structuur
5	B_t [m]	Breedte van de teen van de structuur
6	γ_f [-]	Ruwheids- /doorlatendheidsfactor van de structuur
7	$\cot\alpha_d$ [-]	Cotangens van de hellingshoek van de structuur onder de berm
8	$\cot\alpha_u$ [-]	Cotangens van de hellingshoek van de structuur boven de berm
9	$\cot\alpha_{excl}$ [-]	Cotangens van de gemiddelde hellingshoek van de structuur, zonder bijdrage van de berm
10	$\cot\alpha_{incl}$ [-]	Cotangens van de gemiddelde hellingshoek van de structuur, met bijdrage van de berm
11	R_c [m]	Hoogte van de kruin van de structuur t.o.v. swl
12	B [m]	Breedte van de berm
13	h_b [m]	Waterdiepte op de berm
14	$\tan\alpha_B$ [-]	Tangens van de hellingshoek van de berm
15	B_h [m]	Breedte van de horizontaal geschematiseerde berm
16	A_c [m]	Hoogte van de kruin van de deklaag van de structuur t.o.v. swl

17 G_c [m] Kruinbreedte van de structuur

De eerste stap bij het bepalen van de structurele parameters voor een proef bestaat erin de beproefde sectie op te delen in drie gebieden (figuur 2).
Het belangrijkste gebied voor de golven is het gebied rond de swl (stil water lijn), hier 'centre area' genoemd, en kan benaderd worden door het gebied tussen $1.5H_{m0\ toe}$ boven en onder de swl (Van der Meer et al., 1998). Boven en onder de 'centre area' bevindt zich de 'upper area' respectievelijk de 'lower area'. Het splitsen in deze 3 gebieden vergemakkelijkt het benoemen van de teen, de eventuele berm en de kruin van de structuur. De teen is veelal gelegen in de 'lower area' van de structuur, de berm in de 'centre area' en de kruin in de 'upper area' (figuur 2).
Hierna wordt in detail uitgelegd hoe de 17 structurele parameters precies worden bepaald.

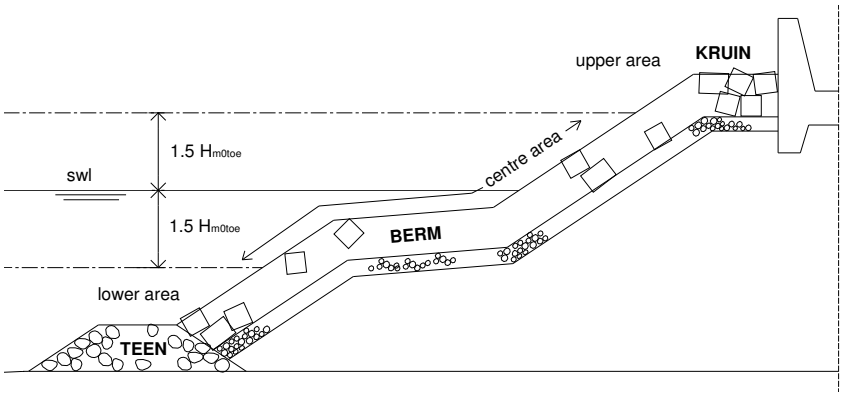

Figuur 2 Typische ligging van een berm, een kruin en een teen

De parameter **h_{deep} [m]** verwijst naar de waterdiepte op diep water, of meer concreet naar de waterdiepte waar de golfkarakteristieken $H_{m0\ deep}$, $T_{p\ deep}$, $T_{m\ deep}$ and $T_{m-1,0\ deep}$ bepaald zijn (figuur 3). Voor fysische modelproeven uitgevoerd in een golfgoot verwijst h_{deep} dus niet noodzakelijk naar de grootste waterdiepte in de golfgoot.

De parameter **m [-]** beschrijft de helling van de vooroever (figuur 3). Wanneer het voorland niet uniform hellend is moet de waarde van m benaderd worden. Aangezien vooral de vooroever net voor de structuur (het meest ondiepe gebied) door de golven gevoeld wordt, wordt de vooroever benaderd over een horizontale afstand van ongeveer 2 golflengtes L_0 voor de structuur.

Bij een vlakke vooroever is de waarde van m theoretisch oneindig. Aangezien een eindige waarde meer werkbaar is, werd in dergelijke gevallen een waarde m = 1000 opgenomen in de databank.

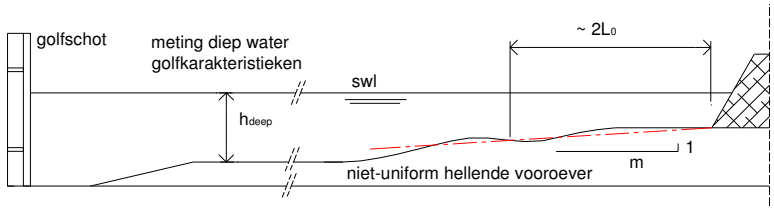

Figuur 3 Bepaling van h_{deep} en m

De parameter **h [m]** verwijst naar de waterdiepte net voor de structuur (figuur 4). Bij een vlakke bodem in een golfgoot is $h = h_{deep}$.

De parameters **h_t [m]** en **B_t [m]** beschrijven de teen van de structuur (figuur 4). De waarde van h_t wordt gemeten in het midden van de teen, B_t wordt gemeten op de top van de teen. Als de structuur geen teen heeft, is $h_t = h$ en $B_t = 0$m.

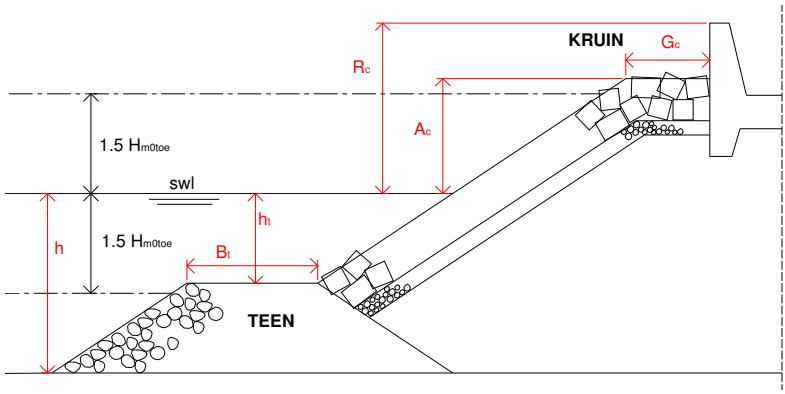

Figuur 4 Bepaling van h, h_t , B_t en van R_c, A_c en G_c

De berm van een structuur wordt beschreven aan de hand van de parameters **B [m]**, **h_b [m]**, **$\tan\alpha_B$ [-]** en **B_h [m]** (figuur 5).
De waterdiepte op de berm h_b wordt gemeten in het midden van de berm. Als de berm gelegen is boven de swl, dan is de waarde van h_b negatief. Het verschil tussen de breedte van de originele berm B en de breedte van de horizontaal geschematiseerde berm B_h wordt verduidelijkt in figuur 5. De parameter B_h kan gebruikt worden als vervanging voor de parameters B en $\tan\alpha_B$.

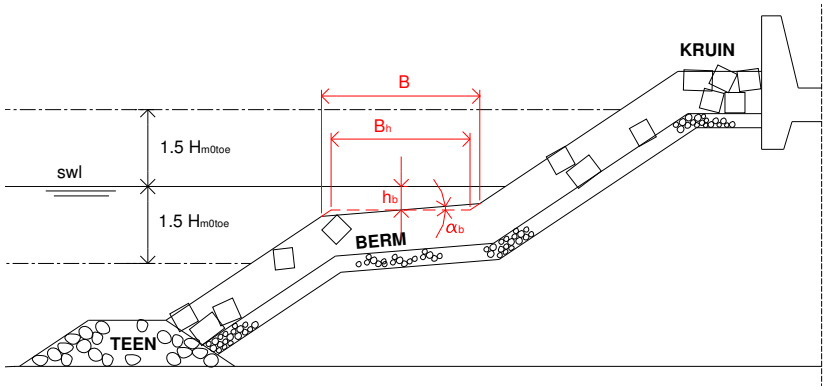

Figuur 5 Bepaling van B, B_h, $\tan\alpha_B$ en h_b

De parameters **R_c [m]**, **A_c [m]** en **G_c [m]** beschrijven de kruin van de structuur (figuur 4). De kruinhoogte R_c wordt verticaal gemeten vanaf de swl tot het punt waar overslag gemeten wordt. De parameter A_c verwijst naar de verticale afstand gemeten vanaf de swl tot het hoogste punt van de deklaag van de stortsteengolfbreker. De parameter R_c kan een waarde groter dan, gelijk aan of kleiner dan de parameter A_c aannemen, afhankelijk van het al dan niet aanwezig zijn van een kruinmuur en de hoogte ervan ten opzichte van de deklaag. De parameter G_c verwijst naar de kruinbreedte.
Wanneer de structuur geen stortsteengolfbreker betreft, vervalt de definitie van de parameter A_c . Deze laatste kan dan samen met R_c en G_c gebruikt worden om de kruin van de structuur in detail te beschrijven (figuur 6).

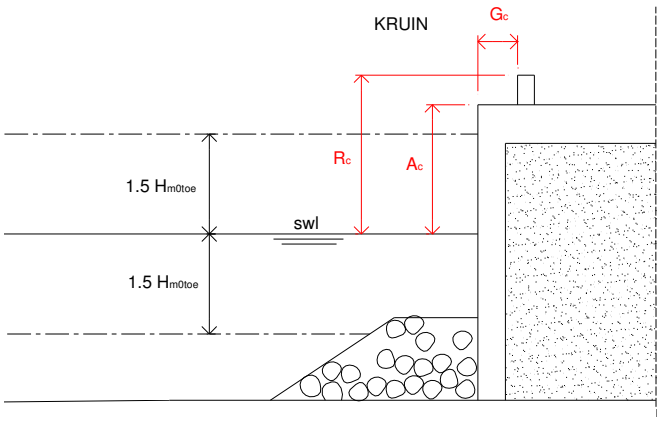

Figuur 6 Gebruik van A_c samen met R_c en G_c om de kruin van een structuur te beschrijven

De parameters **cotα$_d$ [-]**, **cotα$_u$ [-]**, **cotα$_{excl}$ [-]** en **cotα$_{incl}$ [-]** beschrijven de helling(en) van de structuur (figuur 7) op drie verschillende manieren, i.e.:

- met cotα$_d$ en cotα$_u$ of
- met cotα$_{excl}$ of
- met cotα$_{incl}$

De kruin en de teen van de structuur worden bij het bepalen van de hellingen buiten beschouwing gelaten aangezien deze reeds door aparte parameters beschreven worden.
De parameters cotα$_d$ en cotα$_u$ verwijzen naar de helling van de structuur onder respectievelijk boven de berm.
De parameters cotα$_{excl}$ en cotα$_{incl}$ verwijzen naar gemiddelde, berekende hellingen en kunnen gebruikt worden om de structuur te beschrijven aan de hand van één enkele parameter. Bij cotα$_{incl}$ wordt de aanwezige berm mee in beschouwing genomen in de gemiddelde helling, bij cotα$_{excl}$ wordt de aanwezige berm niet beschouwd.
Wanneer geen berm aanwezig is, is cotα$_{excl}$ = cotα$_{incl}$.

Figuur 7 verduidelijkt hoe de 4 hellingsparameters bepaald worden.
De hellingshoek α$_u$ wordt bepaald door het punt van de structuur op een hoogte van 1.5H$_{m0\ toe}$ boven de swl te verbinden met het uiterste punt van de berm, verst weg van zee. Wanneer de kruin zich lager bevindt dan 1.5H$_{m0\ toe}$ boven de swl, dan wordt om α$_u$ te bepalen het beginpunt van de kruin genomen in plaats van het punt op 1.5H$_{m0\ toe}$ boven de swl.
Analoog wordt de hellingshoek α$_d$ bepaald door het punt op een diepte van 1.5H$_{m0\ toe}$ onder de swl te verbinden met het uiterste punt van de berm, dichtst bij zee. Wanneer de teen van de structuur hoger gelegen is dan 1.5H$_{m0\ toe}$ onder de swl, dan wordt om α$_d$ te bepalen het hoogste punt van de teen genomen ipv het punt 1.5H$_{m0\ toe}$ onder de swl.
De gemiddelde hellingshoek α$_{incl}$ wordt bepaald door het punt 1.5H$_{m0\ toe}$ boven de swl te verbinden met het punt 1.5H$_{m0\ toe}$ onder de swl. Een eventuele berm wordt hierbij meegenomen. De gemiddelde hellingshoek α$_{excl}$ wordt bepaald door de breedte B$_h$ af te trekken van de horizontale afstand die α$_{incl}$ bepaalt. Ook hier wordt een lage kruin en/of een hoge teen niet in rekening gebracht.

Het gebruik van twee hellingsparameters, i.e. cotα$_u$ en cotα$_d$, leidt vaak tot een betere beschrijving van de structuur dan wanneer maar één enkele parameter, i.e. cotα$_{incl}$ of cotα$_{excl}$, gebruikt wordt. Figuur 7 illustreert dit duidelijk.

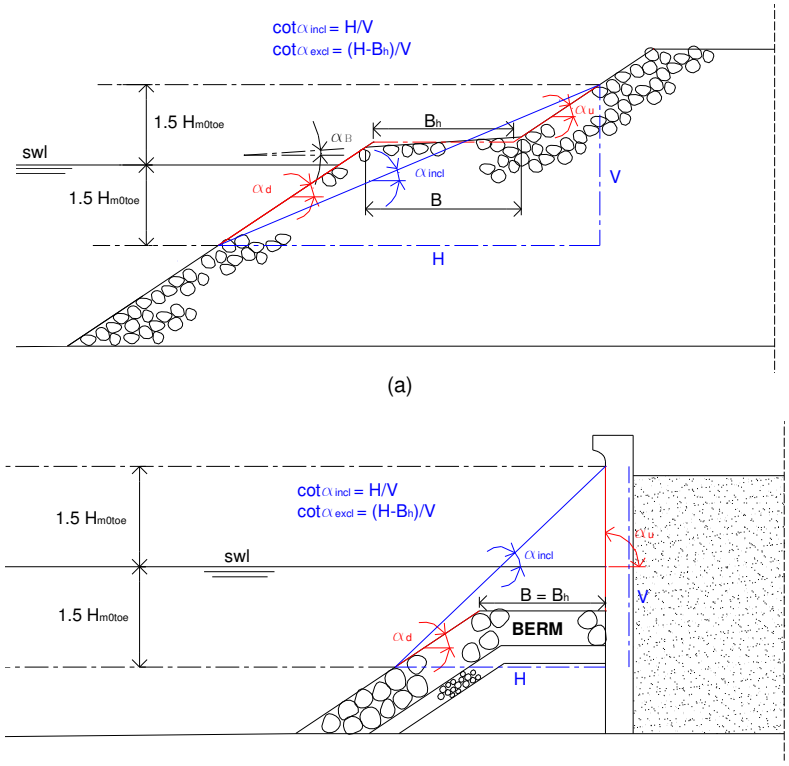

Figuur 7 Bepaling van de hellingsparameters van een structuur

Bij de aanwezigheid van een grote parapet kan de waarde van $\cot\alpha_u$ negatief worden.

Een parapet betreft een zeewaarts overhangend deel van een verticale muur, met als doel de golven terug zeewaarts te 'keren' (zie bijvoorbeeld figuur 8). De precieze invloed van een parapet op golfoverslag is op dit ogenblik (eind 2004 - begin 2005) nog niet gekend, maar onderzoek is wel lopende (Pearson et al., 2004a).

De invloed van een grote parapet (waar 'grote' verwijst naar het feit dat de parapet de volledige structuur domineert) wordt in dit proefschrift meegenomen als een negatieve waarde van $\cot\alpha_u$ (figuur 8). De structuur wordt beschouwd als een 'samengestelde helling' waarbij het overgangspunt tussen de 2 hellingen beschreven wordt door de parameter h_b. De ligging van het overgangspunt wordt eerder arbitrair gekozen, maar wel zodanig dat de 2 hellingen de structuur goed benaderen.

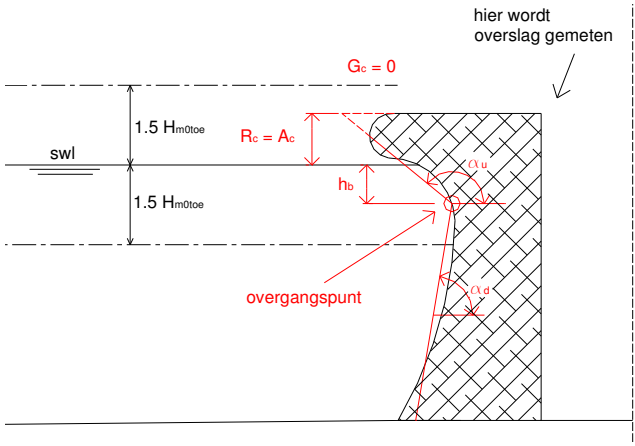

Figuur 8 Schematisatie van een grote parapet

Een 'kleine' parapet, gedefinieerd als een parapet die slechts een klein onderdeel uitmaakt van de gehele structuur, wordt in rekening gebracht via de waarde van γ_f .

De parameter **γ_f [-]** is de laatste structurele parameter en een indicatie voor het gecombineerde effect van ruwheid en doorlatendheid van de structuur. Voor een gladde, ondoorlatende structuur is γ_f = 1. Het reducerende effect van ruwe, doorlatende structuren op golfoverslag (en golfoploop) wordt weergegeven door een waarde van $\gamma_f < 1$.
De introductie van een ruwheidfactor dateert van rond 1950 toen Russisch onderzoek met regelmatige golven werd uitgevoerd naar de invloed van ruwheid op golfoploop. Recentere ruwheidfactoren worden voorgesteld in TAW (2002) en zijn afgeleid uit golfoploopproeven uitgevoerd tussen 1974 en 2002 met onregelmatige golven.
Binnen het CLASH project werden overslagproeven uitgevoerd om het gecombineerde effect van ruwheid en doorlatendheid van stortsteengolfbrekers op golfoverslag te onderzoeken. Gedetailleerde informatie over dit onderzoek is te vinden in Pearson et al., 2004b. Er werden γ_f -waarden bepaald voor stortsteengolfbrekers met verschillende types deklaag, zie tabel 2. Naast deze experimenteel bepaalde waarden werden voor een aantal niet-beproefde secties schattingen gemaakt van de γ_f -waarde, gebaseerd op proeven verzameld in de databank. Ook deze waarden zijn weergegeven in tabel 2. Aangezien niet ondersteund door intensief onderzoek dienen de geschatte waarden als voorlopige waarden beschouwd te worden.

Tabel 2 γ_f -waarden in de databank

Nieuwe, experimenteel bepaalde γ_f -waarden (Pearson et al., 2004b)	
Type deklaag	**γ_f**
Glad, ondoorlatend oppervlak	1.00
Rotsblokken (1 laag, ondoorlatende kern)	0.60
Rotsblokken (1 laag, doorlatende kern)	0.45
Rotsblokken (2 lagen, ondoorlatende kern)	0.55
Rotsblokken (2 lagen, doorlatende kern)	0.40
Kubussen (1 laag, willekeurige plaatsing)	0.50
Kubussen (2 lagen, willekeurige plaatsing)	0.47
Antifers	0.47
HARO's	0.47
Accropodes	0.46
X-blocks	0.45
Core-locs	0.44
Tetrapodes	0.38

Geschatte γ_f -waarden op basis van proeven verzameld in de databank	
Type deklaag	**γ_f**
SHEDS	0.55
Seabeas	0.50
Bermgolfbreker (vervormbaar)	0.40
Dolossen	0.43
Ijslandse bermgolfbreker (niet vervormbaar)	0.35

Het dient vermeld dat structuren met nog andere types deklaag dan hierboven aangehaald in de databank aanwezig zijn. Sommige deklagen bestaan uit zeer specifieke blokken, andere structuren bestaan uit een ondoorlaatbare ondergrond met een energie-dissiperende bovenlaag, vb. een getrapte helling. Daarnaast kunnen ook samengestelde structuren met verschillende types deklaag onderscheiden worden. Telkens werd een welbeschouwde schatting gemaakt van de bijhorende γ_f -waarde.

Zoals hoger vermeld, wordt de invloed van een kleine parapet mee in rekening gebracht in de waarde van de parameter γ_f . De methode hier toegepast is een uitbreiding van de methode voorgesteld in TAW (2003) voor verticale muren, waar een parapet in rekening wordt gebracht als een verhoogde ruwheid van de structuur gevoeld door de golven.
In een eerste fase wordt de waarde van γ_f bepaald enkel op basis van de werkelijke ruwheid en doorlatendheid van de structuur, zoals hierboven uitgelegd. Deze waarde wordt $\gamma_{farmour}$ genoemd. Pas in een tweede fase wordt een eventuele correctie op deze waarde uitgevoerd voor het in rekening brengen van een parapet, zoals weergegeven in volgende vergelijkingen:

Voor een **ruwe** structuur, i.e. $\gamma_{f\ armour} < 0.9$:

$$\begin{array}{l} \text{als } R_c / H_{m0\ toe} \geq 0.5 \quad : \gamma_f = \gamma_{f\ armour} - 0.05 \\ \text{als } R_c / H_{m0\ toe} < 0.5 \quad : \gamma_f = \gamma_{f\ armour} \end{array} \tag{3}$$

Voor een **gladde** structuur, i.e. $\gamma_{f\ armour} \geq 0.9$:

$$\begin{array}{l} \text{als } R_c / H_{m0\ toe} > 1 \quad : \gamma_f = \gamma_{f\ armour} - 0.3 \\ \text{als } R_c / H_{m0\ toe} \leq 0.5 \quad : \gamma_f = \gamma_{f\ armour} \\ \text{als } 0.5 < R_c / H_{m0\ toe} \leq 1 \quad : \text{interpolatie} \end{array} \tag{4}$$

waarbij γ_f verwijst naar de finale waarde van de parameter waarbij een eventuele invloed van een kleine parapet in rekening is gebracht.

Vergelijkingen (3) en (4) tonen aan dat de reductie van $\gamma_{f\ armour}$ afhangt van de waarde van $R_c / H_{m0\ toe}$. Voor lage waarden van $R_c / H_{m0\ toe}$ heeft de parapet geen invloed: de golven lopen gewoon over de structuur. Voor ruwe structuren is de reductie beperkt tot maximaal 0.05, om onrealistisch lage waarden van γ_f te vermijden.

Alle geschatte waarden van γ_f zijn in de databank gemarkeerd in rood. Dit betekent dat enkel de waarden uit de bovenste helft van tabel 2, waarbij geen kleine parapet in rekening gebracht wordt, niet gemarkeerd zijn.

3.5 Bepalen van de algemene parameters

Volgende 3 algemene parameters zijn opgenomen in de databank:

1	Name	Parameter die een unieke naam toekent aan elke proef
2	RF [-]	'Betrouwbaarheidsfactor', geeft een indicatie van de betrouwbaarheid van de proef, kan waarden 1, 2, 3 of 4 aannemen
3	CF [-]	'Complexiteitsfactor', geeft een indicatie van de complexiteit van de sectie, kan waarden 1, 2, 3 of 4 aannemen.

De parameter **Name** betreft een uniek nummer toegekend aan iedere test, bestaande uit 6 getallen, i.e. xxx-xxx. De eerste 3 getallen verwijzen naar een bepaalde proevenreeks, de laatste 3 getallen verwijzen naar de proef binnen de reeks. Vb. 100-001 en 100-002 verwijzen naar proef 1 en proef 2 uit een proevenreeks die het kenmerk '100' kreeg.

De betrouwbaarheidsfactor **RF [-]** en de complexiteitsfactor **CF [-]** geven een indicatie van de betrouwbaarheid van de uitgevoerde proef respectievelijk de complexiteit van de beproefde sectie. Een waarde 1 verwijst naar een zeer betrouwbare proef respectievelijk een eenvoudige sectie. Waarden 2 en 3 zijn gradaties, verwijzend naar minder betrouwbare proeven en meer complexe secties. Een waarde 4 verwijst naar een onbetrouwbare proef respectievelijk een zeer complexe sectie. Deze laatste proeven zullen wegens niet betrouwbaar genoeg buiten beschouwing gelaten worden voor de ontwikkeling van een voorspellingsmethode.
De waarde van de parameter RF toegekend aan een proef hangt af van:

- de precisie door de onderzoeker aan de dag gelegd tijdens het uitvoeren van de metingen en de analyse van de gegevens,
- de beperkingen/mogelijkheden van de testfaciliteit waarin de proeven uitgevoerd werden, en
- de berekeningen en schattingen uitgevoerd om de parameters in de databank te bepalen.

De waarde van de parameter CF toegekend aan een proef hangt enkel af van de mogelijkheid om de sectie nauwkeurigheid te beschrijven aan de hand van de gekozen structurele parameters.

3.6 Opbouw van de databank

De databank is beschikbaar op de bijgevoegde CD-ROM onder de vorm van een rekenblad en bestaat uit 10532 rijen (voor elke proef één rij) en 33 kolommen. Naast de hoger vermelde 31 kolommen waarin de hydraulische, structurele en algemene parameters worden vermeld, bevat de databank 2 extra kolommen.
De eerste extra kolom kreeg de naam ‘Remark’. In deze kolom wordt het afgeraden om bepaalde proeven te gebruiken voor de ontwikkeling van een neurale voorspellingsmethode. De model- en schaaleffecten mogelijks aanwezig in kleinschalige modelproeven zijn hiervoor een van de redenen (zie verder punt 4). Een opmerking wordt gegeven voor prototype proeven, proeven uitgevoerd met artificiële wind in laboratorium en proeven uitgevoerd op een sectie die in realiteit niet voorkomt.
De tweede extra kolom kreeg de naam ‘Reference’ en geeft voor de openbare proeven een referentie die geïnteresseerde onderzoekers toelaat om verdere details over de proeven op te zoeken.

4 Ontwikkeling van een neurale voorspellingsmethode voor golfoverslag

4.1 Neurale netwerken: een inleiding

Wanneer de auteur in dit proefschrift spreekt over neurale netwerken (NNen), doelt de auteur op 'artificiële' neurale netwerken. Artificiële NNen behoren tot het vakgebied van de artificiële intelligentie en kunnen in deze context gedefinieerd worden als systemen die intelligentie simuleren door de structuur van onze hersenen na te bootsen. Figuur 9 geeft een schematische voorstelling van een biologisch neuron: het cellichaam is voorzien van aanhangsels die input ontvangen, 'dendrieten', en 'axons' die via synapsen de output van het neuron naar dendrieten van andere neuronen overdragen.

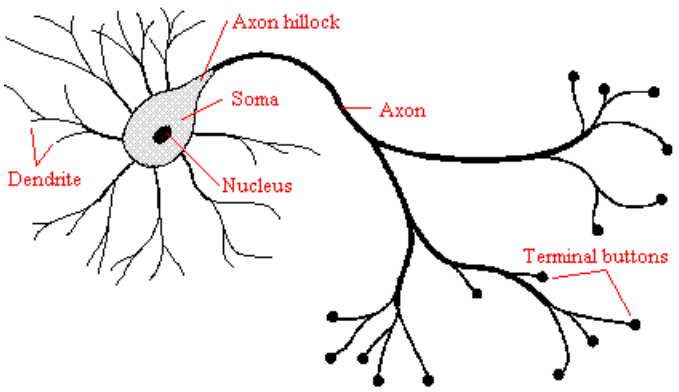

Figuur 9 Schematische voorstelling van een biologisch neuron (uit Jain et al., 1996)

Artificiële NNen zijn gebaseerd op deze biologische neuronen en kunnen getraind worden op gekende input-output patronen. De NNen die in dit proefschrift gebruikt worden zijn 'multilayer perceptrons' (MLP's), opgebouwd uit meerdere input parameters, één verborgen laag en één enkele output parameter (figuur 10). Deze netwerken vallen onder de 'feedforward' modellen, wat impliceert dat de informatie in dergelijke systemen enkel in voorwaartse richting verloopt, i.e. er zijn geen verbindingen die uitwisseling van informatie in achterwaartse richting of binnen een bepaalde laag toelaten.

De output van de weergegeven MLP wordt als volgt berekend:

$$y = \sum_{r=1}^{m} w_r \, f\left(\sum_{j=1}^{n} v_{rj} \, x_j + b_r \right) \tag{5}$$

met input X Є $\Re^n$, output y Є $\Re$, gewichtenmatrices W Є $\Re^{1 \times m}$, V Є $\Re^{m \times n}$ en bias vector β Є $\Re^m$, waarbij n de dimensie van de input ruimte is, m het aantal neuronen in de verborgen laag en $\Re$ de verzameling van de reële getallen.

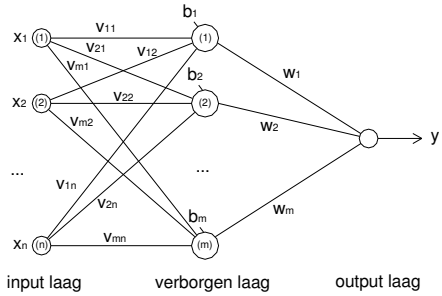

Figuur 10 Multilayer perceptron opgebouwd uit één verborgen laag en één output parameter

Vertrekkend van een bepaalde netwerkconfiguratie, rest nog het bepalen van de onbekende gewichten, w_r en v_{rj} , en de bias-waarden, b_r . Deze parameters worden bepaald tijdens het zogenaamde 'trainingsproces' van het NN. Door verschillende gekende input-output patronen aan het netwerk te presenteren, 'leert' het netwerk de relatie tussen beide.
Er bestaan verschillende algoritmes voor het trainen van NNen. Zonder hier verder in detail op in te gaan, kan vermeld worden dat in dit proefschrift het 'Levenberg-Marquardt' algoritme gebruikt wordt.

Bij het ontwikkelen van een NN wordt de beschikbare dataset vaak opgesplitst in een 'trainingset' en een 'testset', waarbij de trainingset gebruikt wordt om het netwerk te trainen, en de testset om het netwerk te testen. Het is hierbij belangrijk een goed generalisatiegedrag te bekomen. Dit betekent dat de bedoeling van het netwerk is om de onderliggende functie te leren, en niet om de input-output patronen waarop het getraind wordt te memoriseren.
Binnen dit proefschrift wordt 'Bayesiaanse optimalisatie' van de parameters toegepast, wat een goede generalisatie van het netwerk tot gevolg heeft (Foresee en Hagan, 1997).

Om optimaal gebruik te kunnen maken van de beschikbare data (i.e. om het gebruik van een testset te vermijden), kan de 'bootstrap methode' toegepast worden.
De bootstrap methode werd initieel voorgesteld door Efron in 1979, voor het bepalen van de standaard afwijking van een schatter $\hat{\theta}$ die berekend is op basis

van een dataset (Efron, 1982). Bij de bootstrap methode worden subsets van de volledige dataset geanalyseerd waarbij een subset gegenereerd wordt door willekeurig te selecteren *met herplaatsing* uit de volledige dataset. Dit laatste betekent dat op het ogenblik dat een datapunt geselecteerd wordt uit de volledige dataset, het teruggeplaatst wordt voor het selecteren van een volgend datapunt. Theoretisch betekent dit dat een subset van N datapunten, N dezelfde punten kan bevatten. De basisgedachte van de bootstrap methode bestaat erin dat iedere op deze manier gegenereerde subset, een goede weergave is van de volledige dataset en van de volledige inputruimte. De standaardafwijking van de schatter $\hat{\theta}$, bepaald op basis van de volledige dataset, wordt verondersteld gelijk te zijn aan de standaardafwijking van de verschillende waarden voor deze schatter $\hat{\theta}_{(b)}$ bepaald op basis van verschillende bootstrap subsets.

Het trainen van een NN (met een vaste netwerkconfiguratie) met verschillende bootstrap subsets, resulteert in verschillende bootstrap netwerken. Deze kunnen gebruikt worden om een beter finaal model te bekomen, zie vergelijking (6): het finaal model f(.) wordt bepaald als een gemiddelde van alle bootstrap netwerken $f_b(.)$. Met spreekt ook wel van een 'comité van netwerken'.

$$f(x) = \frac{1}{B}\sum_{b=1}^{B} f_b(x) \tag{6}$$

Hierbij verwijst B naar het aantal bootstrap subsets en corresponderende netwerken.

De bootstrap methode laat bovendien toe om een schatting te maken van de betrouwbaarheid van een voorspelling. Efron en Tibshirani (1993) beschrijven hiervoor verschillende methodes. De methode toegepast in dit proefschrift is gebaseerd op percentielen van de distributie van de verschillende bootstrap voorspellingen.
Het 90% percentiel interval voor de voorspelling f(x) wordt bepaald door de op 5% na kleinste voorspelling $f_b(x)$ en de op 5% na grootste voorspelling $f_b(x)$ (met b = 1, …, B).

4.2 Toepassing van neurale netwerken in dit proefschrift

In dit proefschrift worden NNen gebruikt om een voorspellingsmethode te ontwikkelen voor golfoverslag over golfbrekers en zeeweringen. Hoewel de meest logische optie hiervoor één neuraal netwerk is, wordt in dit proefschrift geopteerd voor het gebruik van 2 opeenvolgende neurale netwerken:

- een NN voor de classificatie van overslag, de zogenaamde 'classifier' en

- een tweede NN voor de bepaling van de hoeveelheid overslag, de zogenaamde 'quantifier'.

De classifier klasseert golfoverslag als 'significant' of als 'verwaarloosbaar', i.e. $q > 0$ $m^3/s/m$ of $q = 0$ $m^3/s/m$. Enkel als de classifier overslag $q > 0$ $m^3/s/m$ voorspelt, wordt de quantifier gebruikt om het gemiddelde overslagdebiet q te bepalen. De classifier fungeert bijgevolg als filter voor de quantifier.
Er wordt in dit proefschrift aangetoond dat dit resulteert in een significant beter eindresultaat dan wanneer slechts één enkel netwerk (de quantifier) gebruikt wordt.

In een eerste fase van het ontwikkelen van classifier en quantifier wordt op basis van training- en testsets een optimale netwerkconfiguratie bepaald voor beide netwerken. Daarna wordt de bootstrap methode gebruikt om optimaal gebruik te maken van de beschikbare data voor de ontwikkeling van de finale netwerken.
Voor de quantifier wordt een 'comité van netwerken' voorgesteld als finaal model, waarbij 90% percentiel intervallen beschikbaar zijn voor iedere voorspelling. Voor de classifier wordt de bootstrap methode gebruikt om een optimale beslissingsgrens vast te leggen voor de classificatie van een datapunt (zie verder punt 4.6).

4.3 Parameters in het finaal overslagmodel

Slechts een deel van de parameters opgenomen in de CLASH databank worden gebruikt voor de ontwikkeling van de neurale voorspellingsmethode. Tabel 3 geeft een overzicht van de parameters gebruikt in de finale classifier en quantifier, samen met hun functie in de modellen.

Voor zowel classifier als quantifier worden dezelfde **input parameters** gebruikt. De geselecteerde input parameters geven een beknopt maar volledig overzicht van een overslagproef. Het dient opgemerkt dat enkel de golfparameters aan de teen van de constructie gebruikt worden. In eerste instantie werd ook de parameter $H_{m0\ deep}$ meegenomen als input parameter, doch onderzoek wees uit dat deze parameter geen significante bijdrage leverde in de voorspellingsmethode.

In een eerste fase wordt de quantifier ontwikkeld. Hiervoor wordt de **output parameter** q omgevormd naar zijn logaritme, i.e. log(q). Het trainen van de quantifier op log(q) in plaats van op q levert betere voorspellingen op voor waarden van $q < 10^{-2}$ $m^3/s/m$, maar heeft ook tot gevolg dat de quantifier niet kan getraind worden op waarden $q = 0$ $m^3/s/m$. Ook het voorspellen van waarden $q = 0$ $m^3/s/m$ door de quantifier is niet mogelijk. Verder zal bovendien worden aangetoond dat de quantifier niet in staat blijkt kleine overslagwaarden te voorspellen voor

nulmetingen, wat de directe aanleiding is voor het ontwikkelen van een classifier als filter voor de quantifier.
De output parameter q wordt voor de ontwikkeling van de classifier vervangen door 2 discrete waarden, i.e. +1 en -1, verwijzend naar een situatie waar significante respectievelijk verwaarloosbare of geen overslag optreedt.

Tabel 3 Parameters uit de CLASH databank gebruikt in de finale neurale voorspellingsmethode

Aard		Parameter	Functie
hydraulisch	1	$H_{m0\ toe}$ [m]	input
	2	$T_{m\ -1,0\ toe}$ [s]	input
	3	β [°]	input
	4	q [m^3/s/m]	output
structureel	1	h [m]	input
	2	h_t [m]	input
	3	B_t [m]	input
	4	γ_f [-]	input
	5	$\cot\alpha_d$ [-]	input
	6	$\cot\alpha_u$ [-]	input
	7	R_c [m]	input
	8	h_b [m]	input
	9	B_h [m]	input
	10	A_c [m]	input
	11	G_c [m]	input
algemeen	1	RF [-]	gewichtsfactor
	2	CF [-]	gewichtsfactor

De factoren RF en CF worden voor de ontwikkeling van beide NNen samengevoegd tot een **gewichtsfactor**, die een indicatie geeft van de algemene betrouwbaarheid van een proef. In overeenstemming met Pozueta et al. (2004b) wordt de gewichtsfactor gedefinieerd als:

$$\text{gewichtsfactor} = (4 - RF) * (4 - CF) \quad (7)$$

De waarde van de gewichtsfactor is gelinkt aan het aantal keer dat eenzelfde proef gebruikt wordt als input tijdens het trainen en het testen van de netwerken. Hoe meer een proef gebruikt wordt als input, hoe meer de netwerken focussen op deze input. Dit impliceert dat de netwerken gedwongen worden om meer aandacht te besteden aan de meest betrouwbare proeven.
Zowel RF als CF kunnen waarden aannemen van 1 tot 4 wat betekent dat de meest betrouwbare proeven tot 9 keer als input gebruikt worden. Daartegenover staat dat onbetrouwbare proeven (RF of CF = 4, dus gewichtsfactor = 0) helemaal niet gebruikt worden voor het ontwikkelen van de NNen.

4.4 Model- en schaaleffecten

De CLASH databank is samengesteld uit proeven op zeer uiteenlopende schaal, variërend van prototype metingen tot kleinschalige proeven. Om onderlinge vergelijking van de proeven mogelijk te maken, worden alle proeven verschaald volgens de in coastal engineering wijdverbreide Froude modelwet, waarbij de parameter $H_{m0\ toe}$ als lengteschaal N_L gekozen wordt. Alle input parameters en voor de quantifier ook de output parameter worden verschaald, i.e. $R_c \rightarrow R_c / H_{m0\ toe}$; $T_{m-1,0\ toe} \rightarrow T_{m-1,0\ toe} / (H_{m0\ toe})^{0.5}$; $q \rightarrow q / (H_{m0\ toe})^{1.5}$ etc.

Dit stemt overeen met het verschalen van alle proeven naar een fictieve situatie waar een golfhoogte $H_{m0\ toe}$ = 1m optreedt. Bijgevolg verdwijnt één input parameter, i.e. $H_{m0\ toe}$, uit de inputruimte van de netwerken.

De verschaalde parameterwaarden worden verder in de tekst aangeduid met een 's' in superscript voor de parameter, i.e. $R_c / H_{m0\ toe} = {}^{s}R_c$; $T_{m-1,0\ toe} / (H_{m0\ toe})^{0.5} = {}^{s}T_{m-,0\ toe}$; $q / (H_{m0\ toe})^{1.5} = {}^{s}q$ etc.

Voor de parameters γ_f, $\cot\alpha_u$, $\cot\alpha_d$ en β is de waarde voor en na verschaling naar de situatie $H_{m0\ toe}$ = 1m gelijk, i.e. ${}^{s}\gamma_f = \gamma_f$, ${}^{s}\cot\alpha_u = \cot\alpha_u$, ${}^{s}\cot\alpha_d = \cot\alpha_d$ en ${}^{s}\beta = \beta$.

Het vermoeden dat model- en schaaleffecten kleinschalige overslagmetingen beïnvloeden onder specifieke omstandigheden (De Rouck et al., 2001), werd bevestigd door het CLASH onderzoek gevoerd naar dit onderwerp (Kortenhaus et al., 2005). Dit onderzoek resulteerde in een CLASH schaalprocedure, met als belangrijkste onderdeel een 'schaalmap' die model- en schaaleffecten identificeert en correctiefactoren voorstelt om overeenkomstige prototype overslagdebieten te berekenen.

De CLASH schaalprocedure dient toegepast op overslagresultaten afkomstig van kleinschalige modelproeven *die opgeschaald zijn tot prototype resultaten volgens Froude*. Dergelijke resultaten worden in onderhavige tekst q_{ss} genoemd.

Kleinschalige proeven worden in deze context gedefinieerd als modelproeven met een gemeten golfhoogte $H_{m0\ toe}$ *kleiner dan 0.5m*. Dit betekent ook dat de schaalprocedure enkel mag toegepast worden als *de overeenkomstige golfhoogte $H_{m0\ toe}$ in de schaal waar het finaal overslagdebiet vereist is, groter is dan 0.5m*. Voor alle andere gevallen dient geen correctie toegepast.

In figuur 11 is de CLASH schaalmap weergegeven. Ruwe hellende structuren worden onderscheiden van andere structuren. De schaalmap geeft 3 mogelijke resultaten:

- q_{scale_wind}: relevant voor ruwe hellende structuren, houdt rekening met mogelijke schaaleffecten en met het modeleffect wind
- q_{scale_nowind}: relevant voor ruwe hellende structuren, houdt enkel rekening met mogelijke schaaleffecten
- q_{wind}: relevant voor verticale structuren en gladde (hellende) structuren, houdt rekening met het modeleffect wind

De in figuur 11 weergegeven correctiefactoren f_{wind} , f_{scale_nowind} en f_{scale_wind} worden gedefinieerd in tabel 4.

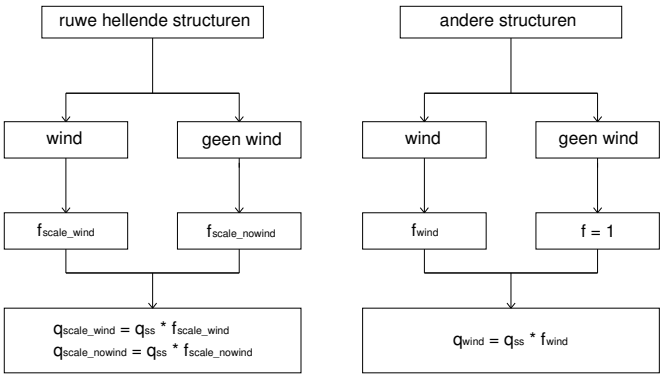

Figuur 11 CLASH schaalmap

Tabel 4 CLASH correctiefactoren

Waarde van q_{ss}	**f_{wind}**	**f_{scale_nowind}**	**f_{scale_wind}**
$q_{ss} < 1.10^{-5}$ m^3/s/m	4	16	24
1.10^{-5} m^3/s/m ≤ q_{ss} ≤ 1.10^{-2} m^3/s/m	$1+3.\left(\frac{-\log q_{ss}-2}{3}\right)^3$	$1+15.\left(\frac{-\log q_{ss}-2}{3}\right)^3$	$1+23.\left(\frac{-\log q_{ss}-2}{3}\right)^3$
$q_{ss} > 1.10^{-2}$ m^3/s/m	1	1	1

De CLASH schaalmap kan niet toegepast worden als de gemeten overslag in het laboratorium q = 0 m^3/s/m. In Kortenhaus et al. (2005) wordt een methode beschreven om kleine overslagdebieten te schatten voor dergelijke nulmetingen, waarop de schaalmap wel kan toegepast worden. De basisgedachte is hier dat de nulwaarde tijdens de kleinschalige overslagproef het gevolg is van het niet meer meetbaar zijn van de zeer kleine overslaghoeveelheid in het laboratorium.
De methode vertrekt van beschikbare niet-nulmetingen van eenzelfde proevenreeks (i.e. dezelfde beproefde sectie) met gelijkaardige golfkarakteristieken. De dimensieloze overslagdebieten $\frac{q}{\sqrt{gH_{m0\ toe}^3}}$ worden uitgezet versus de dimensieloze kruinhoogtes $R_c / H_{m0\ toe}$ (of $A_c / H_{m0\ toe}$, afhankelijk van de beschouwde sectie). Vervolgens wordt door deze niet-nulwaarden een empirische formule gefit.

Vertrekkend van de beschikbare $R_c/H_{m0\ toe}$ -waarde (of $A_c/H_{m0\ toe}$ -waarde) van de nulmeting, wordt de empirisch voorspelde waarde $\frac{q_{est}}{\sqrt{gH_{m0\ toe}^3}}$ afgelezen. De kleinschalige niet-nulschatting q_{est} wordt vervolgens omgerekend naar grote schaal, waarna de CLASH schaalmap kan toegepast worden.

Aangezien de meerderheid van de proeven in de databank kleinschalige proeven betreft, wordt een neurale kleinschalige voorspellingsmethode ontwikkeld, i.e. overslag wordt voorspeld op kleine schaal met de neurale voorspellingsmethode. Om verwarring van de classifier en quantifier te vermijden, dienen proeven die op kleine schaal een ander resultaat zouden geven ten gevolge van model- en/of schaaleffecten, uitgesloten te worden voor de ontwikkeling van de NNen. Studie van de data in de databank leert dat enkel de prototype metingen dienen worden uitgesloten.
Daarnaast worden ook kleinschalige proeven met artificiële windgeneratie verwijderd voor de ontwikkeling van de NNen, aangezien wind niet in rekening gebracht wordt als input.
Concreet betekent dit dat het aantal beschikbare data voor de ontwikkeling van de NNen gereduceerd wordt van 10532 tot 9071, waarvan 8195 data met $q \neq 0$ m^3/s/m en 876 data met $q = 0$ m^3/s/m. Hierbij zijn ook de proeven met RF of CF = 4 (dus gewichtsfactor = 0) in mindering gebracht.

4.5 Ontwikkeling van een neurale quantifier voor $q \neq 0$ m^3/s/m

4.5.1 Finale quantifier ontwikkeld met de bootstrap methode

De quantifier wordt getraind op de niet-nuldata aanwezig in de databank. Het betreft hier in totaal 8195 betrouwbare overslagproeven (i.e. RF en CF ≠ 0) wat overeenkomt met 46328 'gewogen' proeven, i.e. het aantal proeven dat bekomen wordt wanneer elke proef vermenigvuldigd wordt met zijn gewichtsfactor.

De optimale netwerkconfiguratie wordt bepaald door het trainen en testen van de quantifier met een (gewogen) trainingset respectievelijk (gewogen) testset. Het gedrag van een netwerk wordt beoordeeld op basis van de vierkantswortel uit de gemiddelde kwadratische afwijking bekomen voor de testset (de 'rms-error' of 'rmse' van de testset), als volgt gedefinieerd:

$$rmse\_test = \sqrt{\frac{1}{N_{test}} \sum_{n=1}^{N_{test}} \left[log(^s q_{measured})_n - log(^s q_{NN})_n \right]^2} \qquad (8)$$

waarbij N_{test} het aantal (gewogen) testdata is, $\log({}^{s}q_{measured})$ de logaritme van de gewenste output en $\log({}^{s}q_{NN})$ de logaritme van de output voorspeld door het netwerk. ${}^{s}q_{measured}$ en ${}^{s}q_{NN}$ zijn weergegeven in $m^3/s/m$.
Hoe lager de waarde van rmse_test, hoe beter het netwerk.

De optimale configuratie van de quantifier is weergegeven in figuur 12. Het netwerk bestaat uit 13 verschaalde input parameters, één verborgen laag met 25 verborgen neuronen en één output parameter, i.e. de logaritme van het verschaalde overslagdebiet, $\log({}^{s}q)$.

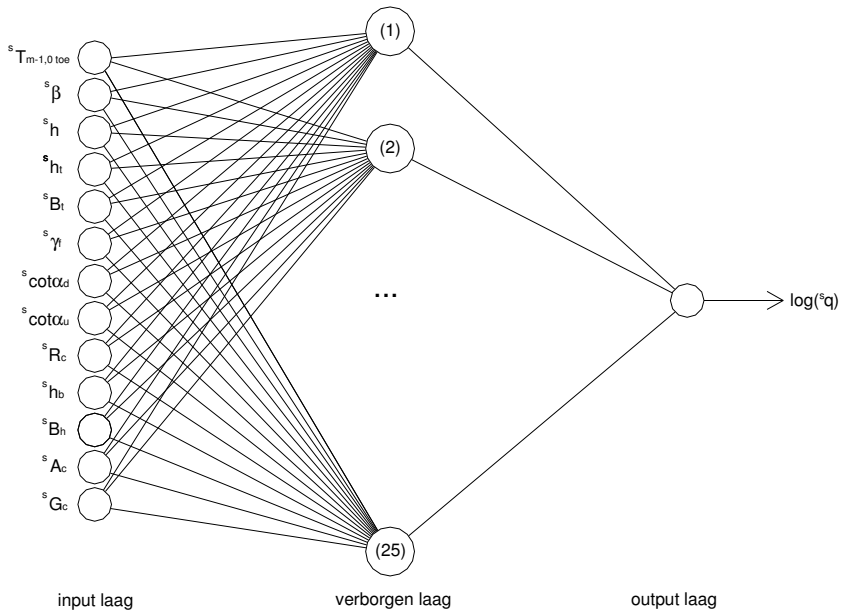

Figuur 12 Geoptimaliseerde netwerkconfiguratie van de quantifier

De finale quantifier wordt vervolgens ontwikkeld met behulp van de bootstrap methode. Hiertoe worden 100 bootstrap netwerken getraind op basis van 100 bootstrap subsets. Elke subset bevat evenveel data als de originele, gewogen dataset (i.e. 46328 data), en wordt gesampled *met herplaatsing* uit de originele, gewogen dataset.
De finale quantifier bestaat uit het comité van 100 netwerken: een voorspelling met de finale quantifier wordt bepaald als de gemiddelde waarde van 100 voorspellingen, bekomen met de 100 bootstrap netwerken. Daarnaast wordt voor iedere voorspelling het 90% percentiel interval gegeven, berekend op basis van de distributie van de bootstrap voorspellingen (zie punt 4.1).

De voorspellingen voor de originele dataset door de finale quantifier zijn grafisch weergegeven in figuur 13. De voorspelde waarden ${}^{s}q_{NN}$ zijn uitgezet versus de gemeten waarden ${}^{s}q_{measured}$. De gewogen rms-error is 0.3100.

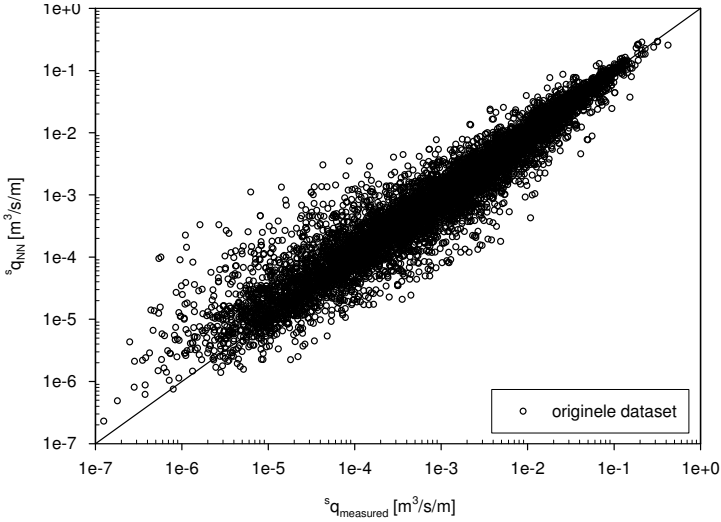

Figuur 13 Voorspelling door het comité van netwerken voor de originele dataset (8195 data)

Het gedrag van de finale quantifier voor de originele dataset kan ook beschreven worden aan de hand van de maximale foutfactoren bekomen voor deze dataset (waarbij een klein percentage uitschieters buiten beschouwing wordt gelaten). De foutfactor voor overpredictie (${}^{s}q_{NN} > {}^{s}q_{measured}$) wordt hier gedefinieerd als ${}^{s}q_{NN} / {}^{s}q_{measured}$ terwijl de foutfactor voor onderpredictie (${}^{s}q_{NN} < {}^{s}q_{measured}$) wordt gedefinieerd als ${}^{s}q_{measured} / {}^{s}q_{NN}$.
Tabel 5 toont de maximale foutfactoren voor de originele dataset, variërend naargelang het percentage uitschieters dat buiten beschouwing gelaten wordt. Bij het beschouwen van (100-x)% van de dataset, worden de 0.5*x% grootste factoren voor overpredictie en de 0.5*x% grootste factoren voor onderpredictie niet beschouwd.

Tabel 5 Maximale foutfactoren voor de originele dataset (gewogen waarden)

% van de dataset beschouwd	(100%)	99%	95%	90%
maximale foutfactor voor overpredictie	(203.55)	31.35	**5.35**	3.34
maximale foutfactor voor onderpredictie	(27.48)	10.21	**3.62**	2.78

De maximale foutfactoren overeenkomend met de volledige dataset staan tussen haakjes aangezien deze niet representatief zijn voor het gedrag van de quantifier. De waarden overeenkomend met 95% staan in vet en kunnen als goede maat voor het gedrag van de quantifier aanvaard worden.

4.5.2 Toepassingsdomein van de quantifier

Een NN is enkel in staat betrouwbare voorspellingen te maken binnen het domein van de data waarop het getraind werd. Om extrapolatie van het netwerk te vermijden, is het zeer belangrijk grenzen van toepasbaarheid op te stellen voor de quantifier.
Aangezien de inputruimte van de quantifier een 13-dimensionale ruimte betreft, dient nieuwe input voor de quantifier in deze 13-dimensionale ruimte binnen de wolk van data waarop het netwerk getraind werd te liggen. Aan de hand van een matrixplot (zie annex) krijgt men een idee van de ligging van de trainingsdata in de 13-dimensionale ruimte. In dergelijke plot worden alle parameters tegenover elkaar uitgezet, hier resulterend in 13x13 figuren. Op de diagonaal zijn de histogrammen van de individuele parameters weergegeven.

Studie van elk van de input parameters individueel, en studie van hun gecombineerd voorkomen aan de hand van de matrixplot, resulteert in grenzen van toepasbaarheid voor iedere input parameter (zie tabel 6). Er wordt onderscheid gemaakt tussen waarden van $\gamma_f = 1$ en $\gamma_f < 1$, aangezien studie van de matrixplot uitwijst dat vaak andere parameterlimieten optreden voor deze onderscheiden waarden van γ_f (wat kan verklaard worden door de verschillende types structuren).

Tabel 6 Grenzen van toepasbaarheid voor de quantifier

		$\gamma_f = 1$			$\gamma_f < 1$	
1	3.00	$\leq {}^{s}T_{m\text{-}1,0\ toe}$ [s] $\leq$	22.00	3.00	$\leq {}^{s}T_{m\text{-}1,0\ toe}$ [s] $\leq$	12.00
2	0	$\leq {}^{s}\beta$ [°] $\leq$	60.00	0	$\leq {}^{s}\beta$ [°] $\leq$	60.00
3	1.00	$\leq {}^{s}h$ [m] $\leq$	20.60	1.00	$\leq {}^{s}h$ [m] $\leq$	13.30
4	1.00	$\leq {}^{s}h_t$ [m] $\leq$	20.50	0.65	$\leq {}^{s}h_t$ [m] $\leq$	13.30
5	0	$\leq {}^{s}B_t$ [m] $\leq$	11.40	0	$\leq {}^{s}B_t$ [m] $\leq$	5.00
6	1.00	$\leq {}^{s}\gamma_f$ [-] $\leq$	1.00	0.35	$\leq {}^{s}\gamma_f$ [-] $\leq$	0.95
7	0	$\leq {}^{s}\cot\alpha_d$ [-] $\leq$	7.00	0	$\leq {}^{s}\cot\alpha_d$ [-] $\leq$	5.30
8	-5.00	$\leq {}^{s}\cot\alpha_u$ [-] $\leq$	6.00	0	$\leq {}^{s}\cot\alpha_u$ [-] $\leq$	8.00
9	0	$\leq {}^{s}R_c$ [m] $\leq$	5.00	0.25	$\leq {}^{s}R_c$ [m] $\leq$	2.80
10	-1.00	$\leq {}^{s}h_b$ [m] $\leq$	3.60	-1.00	$\leq {}^{s}h_b$ [m] $\leq$	1.20
11	0	$\leq {}^{s}B_h$ [m] $\leq$	16.20	0	$\leq {}^{s}B_h$ [m] $\leq$	6.20
12	0	$\leq {}^{s}A_c$ [m] $\leq$	4.00	0.10	$\leq {}^{s}A_c$ [m] $\leq$	2.90
13	0	$\leq {}^{s}G_c$ [m] $\leq$	7.60	0	$\leq {}^{s}G_c$ [m] $\leq$	5.40

Voor simulaties met de quantifier is het vereist dat elke input parameter gesitueerd is binnen de vooropgestelde grenzen.

4.5.3 Simulaties met de quantifier

Om het gedrag van de ontwikkelde quantifier te bestuderen, worden verschillende simulaties uitgevoerd. Hier worden enkel de resultaten voor de nulmetingen besproken. In punt 4.6 bij de resultaten van de combinatie classifier-quantifier zijn meer resultaten weergegeven.

Van de 876 nulmetingen die niet konden gebruikt worden voor het trainen van de quantifier, worden er 657 als betrouwbaar bestempeld (zie verder punt 4.6.1). Van deze 657 metingen vallen er 309 buiten het toepassingsdomein van de quantifier. De quantifier mag bijgevolg niet gebruikt worden om voor deze data een voorspelling te maken.

In figuur 14 is de quantifier simulatie ${}^{s}q_{NN}$ voor de resterende 348 nuldata weergegeven. Voor elke voorspelling is ook het 90% percentiel interval gegeven. De voorspellingen zijn gesorteerd van groot naar klein.

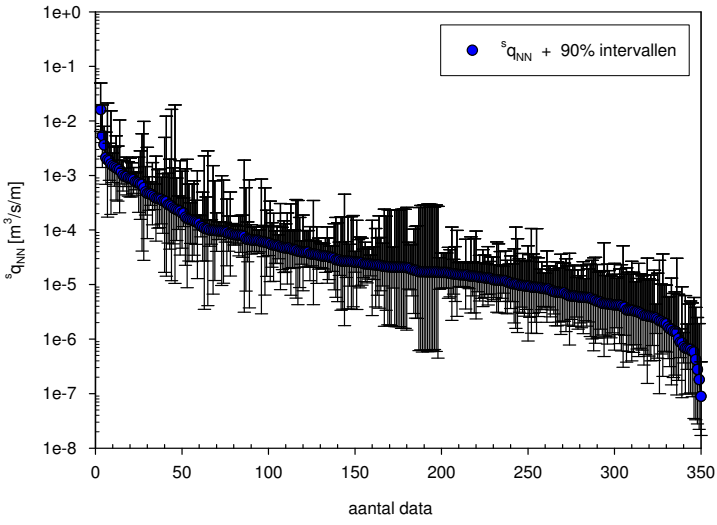

Figuur 14 Quantifier simulatie van 348 nulmetingen

Hoewel een groot deel van de nulmetingen buiten het toepassingsdomein van de quantifier valt, toont figuur 14 dat voor de meerderheid van de gesimuleerde nulmetingen grote waarden van ${}^{s}q_{NN}$ bekomen worden. De betrouwbaarheids-intervallen zijn veelal eerder smal, wat resulteert in een valse impressie van een goede voorspelling.

Hieruit volgt dat de quantifier niet in staat is om te generaliseren voor overslagdebieten q = 0 m^3/s/m, wat de directe aanleiding was voor het ontwikkelen van de classifier als filter voor de quantifier.

4.6 Ontwikkeling van een neurale classifier voor q

4.6.1 Finale classifier ontwikkeld met de bootstrap methode

De classifier wordt slechts getraind op 2 mogelijke output waarden, i.e. +1 voor significante overslag en -1 voor geen of verwaarloosbare overslag.
Zorgvuldig screenen van de 876 beschikbare nuldata (4535 gewogen data) leidt tot een selectie van 657 'betrouwbare' nuldata (3521 gewogen data). Hierbij verwijst 'betrouwbaar' voornamelijk naar een goede meetnauwkeurigheid in het laboratorium. Daarnaast wordt gemeten overslag $^{s}q < 10^{-6}$ m^3/s/m beschouwd als verwaarloosbare overslag, wat resulteert in 41 extra data (189 gewogen data) voor klasse -1. In totaal zijn dus 657 + 41 = 698 data (3521 + 189 = 3710 gewogen data) beschikbaar voor klasse -1, versus 8195 - 41 = 8154 data (46328 - 189 = 46139 gewogen data) voor klasse +1.

Om te vermijden dat een classifier bekomen wordt die a priori significante overslag voorspelt, worden voor het trainen van de classifier bij voorkeur slechts evenveel niet-nuldata als nuldata gebruikt. Aangezien slechts 698 nuldata beschikbaar zijn, betekent dit een selectie van 698 niet-nuldata uit de 8154 beschikbare data voor klasse +1, en dus onvermijdelijk een groot verlies aan informatie.

Er kunnen twee redenen aangehaald worden waarom het aantal nuldata zoveel kleiner is dan het aantal niet-nuldata in de databank.
Een eerste reden betreft de interesse van onderzoekers, die voornamelijk uitgaat naar niet-nuldata. Dikwijls is het zelfs zo dat onderzoekers nulmetingen niet rapporteren.
Een tweede reden is dat bij parametrische testen, die vaak uitgevoerd worden in laboratoria, de proeven stopgezet worden van zodra een nul gemeten wordt. Het meest frequent zijn overslagproeven op een vaste structuur met een dalende waterstand, wat resulteert in stijgende waarden van R_c /$H_{m0\ toe}$ (voor vaste golfparameters). Van zodra geen overslag meer gemeten wordt, worden de proeven stopgezet aangezien de onderzoeker weet dat voor nog lagere waterstanden automatisch ook geen overslag gemeten zal worden. Een andere mogelijkheid zijn proeven waarbij de beproefde sectie zelf aangepast wordt, zoals bijvoorbeeld proeven met toenemende kruinbreedte G_c . Ook hier worden de metingen vaak stopgezet zodra een nul gemeten wordt.
Het gevolg van deze parametrische testen is niet alleen een klein aantal nuldata in de databank, maar bovendien een slechte verdeling van de nuldata in de volledige

nulruimte: de nuldata hebben voornamelijk betrekking op de grens geen overslag - wel overslag.

Om dit probleem op te lossen, worden uit de bestaande nuldata twee sets artificiële nuldata gegenereerd, waarbij de nulruimte in twee richtingen uitgebreid wordt:

- artificiële nuldata met hogere waarden van ${}^{s}R_c$ worden gegenereerd
- artificiële nuldata met hogere waarden van ${}^{s}G_c$ worden gegenereerd

Men kan nog andere artificiële nuldata bedenken, doch bovenstaande data worden beschouwd als meest relevant, waarbij de nadruk gelegd wordt op de eerste set van artificiële data.

De eerste set artificiële data wordt gegenereerd door de input parameters van de beschikbare nuldata over te nemen, behalve de waarde van ${}^{s}R_c$, die verhoogd wordt met een factor (1+x). Om realistische artificiële secties te bekomen dient de parameter ${}^{s}A_c$ mee verhoogd te worden, i.e. met een factor [1+x* (${}^{s}R_c$ / ${}^{s}A_c$)]. Op deze manier wordt de kruinconfiguratie van de structuur behouden (figuur 15).
Verschillende combinaties van x -waarden worden geprobeerd, waarbij uiteindelijk waarden van x = 0.1, 0.2, 0.3 en 0.5 worden weerhouden. Dit betekent dat voor iedere nulmeting 4 extra artificiële nuldata bekomen worden.

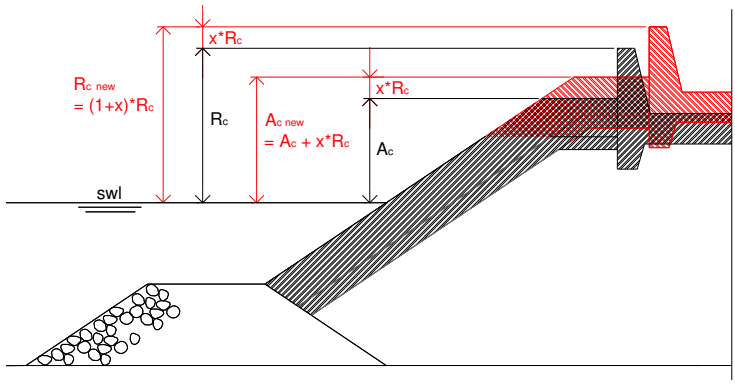

Figuur 15 Generatie van artificiële data door het verhogen van R_c (en A_c)

De tweede set artificiële data wordt gegenereerd door opnieuw de input parameters van de originele nuldata over te nemen, maar nu enkel de waarde van ${}^{s}G_c$ te verhogen met een factor (1+y). Alle andere input parameters blijven hier behouden. Uiteindelijk worden waarden van y = 0.2 en 0.5 weerhouden, wat 2 extra artificiële nuldata betekent per nulmeting. Er worden bewust minder artificiële

data gegenereerd vertrekkend van ${}^{s}G_c$, aangezien dergelijke parameterproeven minder voorkomen. Nuldata met ${}^{s}G_c$ = 0m worden niet gebruikt voor de generatie van artificiële data aangezien deze sowieso tot onrealistische secties leiden.

Het resultaat van het genereren van artificiële nuldata is een duidelijk toegenomen aantal beschikbare data in klasse -1: 4206 in plaats van de oorspronkelijke 698 (22550 gewogen nuldata in plaats van 3710 gewogen nuldata), met bovendien een betere spreiding in de nulruimte. Daarnaast kan voor de training van de classifier ook een groter aantal van de beschikbare niet-nuldata gebruikt worden.

De optimale netwerkconfiguratie wordt zoals voor de quantifier bepaald door het trainen en testen van de classifier met een (gewogen) trainingset respectievelijk (gewogen) testset. Het gedrag van een netwerk wordt opnieuw beoordeeld op basis van vergelijking (8) waarbij de waarden van $\log({}^{s}q)$ vervangen worden door de waarden +1 of -1. Vergelijking (8) kan bijgevolg gereduceerd worden tot:

$$(rmse\_test)^2 * 25 = perc\_wrong\_test \qquad (9)$$

waarbij perc_wrong_test het percentage verkeerd geklasseerde testdata betreft.

De uiteindelijke netwerkconfiguratie van de classifier is vergelijkbaar met de configuratie weergegeven in figuur 12. Dezelfde 13 verschaalde input parameters worden gebruikt, doch het aantal verborgen neuronen is slechts 20 en de output wordt vervangen door de waarde +1 of -1, afhankelijk van de klasse.

De finale classifier wordt ontwikkeld met behulp van de bootstrap methode. Hiertoe worden 61 bootstrap netwerken getraind op basis van 61 bootstrap subsets die als volgt bepaald worden:

- 22550 data worden gesampled *met herplaatsing* uit de 22550 gewogen data uit klasse -1,
- een even groot aantal, i.e. 22550 data, worden gesampled *met herplaatsing* uit de 46139 gewogen data uit klasse +1,
- beide samples worden samengevoegd tot één bootstrap subset met 2*22550 = 45100 data

De 61 bootstrap netwerken worden gebruikt om een optimale beslissinggrens te bepalen voor het uiteindelijk toekennen van een voorspelling aan klasse +1 of -1. De basisgedachte hier is dat het gevaarlijker is vanuit ontwerpstandpunt een niet-nulmeting als verwaarloosbare overslag te klasseren dan een nulmeting als significante overslag te klasseren.
De beslissinggrens wordt uiteindelijk bepaald als volgt: een voorspelling wordt toegekend aan klasse +1 van zodra er meer dan 5 van de 61 bootstrap netwerken

klasse +1 voorspellen. Met dit beslissingscriterium wordt 3.09% van de gewogen originele dataset fout geklasseerd, waaronder 19.29% van de 3710 nuldata en 1.80% van de 46139 niet-nuldata.

Ten gevolge van het strenge beslissingscriterium voor klasse -1 (i.e. een punt wordt slechts toegekend aan klasse -1 op het ogenblik dat er 56 of meer bootstrap netwerken klasse -1 voorspellen) is de classifier geneigd in het overgangsgebied van significante naar verwaarloosbare overslag niet-nul te voorspellen, wat resulteert in een 'veilige' voorspelling.

4.6.2 Toepassingsdomein van de classifier

Analoog als voor de quantifier worden ook voor de classifier strikte grenzen van toepasbaarheid opgesteld, zie tabel 7. Aangezien de classifier getraind is op basis van alle niet-nuldata + extra nuldata, zijn de grenzen gelijk aan of uitgestrekter dan deze van de quantifier.

Tabel 7 Grenzen van toepasbaarheid voor de classifier

		$\gamma_f = 1$			$\gamma_f < 1$	
1	3.00	$\leq {}^sT_{m-1,0\ toe}$ [s] $\leq$	22.00	3.00	$\leq {}^sT_{m-1,0\ toe}$ [s] $\leq$	12.00
2	0	$\leq {}^s\beta$ [°] $\leq$	60.00	0	$\leq {}^s\beta$ [°] $\leq$	60.00
3	1.00	$\leq {}^sh$ [m] $\leq$	20.60	1.00	$\leq {}^sh$ [m] $\leq$	13.30
4	1.00	$\leq {}^sh_t$ [m] $\leq$	20.50	0.65	$\leq {}^sh_t$ [m] $\leq$	13.30
5	0	$\leq {}^sB_t$ [m] $\leq$	11.40	0	$\leq {}^sB_t$ [m] $\leq$	5.00
6	1.00	$\leq {}^s\gamma_f$ [-] $\leq$	1.00	0.35	$\leq {}^s\gamma_f$ [-] $\leq$	0.95
7	0	$\leq {}^s\cot\alpha_d$ [-] $\leq$	7.00	0	$\leq {}^s\cot\alpha_d$ [-] $\leq$	5.30
8	-5.00	$\leq {}^s\cot\alpha_u$ [-] $\leq$	6.00	0	$\leq {}^s\cot\alpha_u$ [-] $\leq$	8.00
9	0	$\leq {}^sR_c$ [m] $\leq$	7.50	0.25	$\leq {}^sR_c$ [m] $\leq$	4.20
10	-1.00	$\leq {}^sh_b$ [m] $\leq$	3.60	-1.00	$\leq {}^sh_b$ [m] $\leq$	1.20
11	0	$\leq {}^sB_h$ [m] $\leq$	16.20	0	$\leq {}^sB_h$ [m] $\leq$	6.20
12	0	$\leq {}^sA_c$ [m] $\leq$	6.00	0.10	$\leq {}^sA_c$ [m] $\leq$	4.35
13	0	$\leq {}^sG_c$ [m] $\leq$	11.40	0	$\leq {}^sG_c$ [m] $\leq$	8.10

4.6.3 Simulaties met de classifier als filter voor de quantifier

Het finaal voorspellingsmodel bestaat uit de combinatie classifier-quantifier en kan getest worden aan de hand van een aantal proevenreeksen.

Enerzijds zijn de CLASH prototype metingen beschikbaar. Simulatie van de prototype situaties, gecorrigeerd voor mogelijke model- en schaaleffecten volgens de CLASH schaalprocedure, resulteert in schattingen die kunnen vergeleken worden met de beschikbare metingen. Hier wordt het resultaat beschreven dat bekomen wordt voor de Ostia meetsite.

Anderzijds kunnen kunstmatige proevenreeksen gegenereerd worden voor situaties waarvan het overslagresultaat beschreven wordt door empirische formules. Vergelijking met deze formules geeft een idee van het gedrag van het opgestelde voorspellingsmodel. Hier wordt overslag over een stortsteengolfbreker beschreven.

De Ostia meetsite is gesitueerd te Ostia, bij Rome (Italië). De structuur bestaat uit een stortsteengolfbreker met rotsblokken als deklaagelementen. In totaal zijn 77 prototype overslagmetingen beschikbaar, gemeten tijdens 7 stormen (2003-2004). Gedetailleerde informatie over de Ostia prototype metingen is te vinden in Franco et al., 2004.
De verschaalde input parameters van de metingen vallen alle binnen de grenzen van toepasbaarheid opgesteld in tabellen 6 en 7, wat betekent dat alle metingen kunnen gesimuleerd worden.
In een eerste fase worden de data door de classifier geklasseerd. De classifier klasseert 69 van de 77 data als significante overslag. Voor deze data wordt met de quantifier een gemiddeld overslagdebiet bepaald.
De overblijvende 8 data worden door de classifier geklasseerd als verwaarloosbare overslag. Er wordt aangenomen dat de verwachte model- en schaaleffecten aan de basis liggen van deze nul-classificatie en bijgevolg kan de CLASH schaalprocedure gebruikt worden om voor deze data een kleine overslagwaarde te schatten (zie punt 4.4). De 69 overslagvoorspellingen bekomen met de quantifier worden uitgezet in een grafiek waarbij het dimensieloos overslagdebiet $\frac{q}{\sqrt{gH_{m0\ toe}^3}}$ versus de dimensieloze kruinhoogte $R_c / H_{m0\ toe}$ weergegeven wordt, zie figuur 16. De best passende TAW voorspellingslijn voor niet-brekende golven op ruwe hellingen (TAW, 2002) wordt door deze datapunten gefit, resulterend in een γ_f -waarde van 0.38 in de TAW -formule.
Voor de door de classifier als verwaarloosbare overslag geklasseerde datapunten, wordt een waarde $\frac{q_{ss\_est}}{\sqrt{gH_{m0\ toe}^3}}$ afgelezen, waarbij de gekende $R_c / H_{m0\ toe}$ -waarden het uitgangspunt zijn. Figuur 16 toont de gevolgde methodiek.

De kleine niet-nulschattingen q_{ss_est} (8 in totaal) worden nu samen met de quantifier voorspellingen voor de overige 69 data gebruikt om de overeenkomstige prototype overslagdebieten te bepalen. Aangezien het hier een ruwe, hellende structuur betreft, worden aanzienlijke model- en schaaleffecten verwacht. Toepassing van de factor f_{scale_wind} zoals beschreven in punt 4.4, i.e. $q_{proto} = q_{ss} * f_{scale\_wind}$, levert gecorrigeerde schattingen op voor de prototype metingen.

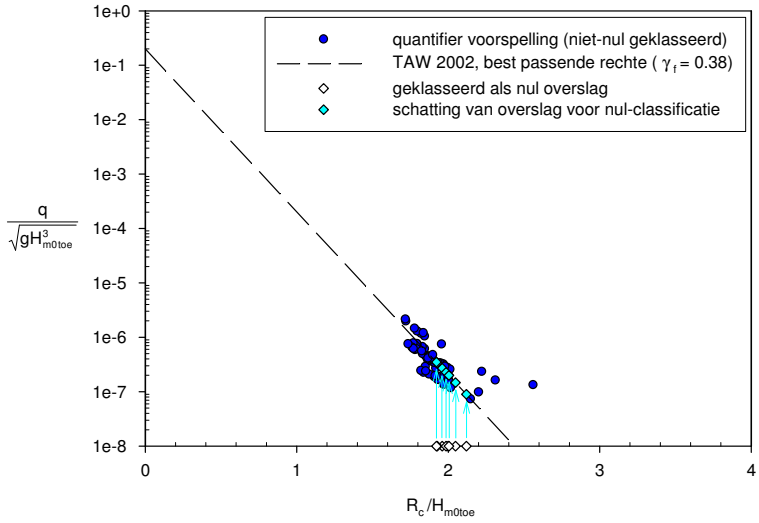

Figuur 16 Schatting van een kleine overslagwaarde voor de als verwaarloosbare overslag geklasseerde Ostia data, gebaseerd op quantifier voorspellingen van de als significante overslag geklasseerde Ostia data

In figuur 17 zijn zowel de 69 door de quantifier voorspelde waarden, $^{s}q_{NN}$, als de 8 geschatte waarden, $^{s}q_{ss\_est}$, weergegeven. Daarnaast zijn ook de prototype voorspellingen, $^{s}q_{NN\_corr\_final}$, weergegeven waarbij de verwachte model- en schaaleffecten in rekening werden gebracht.

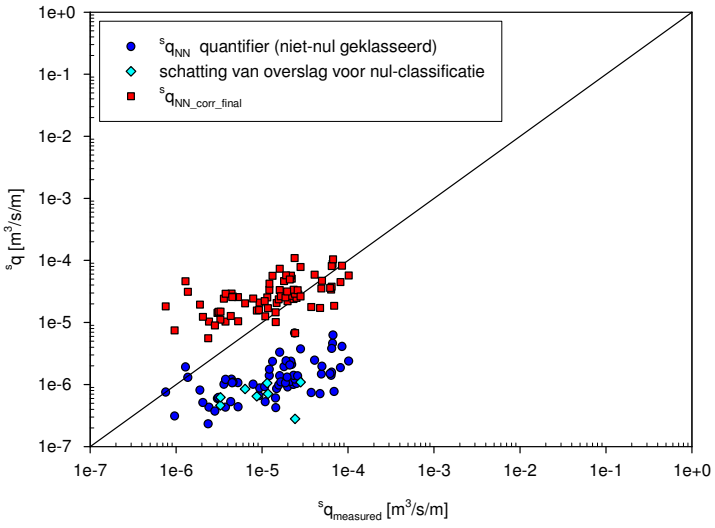

Figuur 17 Gecombineerde classifier-quantifier voorspelling van Ostia data

De uiteindelijke rms-error van de gecorrigeerde waarden ${}^{s}q_{NN\_corr\_final}$ is 0.5249. Figuur 17 toont aan dat de uiteindelijke prototype voorspellingen behoorlijk goed overeenkomen met de gemeten waarden, hoewel voor kleine gemeten waarden een overpredictie lijkt op te treden. Het vermoeden bestaat dat de overpredictie voor de kleine waarden van ${}^{s}q_{measured}$ een gevolg is van het aan de rand van het toepassingsdomein gesitueerd zijn van de data. Het is echter ook mogelijk dat de CLASH schaalprocedure bijdraagt tot/de reden is van deze overpredicties.

Een tweede mogelijkheid om het gedrag van de combinatie classifier-quantifier te testen is aan de hand van kunstmatige proevenreeksen. Het voorbeeld hier beschouwd betreft overslag over een eenvoudige stortsteengolfbreker waarbij de deklaag bestaat uit rotsblokken. Volgende golfkarakteristieken worden verondersteld: $\beta = 0°$ (loodrechte golfaanval) en ${}^{s}T_{m-1,0\ toe} = 4.91s$ (wat overeenkomt met een golfsteilheid $s_0 = 0.043$). De waterdiepte wordt vastgelegd op ${}^{s}h = 7.14m$. De helling van de golfbreker is 1:2 en de kruinbreedte ${}^{s}G_c$ bedraagt 0.9m (wat overeenkomt met 2 à 3 rotsblokken). De ruwheid/doorlatendheid van de golfbreker wordt beschreven door $\gamma_f = 0.4$ (zie tabel 2).
De kunstmatige dataset wordt gegenereerd door de kruinhoogte van de structuur te variëren binnen de toelaatbare grenzen van classifier en quantifier.
Het resultaat kan als volgt worden samengevat (figuur 18):

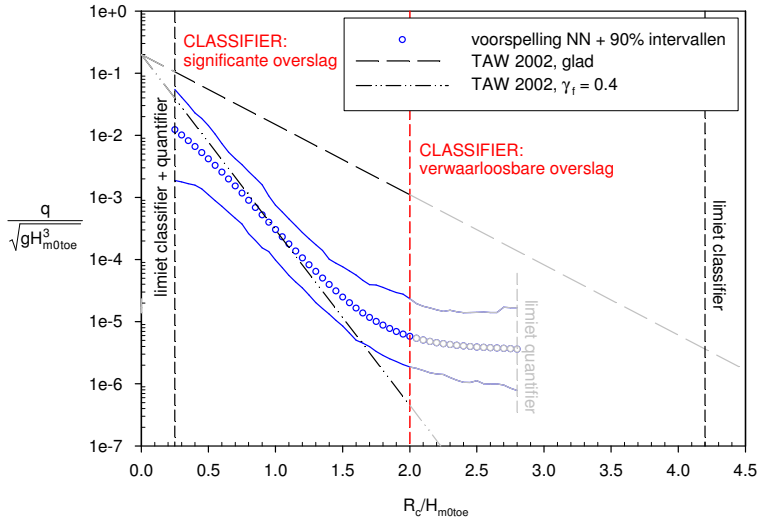

Figuur 18 Gecombineerde classifier-quantifier voorspelling van golfoverslag over een stortsteengolfbreker met een deklaag opgebouwd uit rotsblokken

- De classifier voorspelt enkel significante overslag over de beschouwde stortsteengolfbreker onder vermelde golfaanval voor waarden van $0.25m \leq {}^{s}R_c \leq 2m$. Voor waarden van $2m < {}^{s}R_c \leq 4.2m$ wordt geen of verwaarloosbare overslag verwacht. Voor waarden van ${}^{s}R_c > 4.2m$ en waarden van ${}^{s}R_c < 0.25m$ kan de classifier geen betrouwbare uitspraak doen, aangezien deze gebieden buiten de toepassingsgrenzen van de classifier vallen.
- Voor waarden van $0.25m \leq {}^{s}R_c \leq 2m$ kan de quantifier gebruikt worden om precieze overslagdebieten te bepalen. De resultaten zijn weergegeven in figuur 18 in blauw. Ter vergelijking is de door TAW (2002) voorspelde golfoverslag (niet-brekende golven) over de beschouwde structuur weergegeven, waarbij $\gamma_f = 0.4$. Figuur 18 toont aan dat de quantifier voorspelling de TAW -lijn goed benadert in het gebied $0.25m \leq {}^{s}R_c \leq 2m$.
  Hoewel waarden van $2m \leq {}^{s}R_c \leq 2.8m$ ook nog binnen het toepassingsdomein van de quantifier vallen, mag de quantifier daar niet gebruikt worden, aangezien de classifier er geen of verwaarloosbare overslag voorspelt. De voorspelling van de quantifier in dat gebied is in figuur 18 weergegeven in licht grijs. Het is duidelijk dat de quantifier in dit gebied te hoge overslag zou voorspellen, wat bevestigt dat de classifier een duidelijke meerwaarde levert in de uiteindelijke voorspellingsmethode.

5 Conclusies en voorstellen voor verder onderzoek

5.1 Conclusies

De 5 doelstellingen vooropgesteld in punt 1.4 werden bereikt.

In een eerste fase van het onderzoek werd een literatuurstudie naar bestaande modellen voor golfoverslag uitgevoerd. Speciale aandacht werd gegeven aan de invloedsfactoren die voorkomen in deze modellen, met het oog op het opstellen van de databank in een latere fase van het onderzoek.

In een volgende fase werden bestaande gegevens over overslagmetingen opgespoord. Deze fase kaderde in het CLASH project. Tijdens dit 3-jarig project werden meer dan 10000 overslagmetingen verzameld, zowel uit openbaar als uit vertrouwelijk onderzoek. De verzamelde gegevens werden zeer grondig bestudeerd en beoordeeld op betrouwbaarheid. Het verzamelen en screenen van alle gegevens vergde een grote inspanning en veel tijd maar was onontbeerlijk om tot een goede databank te komen.

De gegevens werden gecompileerd in één databank, waarbij iedere meting door 31 parameters (en 2 opmerkingen) wordt beschreven. De grootste moeilijkheid

was het kiezen van geschikte parameters die een goed totaalbeeld geven van een overslagproef op een willekeurige sectie. Naast structurele parameters en golfparameters, werden ook 2 parameters gebruikt om de complexiteit van de sectie respectievelijk de betrouwbaarheid van de meting te beschrijven. Deze 2 parameters werden verder gebruikt bij het ontwikkelen van de neurale voorspellingsmethode. De uiteindelijke CLASH databank bestaat uit 10532 proeven, afkomstig van 163 verschillende proevenreeksen, en is het eerste belangrijke resultaat bereikt in dit proefschrift. Het nut van deze uitgebreide databank is tweeledig:

- De databank is een schat aan informatie voor onderzoekers in verschillende onderzoeksdomeinen. Het betreft een unicum aan gegevens, nooit voorheen werd dergelijke poging gedaan om overslaggegevens te verzamelen en te compileren.
- De databank werd verder gebruikt voor het ontwikkelen van twee algemeen toepasbare voorspellingsmethodes voor golfoverslag. Naast de CLASH voorspellingsmethode (Pozueta et al., 2004a and 2004b), werd in dit proefschrift, onafhankelijk van CLASH, een tweeledig neuraal netwerk opgesteld.

Hoewel het fundamentele doel van de databank het trainen van een neuraal netwerk was, moet het belang van de databank op zich benadrukt worden. Onderzoekers kunnen overslaggegevens die betrekking hebben op specifieke structuren selecteren en verder gebruiken ter validatie van nieuw analytisch of numeriek onderzoek. Daarnaast kan de databank ook gebruikt worden voor zaken die niet onmiddellijk gerelateerd zijn aan overslag. De mogelijkheid om diep water golfkarakteristieken te vergelijken met golfkarakteristieken aan de teen van een constructie kan hier vermeld worden.
De databank is beschikbaar op de CD-ROM in bijlage.

In een volgende fase van het onderzoek werd een tweeledig neuraal netwerk ontwikkeld, dat in staat is om golfoverslag over een willekeurige structuur te voorspellen. Het eerste netwerk, de ‘classifier’, heeft als taak om golfoverslag te beoordelen als significant of verwaarloosbaar. Het tweede netwerk, de ‘quantifier’, dient vervolgens om de door de classifier als significant beoordeelde overslagsituaties te kwantificeren, i.e. een bijhorend gemiddeld overslagdebiet te bepalen.
Voor beide modellen werd een MLP met één verborgen laag voorgesteld. Na het bepalen van een optimale netwerkconfiguratie werd de bootstrap methode toegepast. Naast het optimale gebruik van de data, laat de bootstrap methode toe een indicatie van de betrouwbaarheid te geven voor iedere quantifier voorspelling. De bootstrap netwerken worden bij de classifier gebruikt om een optimale beslissingsgrens te bepalen.

Om te vermijden dat de netwerken gebruikt worden buiten de parameterwaarden van de data waarop ze getraind zijn, werd voor beide netwerken een strikt toepassingsdomein afgebakend.
Het finaal tweeledig neuraal model is het tweede belangrijk resultaat bereikt in dit proefschrift. Vertrekkend van 14 input parameters (door het netwerk getransformeerd tot 13 verschaalde input parameters, waarbij $H_{m0\ toe}$ = 1m), wordt een (kleinschalige) voorspelling gegeven. Wanneer de classifier verwaarloosbare overslag voorspelt, wordt de quantifier niet verder gebruikt. In het andere geval kwantificeert de quantifier het gemiddelde overslagdebiet en geeft een indicatie van de betrouwbaarheid.

In een laatste fase van het onderzoek werd de ontwikkelde voorspellingsmethode gevalideerd. Hiervoor werden enerzijds beschikbare prototype gegevens gebruikt, anderzijds werden een aantal kunstmatige datasets beschouwd.
Na simulatie van de prototype metingen, werd de CLASH schaalprocedure gebruikt om overeenkomstige prototype resultaten te bekomen. De resultaten bekomen voor de Ostia metingen zijn goed, hoewel voor kleine gemeten overslagwaarden een overpredictie lijkt op te treden. Ook voor andere prototype simulaties kan men diezelfde trend onderscheiden. De overpredicties kunnen zowel afkomstig zijn van de neurale voorspellingsmethode zelf, als van de CLASH schaalprocedure.
Vergelijking van de voorspellingen bekomen voor kunstmatige datasets met bestaande empirische formules toont aan dat de finale voorspellingsmethode goede resultaten oplevert. Er werd bovendien aangetoond dat de classifier een significante meerwaarde levert bovenop het gebruik van de quantifier alleen als voorspellingsmethode: door het 'filtereffect' van de classifier worden grote overpredicties vermeden.

5.2 Voorstellen voor verder onderzoek

In eerste instantie zou de auteur graag de ontwikkelde voorspellingsmethode verder gevalideerd zien. Hiervoor zijn nieuwe resultaten van overslagproeven nodig die toelaten het netwerk te testen en eventueel kunnen leiden tot uitbreidingen/beperkingen van het parameterdomein waarbinnen simulaties kunnen uitgevoerd worden.
Daarnaast kan de specifieke invloed van de input parameters op golfoverslag bestudeerd worden. Hiervoor kunnen enerzijds kunstmatige datasets aangewend worden waarvan de voorspellingen kunnen vergeleken worden met bestaande empirische formules. Anderzijds kunnen ook hier nieuwe fysische modelproeven gebruikt worden als validatie.

Op basis van de beschikbare CLASH prototype meetgegevens werd geconcludeerd dat de combinatie neurale voorspellingsmethode - CLASH schaalprocedure soms te hoge overslagvoorspellingen oplevert, voornamelijk voor kleine gemeten overslagdebieten. Gedetailleerde studie van het gedrag van de neurale voorspellingsmethode voor kleine overslagmetingen kan een antwoord geven op de vraag of het model in sommige gevallen inderdaad tot overpredicties leidt. Daarnaast is het aangeraden om ook de CLASH schaalprocedure verder te valideren met nieuwe beschikbare prototype meetgegevens.

Tijdens het opstellen van de neurale voorspellingsmethode werd verondersteld dat de gegevens afkomstig van eenzelfde proevenreeks onafhankelijk zijn van elkaar. Vermoedelijk is dit niet helemaal correct. Hoe groot de onderlinge afhankelijkheid van data binnen een proevenreeks is en wat de precieze impact hiervan is op de neurale voorspellingsmethode zou verder onderzocht kunnen worden.

Het is aan te raden de invloed van wind op golfoverslag verder te onderzoeken. Ook het modelleren van wind in laboratoria vereist verder onderzoek. De fysische modelproeven uitgevoerd met artificiële wind zijn op dit ogenblik niet verder gebruikt wegens het ontbreken van kennis op dit gebied.

Een belangrijk voordeel van de ontwikkelde neurale voorspellingsmethode is de algemene toepasbaarheid ervan. Nochtans is het bekend dat de fysische processen die optreden tijdens golfoverslag over hellende structuren fundamenteel verschillen van de fysische processen bij golfoverslag over verticale wanden. Het gevolg hiervan is dat de invloedsparameters verschillen. Bovendien bevat de databank een groter aantal proeven op hellende structuren dan op verticale wanden, wat zou kunnen leiden tot een gemiddeld slechtere performantie van de neurale voorspellingsmethode voor verticale wanden.
Vandaar de suggestie om twee gescheiden voorspellingsmodellen te ontwikkelen: een model voor hellende structuren versus een model voor verticale structuren. Een eventuele betere performantie voor beide aparte modellen zou kunnen afgewogen worden tegenover het nadeel van het opsplitsen van het bestaande tweeledige model in 2 aparte modellen. Een extra moeilijkheid bij het opsplitsen van de structuren bestaat erin de samengestelde structuren te klasseren als overwegend hellende of overwegend verticale structuren.

Tot slot wil de auteur nog eens de aandacht vestigen op de grote waarde van de opgestelde databank met overslaggegevens. Het zou zeer interessant zijn om deze unieke verzameling gegevens up-to-date te houden, i.e. verder aan te vullen met nieuwe overslaginformatie die beschikbaar komt.

CHAPTER 1
INTRODUCTION

1.1 Rationale

Coastal structures are designed to protect (often densely populated) coastal regions against wave attack, storm surges, flooding and erosion. The crest height plays a predominant role in the protective function of these structures. Due to climate changes, the sea level is rising and more severe storms occur (see Carter et al., 1988). This emphasises the importance of the design of these protective structures. The amount of sea water transported over the crest of a coastal structure, referred to as 'wave overtopping', is a critical design factor in this context.

Design of coastal structures should lead to an 'acceptable' overtopping amount. Which amount is assessed as acceptable is revealed by socio-economical reasons. High crested coastal structures preventing any overtopping are preferably avoided as these structures are extremely expensive. Moreover, such structures impose visual obstructions where the broad view on the sea is an important tourist attraction with an economical impact. However, the design of (lower crested) coastal structures should provide safety for people and vehicles on the structure, and avoid structural damage as well as damage to properties behind the structure. The preservation of the economical function of the structure under bad weather conditions is also an important factor and has an additional influence on the design.

Nevertheless, there is a lack of reliable and robust prediction methods for wave overtopping at coastal structures. Most frequently applied for structure design are empirical models, set up based on laboratory overtopping measurements. However, these models can only be applied within a restricted range (i.e. the test range of the data on which the model is based), and only a limited range of structure configurations is covered. In addition, it is hard to find suitable prediction methods applicable for structures not having a standard structure geometry.
Finally, present prediction methods may be subject to model and scale effects, resulting in differences between prototype and model response. This follows a.o. from a conclusion of the EC project OPTICREST (De Rouck et al., 2001). In this

project wave run-up $Ru_{2\%}$, i.e. the run-up exceeded by 2% of the waves, on a rubble mound slope measured during full scale storms, was found to be approximately 20% higher than observed during reproductions of these storms in small scale test facilities. Since wave overtopping is closely related to wave run-up, this resulted in the presumption that model and scale effects may also be present in small scale overtopping tests.

1.2 Wave overtopping

'Wave overtopping' or briefly 'overtopping' is defined as the sea water which is flowing over the crest of a coastal structure land-inward (figure 1). Overtopping is related to wave run-up as overtopping occurs when wave run-up levels reach the crest of the structure and pass over it. However, besides this so-called 'green water' flowing over the structure, also 'spray' is considered as wave overtopping. Spray concerns fine droplets of water which are generated by waves breaking on or seaward of the structure and carried over the structure crest under their own momentum and/or driven by wind.

Research on wave overtopping in laboratories seldom considers the effect of wind on (spray) overtopping, which however may have a considerable (relative) contribution for small overtopping discharges.

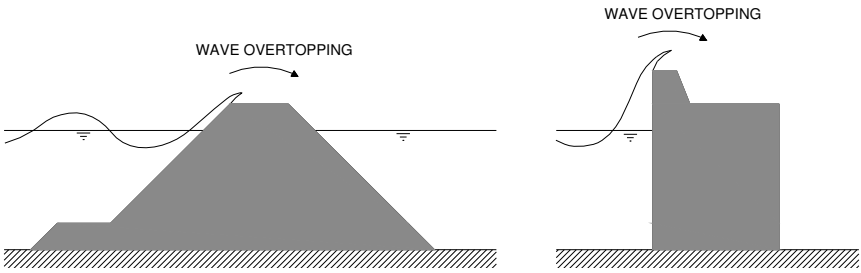

Figure 1.1 Definition of wave overtopping at coastal structures

Two approaches to measuring and assessing wave overtopping at coastal structures can be distinguished. The first approach considers the overtopping volume per overtopping wave. The second and most applied approach considers mean overtopping discharges over certain time intervals and per meter structure width, i.e. q in $m^3/s/m$ or l/s/m. The uneven distribution of overtopping in time and in space caused by irregular wave action is the basic reason for the assessment of overtopping by means of mean overtopping discharges. The latter are found to be 'stable', i.e. reproducible, over time intervals of about 1000 waves.

Within this work the mean overtopping discharge per meter run, q, expressed in $m^3/s/m$, is taken as a starting point: a neural prediction method for mean overtopping discharges has been developed. This corresponds to the most common approach to design coastal structures, i.e. based on mean overtopping discharges. A typical example are the 'guidelines for safety assessment for dikes' set up in the Netherlands by the Technical Advisory Committee on Flood Defence (see TAW, 2002). The huge amount of available data regarding mean overtopping discharge measurements was an extra benefit of considering mean overtopping discharges in this work.

1.3 The CLASH framework

The project 'CLASH' (Crest Level Assessment of coastal Structures by full scale monitoring, neural network prediction and Hazard analysis on permissible wave overtopping), supported by the European Commission, was intended to improve the knowledge on the phenomenon of overtopping and originates from two observations, i.e.:

- the lack of generally applicable prediction methods for crest height design or assessment with respect to wave overtopping and
- the fact that small scale tests underestimate wave run-up on rough slopes.

The CLASH project, under contract no. EVK3-CT-2001-00058, ran from January 2002 until December 2004 (www.clash-eu.org). The research described in this thesis is partly performed within the framework of the CLASH project. Detailed information on the overall CLASH project is summarised in the final project report, see De Rouck et al. (2005).

The main objectives within the CLASH project were:

1) to solve the problem of suspected model and scale effects for overtopping,
2) to develop a generally applicable overtopping prediction method based on many existing datasets gathered in a database on wave overtopping,
3) to define guidelines for tolerable overtopping limits.

In view of solving the problem of suspected model and scale effects, prototype overtopping was measured at 3 European sites within the CLASH project:

- the Zeebrugge measurement site (Belgium), consisting of a rubble mound structure armoured with antifer cubes,
- the Ostia measurement site (Italy), consisting of a rubble mound structure armoured with rocks and
- the Samphire Hoe measurement site (United Kingdom), consisting of a vertical wall with a rubble mound protection in front of it.

The research on model and scale effects required the simulation of the measured prototype storms in various laboratories on a smaller scale. Two-dimensional

simulations in wave flumes as well as three-dimensional simulations in wave basins were performed. Finally, numerical simulations were carried out, providing a third tool to fulfil the first CLASH objective.
The final outcome of the CLASH research performed on model and scale effects confirms the presumption that these effects do affect small scale overtopping measurements under certain circumstances, and resulted in a 'CLASH scaling procedure' quantifying expected model and scale effects for specific situations. For details on this subject reference is made to the corresponding CLASH report, see Kortenhaus et al. (2005).

The second CLASH objective required in a first phase the set-up of a database on existing overtopping information. The set-up of this database is a part of this thesis. Besides gathering overtopping information, thorough screening of the data was carried out. The database was made homogeneous by so-called 'white spot tests' (i.e. additional physical model tests) which were performed within CLASH to fill up the lacking knowledge in the database. The set-up of the overtopping database is described in detail in chapter 3 of this thesis, and in the corresponding CLASH report (Van der Meer et al., 2005b). The final CLASH overtopping database is publicly available (Van der Meer et al., 2005a) and is enclosed on a CD-ROM.
In a second phase, the considered CLASH objective required the development of a generic prediction method for mean overtopping discharges, based on the created CLASH overtopping database. The sophisticated technique of neural network modelling was applied to achieve this, resulting in a CLASH prediction method (see Pozueta et al., 2004a and 2004b).
Separately from the CLASH project, but based on the same CLASH database, a comparable neural prediction method for wave overtopping at coastal structures has been developed in this thesis. Both the CLASH prediction method and the prediction method described in this thesis concern small scale prediction methods, i.e. overtopping discharges to be expected in a small scale model are predicted. The main difference between both prediction methods is that in this thesis a sequence of 2 neural models is proposed, whereas the CLASH prediction method is only composed of 1 single network. It is shown in this thesis that the use of 2 subsequent neural models has a significant added value versus the use of only 1 neural model: large overpredictions due to the inability of a single neural model to predict zero or very small overtopping discharges are avoided. As both the CLASH network and the network described in chapter 4 of this thesis were developed at about the same time, a detailed comparison of the performance of both networks falls beyond the scope of this thesis.

The third and final CLASH objective was to derive/refine overtopping limits for hazard to people and vehicles, and for damage to property. The impact of wave overtopping on social and economical life in densely populated areas near the

coast was also considered. The final outcome of this subject is described in two CLASH reports, see Bouma et al. (2004) and Allsop (2005).

Within this thesis various references to the CLASH project and results obtained within the CLASH project are made. The CLASH results corresponding to the first objective, are used in the last phase of this work to check the combination 'neural model - CLASH scaling procedure', i.e. neural simulations of the prototype measurements are corrected corresponding to the expected model and scale effects, and finally compared to the prototype overtopping measurements. The set-up of the overtopping database frames in the CLASH project, whereas the development of the sequence of 2 neural models within this work is performed outside CLASH. The CLASH result of the third objective is referred to in this work as the most recent information on tolerable overtopping limits, which may serve to assess predicted overtopping discharges and corresponding crest levels of coastal structures.

1.4 Objectives

The research described in this work can be split up in two main parts. The first part concerns the creation of an extensive database on wave overtopping. The second part concerns the development of a neural prediction method, providing a generally applicable prediction method for wave overtopping at coastal structures. The second part is based on the outcome of the first part.

The main objectives of this research can be formulated as follows:

1) *to carry out a literature survey on existing models for wave overtopping, with the specific goal to investigate the parameters influencing the phenomenon of wave overtopping*

2) *to gather as much existing data as possible on overtopping measurements, and to screen these data on consistency, in order to get a homogeneous collection of data on overtopping measurements*

3) *to set up a database on wave overtopping by schematising each single overtopping test of the gathered data by means of a fixed number of parameters, where information on the wave characteristics, the structure geometry, as well as the reliability of the test is included*

4) *to develop a generally applicable prediction method for wave overtopping in small scale tests, by training neural models with data from the overtopping database*

5) to check the performance of the developed prediction method based on

- *the available CLASH prototype measurements and the CLASH scaling procedure accounting for model and scale effects,*
- *synthetic datasets considering overtopping at specific structure types for which the overtopping performance is known.*

1.5 Methodology

To meet the objectives mentioned in previous section, several steps are taken. An overall view of the methodology and the contents of this thesis is presented here.

In a first phase of the thesis a literature survey on wave overtopping is set up. This summary of research performed on wave overtopping is described in chapter 2. Existing models predicting mean overtopping discharges as well as the distribution of individual overtopping waves are studied. Special attention is given to the parameters which are found to influence the overtopping phenomenon. The knowledge on parameters influencing overtopping is of direct use for the set-up of the overtopping database, as all overtopping tests have to be schematised by parameters assessed as possibly influencing the overtopping phenomenon.
In the same chapter existing limits of tolerable overtopping are discussed.

In a second phase existing overtopping data are gathered and an overtopping database is created. This phase frames in the CLASH project and is described in chapter 3. Overtopping data are gathered from partners within the CLASH project as well as from other authorities in and outside Europe. Although only briefly described in this thesis, gathering and screening the data was a comprehensive task. Various preliminary methodologies preceding the final schematisation procedure are not discussed. Chapter 3 focuses on the final methodology of schematising each overtopping test by means of a restricted number of parameters. In addition, the lay-out and the contents of the finalised database are studied in more detail.

In a third and last phase of this thesis a generally applicable overtopping prediction method is developed and validated. Chapter 4 describes the research performed in this respect. The neural prediction method is based on the CLASH overtopping database, but is developed outside CLASH, i.e. separately from the CLASH prediction method. The final neural prediction method proposed within this work is composed of two subsequent neural models: a so-called ‘classifier’, followed by a so-called ‘quantifier’.
Chapter 4 successively treats the general methodology of neural networks, the selection and preprocessing of the data from the database to serve as input for the

neural models, the development of the neural quantifier and the development of the neural classifier.

In chapter 5 the general conclusions of this thesis are compiled. In addition, recommendations for further research are given.

The extensive database on wave overtopping is enclosed on a CD-ROM.

CHAPTER 2
LITERATURE SURVEY ON WAVE OVERTOPPING

2.1 Introduction

This chapter aims to give a concise summary of the research which has been performed to the phenomenon of wave overtopping since halfway previous century.
In this introduction first the evolution in overtopping-related research is dealt with, followed by a short overall view of the contents of this chapter. Further, some specific points of interest in this literature survey are focussed on.

2.1.1 Approach to the overtopping phenomenon

Initial research on the overtopping phenomenon started in the 1950's. Saville (1955) was one of the first researchers to perform overtopping tests with regular waves. Ever since overtopping research has gained more and more attention and several models to predict wave overtopping at various structure types have been developed. Mainly physical model experiments but also prototype measurements provide the basic data for this research. During the first few decades overtopping was simulated in laboratories with regular waves only. Later on, irregular wave generation became standard, resulting in an improved accuracy of the developed prediction methods. The first well-known overtopping model based on irregular wave experiments in laboratory is the formula of Owen (1980). Even now, Owen's formula is used for the design of sloping structure types.

The majority of overtopping research published in literature considers mean overtopping discharges q, expressed as flow rates per meter run of the defence structure ($m^3/s/m$ or l/s/m). Also limits for tolerable overtopping are most frequently expressed using mean overtopping discharges. The mean overtopping discharge over about 1000 waves is a 'stable' parameter, in contrast to the volume of an individual overtopping wave. Due to the uneven distribution in time and space of overtopping, the local overtopping discharge from one single wave can be up to 100 times the measured time-averaged overtopping discharge during the storm peak.

However, the maximum individual overtopping volume of a wave may also be of large significance, both for damage to structures and hazard to people. Consequently, recent research on individual overtopping volumes and related probability distributions has been performed. The research performed by Franco et al. (1994) presents the first results on the distribution of individual overtopping volumes.

2.1.2 Contents of literature survey

Considering mean overtopping discharges, several types of overtopping models have been developed. This thesis gives an overall view of the most important models, i.e.:

- empirical models (= regression models)
  - simple regression models
  - weir-models
  - models based on run-up
  - graphical models
- numerical models

First, empirical models are distinguished from numerical models. Empirical models are regression models, based on available overtopping data from physical model experiments. These models are treated in section 2.2. Numerical models, treated in section 2.3, simulate overtopping events in numerical wave flumes. Basically, the latter models solve a series of differential equations describing fluid flow in front of and on the structure. The emphasis is put on the empirical models, the most studied and the most applied models through the years by far.

Four groups of empirical models are treated in this thesis. The first and most extensive examined group concerns simple regression models. Typically, in these models a relationship between a dimensionless discharge and a dimensionless crest freeboard is proposed, with certain parameters to be estimated starting from the available physical model tests. Nowadays these models are still the basis of the design of a lot of coastal structures. The second and third group of empirical models contain more physics than the simple regression models. The second group of models is based on the weir analogy. Kikkawa (1968) introduced this theoretical approach of overtopping. The third group considers models based on run-up measurements, i.e. overtopping is derived from run-up. Finally, the last group of empirical models mentioned in this thesis concerns graphical models. Some researchers present their results graphically, which leads to design diagrams for overtopping. The design diagrams of Goda (1985) are a well-known example.

Following to this survey of overtopping models for mean overtopping discharges, in section 2.4 individual overtopping volumes of waves are studied in more detail.

Finally, in section 2.5 limits of tolerable overtopping discharges are considered. Several studies resulted in guidance on limits for mean overtopping discharges providing both safety of traffic and structural safety. Recently, limits for individual overtopping volumes have also been studied. However, methods to predict peak volumes are less validated. The fact that data related to individual overtopping measurements are rare plays a role here.

2.1.3 Points of interest

In the past it was typical for traditional wave overtopping research to concentrate on one specific structure type. As will be seen in this chapter this resulted in corresponding overtopping models only applicable for one structure type. Vertical structures are often distinguished from sloping structure types (smooth or rough) in this context. However, also for composite structure types overtopping models were developed.
The developed neural prediction method within this thesis has been trained using a database in which all structure types are integrated. The final result consists of a single 'model' (composed of 2 subsequent neural models) which is able to predict overtopping at any coastal structure type. It is clear that the overall predictive capacity of the neural prediction method is particularly advantageous.

The empirical models developed until now use only a restricted number of wave parameters and structural parameters to predict mean overtopping discharges. The fact that each model is valid for only one specific structure type contributes to this. Considering various proposed overtopping models, it is seen that overtopping is influenced by many wave and structure characteristics.
Several researchers proposed correction factors for existing simple overtopping models. These correction factors account for additional influences on overtopping which were not considered in the original model, for example oblique wave attack.

All models treated in this chapter were set up based on model experiments on wave overtopping. This implies that all models are in fact models predicting wave overtopping *in laboratory*, where no or little attention has been given to possible model and scale effects. In chapter 4 the influence of the presence of model and scale effects in laboratory measurements on the development of the neural prediction method will be treated in detail. In this chapter no further attention is given to these effects.

This section's aim is not to describe all overtopping models and formulae in detail, but rather to present an overall view of the distinguished models for overtopping as well as of the evolution of the wave overtopping research through the years. The reader should achieve an idea of the evolution of the knowledge on the overtopping phenomenon and the physics behind it. Only irregular wave overtopping models are considered. However, some models predicting regular wave overtopping are mentioned, as these serve as a basis for irregular wave overtopping models, e.g. the model of Weggel (1976) and Kikkawa (1968).
In view of developing a neural prediction method for overtopping, it is very important to define the parameters influencing overtopping. Therefore, in this survey special attention is given to the parameters included in existing overtopping models. The quantification of the effect of influencing parameters by various researchers is not considered in detail.

It should be noted that the wave characteristics which are mentioned in this section always refer to the incident wave characteristics at the toe of the structure. In case the deep water wave characteristics are used, this is explicitly mentioned in the text.
One can remark that many researchers take non-breaking waves as starting point, where the wave period at the toe is supposed to equal or approximate the deep water wave period.

In this chapter several formulae are described. The author consistently used the same notation for the same parameters in all formulae. All frequently used parameters are included in the 'list of symbols' enclosed in the front of this thesis. Rarely used parameters which are not included in this list, are explained in the text at the moment these are used.

2.2 Empirical models

2.2.1 Simple regression models

This section focuses on the research performed on simple regression models for overtopping.

Two frequently appearing types of regression models are distinguished, i.e.:

type A $$Q^* = a \,.\, exp\left[-\left(b \,.\, R^*\right)\right] \quad (2.1)$$

type B $$Q^* = a \,.\, R^{*-(b)} \quad (2.2)$$

where Q* refers to a dimensionless mean overtopping discharge per meter structure width and R* to a dimensionless crest freeboard. The parameters a and b are fitted coefficients.

Within one model various values of a and b are often proposed, related to specific structure characteristics which are tested, e.g. the structure slope, the roughness of the structure surface and the crest width. Some researchers include specific structure characteristics in the dimensionless parameters Q* and R* of eqs. (2.1) and (2.2), leading to a more generally applicable overtopping formula. Examples are the formulae proposed by Pedersen (1996) and Hebsgaard et al. (1998), see further in this section. However, this attempt is hardly ever adapted. The need of a large uniform dataset describing overtopping at various structure types to create such formulae may be mentioned here as a reason why these formulae are rather scarce.

Regression models developed for smooth sloping structures are considered first in this section. These models are often extended to rough sloping structures and to specific crest configurations. This first class of models is discussed in section 2.2.1.1, whereas models for vertical walls, a second class of models, are treated in section 2.2.1.2. The physics related to overtopping at vertical walls are different from these related to sloping structure types. This is reflected by the different influences found for certain wave and structural parameters in the overtopping models. The behaviour of composite structure types, which are e.g. composed of a vertical wall with a rubble mound protection in front of it, depends on the specific structure geometry with corresponding wave characteristics. Composite structure types are mentioned in section 2.2.1.1 as well as in section 2.2.1.2, as structure types for which the basic model is extended.
Additional influencing parameters for overtopping, often represented by researchers as correction factors to be added to the empirical model, are treated in section 2.2.1.3.

2.2.1.1 Sloping structures

Table 2.1 gives an overall view of the models considered in this section. For each model the dimensionless parameters Q* and R* are represented. The table facilitates the comparison of the models and allows keeping an overall view while going through this section.

Table 2.1 Simple regression models for sloping structures

	Model type [1]	Q*	R*
Owen (1980)	Type A	$\frac{q}{g\,H_s\,T_m}$	$\frac{R_c}{T_m\sqrt{gH_s}}\cdot\frac{1}{\gamma_f}$
TAW (2002)	Type A	for $\gamma_b\xi_0 <\approx 2$; plunging conditions	
		$\frac{q}{\sqrt{g\,H_{m0}^3}}\cdot\sqrt{\frac{s_0}{\tan\alpha}}\cdot\frac{1}{\gamma_b}$	$\frac{R_c}{H_{m0}}\cdot\frac{\sqrt{s_0}}{\tan\alpha}\cdot\frac{1}{\gamma_b\,\gamma_f\,\gamma_\beta\,\gamma_v}$
		for $\gamma_b\xi_0 >\approx 2$; surging conditions	
		$\frac{q}{\sqrt{g\,H_{m0}^3}}$	$\frac{R_c}{H_{m0}}\cdot\frac{1}{\gamma_f\,\gamma_\beta}$
		$\xi_0 > 7$ (heavy wave breaking on shallow foreshore)	
		$\frac{q}{\sqrt{g\,H_{m0}^3}}$	$\frac{R_c}{H_{m0}(0.33+0.022\xi_0)}\cdot\frac{1}{\gamma_f\,\gamma_\beta}$
Bradbury and Allsop (1988) + Aminti and Franco (1988)	Type B	$\frac{q}{g\,H_s\,T_m}$	$\frac{R_c^2}{H_s\,T_m\sqrt{g\,H_s}}$
Pedersen (1996)	Type B	$\frac{q\,T_m}{L_{0m}^2}$	$\frac{H_s^5}{R_c^3\,A_c\,G_c\,\cot\alpha}$
Hebsgaard et al. (1998)	Type A	$\frac{q}{ln(s_{0p})\sqrt{g\,H_s^3}}$	$\frac{-1.6\,(\cot\alpha)^{0.3}\,(2\,R_c+0.35\,G_c)}{\gamma_f\,H_s\,\sqrt{\cos\beta}}$
Ahrens and Heimbaugh (1986, 1988)	Type A	$\frac{q}{\sqrt{g\,H_s^3}}$	$\frac{R_c}{(H_s^2\,L_{0p})^{1/3}}$

[1] see eqs. (2.1) and (2.2)

A well-known overtopping model originating from laboratory tests performed with irregular waves is the regression model proposed by **Owen (1980)**. Owen (1980) presents an overtopping model of type A to describe overtopping at a smooth sloping structure, i.e:

$$\frac{q}{g\,H_s\,T_m} = a\,.\,exp\left(-b\,.\,\frac{R_c}{T_m\sqrt{g\,H_s}}\right) \qquad (2.3)$$

Both the dimensionless crest freeboard parameter R* and the dimensionless overtopping discharge Q* include the significant wave height and mean period of the incident waves.
The model is based on over 500 model tests with irregular waves performed on an impermeable smooth slope. In some cases the slope is fronted by a flat berm. The generalised profile of the tests by Owen (1980) is shown in figure 2.1.

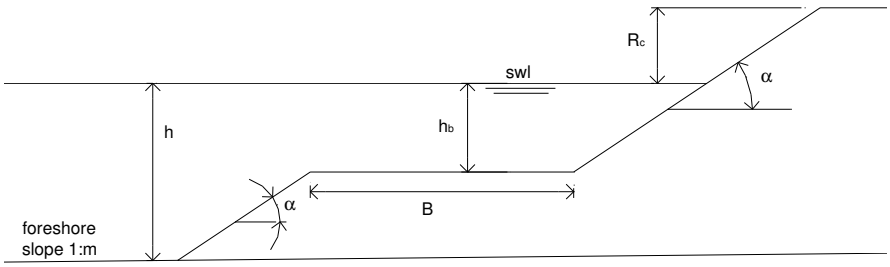

Figure 2.1 Generalised profile of tests by Owen (1980)

In case of a simple sloping structure the empirically determined parameters a and b account only for the slope of the structure. Table 2.2 summarises the corresponding values proposed by Owen (1980).
For bermed slopes the parameters a and b account in addition for the berm dimensions, i.e. the berm width B and the berm depth h_b (see figure 2.1). For the corresponding values of a and b is referred to Owen (1980).

Table 2.2 Values for parameters a and b for simple smooth slopes (Owen, 1980)

Structure slope 1:cotα	a	b
1:1	0.0079	20.12
1:1.5	*0.0102*	*20.12*
1:2	0.0125	22.06
1:2.5	*0.0145*	*26.10*
1:3	*0.0163*	*31.90*
1:3.5	*0.0178*	*38.90*
1:4	0.0192	46.96
1:4.5	*0.0215*	*55.70*
1:5	*0.0250*	*65.20*

bold type : values derived from model tests

italic type : *values derived by interpolation based on published run-up data (Shore Protection Manual, U.S. Army Corps of Engineers, 1978)*

Owen (1980) extends his model to sloping structures with surface roughness by introducing a reduction coefficient γ_f. The reduction coefficient is included in the formula as follows:

$$\frac{q}{g\,H_s\,T_m} = a\,.\,exp\left(-b\,.\,\frac{R_c}{T_m\sqrt{g\,H_s}}\,.\,\frac{1}{\gamma_f}\right) \tag{2.4}$$

The values of γ_f recommended by Owen (1980) concern published values for the effect of roughness on wave run-up.
Finally, based on additional tests, Owen (1980) proposes correction factors for the coefficients a and b to apply under oblique wave attack, i.e. $\beta \neq 0°$.
For values of γ_f and correction factors for $\beta \neq 0°$ is referred to Owen (1980).

Comparable to Owen (1980), **Van der Meer (1993)** develops an overtopping model of type A for overtopping at impermeable smooth slopes. Van der Meer (1993) finds that 'plunging conditions', corresponding to waves breaking on a slope, show a different overtopping behaviour from 'surging conditions' or non-breaking waves on a slope. The breaker parameter ξ_0 (combined with a reduction factor to account for the presence of a berm) is used to separate both conditions. The difference between the corresponding two types of 'breakers' is shown in figure 2.2.

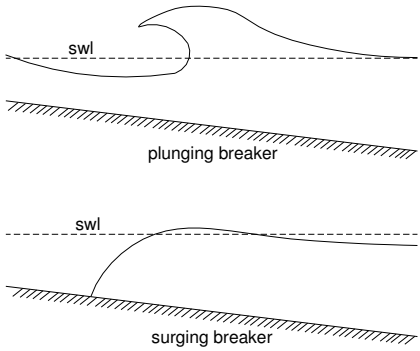

Figure 2.2 Plunging versus surging breakers

Van der Meer (1993) proposes a set of two equations, both of type A, which are extended for application for rough and bermed slopes as well. The research performed on run-up and overtopping by De Waal and Van der Meer (1992) is on the basis of the proposed overtopping model. The data from Owen (1980) and Führboter et al. (1989) are also used.
The original model proposed by Van der Meer (1993) has been improved subsequently (see Van der Meer and Janssen, 1995, and TAW, 1997) resulting in the most recent form in **TAW (2002)**, see eqs. (2.5a) and (2.5b):

- for $\gamma_b\xi_0 <\approx 2$; i.e. plunging conditions

$$\frac{q}{\sqrt{g\,H_{m0}^3}} \cdot \sqrt{\frac{s_0}{\tan\alpha}} = 0.067\,.\,\gamma_b\,.exp\left(-4.75\,.\,\frac{R_c}{H_{m0}}\,.\,\frac{\sqrt{s_0}}{\tan\alpha}\,.\,\frac{1}{\gamma_b\;\gamma_f\;\gamma_\beta\;\gamma_v}\right) \qquad (2.5a)$$

and standard deviation σ of coefficient b = 4.75 : σ = 0.5

- for $\gamma_b\xi_0 >\approx 2$; i.e. surging conditions

$$\frac{q}{\sqrt{g\,H_{m0}^3}} = 0.2\,.\,exp\left(-2.6\,.\,\frac{R_c}{H_{m0}}\,.\,\frac{1}{\gamma_f\;\gamma_\beta}\right) \qquad (2.5b)$$

and standard deviation σ of coefficient b = 2.6 : σ = 0.35

where γ_b , γ_f , γ_β and γ_v are reduction factors to account respectively for the presence of a berm, surface roughness, oblique and short-crested waves and the presence of a small wall on the slope (see TAW, 2002).

The factor γ_b accounts for the berm depth h_b , the berm width B and the slope of the berm α_B . The factor γ_β accounts for values of $\beta > 0°$. In addition, short-crested waves are distinguished from long-crested waves. The factor γ_v accounts for the dimensions of the small wall on the slope.

Dependent on the value of $\gamma_b\xi_0$, a measure for the wave conditions, different dimensionless parameters are proposed. Van der Meer (1993) finds that the wave period influences the overtopping results for plunging wave conditions, whereas this is not the case for surging wave conditions. The influence of the slope of the structure, α, the presence of a berm, and the presence of a vertical wall on top of the structure slope, is only accounted for in case of plunging wave conditions. For surging wave conditions on a slope, only the wave height is included in both dimensionless parameters. This is in contrast to the proposed model (2.3) by Owen (1980), who includes the wave period as well as the slope of the structure in his model, independent of the nature of the waves.

The model proposed by TAW (2002) advises to use spectral wave parameters. For the significant wave height the spectral value H_{m0} and for the wave period the mean period $T_{m-1,0}$ is advised. These parameters are found to account for the shape of the wave spectrum in the best way.

For wave overtopping on shallow foreshores, typically characterised by large values of the breaker parameter ξ_0 on relatively gently sloping structure slopes, TAW (2002) prescribes eq. (2.6). It concerns an adaptation of eq. (2.5b). The dimensionless crest freeboard encloses the breaker parameter, which implies that the structure slope as well as the wave period are included.
The procedure takes into account that due to very heavy breaking waves, spectra may be 'flattened out' and long waves may be present, leading to much higher overtopping than obtained with the formulae (2.5a) and (2.5b). Eqs. (2.5a) and (2.5b) are used for $\xi_0 < 5$, and eq. (2.6) for shallow foreshores with $\xi_0 > 7$. In between, linear interpolation on the logarithm of q is performed.

$$\frac{q}{\sqrt{g\,H_{m0}^3}} = 0.12\,.\,exp\left(-\frac{R_c}{\gamma_\beta\;\gamma_f\;H_{m0}\;(0.33 + 0.022\;\xi_0)}\right) \qquad (2.6)$$

and standard deviation σ of coefficient a = 0.12 : σ = 0.24

It should be mentioned that the models proposed by TAW (2002) enclose a lot of information on the structure geometry. This is achieved by the reduction factors, accounting for various influences.

Bradbury and Allsop (1988) propose a model of type B to describe overtopping at rock armoured sloping structures, see eq. (2.7). The dimensionless parameters Q* and R* enclose the same influencing parameters as included in Owen's model (1980), see eq. (2.3).

$$\frac{q}{g\,H_s\,T_m} = a\,.\left(\frac{R_c^2}{H_s\,T_m\sqrt{g\,H_s}}\right)^{-b} \tag{2.7}$$

The model is based on approximately 240 model tests on rock armoured, impermeable slopes with crown walls. The generalised profile is shown in figure 2.3.

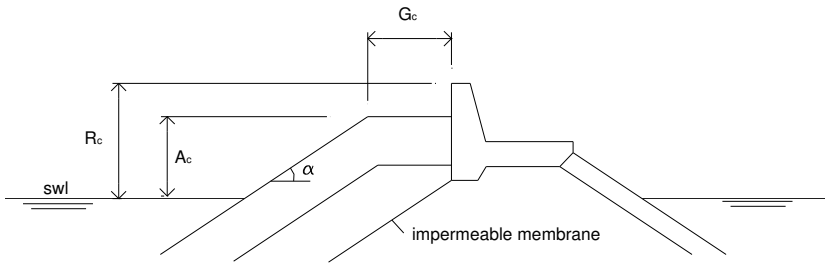

Figure 2.3 Generalised profile of tests by Bradbury and Allsop (1988)

The fitted coefficients a and b account for the crest width G_c , the crest freeboard R_c and the armour crest freeboard A_c . The slope of the structure is constant for all tests, i.e. cotα = 2. Values of G_c/H_s = 0.79 - 1.7 correspond to a crest width of three stone diameters, values of G_c/H_s = 1.6 - 3.3 correspond to a crest width of 6 stone diameters. Table 2.3 presents the values for a and b proposed by Bradbury and Allsop (1988).

Table 2.3 Values for parameters a and b for rock armoured slopes (Bradbury and Allsop, 1988)

G_c / H_s	G_c / R_c	A_c / R_c	$a \cdot 10^9$	b
0.79 - 1.7	0.58	0.21	3.6	4.4
	0.75	0.28	6.7	3.5
	0.83	1.00	1.30	3.8
	0.88	0.32	1.8	3.6
	1.07	0.39	5.3	3.5
	1.07	0.71	1.6	3.2
	1.07	1.00	0.37	2.9
1.6 - 3.3	2.14	0.39	1.0	2.8

With reference to the research performed by Bradbury and Allsop (1988), **Aminti and Franco (1988)** prescribe additional values for the empirical parameters a and b. Testing of typical breakwater cross-sections comparable with figure 2.3 is on the basis (one sea state). Values of the parameters a and b are determined for various armour layers, structure slopes and crest widths, see table 2.4.

Table 2.4 Values for parameters a and b for rock armoured slopes (Aminti and Franco, 1988)

armour type	cotα	G_c / H_s	$a \cdot 10^8$	b
rocks	2.00	1.10	17	2.41
		1.85	19	2.30
		2.60	2.3	2.68
	1.33	1.10	5.0	3.10
		1.85	6.8	2.65
		2.60	3.1	2.69
cubes	2.00	1.10	8.3	2.64
		1.85	15	2.43
		2.60	84	2.38
	1.33	1.10	62	2.20
		1.85	17	2.42
		2.60	1.9	2.82
tetrapods	2.00	1.10	1.9	3.08
		1.85	1.3	3.80
		2.60	1.1	2.86
	1.33	1.10	5.6	2.81
		1.85	1.7	3.02
		2.60	0.92	2.98

Also in **Pedersen and Burcharth (1992)** and **Pedersen (1996)** research on overtopping at comparable structure types is described, i.e. rock armoured permeable slopes with crown walls are considered.
Similar to Bradbury and Allsop (1988) and Aminti and Franco (1988) the final model prescribed by Pedersen (1996) belongs to type B. However, different dimensionless parameters are proposed:

$$\frac{q\,T_m}{L_{0m}^2} = 3.2 * 10^{-5}\ \frac{H_s^5}{R_c^3\ A_c\ G_c\ \cot\alpha} \tag{2.8}$$

and standard deviation σ of factor a = $3.2 * 10^{-5}$: σ = $0.3 * 10^{-5}$

The model is based on over 370 tests. The dimensionless discharge Q* only takes into account the mean wave period. The significant wave height is included in the dimensionless crest freeboard R*. In addition, this last parameter contains the crest width G_c , the armour crest freeboard A_c and the structure slope α.
In contrast with previous models, the model by Pedersen (1996) includes the dominating structural parameters into the model, leading to only one equation with fixed values for the fitted parameters. According to Pedersen (1996), eq. (2.8) gives conservative estimates for small overtopping discharges.

Hebsgaard et al. (1998) investigate overtopping at traditional rubble mound breakwaters without superstructure. All tests are carried out with quarry rock as armour. The derived expression by Hebsgaard et al. (1998) is of type A, see eq. (2.9). Also the influence of oblique long-crested wave attack, β > 0°, is searched for and included.

$$\frac{q}{ln(s_{0p})\sqrt{g\ H_s^3}} = -0.3\ .\ exp\left(\frac{-1.6\ (\cot\alpha)^{0.3}\ (2\ R_c + 0.35\ G_c)}{\gamma_f\ H_s\ \sqrt{\cos\beta}}\right) \tag{2.9}$$

where γ_f is a factor determined to account for the type of armour.
Eq. (2.9) is originally set up for rock armoured slopes, but limited testing of the expression by Hebsgaard et al. (1998) results in additional values for γ_f for artificial armour units (see Hebsgaard et al., 1998).
The dimensionless discharge Q* includes the wave height as well as the wave period. The dimensionless crest freeboard encloses the wave height, the crest width G_c , the slope of the structure α, and in addition the influence of the angle of wave attack and the armour type is included. Comparable to the model proposed by Pedersen (1996), Hebsgaard et al. (1998) include all tested influencing parameters into their model.

Ahrens and Heimbaugh (1986, 1988) perform overtopping tests on several seawall and revetment designs. For all structure types, Ahrens and Heimbaugh (1986, 1988) propose the same three overtopping models, see eqs. (2.10), (2.11) and (2.12). A part of the tested structures concern sloping structures, but composite structure types and vertical walls are also tested. Consequently, the models proposed by Ahrens and Heimbaugh (1986, 1988) are also mentioned in section 2.2.1.2, describing overtopping models for vertical structures.
The first model considers the dimensional overtopping discharge q as a function of R*. The second model considers a dimensionless overtopping discharge Q* as a function of R* (i.e. type A). The third model is the most complex model and adds an additional dimensionless parameter X* to model 2.

Model 1 : $q = a \cdot \exp(-b \cdot R^*)$ (2.10)
Model 2 : $Q^* = a \cdot \exp(-b \cdot R^*)$ (2.11)
Model 3 : $Q^* = a \cdot \exp(-b \cdot R^* - c \cdot X^*)$ (2.12)

where $Q^* = \frac{q}{\sqrt{g\, H_s^3}}$ and $R^* = \frac{R_c}{\left(H_s^2\, L_{0p}\right)^{1/3}}$.

The parameter X* is a dimensionless parameter, which is determined by Ahrens and Heimbaugh (1986, 1988) for each dataset as the parameter which improves the predictive ability of model 3 over model 2 most.
Similar to the model proposed by Van der Meer (1993) for surging wave conditions, the dimensionless discharge parameter Q* contains only a characteristic wave height parameter. The dimensionless crest freeboard R* on the other hand contains a characteristic period parameter in addition. For the sloping and composite structure types, Ahrens and Heimbaugh (1986, 1988) propose dimensionless parameters $X^* = (s_{0p})^{0.5}$, B/L_{0p} or H_s/h_b , where B and h_b refer to the width respectively depth of a present berm.

The results are presented by Ahrens and Heimbaugh (1986, 1988) with specific values for the fitted coefficients a, b and c (this last one only for model 3) for each structure type, which explains why the values are not included in this thesis. Moreover, Ahrens and Heimbaugh (1986, 1988) find that small changes in geometry configuration can have an important influence on the overtopping rate, which confirms that one should be careful when applying the developed models to structure types with (even slightly) varying structure characteristics.

2.2.1.2 Vertical structures

Comparable to table 2.1 for sloping structures, an overall view of the considered regression models for vertical structures is given in table 2.5.

Table 2.5 Simple regression models for vertical structures

	Model type [1]	Q*	R*
Ahrens and Heimbaugh (1986, 1988)	Type A	$\frac{q}{\sqrt{g\,H_s^3}}$	$\frac{R_c}{\left(H_s^2\,L_{0p}\right)^{1/3}}$
Franco et al. (1994, 1999)	Type A	$\frac{q}{\sqrt{g\,H_s^3}}$	$\frac{R_c}{H_s}\cdot\frac{1}{\gamma}$
Allsop et al. (1995)		general + reflecting waves : h* > 0.3	
	Type A	$\frac{q}{\sqrt{g\,H_s^3}}$	$\frac{R_c}{H_s}$
		impacting waves : h* ≤ 0.3	
	Type B	$\frac{q}{\sqrt{g\,h^3}\,h^{*2}}$	$\frac{R_c}{H_s}.h^*$
Besley et al. (1998)		impacting waves : h* ≤ 0.3 large mound : d* ≤ 0.3	
	Type B	$\frac{q}{\sqrt{g\,d^3}\,d^{*2}}$	$\frac{R_c}{H_s}.d^*$

[1] see eqs. (2.1) and (2.2)

The research performed by **Ahrens and Heimbaugh (1986, 1988)** is mentioned once more as they consider overtopping at a simple vertical wall (with a small recurve) as well. The three proposed overtopping models were given in the previous section, i.e. eqs. (2.10), (2.11) and (2.12). The parameter X* is determined as R_c/h for the vertical wall.

Franco et al. (1994) study the overtopping response of various caisson breakwaters. Several series of model tests are considered (see Franco, 1993 and 1994). The studied structures consist of traditional vertical-face caissons, perforated ones, caissons with shifted sloping parapets and caissons with a rubble mound protection (i.e. composite structure types).
Franco et al. (1994) start from a model to describe overtopping at vertical walls identical to the model of TAW (2002) for surging wave conditions on smooth dikes,

i.e. type A, with the same dimensionless parameters. The following equation, based on tests within the range $0.9 < R_c/H_s < 2.3$ and for relatively deep water, is proposed:

$$\frac{q}{\sqrt{g\,H_s^3}} = 0.2\,.\,exp\left(-4.3\,.\,\frac{R_c}{H_s}\,.\,\frac{1}{\gamma}\right) \qquad (2.13)$$

The value of the influencing parameter γ depends on the specific structure geometry (see Franco et al., 1994).
Franco et al. (1994) conclude that the overtopping of horizontally composite breakwaters is influenced by porosity, slope, width and elevation of the mound.

Based on additional model tests, **Allsop et al. (1995)** find that eq. (2.13) of Franco et al. (1994) underestimates overtopping discharges for larger values of R_c/H_s. As the bathymetry and the crest of the model structure are fixed during testing, larger values of R_c/H_s correspond to smaller values of h/H_s. According to Allsop et al. (1995) effects of wave breaking are on the origin of the larger overtopping discharges for these smaller values of h/H_s.
Initially, Allsop et al. (1995) propose the same model as Franco et al. (1994) to predict overtopping at vertical walls, with new fitted parameters, i.e.:

$$\frac{q}{\sqrt{g\,H_s^3}} = 0.03\,.\,exp\left(-2.05.\,\frac{R_c}{H_s}\right) \qquad (2.14)$$

Eq. (2.14) is valid within a wider range, i.e. $0.03 < R_c/H_s < 3.2$, and in deep water as well as in shallow water. For values of $R_c/H_s > 1$ significantly higher overtopping discharges are predicted compared to Franco et al. (1994).

Further research by Allsop et al. (1995) shows that the overtopping performance of vertical walls is dependent upon the type of incident wave conditions. In deep water the waves generally hit the structure and are reflected back seawards, i.e. so-called 'reflecting' waves. In limited water depth the waves are inclined to break over the seawall, i.e. so-called 'impacting' waves.
Allsop et al. (1995) define a wave parameter which dictates whether waves at the structure are dominating reflecting or impacting, i.e.:

$$h^* = (h/H_s)\,.\,(2\pi h/gT_m^2) \qquad (2.15)$$

where h is the water depth in front of the vertical wall.

Waves are defined as dominating reflecting when h* > 0.3 and dominating impacting when h* ≤ 0.3.
For reflecting waves, i.e. data with h* > 0.3, Allsop et al. (1995) propose to use eq. (2.14) where the parameter values of a and b are replaced:

$$\frac{q}{\sqrt{g\,H_s^3}} = 0.05\,.\,exp\left(-2.78\,.\,\frac{R_c}{H_s}\right) \tag{2.16}$$

where $0.03 < R_c/H_s < 3.2$.
For impacting waves, i.e. data with h* ≤ 0.3, a new model of type B is proposed, composed of new dimensionless parameters, including h*:

$$\frac{q}{\sqrt{g\,h^3\,h^{*2}}} = 1.37\,.\,10^{-4}\left(\frac{R_c}{H_s}\,.\,h^*\right)^{-3.24} \tag{2.17}$$

where $0.05 < \frac{R_c}{H_s}\,.\,h^* < 1.00$.
This implies that the water depth at the structure as well as the wave period have an additional influence on overtopping for impacting waves.

In case of impacting waves, **Besley et al. (1998)** propose an adapted overtopping model of type B, which accounts for the influence of a large mound present in front of a vertical wall. A large mound is defined as a mound with a value of d* ≤ 0.3, with:

$$d^* = (d/H_s)\,.\,(2\pi h/gT_m^2) \tag{2.18}$$

where d refers to the water depth on the mound (which is situated below swl).
Following model is proposed:

$$\frac{q}{\sqrt{g\,d^3\,d^{*2}}} = 4.63\,.\,10^{-4}\left(\frac{R_c}{H_s}\,.\,d^*\right)^{-2.79} \tag{2.19}$$

where $0.05 < \frac{R_c}{H_s}\,.\,d^* < 1.00$.
The water depth on the mound is an additional influencing parameter in this case.

A small mound, defined as having a value of d* > 0.3, is found to have little effect on the overtopping phenomenon by Besley et al. (1998) and should not be considered.

Bruce et al. (2001) extend the prediction method by Allsop et al. (1995) for impacting waves on battered walls (1:10 or 1:5). Eq. (2.17) is proposed with modified coefficients for both types of walls (see Bruce et al., 2001).

In addition to the research performed by Franco et al. (1994), further research by **Franco and Franco (1999)** leads to new values for the parameters a, b and γ in eq. (2.13). The values result from the reanalysis of the data used by Franco et al. (1994), with additional results of 3D model studies performed at DH (Delft Hydraulics) in 1994 by a team of Italian, Danish and Dutch researchers, see Franco et al. (1995) and Franco (1996).
Eq. (2.20) shows the new model proposed by Franco and Franco (1999) for overtopping at vertical walls. The model is extended for the effect of oblique and short-crested waves, and variations of the wall geometry (permeable, with nose).

$$\frac{q}{\sqrt{g\,H_s^3}} = 0.082\,.\,exp\left(-3\,.\,\frac{R_c}{H_s}\,.\,\frac{1}{\gamma}\right) \qquad (2.20)$$

and standard deviation σ of factor b = 3 : σ = 0.26

The influencing factor γ is composed of two separate influencing factors, i.e. γ_β and γ_s, which account for the influence of oblique and short-crested waves respectively the influence of the front geometry of the breakwater. The factor γ_β differs from the one proposed by TAW (2002). However, similar to TAW (2002), the proposed values for γ_β account for the angle of wave attack β, and in addition distinguish short-crested waves from long-crested waves. For values of these factors is referred to Franco and Franco (1999).
Eq. (2.20) is based on tests in relatively deep water with $0.3 < R_c/H_s < 2.7$.

In figure 2.4 a graphical comparison between the proposed regression formulae for overtopping at simple vertical walls is shown. As all formulae have their own restricted range of applicability, corresponding to the parameter ranges of the model tests on which the model is based, the formulae should not be used for the entire range of R_c/H_s represented on the figure. However, to facilitate comparison, the lines are extended up to $R_c/H_s = 0$ at the left side and up to $Q^* = 10^{-6}$ at the right side.

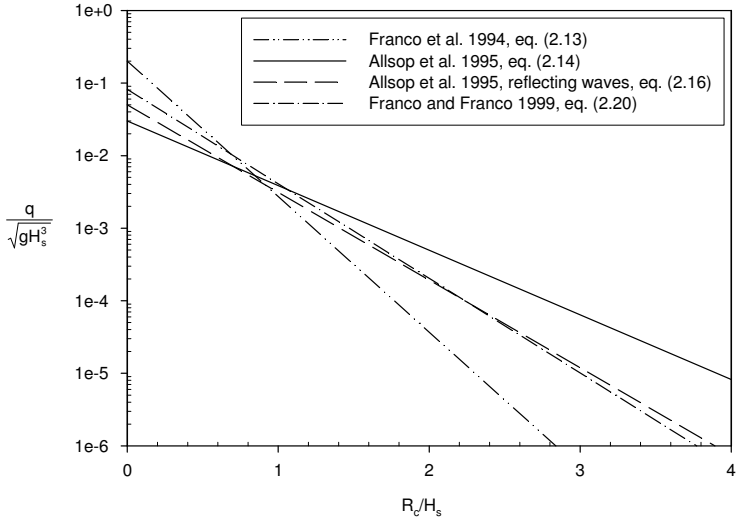

Figure 2.4 Comparison of simple regression models for vertical walls

For values of $R_c/H_s > \approx 1$, Franco and Franco (1999) predict overtopping values for simple vertical walls in between the older formula of Franco et al. (1994) and the generally applicable formula of Allsop et al. (1995). As shown in figure 2.4, eq. (2.20) of Franco and Franco (1999) is about the same as eq. (2.16) of Allsop et al. (1995) set up for reflecting waves, which is reasonable as Franco and Franco (1999) consider relatively deep water conditions.

2.2.1.3 Influencing factors

The majority of existing regression formulae mentioned in section 2.2.1.1 and section 2.2.1.2 make use of a restricted number of parameters to determine the overtopping discharge.

For sloping structure types, the dimensionless discharge parameter Q* and the dimensionless crest freeboard parameter R* are often composed of the overtopping discharge q, the crest freeboard R_c and a characteristic wave height and wave period. However, a wave period parameter is not noticed in all models. In TAW (2002) for example no period parameter is mentioned in the model for surging wave conditions.

Additionally, parameters describing the structure geometry more specifically are sometimes added. The structure slope α, the crest width G_c , the armour crest freeboard A_c , the berm width B and the berm depth h_b are such parameters. These structural parameters may be added as direct parameters in the equation (e.g. Pedersen, 1996, Hebsgaard, 1998) or may be present in correction factors added

to the equation (e.g. TAW, 2002). If lacking, these parameters are sometimes accounted for by assigning various values to the empirical coefficients a and b in eqs. (2.1) and (2.2) for different discrete values of these structural parameters. The models proposed by Owen (1980), Bradbury and Allsop (1988) and Aminti and Franco (1988) are such examples.
Besides the above mentioned influencing factors sometimes a correction factor is present to account for

- the roughness (and related permeability) of the structure and
- oblique wave attack and (sometimes) short-crestedness of the waves.

For vertical structure types the same basic parameters are included in the dimensionless discharge parameter Q* and the dimensionless crest freeboard parameter R*, i.e. the overtopping discharge q, the crest freeboard R_c and a characteristic wave height and wave period. A wave period parameter is not always included.
The water depth in front of the vertical wall h, or on the mound in front of it d, are noticed as additional parameters directly present in the equations.
Finally, correction factors are added to the models by Franco et al. (1994) and Franco and Franco (1999) to account for

- structure characteristics such as the presence of a small recurve, a perforated front and deck, a typical crest configuration… and
- oblique wave attack and short-crestedness of the waves.

The influence of oblique wave attack and short-crestedness of the waves on overtopping at vertical walls differs from its influence on sloping structure types (see Franco and Franco, 1999).

However, apart from the mentioned studies, much more research on influencing factors for overtopping has been performed. Additional guidance to account for specific influences of parameters which are not considered in the regression formulae is the result. It is not the aim to discuss the effect of all these parameters in detail in this thesis. Only a summary of influencing factors and most important references to the research describing these factors are given.

For sloping structures, the influence of the combined effect of roughness and permeability of the structure on the overtopping phenomenon is studied quite extensively. The first γ_f -values are proposed by Owen (1980) and concern factors originally set up for run-up. Later also De Waal and Van der Meer (1992, more recent TAW, 2002) study this subject regarding overtopping with run-up measurements on the basis. Hebsgaard et al. (1998) derive limited γ_f -values from overtopping measurements. The latest research on the effect of roughness and permeability of slopes on overtopping is performed within the CLASH project, see Pearson et al. (2004b). Besides new model tests on overtopping, also previous

overtopping measurements by Aminti and Franco (1988) are considered in this research.
The results obtained by Pearson et al. (2004b) are used further in this thesis (see chapter 3, section 3.6.3.8). More detailed information is given in the corresponding section.

The influence of oblique wave attack and short-crestedness of the waves on wave overtopping depends on the structure type. The research performed by Owen (1980), Hebsgaard et al. (1998), Franco and Franco (1999), and TAW (2002, originating from De Waal and Van der Meer, 1992) has been mentioned before. The work performed by Juhl and Sloth (1994), Banyard and Herbert (1995), Pilarczyk and Zeidler (1996), and Sakakiyama et al. (1996) may be added.

Wind is another factor worthwhile to be mentioned as having a possible influence on wave overtopping. De Waal et al. (1992, 1996), Ward et al. (1992, 1994), Medina et al. (1998) and González-Escriva et al. (2002) all report on the influence of wind on overtopping.

The influence of recurve walls on overtopping, both on top of sloping structures and as a recurve of simple vertical walls, is also studied. Bradbury and Allsop (1988), Owen and Steele (1991), Juhl (1992), Banyard and Herbert (1995), Herbert and Owen (1995), Cornett et al. (1999), Kortenhaus et al. (2001), Kortenhaus et al. (2003), TAW (2003), and Pearson et al. (2004a) are referred to for this subject. Few direct guidance on the influence of recurve walls is present at the moment of writing this thesis. However, studies are still going on for this subject.

The influence of the shape of the spectrum on overtopping is accounted for in TAW (2002), by advising the use of the spectral parameters H_{m0} and $T_{m-1,0}$. The parameter H_{m0} is a parameter representative for the incident total wave energy, whereas Van Gent et al. (2001a) show that the parameter $T_{m-1,0}$ is the best period parameter to describe phenomena as wave run-up and overtopping.

Finally, the positioning of armour units on a slope is referred to as influencing overtopping measurements by Medina et al. (2003).

More detailed information on the influencing factors discussed in this section is available in the corresponding publications from the reference list.

2.2.2 Models with overtopping as function of run-up

Some overtopping models write the overtopping discharge as a function of the wave run-up levels which would occur if the structure was high enough to prevent overtopping.

Focussing on models based on irregular wave overtopping measurements, table 2.6 gives an overall view of models considered in this section. It is possible to consider the mentioned equations as regression models of type A, i.e. eq. (2.1) from section 2.2.1. Doing so, the corresponding dimensionless parameters Q* and R* are represented in table 2.6.

Table 2.6 Models with overtopping as function of run-up

	Model type [1]	Q*	R*
Weggel (1976) + Ahrens (1977)	Type A	$\frac{q}{\sqrt{g\,H_0'^3}}$	$tanh^{-1}\left(\frac{R_c}{Ru}\right)$
De Waal and Van der Meer (1992)	Type A	$\frac{q}{\sqrt{g\,H_s^3}}$	$\frac{Ru_{2\%} - R_c}{H_s}$
Schüttrumpf (2001)	Type A	$\frac{q}{\sqrt{2\,g\,H_s^3}}$	$\frac{R_c}{Ru_{2\%}}$

[1] see eqs.(2.1) and (2.2)

Weggel (1976) is the first to develop an empirical model to predict overtopping based on run-up, see eq. (2.21). The overtopping tests by Saville (1955), who measures overtopping of regular waves at smooth (sloping and vertical) structures, are on the basis of it. Consequently, the model of Weggel (1976) is only valid for monochromatic waves.

$$\frac{q}{\sqrt{g\,H_0'^3}} = a.exp\left\{-\left(\frac{0.217}{b'}\right).tanh^{-1}\left(\frac{R_c}{Ru}\right)\right\} \tag{2.21}$$

where $0 \leq R_c / Ru < 1$, where H'_0 is the equivalent deep water wave height and Ru the run-up on the structure that would occur if the structure was high enough to prevent overtopping. The parameters a and b' are empirically determined coefficients which depend on the incident wave characteristics and on the structure geometry. Values of a and b' are given by Weggel (1976) for different structure slopes, vertical walls and recurve walls. It is clear that the parameter b from eq. (2.1) equals 0.217/b'.

Ahrens (1977) extrapolates Weggel's equation to irregular waves by summing up the overtopping contributions from each run-up in an irregular sea, keeping the parameters a and b constant. Ahrens (1977) assumes therefore that wave run-up is Rayleigh distributed.
The assumptions of Ahrens on which he relies to develop a model for irregular wave overtopping are found to be unacceptable. The Rayleigh distribution of run-up is only correct in case of deep water and also the assumption of constant values of a and b is found by some researchers to be unacceptable (see Douglass, 1986, and Medina et al. 2002).

In **De Waal and Van der Meer (1992)** overtopping is related to a 'shortage in crest height' ($Ru_{2\%}$ - R_c)/H_s instead of to R_c /H_s as proposed later by Van der Meer (see Van der Meer, 1993, and more recent TAW, 2002: eq. (2.5a) and (2.5b)). De Waal and Van der Meer (1992) propose following model for overtopping at smooth dikes:

$$\frac{q}{\sqrt{gH_s^3}} = 8.10^{-5}\ exp\left(3.1 . \frac{Ru_{2\%} - R_c}{H_s}\right) \tag{2.22}$$

where $Ru_{2\%}$ is the wave run-up exceeded by 2% of the wave run-up events on a non-overtopped slope.
This early model proposed by De Waal and Van der Meer (1992), gives similar results as the model developed later by Van der Meer (1993). However, eq. (2.22) shows a more limited range of applicability than eq. (2.5a) and (2.5b), i.e. for large overtopping discharges and for values of R_c much lower than $Ru_{2\%}$ eq. (2.22) is assessed as less reliable.
Considering eq (2.22) as a regression model of type A (see eq. (2.1)) results in values of coefficients a and b of 8.10^{-5} respectively -3.1.

A recent overtopping model expressing the overtopping discharge as a function of the fictitious run-up level, is proposed by **Schüttrumpf (2001)**, describing overtopping of irregular waves at smooth dikes:

$$\frac{q}{\sqrt{2\ g\ H_s^3}} = 0.038 . \xi_m . exp\left(-5.5 . \frac{R_c}{Ru_{2\%}}\right) \qquad \text{for } \xi_m < 2 \tag{2.23a}$$

$$\frac{q}{\sqrt{2\ g\ H_s^3}} = \left(0.096 - \frac{0.160}{\xi_m^3}\right) . exp\left(-5.5 . \frac{R_c}{Ru_{2\%}}\right) \qquad \text{for } \xi_m \geq 2 \tag{2.23b}$$

where $Ru_{2\%}$ is the wave run-up value exceeded by 2% of the wave run-up events on a non-overtopped slope. Considering eqs. (2.23a) and (2.23b) as regression models of type A (see eq. (2.1)) results in a value of coefficient a dependent on the breaker parameter ξ_m and a value of coefficient b = 5.5.

The model proposed by Schüttrumpf (2001) is developed in a way that the boundary conditions are fulfilled, i.e. for tests with no freeboard (R_c = 0m) and for tests without overtopping ($R_c > Ru_{2\%}$). The equations are developed in two phases. In a first phase the weir-analogy (see next section) is used to determine an expression for the coefficient a, fulfilling the boundary-condition for R_c = 0m. In a second phase the coefficient b is determined, fulfilling the boundary-condition for $R_c > Ru_{2\%}$.

2.2.3 Weir-models

Overtopping models which are based on the analogy of the flow over a weir are called 'weir-models'. Two weir-models are considered in this section, both corresponding to regression models of type B (see eq. (2.2), section 2.2.1). Table 2.7 shows the corresponding dimensionless parameters Q* and R*.

Table 2.7 Weir-models

	Model type [1]	Q*	R*
Kikkawa (1968)	Type B	$\frac{q}{\sqrt{2\,g\,H_0^3}}$	$\frac{kH_0 - R_c}{kH_0}$
Hedges and Reis (1998)	Type B	$\frac{q}{\sqrt{g\,(CH_s)^3}}$	$\frac{CH_s - R_c}{CH_s}$

[1] see eqs.(2.1) and (2.2)

The flow rate over a weir is given by the Poleni-formula, i.e.:

$$Q = \frac{2}{3}\,\theta\,B\,\sqrt{2g}\;y^{3/2} \tag{2.24}$$

where Q is the instantaneous discharge over the weir (in m^3), θ is the discharge coefficient, B is the width of the weir and y is the energy height, composed of kinetic and potential energy.

Kikkawa (1968) introduces the weir-model to calculate overtopping at seawalls as follows:

$$q'(t) = \frac{2}{3}\,\theta\,\sqrt{2g}\;(E(t) - R_c)^{3/2} \qquad \text{if } E(t) > R_c \tag{2.25a}$$

$$q'(t) = 0 \qquad \text{if } E(t) \le R_c \tag{2.25b}$$

where q'(t) is the instantaneous discharge per unit length of the seawall (in m^3/m), θ is the discharge coefficient, E(t) is the energy height function and t is the time. The energy height function E(t) is approximated by the surface elevation above swl at the seawall η(t), i.e. the kinetic energy height is ignored.
Kikkawa (1968) assumes regular waves and expresses the surface elevation η(t) at the location of the seawall as a sine function, or even more simple, as a linear approximation of the sine function with amplitude kH_0 (see figure 2.5). H_0 refers to

the deep water wave height of the regular wave, where k is a factor to be determined empirically.

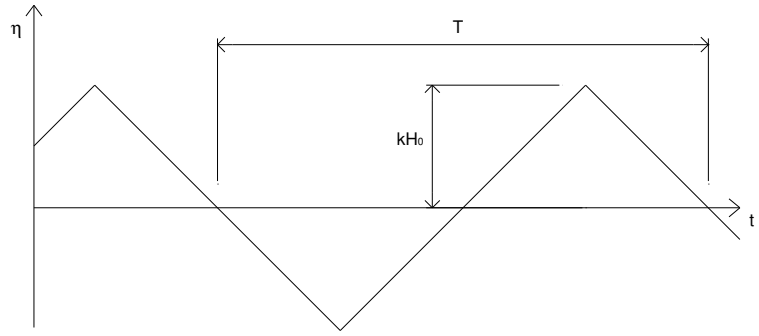

Figure 2.5 Linear approximation of surface elevation at the location of the seawall

If the surface elevation η(t) is approximated by a linear function as shown in figure 2.5, integration over the wave period T leads to the following expression:

$$\frac{q}{\sqrt{2gH_0^3}} = \frac{2}{15}\,\theta\, k^{3/2}\left(1-\frac{R_c}{kH_0}\right)^{5/2} \qquad \text{for } 0 \le R_c < kH_0 \qquad (2.26a)$$

$$\frac{q}{\sqrt{2gH_0^3}} = 0 \qquad \text{for } R_c \ge kH_0 \qquad (2.26b)$$

Kikkawa (1968) determines the value of the discharge coefficient θ = 0.5 for a rectangular weir. The parameter k is a function of the structure geometry and the wave steepness.
The proposed model only predicts overtopping for $R_c < kH_0$.

Hedges and Reis (1998) suggest a regression model for wave overtopping of random waves at a sloping structure of a form based on eq. (2.26a) and (2.26b), i.e.:

$$\frac{q}{\sqrt{g(CH_s)^3}} = A\left(1-\frac{R_c}{(CH_s)}\right)^B \qquad \text{for } 0 \le \frac{R_c}{CH_s} < 1 \qquad (2.27a)$$

$$\frac{q}{\sqrt{g(CH_s)^3}} = 0 \qquad \text{for } \frac{R_c}{CH_s} \ge 1 \qquad (2.27b)$$

where A, B and C are regression coefficients dependent on the structure geometry, and where CH_s = Ru_{max} = the maximum wave run-up induced by the random waves.

The parameter A represents the dimensionless overtopping discharge at the structure when the freeboard is zero. The parameter B determines the shape of the overtopping model. Hedges and Reis (1998) estimate the values of A and B based on the overtopping data of Owen (1980).
The parameter C determines the maximum run-up level and is consequently dependent on the level of confidence associated with the prediction of the maximum run-up level. If the parameter C is changed, corresponding changes occur in the values of A and B. As the data from Owen do not provide zero overtopping measurements and only few small overtopping measurements, the parameter C is estimated by Hedges and Reis (1998) from run-up measurements on slopes for which there is no overtopping.
Hedges and Reis (1998) propose regression coefficients for various structure slopes and levels of confidence of the maximum run-up level. In addition, 2 types of fitting procedures are considered, resulting in different values of the empirical coefficients. For details Hedges and Reiss (1998) is referred to.

2.2.4 Graphical models

Some researchers present diagrams containing overtopping information in a graphical form. A disadvantage of graphical models is that interpolation of the diagrams by the user is required.

The design diagrams of **Goda (1985)** are well-known. They are set up for the estimation of overtopping discharges at simple vertical walls and block mounded seawalls, i.e. vertical walls with a rubble mound structure composed of concrete armour units in front of these. The diagrams are based on model tests with irregular waves (Goda, 1975).
In each graph, a dimensionless overtopping discharge Q* is represented versus a dimensionless water depth at the toe of the structure h/H_0', with in addition lines of constant dimensionless crest freeboard R*, with

$$Q^* = \frac{q}{\sqrt{2gH_0'^3}} \tag{2.28a}$$

$$R^* = \frac{R_c}{H_0'} \tag{2.28b}$$

where H'_0 refers to the equivalent deep water wave height (see Goda, 1985).
For both structure types, simple vertical walls and block mounded vertical walls, 6 design graphs are set up: bottom slopes of 1:10 and 1:30 are considered in combination with 3 values of the wave steepness, H'_0/L_0 = 0.012, 0.017 and 0.036. L_0 refers to the deep water wave period based on H'_0 and $T_{1/3}$.

Herbert (1993) extends the work of Goda (1985) to bottom slopes of 1:100 and values of s_{0m} = 0.06.

Goda (1985) (and later also Herbert, 1993) uses the deep water wave characteristics in combination with the assumption of a constant bottom slope to determine overtopping discharges. The use of a characteristic deep water wave height is in contrast with the use of a characteristic wave height at the toe of the structure, considered in the majority of overtopping studies.

Jensen and Sorensen (1979) also make use of graphical overtopping models. They present 7 graphs for overtopping at 7 different structures. Their graphs result from model tests on sloping breakwaters with different crest configurations and armour units. For one series of model tests corresponding prototype measurements are available.

In each graph a dimensionless overtopping discharge Q* is represented versus a dimensionless crest freeboard R*, with:

$$Q^* = \frac{q\,T_m}{(B^*)^2} \tag{2.29a}$$

$$R^* = \frac{H_s}{R_c} \tag{2.29b}$$

where B* is a representative breakwater dimension, defined by Jensen and Sorensen (1979) as the horizontal distance from the point where the armour layer intersect with the swl to the limit of the reclamation or to the rear side of the crown wall. It is possible to write the parameter B* in function of 3 structure parameters, i.e. $B^* = G_c + \cot\alpha.A_c$, where G_c is the crest width, A_c the armour crest freeboard and α the slope of the structure.

In some of the graphs additional influencing parameters are marked, i.e. a dimensionless wind speed $U^* = \frac{U}{\sqrt{gB^*}}$ (where U is the wind speed), the slope of the structure α and a dimensionless wave period parameter $T^* = \frac{T_m}{\sqrt{B^*/g}}$.

The waves are measured at a limited distance in front of the breakwater during testing, and are not depth-limited.

The results of Jensen and Sorensen (1979) show that the logarithm of Q* is linearly dependent on R*. They find that the effect of wind is most pronounced for small values of R*, while for high sea states and for high water levels wind has no influence on the amount of overtopping.

The prototype measurements of Jensen and Sorensen (1979) are in agreement with their model test results.

2.3 Numerical models

In this section numerical models capable of simulating wave overtopping at structures are considered. Only the principle of present numerical models is explained, without going into detail to the subject. This section is based on Ingram (2005).

The advantage of numerical models compared to the discussed empirical models is the general applicability: theoretically any validated numerical model can be configured for any structure type and within the overall range covered. However, precise numerical models require a huge amount of computation time, even to simulate only a few waves. Simpler descriptions of the fluid dynamic equations result in much faster calculations, but at cost of the accuracy of the model and moreover, they result in restricted applicability.

Numerical models for overtopping work by solving a system of governing fluid dynamic equations in order to provide a computer model of either a wave flume or a wave basin as required. Ingram (2005) distinguishes two different classes of numerical models, i.e. shallow water models versus surface capturing models.
The first class of models solves the depth integrated non-linear shallow water equations, abbreviated 'NLSW', whereas the second class of models solves the Navier-Stokes equations through the full height of the water column. This second class of models is much more computationally demanding.

One-dimensional shallow water equations are originally developed for near horizontal, free-surface channel flows. NLSW equations are deduced from Navier-Stokes equations by averaging over depth and assuming the pressure distribution in the vertical direction being hydrostatic. Consequently, NLSW models theoretically can only be used for shallow slopes where the vertical component of the wave flow is relatively small. However, in practice it is found that these models provide quite good results for even very steep slopes such as 5:1 and 10:1 (i.e. battered walls). A disadvantage is that the models only provide appropriate results if the position of the seaward boundary is chosen very close to the structure toe. This implies that the models require time-series of nearshore wave conditions as input, which is much more complicated to determine than deepwater time-series. However, present research suggests that careful use of such a model, run with 1000 random waves, may give reasonable estimates of overtopping discharges, i.e. within half an order of magnitude, also for quite steep structure types.
Examples of NLSW models are:

- ANEMONE (Advanced Nonlinear Engineering MOdels for the nearshore Environment), initially developed by **Dodd (1998)**,

- AMAZON, developed by the Centre for Mathematical Modelling and Flow Analysis (CMMFA) at Manchester Metropolitan University, and described by **Mingham and Causon (1998)** and **Causon et al. (2000)**,
- ODIFLOCS (One-DImensional FLOw on and in Coastal Structures) developed by **Van Gent (1994)**.

Opposite to NLSW models, models based on the solution of the Navier-Stokes equations are able to simulate the process of wave overturning, wave breaking and the formation of the overtopping jet. However, these models require quite an amount of computational time, even for simulations of only tens of overtopping waves with high performance computers. Very detailed information is available on the velocity distribution in the water column, but this also requires substantial computational time.
The seaward boundary requires a wave spectrum or the desired mono- or bi-chromatic waves directly. These wave conditions are then used to provide the local velocities in the water column. In order to minimise the computational cost, the seaward boundary also needs to be located reasonably close to the structure.
Within the Navier-Stokes models different mechanisms exist to determine the location of the free surface. The Volume of Fluid (VoF) approach (Hirt and Nichols, 1981) can be mentioned versus the free surface capturing approach (Kelecy and Pletcher, 1997).
Examples of Navier-Stokes models are:

- SKYLLA (**Van der Meer et al., 1992**), developed at Delft Hydraulics
- VOFbreak² (**Troch et al., 2003**), developed at Ghent University
- LVOF (**Li et al., 2004**), developed at Ghent University
- AMAZON-SC (**Qian et al., 2003**), developed at Manchester Metropolitan University

The Navier-Stokes models do not have restrictions on the geometry of the seawall and give good predictions of individual overtopping volumes. Due to the computational cost however, their use is restricted to only a few waves. Their principle use is therefore to provide detailed information about the overtopping process occurring at a specific structure type for specific wave conditions.

Generally, one can expect that in the near future numerical models will be used more intensively for design processes, since processor speed of PC's increases. However, one should be aware of the fact that numerical models are no simple-to-use engineering tools, but research tools which require experienced modellers to operate the numerical codes.
As numerical models are not immediately useful for the research performed in this thesis, numerical models are not further considered here.

2.4 Overtopping volume of an individual wave

The finding that overtopping events occur very unevenly distributed in time and in space, and the experience that overtopping volumes of individual waves may vary significantly, is on the basis of the recent research on individual overtopping volumes and related probability distributions.

Research by **Franco et al. (1994)** and **Van der Meer and Janssen (1995)** shows that the probability function for the overtopping volume per wave and per unit structure width, follows a Weibull distribution. The probability that the overtopping volume per unit width of an individual wave, v, is larger than a specified overtopping volume per unit width, V, is written as:

$$prob\,(v > V) = exp\left[-\left(\frac{V}{A}\right)^{b}\right] \qquad or \tag{2.30a}$$

$$V = A\left(-ln\left[prob\,(v > V)\right]\right)^{1/b} \tag{2.30b}$$

where

$$A = a\,.\,\frac{T_m\,q}{P_{ow}} \tag{2.31}$$

and where P_{ow} is the probability of overtopping per wave (= N_{ow}/N_w), with N_{ow} the number of overtopping waves and N_w the number of incoming waves. The parameters a and b are empirical parameters, dependent on the structure type and wave characteristics.

Eqs. (2.30a), (2.30b) and (2.31) show that the exceedance probability of a given volume is related to the mean overtopping discharge and the overtopping probability.

The proposed Weibull distribution in eqs. (2.30a) and (2.30b) can be used to represent extreme values of the overtopping volume V. The maximum overtopping volume per unit width, produced by one wave out of the total number of overtopping waves, is represented by:

$$V_{max} = A\left[ln\,(N_{ow})\right]^{1/b} \tag{2.32}$$

where A is given by eq. (2.31).

If the run-up levels follow a Rayleigh distribution, the probability of overtopping per wave P_{ow}, may be estimated as:

$$P_{ow} = exp\left[-\left(\frac{R_c}{cH_s}\right)^2\right] \tag{2.33}$$

where the parameter c is dependent of the structure type.

Franco et al. (1994) suggest c = 0.91 for simple vertical walls in relatively deep water.
According to **Besley (1998),** in shallow water the probability of overtopping of vertical walls is larger than obtained with c = 0.91 in eq. (2.33). Besley (1998) states that breaking wave heights are no longer Rayleigh distributed and in addition that the mechanism by which individual waves overtop the structure is no longer dominated by wave run-up. Therefore, in case of impacting waves, i.e. $h^* \leq 0.3$, see section 2.2.1.2 and eq. (2.15), with reference to Allsop (1995), Besley (1998) proposes eq. (2.34) instead of eq. (2.33), i.e.:

$$P_{ow} = 0.031\left[\left(\frac{R_c}{H_s}\right).h^*\right]^{-0.99} \tag{2.34}$$

For sloping structures Van der Meer and Janssen (1995) propose eq. (2.33) with the following expression for the parameter c:

$$c = 0.81\ \xi_{eq}\ \gamma_r\ \gamma_h\ \gamma_\beta \tag{2.35}$$

with a maximum of $c = 1.62\ \gamma_r\ \gamma_h\ \gamma_\beta$

where γ_r, γ_h and γ_β are reduction factors originally determined by Van der Meer and Janssen (1995) for run-up on smooth slopes, accounting for the slope roughness, the influence of a shallow foreshore and both oblique wave attack and directional spreading respectively. ξ_{eq} is the equivalent breaker parameter for a slope with a berm and is defined as $\gamma_b\ \xi_{op}$, where γ_b is a reduction factor for a berm (see Van der Meer and Janssen, 1995).

Analysis of model tests resulted in different values for the empirical parameters a and b in eqs. (2.30) and (2.31) for a variety of structure types.

Besley (1999) summarises different empirical values, see table 2.8. Values for vertical walls (dependent on reflecting or impacting waves) and for sloping structures are given. It is shown that the values of a and b are dependent on the wave steepness.

Table 2.8 Empirical values for parameters a and b in eqs. (2.30) and (2.31) (see Besley, 1999)

	a	b
vertical wall		
reflecting waves, $h^* > 0.3$		
$s_{0p} = 0.02$	0.74	0.66
$s_{0p} = 0.04$	0.90	0.82
impacting waves, $h^* \leq 0.3$	0.92	0.85
sloping smooth structures		
$s_{0p} = 0.02$	0.85	0.76
$s_{0p} = 0.04$	0.96	0.92

2.5 Tolerable overtopping limits

Tolerable overtopping concern overtopping which is acceptable to come over the crest of a structure under the design conditions of the structure. The limits depend primarily on the type of structure and its functionality.
Various research on tolerable overtopping limits has been performed, resulting in guidance on allowable overtopping limits, providing safety for people and vehicles on the structure on the one hand, and structural safety on the other hand. This section gives an overall view of the present knowledge on tolerable overtopping limits.

Guidance on overtopping hazards is primarily based on mean overtopping discharges. Early field studies of tolerable overtopping limits for dikes and revetments are performed by Tsuruta and Goda (1968), Goda (1970) and Fukuda, Uno and Irie (1974). These Japanese studies are on the basis of existing limits for mean overtopping discharges.
Further Jensen (1984) discusses critical values of overtopping at a breakwater. Dutch guidelines on sea dikes (RWS, 1993) indicate allowable overtopping rates for inner slopes, and Smith et al. (1994) report on full scale tests conducted on grass dikes. De Gerloni et al. (1991) and Franco et al. (1994) also investigate critical overtopping discharges, i.e. on breakwater crests for cars and people. Full scale tests as well as numerical modelling of overtopping rates which endanger people are performed by Endoh and Takahashi (1994). Finally, also Herbert (1996) provides information on prototype safety by monitoring overtopping at a vertical seawall.
Table 2.9 summarises the results of these studies and incorporates recommended limits of mean overtopping discharges which provide both safety for traffic and structures. The table is extracted from the Coastal Engineering Manual (U.S. Army Corps of Engineers, 2002).

Table 2.9 Suggested limits for mean overtopping discharges (U.S. Army Corps of Engineers, 2002)

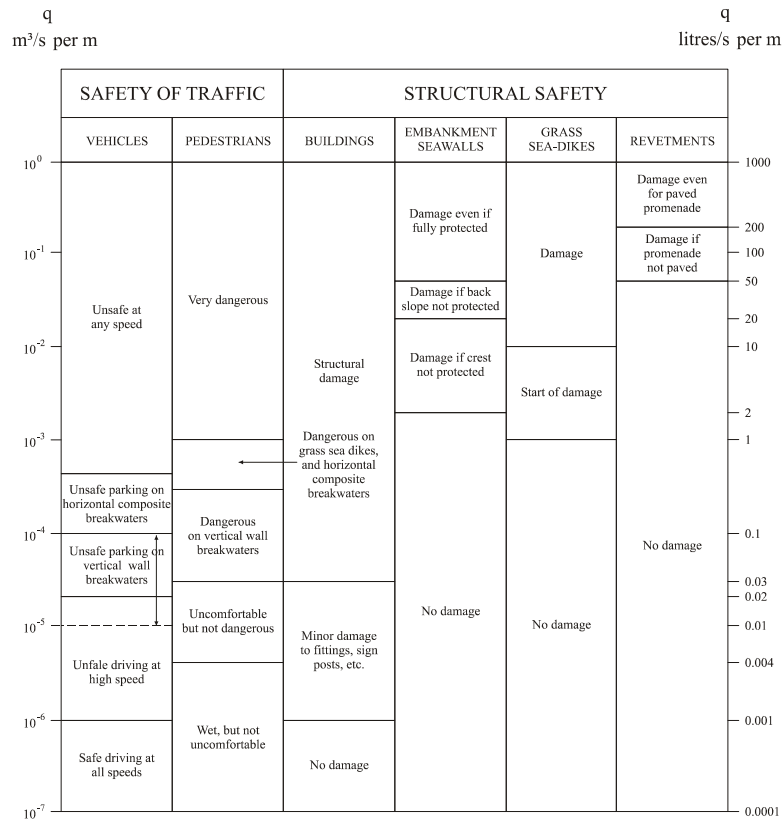

Applying table 2.9 for design of coastal structures, one should be aware of the fact that the maximum overtopping intensities might locally be up to two orders of magnitude larger than the mean overtopping discharge. In addition, also local traditions and individual opinions contribute to the assessment of what is acceptable.

Refinements to table 2.9, including tolerable peak volumes (and overtopping velocities), have been proposed.
First research on individual overtopping volumes is performed by Franco et al. (1994). They perform model tests on limiting overtopping volumes for pedestrians on caisson breakwaters and find that the critical bands of overtopping volume (being dangerous above the upper limit and safe below the lower limit) lie between 0.2 and 2 m^3/m. However, Franco et al. (1994) mention that even a concentrated jet of 0.05 m^3/m on the upper body can be enough to make a person fall down.

The full-scale tests conducted on grass dikes reported by Smith et al. (1994) result in limit discharges for trained staff on the dike of 0.01 $m^3/s/m$. The corresponding maximum volume is reported to be about 1 m^3/m. Compared to the safety limit by Franco et al. (1994) this is clearly higher. However, it is clear that safety limits may be higher for trained staff than those for other users.
In addition, it is found that the effect of individual waves is dependent on the structure geometry. Franco et al. (1994) report that the same overtopping volume is more dangerous if the breakwater is purely vertical than e.g. in case of a composite one. The difference in overflow mechanism is a probable explanation for this fact.
According to Herbert (1996), who monitors overtopping at a vertical seawall at Colwyn Bay, personnel can work safely on the crest up to 10^{-4} $m^3/s/m$. Besley et al. (1998) estimate that the corresponding maximum individual overtopping volume V_{max} is approximately equal to 0.04 m^3/m. For vehicles, discharges larger than 2.10^{-4} $m^3/s/m$ are assessed as dangerous, corresponding to approximately $V_{max} = 0.05$ m^3/m.

Bruce et al. (2002) analyse velocities of waves overtopping vertical walls at both small and large scale tests. It is found that the upward velocity u_z , non-dimensionalised by the inshore wave celerity $c_i = (gh)^{0.5}$, increases clearly for small values of h*, i.e. $h^* < 0.15$. Consequently, hazards may vary with changes of wave breaking characteristics.

Recent research on tolerable overtopping limits is performed within the framework of the CLASH project, see Bouma et al. (2004) and Allsop et al. (2005). The overall aim of this research within CLASH was the derivation/refinement of guidance on various levels of hazard imposed on people by overtopping. On the one hand, measured and hindcast events are compared with records of observed hazards. On the other hand, the risk of economic losses is studied. Table 2.10 is set up during this research and suggests, besides limits of mean overtopping discharges, also limits for peak overtopping volumes. The limits derive from a general precautionary principle informed by previous guidance and by the various observations and measurements made within the CLASH project.

For trained staff under specific conditions table 2.10 allows overtopping discharges up to 10 l/s/m. For common pedestrians these overtopping discharges may be very dangerous, which is mentioned explicitly in table 2.9. Also for vehicles under very specific conditions (i.e. driving at low speed, overtopping by pulsating flows and low levels, no falling jets), higher mean discharge limits are allowed in table 2.10.
Additionally, table 2.10 suggests limits for peak volumes of overtopping. Due to the lower frequency of the peak volumes, rather high limit volumes are found in the table.

Table 2.10 Suggested limits for mean overtopping discharges and peak volumes (Allsop et al. 2005)

Hazard type / reason	Mean discharge, q, in l/s/m	Peak volume, V_{max}[1], in l/m	Comments or other limits
Pedestrians			
Unaware pedestrian, no clear view of the sea, relatively easily upset or frightened, narrow walkway or close proximity to edge	0.03	2-5 at high level or velocity	
Aware pedestrian, clear view of the sea, not easily upset or frightened, able to tolerate getting wet, wider walkway	0.1	20-50 at high level or velocity	
Trained staff, well shod and protected, expecting to get wet, overtopping flows at lower levels only, no falling jet, low danger of fall from walkway	1-10	500 at low level	$d.u^2$ < 1-5 $m^3/s^2.m$ (with d = flow depth and u = velocity)
Vehicles			
Driving at moderate or high speed, impulsive overtopping giving falling or high velocity jets	0.01-0.05	5 at high level or velocity	
Driving at low speed, overtopping by pulsating flows at low levels only, no falling jets	10-50	1000	
Property			
Sinking small boats set 5-10m from wall, damage to larger yachts	10	1000-10000	Volumes depend on vessel position etc., form of overtopping flow and wave transmission
Significant damage of sinking of larger yachts	50	5000-50000	

[1] Overtopping at 'high level' is overtopping flying through the air, overtopping at 'low level' is overtopping flowing over or close to the promenade, velocities depend on the flow depth

2.6 Conclusion

In this chapter a literature review on wave overtopping has been given. Four groups of empirical (regression) models for the prediction of mean overtopping discharges q at various structure types are discussed in detail. Numerical models simulating wave overtopping at structures are considered rather briefly. Further individual wave overtopping volumes and admissible overtopping discharges are treated.

The specific aim of the survey in this chapter was to identify the parameters which have an influence on the overtopping phenomenon, for any structure type. Table 2.11 summarises the findings in this context. All influencing parameters mentioned in any considered overtopping model in this chapter are included in the table. In case the influencing parameter only appears through a correction factor, the corresponding correction factor is given in brackets. For the influencing characteristics which are not quantified up till now no parameter is given.

Table 2.11 Parameters in existing overtopping models influencing overtopping at coastal structures

Influencing characteristics	Parameters
Wave characteristics	
• wave height at deep water/at the toe of the structure	H_s or H_{m0} [m]
• wave period at deep water/at the toe of the structure	T_p, T_m, $T_{1/3}$ or $T_{m-1,0}$ [s]
• wave direction	β [°]
• short-crestedness of the waves	(γ_β)
Structure characteristics	
• slope of the foreshore	1:m
• slope of the structure	α [°]
• crest width	G_c [m]
• crest freeboard	R_c [m]
• armour crest freeboard	A_c [m]
• roughness/permeability of the structure (including various types of armour)	(γ_f)
• berm characteristics	h_b [m], B [m] and α_B [°], (or in γ_b)
• water depth at the toe of the structure	h [m]
• water depth on the mound in front of a vertical wall	d [m]
• positioning of armour units	-
• presence of a recurve wall	-
• dimensions of a small wall on a structure	(γ_v)
• specific front geometry of a vertical wall (e.g. porosity, nose,…)	(γ or γ_s)
Environment characteristic	
• wind	U [m/s]

The knowledge obtained in this chapter regarding the influencing parameters on wave overtopping was of direct use for the set-up of a database on wave overtopping tests (see next chapter), as each overtopping test had to be included in this database by means of a fixed number of parameters.

The concise summary of overtopping prediction methods given in this chapter, with tables and references included, can be used as 'application manual' for engineers focussing on the overtopping phenomenon.

CHAPTER 3
SET-UP OF A DATABASE ON WAVE OVERTOPPING

3.1 Introduction

This chapter discusses the set-up of the extensive CLASH database on wave overtopping at coastal structures (Van der Meer et al., 2005a, see enclosed CD-ROM).

The extensive database on wave overtopping was created in two phases. A first preliminary database, composed of overtopping information originating from before 2003, and consisting of about 6500 tests, was released within CLASH in August 2003 as an intermediate result, see Verhaeghe et al. (2003a and 2003b). In a second phase, from August 2003 to December 2004, this preliminary database was enlarged and improved to a final database, consisting of 10532 overtopping tests, originating from 163 independent test series. In this chapter a description of the set-up and contents of this extended, final database is given. The comprehensive task of gathering and screening the data is described only briefly. More detailed information on the gathering and screening process, as well as on the various preliminary methodologies preceding the final schematisation procedure can be found in the CLASH report, see Van der Meer et al. (2005b).

The purpose of the extensive database on wave overtopping entries is dual:

- The overtopping database on its own provides an inventory of the many reliable overtopping tests ever performed, independent of any place or time. Logically, the obtained inventory is restricted by the ability to find, get and screen the overtopping data within the 3 year duration of CLASH.
  The database is in the first place a useful object for researchers who concentrate on the phenomenon of overtopping. Aspects related to specific structure types can be studied separately, for example by extracting the corresponding data from the database. In addition, data can be used as validation data for new analytical or numerical research on the overtopping phenomenon.
  However, also for non-overtopping related research the database may provide useful information. The possibility to study propagating waves from deep to

more shallow water by comparing deep water wave characteristics with wave characteristics at the toe of the structure is only an example.

- More fundamentally, the overtopping database is used to develop a neural prediction method for mean overtopping discharges at coastal structures. The creation of a generic prediction method for wave overtopping, applicable for all kinds of coastal structures, was the second main objective of the CLASH project. Within the framework of this thesis and separately from the CLASH project, the neural network technique has also been examined to develop a generic overtopping prediction method. The development of this neural prediction method based upon the extensive CLASH database is described in chapter 4 of this work.

3.2 Origin of overtopping data

During the last 30 years, overtopping at coastal structures has been the subject of extensive research, resulting in a lot of overtopping information available at different universities and research institutes all over the world. The first phase of composing a database consisted therefore in collecting as much of these present data as possible. As the data were gathered within the CLASH project, a lot of data originate from CLASH partners, but also data from non-CLASH institutes within Europe as well as from outside Europe contribute to the database. The percentage of data which was received from CLASH partners in the final database amounts to approximately 80%.

Distinction could be made between publicly available data, often related to basic research and already described in literature, and confidential reports, in most cases related to overtopping tests performed for specific sites and practical situations. Approximately 75% of the available data are publicly available date, the remaining 25% are confidential data.
For the confidential data it was required in some cases to visit the involved authorities to get the necessary information. In this context, visits to Delft Hydraulics (The Netherlands), Hydraulic Research Wallingford (United Kingdom) and Modimar (Rome, Italy) were performed.

During the first phase of the set-up of the database, about 6500 tests were gathered. During the second and last phase, not only 4000 new overtopping tests were added, but also some parameters were improved, resulting in an extended ánd improved final database.

The 4000 extra overtopping tests added to the preliminary database can be subdivided in 4 groups:

1) prototype measurements of overtopping, performed within the framework of CLASH, at three European measurement sites:
   Ostia (Italy), Samphire Hoe (United Kingdom) and Zeebrugge (Belgium),
2) extra model tests performed within the framework of CLASH, on scale models of the three mentioned prototype sites, with the aim to draw a conclusion on possible model and scale effects,
3) extra model tests performed within the framework of CLASH, to fill up the gaps, so-called ‘white spots’, in the first database, with the intention to achieve a more homogenous overtopping database,
4) extra gathered overtopping tests from all over the world, originating on the one hand from newly found references to overtopping research performed in the past, and on the other hand from more recently performed overtopping tests.

The first group of tests, i.e. the prototype overtopping measurements performed within CLASH, resulted in 111 additional overtopping tests. These prototype measurements are described in detail in three CLASH reports, one final report for each measurement site (see Franco et al., 2004, Geeraerts et al., 2004a and Pullen, 2004a).

The model tests on the scaled prototype sites were performed within CLASH at six different laboratories, two for each prototype site, providing the second group of tests. This resulted in 567 extra overtopping tests. The laboratory tests are described in detail in three CLASH reports, one report for each simulated prototype site (see Geeraerts et al., 2004c, Kortenhaus et al., 2004 , Pullen, 2004b).

The third group of tests, consisting of the white spot tests performed within CLASH, are tests resulting from the study of the contents of the preliminary database. The intention of these tests was to provide additional information for the database to achieve a more homogeneous database. Homogeneity of the database is favourable from the point of view of the researcher who will use the database for further research, but it is also one of the requirements to reach a good neural prediction method.
In the preliminary database two important types of white spots were detected:

- the influence of the combined effect of surface roughness and permeability
- the effect of oblique wave attack, short-crested waves and directional spreading of the waves

Additionally, the influence of roughness around swl, the effect of low wave steepness ($s_{0p} < 0.01$), the influence of armour height and crest width, the influence of the slope of the berm and the influence of toe details were marked as white spots.
The first two most important white spots resulted in 1162 additional overtopping results, originating from tests on rubble mound structures performed with various armour layers on the one hand, and three-dimensional model tests with oblique wave attack on the other hand. Besides these tests, additional tests were performed with low wave steepness and reshaping breakwaters, leading to 216 extra overtopping results.
For detailed information on the white spot tests in general, and for the specific conclusions on each studied subject, the original reports need to be consulted: for the conclusions on roughness and permeability of rubble mound structures with various armour units, see Pearson et al. (2004b), for the three-dimensional tests, see Lykke Andersen et al. (2004a), for the additional low steepness tests, see Geeraerts et al. (2004b), and for the additional tests on berm breakwaters, see Lykke Andersen et al. (2004b).

The final results of the roughness and permeability study are included in the database by means of the values for the roughness/permeability factor γ_f, see section 3.6.3.

All overtopping tests gathered within CLASH during this second phase of the database set-up add up to approximately 2050 tests, implicating that the remaining ~1950 tests gathered during this period are originating from the fourth group of tests: new information gathered from inside as well as outside Europe.

The improvements on the preliminary database concern mainly the values of the roughness/permeability factor γ_f (see section 3.6.3). As in the first stage of the CLASH project, little was known about the combined effect of roughness and permeability of rubble mound structures armoured with artificial units, this effect was included in the preliminary database by means of estimated values for γ_f , see Verhaeghe et al., 2003a. The white spot tests performed in this context, resulted in more precise roughness/permeability factors γ_f for rubble mound structures with various armour types (see Pearson et al., 2004b). The estimated values of γ_f in the preliminary database were replaced by these recent γ_f -values in the final database.
Other improvements on the preliminary database concern slightly adapted ideas on how to schematise special shaped structures, and new, better definitions of some parameters. This will not be further discussed here, as it concerns only minor changes which were carried out. The final methodology of including the data in the database, which led to the final database is described here.

Table 3.1 gives an overall view of the origin of the gathered tests. For each country the institutes who delivered overtopping information are given, with the respective number of overtopping tests included in the database. If for the same country more than one institution delivered data, the total number of data for the whole country is mentioned in italics in brackets. As mentioned before, the total number of tests included in the overtopping database is 10532, resulting from 163 independent test series.
All Italian data were obtained through Modimar (CLASH partner). Therefore, this institution is added to the country Italy in brackets.

Table 3.1 Origin and nature of tests

Country	Institution	Tests	M [1]	PT [2]
Belgium		*(661)*		
	• Flanders Community Coastal Division (FCCD)	11		11
	• Ghent University	528	528	
	• Waterbouwkundig laboratorium Borgerhout (WLB)	122	122	
Canada				
	• Canadian Hydraulics Centre (CHC)	225	225	
Denmark		*(1390)*		
	• Aalborg University (AAU)	1294	1294	
	• Danish Hydraulic Institute (DHI)	96	96	
Germany				
	• Leichtweiß-Institut für Wasserbau (LWI)	1191	1191	
Iceland		39	39	
Italy (Modimar)		*(1108)*		
	• Enel-Hydro	309	309	
	• Estramed laboratory	126	126	
	• Modimar	194	117	77
	• University of Florence	479	479	
Japan		367	346	21
The Netherlands		*(1247)*		
	• Delta Marine Consultants (DMC)	64	64	
	• Delft Hydraulics (DH)	524	524	
	• Infram	659	659	
Norway		22	22	
Spain				
	• Universitat Politècnica de València (UPV)	284	284	
United Kingdom		*(3211)*		
	• Hydraulic Research Wallingford (HRW)	2177	2154	23
	• University of Edinburgh	794	794	
	• Others	240	240	
United States				
	• Waterways Experiment Station (WES)	787	787	
	TOTAL :	**10532**	**10400**	**132**

[1] model test
[2] prototype measurement

In table 3.1 a distinction is made between model tests which are performed on different model scales in several laboratories, and prototype measurements, originating from overtopping measurements at real sites. The prototype measurements concern only a small percentage of the available data: 132 measurements, corresponding to about 1.3% of the total number of tests.
Within the group of laboratory tests, one can distinct two-dimensional model tests performed in a wave flume, from three-dimensional model tests performed in wave

basins. The basin tests constitute almost 20% of the model tests in the database (1981 tests). The remaining 8419 model tests, i.e. about 80%, concern two-dimensional flume tests.

As the database includes results of large and small scale model tests as well as prototype measurements, one has to reflect on possible model and scale effects present in the database.
Extensive research performed within CLASH showed that model and scale effects are present in small scale overtopping measurements under certain conditions. Detailed information on these CLASH results and the corresponding implication for the development of the neural prediction method is given in chapter 4, section 4.4.2. Here it is only mentioned that tests with $H_{m0\ toe} > 0.5$m should be considered as 'large scale tests' for which in some cases model and scale effects are expected when these tests are carried out on a smaller scale.
The total number of tests with $H_{m0\ toe} > 0.5$m present in the database is 276. These tests concern either prototype measurements or model tests performed in large wave flumes. The model tests performed in large wave flumes enclose tests performed at:

- the CIEM wave flume at Barcelona
  100m length x 3m width x 5m depth
  Universitat Politècnica de Catalunya, Spain
- the Deltagoot at Marknesse
  230m length x 5m width x 7m depth
  Delft Hydraulics Laboratory, The Netherlands
- the Large Wave Flume at Hannover (Groβer Wellen Kanal)
  324m length x 5m width x 7m depth
  Coastal Research Centre, Hannover, Germany

Table 3.2 gives an overall view of the nature of the tests with $H_{m0\ toe} > 0.5$m present in the database. The distinction between rough, sloping structures and others is made in accordance to the CLASH scaling procedure (see further chapter 4, section 4.4.2).

Table 3.2 Nature of tests with $H_{m0\ toe} > 0.5$m

	Total	Of which M [1]	Of which PT [2]
Total number of tests	276	147	129
Of which rough, sloping structures	105	0	105

[1] model test
[2] prototype measurement

Based on the CLASH scaling procedure, recommendations regarding the use of data for the development of a neural prediction method are added to the database. What exactly these recommendations imply is discussed further in this chapter (see section 3.8).

Figure 3.1 gives an overall view of the years in which the overtopping tests included in the database were performed. The exact number of tests for each period is marked in brackets.
Approximately 44% of the overtopping tests have been performed during the last 5 years, from 2000 up to 2004. The tests performed within the CLASH project (about 2050 tests, resulting from prototype measurements, model tests as well as white spot tests, see before) constitute almost 45% of these.
Approximately 10% of the tests, i.e. over 1000 tests, originate from overtopping research dated before 1985. The oldest tests included are the tests of Y. Goda, obtained by his extensive research performed in 1975 (Goda et al., 1975).

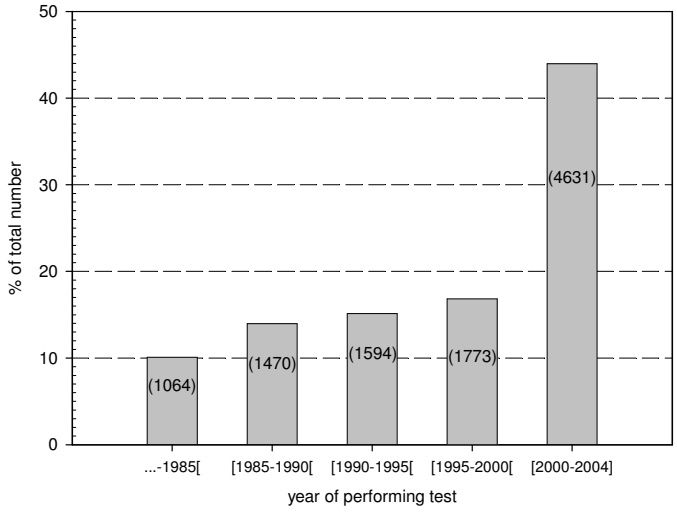

Figure 3.1 Years in which overtopping tests were performed

3.3 Methodology for gathering overtopping information

To obtain a complete and reliable overtopping database as much information as possible was gathered for all test series. Not only information about wave characteristics, test structure and corresponding overtopping discharges, but also information concerning the test facility used to perform the tests, the processing of the measurements and the precision of the work performed was gathered.

For each overtopping measurement, an answer had to be found to the following questions:

- considering the **wave characteristics**:
  - which were the wave characteristics of the measured or generated storm?
    - regular or irregular waves?
    - long-crested or short-crested waves?
    - characteristic wave heights, characteristic wave periods?
    - incident wave angle?

- considering the **test structure**:
  - what kind of structure was tested? (e.g. vertical wall? sloping structure?...)
  - which were the geometrical parameters of the structure?
  - which materials were used to construct the test section?
  - how did the foreshore look like?

- considering the measured **overtopping**:
  - what was measured exactly?
    - the overtopping volume and/or the percentage of waves overtopping?
  - how was the overtopping volume measured?
    - by measuring the increase of the water level or the weight of the overtopping water?

- considering the **test facility** in which the tests were performed (not applicable for prototype tests):
  - which test facility was used?
    - a wave basin or a wave flume? (3D or 2D tests?)
    - what were the possibilities/restrictions of the wave generation system?
  - was reflection compensation performed during testing?
    - active or passive wave absorption?
  - which model scale was used?

- considering the **processing** of the measurements:
  - did the researcher perform time domain analysis and/or spectral domain analysis?
  - did the researcher perform reflection analysis?
    - separation of incident and reflected waves or only determination of total waves?
  - how did the researcher measure incident waves?
    - calibration of the test facility (before construction of the structure) at the location of the structure, measurement of waves at the toe of the structure during testing or only measurement of waves at deep water?

Depending on the answers to these questions, each test could be assessed on reliability and complexity. This was taken into account in the database by defining a 'Reliability Factor' RF and a 'Complexity Factor' CF for each test, which are respectively a measure of the reliability of the performed test and the complexity of the overtopping structure. More detailed information on these two factors is given in section 3.7.

3.4 Parameters in the overtopping database

In view of using the overtopping database for the development of a neural prediction method, each test had to be characterised by a fixed number of parameters. These parameters had to be chosen in such a way that an overall view as complete as possible of the overtopping test was represented by these parameters. The knowledge gathered in chapter 2 on the influencing parameters for the overtopping phenomenon was of direct use here: the influencing characteristics summarised in table 2.11 (see chapter 2) were accounted for as much as possible in the schematisation procedure. In addition, the measured overtopping result, the reliability of the measurement and the complexity of the structure section were included in the database.

The database was set up in such a way that more information than strictly needed for the development of a neural prediction method is included. This resulted in a surplus value of the database on its own for further research purposes. In addition, this allowed for specific parameters for which the influence on the overtopping phenomenon was not yet known at the moment of setting up the database, to let a neural network decide on the importance of these parameters (see further chapter 4).

Three groups of parameters were defined: hydraulic parameters, structural parameters and general parameters. The hydraulic parameters describe the wave characteristics and the measured overtopping, whereas the structural parameters describe the test structure. The general parameters are related to general information about the overtopping test.

The majority of the wave characteristics and structure characteristics summarised in table 2.11 (see chapter 2) were included in the hydraulic respectively structural database parameters. As the majority of overtopping tests included in the database concern small scale tests where wind is not considered, the environmental parameter ‘wind’ mentioned in table 2.11 is not represented in the database. To distinguish the (small number of) small scale tests performed with artificial wind generation from others, a remark was added to these tests in the database (see further section 3.8).

Table 2.11 mentions wave heights and wave periods at deep water as well as at the toe of the structure, corresponding to two possible approaches of overtopping appearing in literature. In the first approach overtopping is related to the deep water wave characteristics, with the slope of the foreshore as an additional influencing parameter in the overtopping model. In the second approach overtopping is related to the wave characteristics at the toe of the structure. As one of the goals of the overtopping database is to provide detailed information on existing overtopping measurements, and to leave open the possibility to use either the wave characteristics at deep water or at the toe of the structure for the development of a neural prediction method, the wave characteristics at both

locations were included in the database. Consequently, also a parameter describing the slope of the foreshore was introduced.

The ultimate number of parameters included in the final database is 31. Below, the parameters are enumerated by group, and a brief description of each of them is given. More detailed information follows in sections 3.5 (hydraulic parameters), 3.6 (structural parameters) and 3.7 (general parameters).

- 11 **hydraulic parameters**:

1	$H_{m0\ deep}$ [m]	Significant wave height from spectral analysis = $4\sqrt{m_0}$, determined at deep water
2	$T_{p\ deep}$ [s]	Peak wave period from spectral analysis at deep water
3	$T_{m\ deep}$ [s]	Mean wave period either from spectral analysis = $\sqrt{m_0/m_2}$, or from time domain analysis (zero-downcrossing) at deep water
4	$T_{m\text{-}1,0\ deep}$ [s]	Mean wave period from spectral analysis at deep water = m_{-1}/m_0
5	β [°]	Angle of wave attack relative to the normal on the structure
6	$H_{m0\ toe}$ [m]	Significant wave height from spectral analysis = $4\sqrt{m_0}$, determined at the toe of the structure
7	$T_{p\ toe}$ [s]	Peak wave period from spectral analysis at the toe of the structure
8	$T_{m\ toe}$ [s]	Mean wave period either from spectral analysis = $\sqrt{m_0/m_2}$, or from time domain analysis (zero-downcrossing) at the toe of the structure
9	$T_{m\text{-}1,0\ toe}$ [s]	Mean wave period from spectral analysis at the toe of the structure = m_{-1}/m_0
10	q [m^3/s/m]	Mean overtopping discharge (volume per second) per meter width
11	P_{ow} [%]	Percentage of the waves resulting in overtopping = $(N_{ow}/N_w).100$

- 17 **structural parameters**:

1	h_{deep} [m]	Water depth at deep water
2	m [-]	Measure of the slope of the foreshore = 1 (unit vertically) : m (units horizontally)
3	h [m]	Water depth in front of the toe of the structure
4	h_t [m]	Water depth on the toe of the structure
5	B_t [m]	Width of the toe of the structure
6	γ_f [-]	Roughness/permeability factor of the structure
7	$\cot\alpha_d$ [-]	Cotangent of the angle that the structure part below the berm makes with a horizontal
8	$\cot\alpha_u$ [-]	Cotangent of the angle that the structure part above the berm makes with a horizontal
9	$\cot\alpha_{excl}$ [-]	Cotangent of the mean angle that the structure makes with a horizontal, excluding the berm
10	$\cot\alpha_{incl}$ [-]	Cotangent of the mean angle that the structure makes with a horizontal, including the berm
11	R_c [m]	Crest freeboard of the structure
12	B [m]	Width of the berm
13	h_b [m]	Water depth on the berm
14	$\tan\alpha_B$ [-]	Tangent of the angle that the (sloping) berm makes with a horizontal
15	B_h [m]	Width of the horizontally schematised berm
16	A_c [m]	Armour crest freeboard of the structure
17	G_c [m]	Crest width of the structure

- 3 **general parameters**:

1	Name	Parameter assigning a unique name to each test
2	RF [-]	'Reliability Factor', giving an indication of the reliability of the test, possible values are 1, 2, 3 or 4
3	CF [-]	'Complexity Factor', giving an indication of the complexity of the test structure, possible values are 1, 2, 3 or 4

3.5 Determination of the hydraulic parameters

The wave characteristics and the measured overtopping are described by means of 11 hydraulic parameters, enumerated in the previous section.
Often several of these parameters were not available in the corresponding report of the test, simply because they were not measured or not written down during performing the test. In this context the following cases could be distinguished:

- only deep water wave characteristics were available, wave characteristics at the toe of the structure were missing
- only wave characteristics at the toe of the structure were available, deep water wave characteristics were missing
- only time domain analysis was performed to determine the wave characteristics
- only one or two of the three spectral wave periods at deep or shallow water were available
- the percentage of waves resulting in overtopping P_{ow} was not measured

With the aim of obtaining a database as complete as possible, if possible an acceptable value was searched for these missing parameters. Well-founded assumptions based on previous research and extra calculations were used to achieve this. Following sections describe these assumptions and calculations in detail. Nevertheless, in some cases it was simply not possible to estimate missing hydraulic parameters accurately. In such cases, preference was given to leave the value of the missing parameter blank in the database. An example concerns the value of P_{ow}, standing for the percentage of waves overtopping. This parameter represents an overtopping result, additional to the mean overtopping discharge and could not be estimated if not measured. Consequently, a blank value in the database is obtained when P_{ow} was not measured. Other cases leading to blank values in the database are treated in section 3.5.2.

The described calculations and estimations in sections 3.5.1 to 3.5.3 all resulted in approximate values for some of the wave characteristics. As this had an influence on the reliability of the values, this fact was incorporated in the database by adapting the value of the reliability factor RF. If any calculations or estimations were needed, a minimum value of 2 was assigned to the factor RF. What the value of RF exactly stands for and how the influence of calculations and estimations was included exactly, is explained in detail in section 3.7.3 .
To distinguish calculated and estimated parameters from measured parameters in the database, the former values are marked with specific colours, depending on the type of the calculation and estimation. More information on this subject is given in section 3.8.

3.5.1 Calculation of incident wave characteristics from given deep water wave characteristics and foreshore

For a part of the gathered overtopping tests, wave characteristics were only available at deep water. In these cases numerical simulations with the SWAN model were made: starting from the deep water wave characteristics and the present foreshore, the wave characteristics at the toe of the structure were calculated.

3.5.1.1 The numerical wave model SWAN

SWAN - acronym for Simulating WAves Nearshore - is a numerical wave model to obtain realistic estimates of wave parameters in coastal areas and inland waters from given wind- , bottom- , and current conditions (see Booij et al., 1999).
The model was developed at the Technical University of Delft, and has been verified by using results from both field measurements and physical model tests. General information about the functionality, physics and limitations of SWAN can be found on the SWAN -site: http://fluidmechanics.tudelft.nl/swan.
The version of SWAN which was used in this thesis is SWAN Cycle III version 40.11 (last revision October 19, 2000). This version is described here.

The SWAN model is based on the wave action balance equation (or energy balance in the absence of currents) with sources and sinks. It concerns a third-generation wave model with first-, second- and third-generation options. The first- and second-generation modes are essentially those of Holthuijsen and de Boer (1988).
In SWAN, wave propagation processes on the one hand and wave generation and dissipation processes on the other hand are implemented. In addition, the wave-induced set-up of the mean sea surface can be computed with SWAN.
Table 3.3 gives a summary of the implemented processes (Booij et al., 1999).

Table 3.3 Wave processes implemented in SWAN

wave propagation processes	wave generation and dissipation processes
• recti-linear wave propagation through geographic space	• generation by wind
• refraction due to variations in bathymetry and current	• dissipation by whitecapping [1]
• shoaling due to variations in bathymetry and current	• dissipation by depth-induced wave breaking
• blocking and reflections by opposing currents	• dissipation by bottom friction
• transmission through, blockage by or reflection from sub-grid obstacles	• three and four wave interactions (triads and quadruplets [2])
	• obstacles

[1] whitecapping:

Whitecapping is a dissipation process which is primary controlled by the steepness of the waves. The whitecapping formulations are based on a pulse-based model (Hasselman, 1974), adapted by the WAMDI group (1988).

[2] triads and quadruplets:

Triads and quadruplets are both wave-wave interactions determining the evolution of the spectrum.

In very shallow water, triad wave-wave interactions are dominant. They transfer energy from lower frequencies to higher frequencies, often resulting in higher harmonics (Beji and Battjes, 1993; low-frequency energy generation by triad wave-wave interactions is not considered here). In SWAN the Lumped Triad Approximation (LTA), derived by Eldeberky (1996) is used for the triad calculations.

In deep water, quadruplet wave-wave interactions dominate the evolution of the spectrum. They transfer wave energy from the spectral peak to lower frequencies (thus moving the peak frequency to lower values) and to higher frequencies (where the energy is dissipated by whitecapping). In SWAN the computations are carried out with the Discrete Interaction Approximation (DIA) of Hasselmann et al. (1985).

One of the limitations of the SWAN model is that it does not account for diffraction, implicating that the model should not be used for the determination of wave characteristics in the immediate vicinity of obstacles and certainly not e.g. in harbours.

Another remark is that both the LTA approximation for the triad wave-wave interactions and the DIA approximation for the quadruplet wave-wave interactions seem to depend on the width of the directional distribution of the wave spectrum.

This implies that both effects are not always performing evenly well. For more detailed information is referred to Booij et al. (1999).
Finally, one can remark that SWAN is not able to model the effect of surf beat, known as low frequency waves (0.005 - 0.05Hz) appearing in the surf zone.

For one-dimensional geographical situations SWAN can be run in 'one-dimensional mode' with two-dimensional calculations. This mode is used in this thesis for the derivation of the wave conditions at the toe of the overtopping structure.

3.5.1.2 Application of SWAN for the set-up of the overtopping database

The majority of the tests included in the database concern model tests with long-crested waves carried out in wave flumes. For this reason the one-dimensional mode of SWAN (with two-dimensional calculations) was used for the calculation of the incident wave characteristics. For the small number of three-dimensional situations, originating from model tests performed in wave basins as well as prototype measurements at real sites, the problem was approximated as a two-dimensional situation. The loss of reliability for these calculations was incorporated in the value of the reliability factor RF (see section 3.7.3). Given the deep water wave characteristics and the bathymetry, the wave characteristics at the toe of the structure could be calculated with SWAN. For the calculations needed, no currents, wind or obstacles were relevant.

It is known that in situations with large energy dissipation between deep water and the toe of the structure (e.g. heavy wave breaking on shallow foreshores), the SWAN model provides less accurate estimates of the wave periods at the toe of the structure, see e.g. Van Gent et al. (2001b). The corresponding mean wave energy levels appear to be predicted rather accurately, leading to reliable values of $H_{m0\ toe}$, also in case of large energy dissipation. The characteristic wave period which was included for each test in the database from the SWAN calculations is the peak period $T_{p\ toe}$, which in general seemed to be predicted better by the SWAN model than the mean period $T_{m-1,0\ toe}$. From the calculated value of $T_{p\ toe}$, the values of other characteristic wave periods $T_{m\ toe}$ and $T_{m-1,0\ toe}$ were estimated (see section 3.5.2). Besides the peak period $T_{p\ toe}$, the value of $H_{m0\ toe}$ is calculated and included in the database.

The reliability of an overtopping test for which SWAN calculations were needed, is lower than if no calculations had to be made. Moreover, it can be stated that the reliability of a single calculation depends on:

- the dimension of the modelled situation: calculations for three-dimensional situations are less reliable as they are approximated by two-dimensional situations,
- the water depth at the toe of the structure: shallow water depths implicate much energy dissipation so less reliable calculations and
- the slope of the foreshore: very steep foreshores, i.e. steeper than ~1:30, lead to less accurate predictions.

The influence of these three factors is included in table 3.8 (see section 3.7.3), which describes in detail how the value of the reliability factor RF was determined in case of SWAN calculations.

3.5.2 Estimation of characteristic wave parameters in relatively deep water

Based on the linear model of deep water waves with a narrow energy spectrum, Longuet-Higgins (1952) showed that the wave heights of these waves obey the Rayleigh distribution. According to this distribution function, the probability that an individual wave height H exceeds some arbitrary value referred to as H_d (with d < design), in the storm characterised by the root-mean-square wave height H_{rms}, can be expressed by:

$$P\,(H > H_d)_{H_{rms}} = exp\left[-\left(\frac{H_d}{H_{rms}}\right)^2\right] \tag{3.1}$$

Since the Rayleigh distribution as described in (3.1) contains only one parameter (H_{rms}), fixed ratios exist between characteristic wave heights, e.g. $H_{1/3} = 1.416\ H_{rms}$, $H_{1/10} = 1.8\ H_{rms}$, $H_{1/20} = 1.94\ H_{rms}$.

One can also state that in case of deep water waves with a narrow energy spectrum, all characteristic wave heights are theoretically proportional to the standard deviation of the surface elevation with known proportionality constants. Starting from $H_{rms} = \sqrt{8\ m_0}$, one also has $H_{1/3} = 4\sqrt{m_0}$ etc. When estimated by m_0 (spectral domain analysis), the notation H_{m0} should be used for the significant wave height (IAHR Working Group on Wave Generation and Analysis, 1989):

$$H_{m0} = 4\sqrt{m_0} \tag{3.2}$$

where m_0 is a measure of the total energy of the storm.

In shallow water, the wave heights no longer obey the Rayleigh distribution. Shoaling, triad interactions and depth-induced breaking become relevant, causing a profile distortion to the linear deep water waves. The consequence is that the approximation $H_{m0} = H_{1/3}$ is no longer valid in shallow water. The manner in which the relationship between H_{m0} and $H_{1/3}$ can be estimated in these cases is explained in section 3.5.3 (Battjes and Groenendijk, 2000).

Contrary to the wave height, the wave period of deep water waves does not exhibit a universal distribution law such as the Rayleigh distribution.
Nevertheless, it has been empirically found that characteristic period parameters are interrelated at deep water. Analysis of field wave data resulted in the following relationships (Goda and Nagai, 1974; Goda, 1985):

$$T_{max} = (0.6 \sim 1.3)\ T_{1/3} \quad (3.3)$$
$$T_{1/10} = (0.9 \sim 1.1)\ T_{1/3} \quad (3.4)$$
$$T_{1/3} = (0.9 \sim 1.4)\ T_m \quad (3.5)$$

With as mean value for many wave records:

$$T_{max} \approx T_{1/10} \approx T_{1/3} \approx 1.2\ T_m \quad (3.6)$$

Also spectral parameters such as T_p and $T_{m0,2}$ can be related with significant wave period parameters such as $T_{1/3}$ and T_m. The following relationship is mentioned for T_p (Goda, 1985):

$$T_p \approx 1.05\ T_{1/3} \quad (3.7)$$

Rice (1944) discovered that the mean period of zero-upcrossing waves T_m can be expressed by:

$$T_m = \sqrt{m_0 / m_2} = T_{m0,2} \quad (3.8)$$

A characteristic wave period for phenomena such as wave run-up and wave overtopping which takes into account the effects of wave energy spectra, is the spectral wave period $T_{m-1,0} = \sqrt{m_{-1} / m_0}$ (Van Gent, 2001a).

For single peaked spectra, a fixed relationship between T_p and $T_{m-1,0}$ is accepted (TAW, 2002):

$$T_p \approx 1.1\ T_{m-1,0} \quad (3.9)$$

In case of missing values for T_p , T_m or $T_{m-1,0}$ in the report describing the overtopping tests, and on condition that the water depth was relatively large at the considered location (avoiding introduced effects of heavy wave breaking), the relationships (3.3) to (3.9) were used to make a reasonable estimation of the missing period parameter.

In more shallow water conditions, the real period relationships probably deviated from the ones obtained with the above mentioned relationships. However, as the wave spectrum in these shallow water depths was not available in most cases, these deep water relationships were, as best available estimation, also used. The less accurate value of some period parameters in these cases was incorporated in the database by the reliability factor RF. Table 3.7 (section 3.7.3) describes in detail how the value of the reliability factor RF was determined when wave period estimations were made.

For double peaked or bi-modal spectra, the value of the peak period T_p is irrelevant. Consequently, for corresponding overtopping tests the value of T_p is left blank in the database.

For a part of the overtopping tests the wave characteristics were only measured at the toe of the structure and not in deep water. In case of relatively deep water at the toe of the structure, it was assumed that wave characteristics in deep water were the same as at the toe. When on the contrary the water depth at the toe was rather shallow, wave breaking was likely to appear. This implicates that the spectral shape of the wave characteristics probably changed drastically compared to at deep water. In these cases the deep water wave characteristics ($H_{m0\ deep}$, $T_{p\ deep}$, $T_{m\ deep}$ and $T_{m-1,0\ deep}$) were left blank in the database.

3.5.3 Determination of $H_{m0\ toe}$ from $H_{s\ toe}$ in shallow water depths

As mentioned in section 3.5.2, wave height distributions in shallow water deviate from those in deep water due to the effects of the restricted depth-to-height ratio. The Rayleigh distribution is no longer valid and the applied relationships between deep water wave heights can no longer be used with a reliable outcome. Battjes and Groenendijk (2000) analysed laboratory data of wave heights on shallow foreshores, which led to generalised empirical parameterisations for the wave height distribution on shallow foreshores of different slopes.

Battjes and Groenendijk (2000) propose a model distribution consisting of two Weibull distributions, of which the parameters are estimated from the laboratory data and expressed in terms of local wave energy (m_0), water depth (h) and bottom slope (1:m). The two Weibull distributions are matched at the transition wave height H_{tr} , leading to the so-called Composite Weibull distribution $F(H_d)$, representing the probability that an individual wave is smaller than or equal to H_d :

$$F(H_d) = P(H \le H_d) = \begin{cases} F_1(H_d) = 1 - exp\left[-\left(\frac{H_d}{H_1} \right)^{k_2} \right] & H_d \le H_{tr} \\ F_2(H_d) = 1 - exp\left[-\left(\frac{H_d}{H_2} \right)^{k_2} \right] & H_d \ge H_{tr} \end{cases} \tag{3.10}$$

with:

- the constraint $F_1(H_{tr}) = F_2(H_{tr})$, to obtain continuity of the distribution function
- exponents k_1 and k_2 shape parameters determining the curvature of the corresponding part of the distribution
- scale parameters H_1 and H_2

The assumed model distribution (3.10) was calibrated and validated with 148 test data which were obtained from experiments performed at Delft Hydraulics from 1993 to 1998. The data concern tests on shallow foreshores with slopes 1:20, 1:30, 1:50, 1:100 and 1:250. References can be found in Battjes and Groenendijk (2000).

Battjes and Groenendijk (2000) normalise all wave heights with the root-mean-square wave height H_{rms} , noted as: $\overline{H_s} = \frac{H_s}{H_{rms}}$.

Relying on the fact that the normalised rooot-mean-square wave height has to equal unity and using eq. (3.10), this leads to the following expression:

$$\overline{H_{rms}} = \sqrt{\overline{H_1}^2 \ \gamma\left[\frac{2}{k_1}+1, \left(\frac{\overline{H_{tr}}}{\overline{H_1}}\right)^{k_1}\right] + \overline{H_2}^2 \ \Gamma\left[\frac{2}{k_2}+1, \left(\frac{\overline{H_{tr}}}{\overline{H_2}}\right)^{k_2}\right]} = 1 \qquad (3.11)$$

where γ(a, x) and Γ(a, x) are incomplete gamma functions (Abramowitz and Stegun, 1964).
The final result as proposed by Battjes and Groenendijk (2000) is a point model (m_0, h, m), with m_0 the zeroth moment of the spectrum, h the local water depth and 1:m the slope of the foreshore. It is described by following parameters and equations:

- the cumulative distribution function (3.10)
- estimated shape parameters $k_1 = 2$ and $k_2 = 3.6$
- parameterisation of the transitional wave height H_{tr} by h and m:
  $$H_{tr} = \left(0.35 + 5.8\,\frac{1}{m}\right) h$$
- parameterisation of the root-mean-square wave height H_{rms} by m_0 and h:
  $$H_{rms} = \left(2.65 + 3.24\,\frac{\sqrt{m_0}}{h}\right)\sqrt{m_0}$$
- values of the scale parameters H_1 and H_2 from solving eq. (3.11) together with the continuity constraint $F_1(H_{tr}) = F_2(H_{tr})$

In figure 3.2 an example is given of the proposed wave height distribution by Battjes and Groenendijk (2000). The distribution is calculated for values of $m_0 = 0.0011m^2$, h = 0.27m and m = 100.
As shown in the figure, the transitional wave height H_{tr} is 0.11m. Values of $H_{1\%}$, $H_{2\%}$, $H_{10\%}$ ... can be easily found.

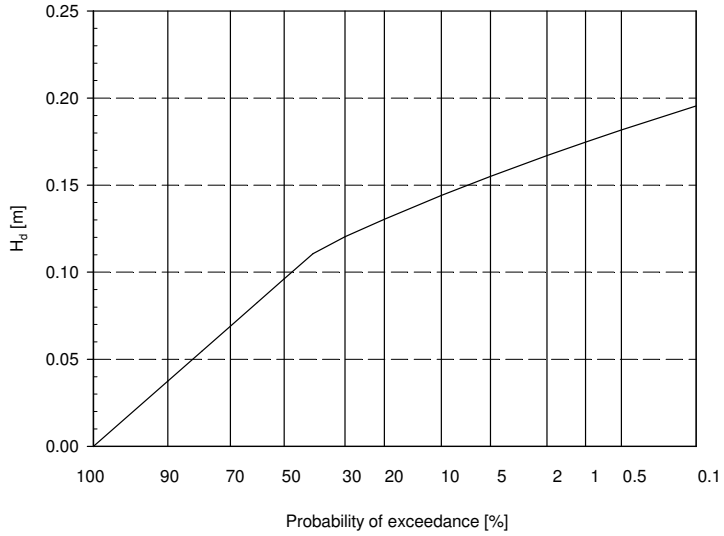

Figure 3.2 Calculated wave height distribution for (m_0, h, m) = (0.0011m², 0.27m, 100)

In case of overtopping tests with a rather shallow water depth at the toe of the structure, the proposed point model by Battjes and Groenendijk (2000) can be used to determine the wave height $H_{m0\ toe}$ if only the wave height $H_{s\ toe} = H_{1/3\ toe}$ is given. The input parameters for the point model are the given value $H_{1/3\ toe}$, the slope of the foreshore 1:m and the water depth h at the toe of the structure, leading to the corresponding value of m_0 at the toe of the structure. Eq. (3.2) finally results in the parameter $H_{m0\ toe}$.

Table 3.7 (section 3.7.3) describes in detail how the value of the reliability factor RF was determined if calculations according to Battjes and Groenendijk (2000) were made.

3.6 Determination of the structural parameters

The starting point for the determination of the structural parameters was the fact that as much as possible overtopping structures had to be schematised by these and only these parameters. Studying a lot of different overtopping sections finally led to the 17 structural parameters as enumerated in section 3.4.
In this section, a detailed description is given of the methodology which is followed to determine these 17 parameters for all overtopping tests included in the database.

3.6.1 General schematisation of the structure in three areas

The first schematisation step of each overtopping structure consists of splitting up the structure into three main parts. The starting point here are the waves which attack the structure, as it is important to schematise the structure in this way the attacking waves 'feel' the structure. This implies that a geometrically identical structure can have a different schematisation depending on the water level and the attacking waves.
The structure part situated around the swl is the most important part for the waves. According to the size of the waves, this area is either larger or smaller. Referring to Van der Meer et al. (1998), the governing part of the structure where the wave action is concentrated on, is defined as the part between $1.5H_{m0\ toe}$ above and $1.5H_{m0\ toe}$ below swl. For the schematisation procedure, the area marked off by the value of $1.5H_{m0\ toe}$ above and $1.5H_{m0\ toe}$ below swl is called the '**centre area**' of the structure. The area below the centre area is called the '**lower area**' of the structure and the area above the centre area is called the '**upper area**' of the structure. Depending on the wave height and the water level, the upper or lower area may be lacking.

Figure 3.3 shows two rubble mound structures where these three main parts are marked.
Depending on the wave height and the water depth near the structure, the centre area can extend the structure slope (figure 3.3 (a)), but it can e.g. also enclose a part of the toe of the structure (figure 3.3 (b)). It is clear that other possibilities may occur.

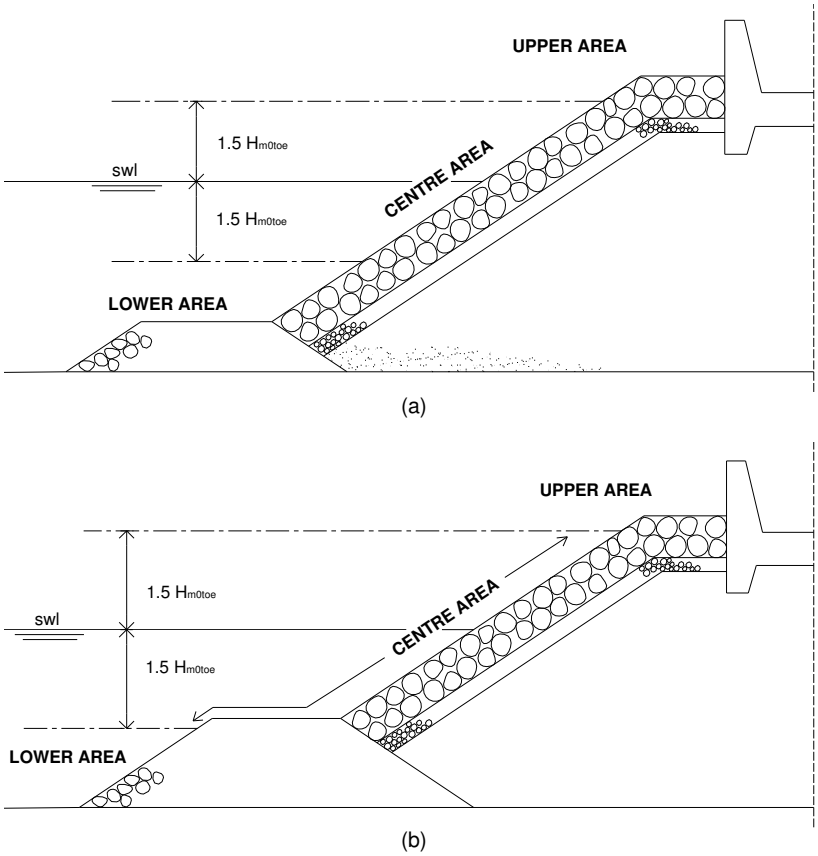

Figure 3.3 Main structure parts of rubble mound structure

3.6.2 Berm, toe and crest of the structure

Looking at structure sections of coastal structures in general (although in the context of this overtopping study), one can often distinguish:

- a structure body, consisting of a vertical wall, a sloping part or a combination of both, and possibly containing a structure berm,
- a structure toe, meant to structurally protect the lower part of the structure, and
- a structure crest, often with a strengthening function for the upper part of the structure.

For the schematisation of a structure section, these three structure parts need to be clearly distinguished. In most cases this distinction is straightforward. However, sometimes confusion can arise. This section examines in detail how the distinction between a berm, a toe and a crest is made in the context of the set-up of the overtopping database. Figures 3.4 to 3.7, which are discussed further in the text one by one, illustrate this.

It is defined that a structure berm is most likely situated in the centre area of the structure (= area between $1.5H_{m0\ toe}$ above and $1.5H_{m0\ toe}$ below swl, see previous section). If the 'berm' ('berm' refers here to the name assigned to it in the corresponding report) is situated lower, it is more likely to be felt by the waves as a toe. If the 'berm' is situated higher, it is more likely to be felt as a crest. In connection with the position of the berm, a toe is defined as most likely to appear in the lower area of the structure (= lower than $1.5H_{m0\ toe}$ below swl) and a crest in the upper area of the structure (= higher than $1.5H_{m0\ toe}$ above swl).
Consequently, it may happen that what is called a 'berm' in the original report, is called a toe or a crest for the database, although the above described levels of toe, berm and crest are not totally binding, i.e.:

- tests with very small values of $H_{m0\ toe}$, leading to a very restricted centre area, are often schematised with a berm which is not situated in the centre area of the structure,
- structure types with quite large toes, situated in relatively shallow water, can be schematised with a toe situated in the centre area of the structure,
- low crested structures of which the upper point of the structure has a level lower than $1.5H_{m0\ toe}$ above swl, are schematised with a crest situated in the centre area of the structure.

The above mentioned examples can be referred to as structures which do not fulfil the most likely position of a berm, a toe or a crest.

In figure 3.4 a typical rubble mound structure is shown. The centre area contains a slightly sloping berm. The crest is situated in the upper area, the toe is situated in

the lower area. This example corresponds with the most common position of the three mentioned structure parts.

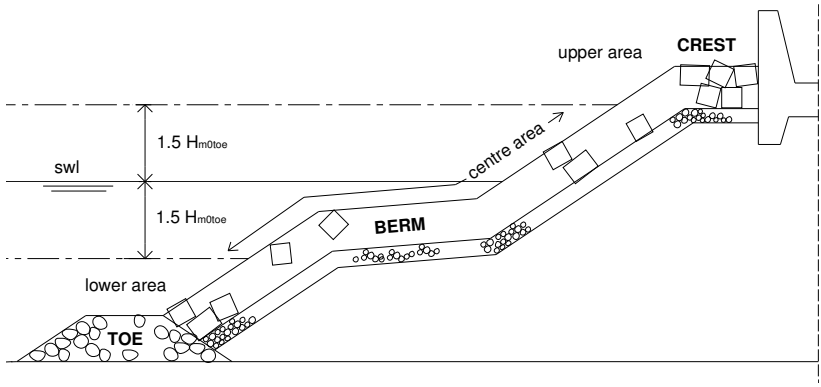

Figure 3.4 Typical position of berm, crest and toe

Figure 3.5 gives an example of a structure with a high situated toe. The different structure materials contribute to the preference of schematising the lower part of the structure here as a large toe and not as a berm.

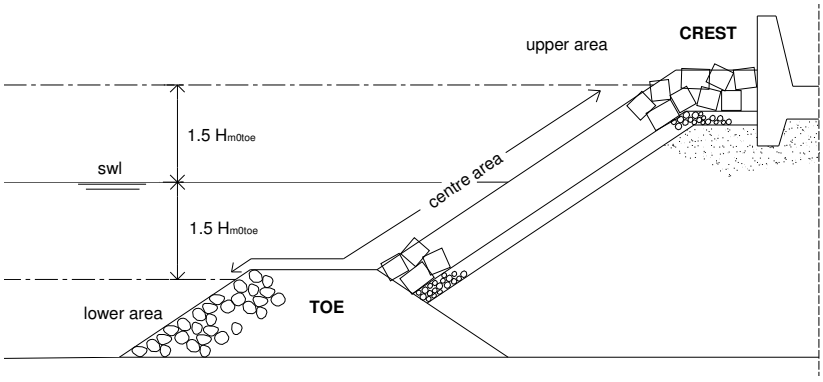

Figure 3.5 Structure type with large toe

Figure 3.6 shows a structure for which the small value of $H_{m0\ toe}$ leads to a situation in which the berm is situated in the lower part of the structure. It is quite obvious in this case that it concerns a berm and not a toe.

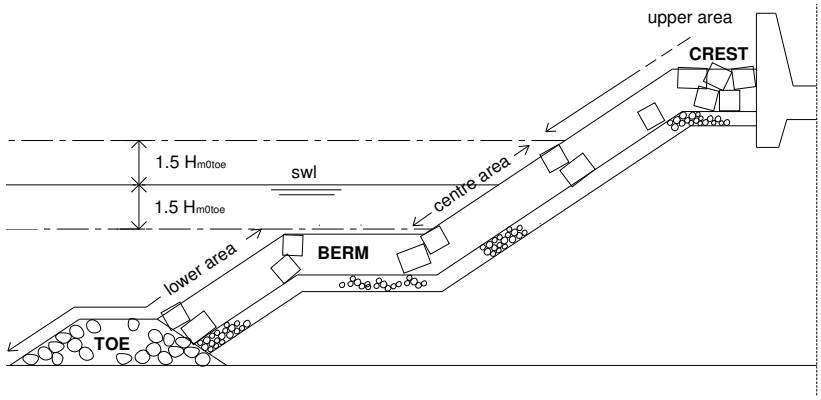

Figure 3.6 Structure type with low situated berm

In figure 3.7 at last an example is given of a structure with a low situated crest. Because of the high water level, the entire structure is situated lower than the $1.5H_{m0\ toe}$ -line above swl.

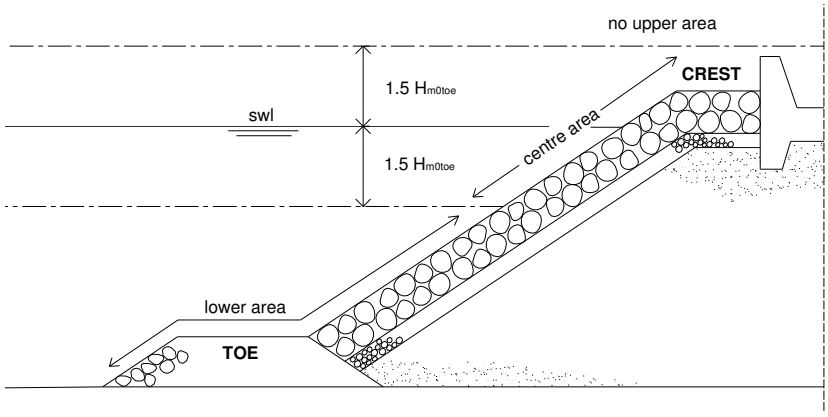

Figure 3.7 Structure type with low situated crest

It is not always straightforward to schematise a horizontal or slightly sloping part of a structure. In some cases more than one schematisation possibility exists.

Apart from the levels of the berm, crest and toe of a structure, some restrictions regarding the slope and the length of a berm are imposed.
In TAW (2002), a berm of a dike is described as a sloping structure part, with a slope in between the horizontal and 1:15. Regarding the schematisation for the overtopping database, slopes less steep than 1:15 are preferred for a berm,

although slopes up to 1:10 are allowed. Slopes steeper than 1:10 are considered as a regular sloping structure part.
In TAW (2002) the berm length is restricted to one fourth of the wave length L_0. Lengths larger than one wave length L_0 correspond to a foreshore and for lengths in between L_0 and $0.25L_0$ one is advised to interpolate between the effect of a berm and a foreshore. In the schematisation procedure for the overtopping database, a berm length up to one wave length is allowed, although berm lengths smaller than $0.25L_0$ are preferred. If the berm is longer than L_0 , it has to be considered as a foreshore. Consequently, in this last case the part of the structure lower than the 'berm' also has to be considered as a part of the foreshore.

Figure 3.8 shows two structures containing a part which is not included as a berm in the database.
Figure 3.8 (a) shows a structure containing a sloping part which is steeper than 1:10 and consequently can not be considered as a berm. Figure 3.8 (b) shows a structure of which the large horizontal part has to be considered as a part of the foreshore. The toe of this last structure is located at the end of the horizontal part, and not in front of it. Section 3.6.5 explains how to schematise these cases exactly.

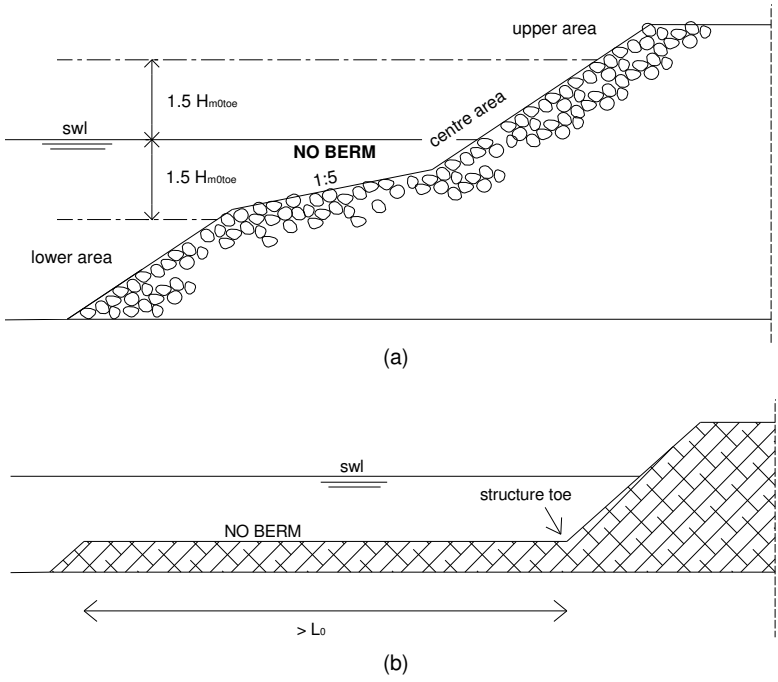

Figure 3.8 Structure 'berms' not considered as berms regarding the schematisation for the database

3.6.3 Structural parameters

This section explains how the structural parameters for a rather easy-to-schematise overtopping structure are determined. In section 3.6.5 the schematisation of more complex sections is covered.

Below the 17 schematisation parameters are given, with a detailed explanation how to determine these.

3.6.3.1 h_{deep} [m]

This is the water depth at deep(er) water. At this water depth the deep wave characteristics $H_{m0\ deep}$, $T_{p\ deep}$, $T_{m\ deep}$ and $T_{m-1,0\ deep}$ are present.
The definition indicates that for laboratory tests, h_{deep} is not necessarily the deepest water depth which appears in the flume or basin. Depending on the location of the wave gauges, the value of h_{deep} is situated between the water depth at the toe of the structure and the deepest water depth in the flume. In figure 3.9 some possibilities of measurement locations of h_{deep} are given. In figure 3.9 (a), the deep water depth corresponds to the water depth in front of the wave paddle of the flume. In figure 3.9 (b) an intermediate water depth is taken as the value for h_{deep} and finally, figure 3.9 (c) considers the special case in which no foreshore is present, resulting in a water depth h_{deep} equal to the water depth just in front of the structure.

3.6.3.2 m [-]

The slope of the foreshore is described by the parameter m by means of 1 (unit measured vertically) : m (units measured horizontally). If no uniform sloping foreshore exists, one has to approximate the value of m. A relevant approximation of m consists of a mean value over a horizontal distance of about 2 wave lengths L_0 in front of the structure. The restriction of the approximation to the foreshore just in front of the structure can be justified as this part is qualifying for the incident wave characteristics.
In figure 3.9 the values of m are indicated. Figure 3.9 (c) is a special case with a flat bottom of the flume. Theoretically the value of m should be equal to infinity in such cases, but as a real, finite value is more workable, in these cases a value of 1000 was assigned to m in the database.

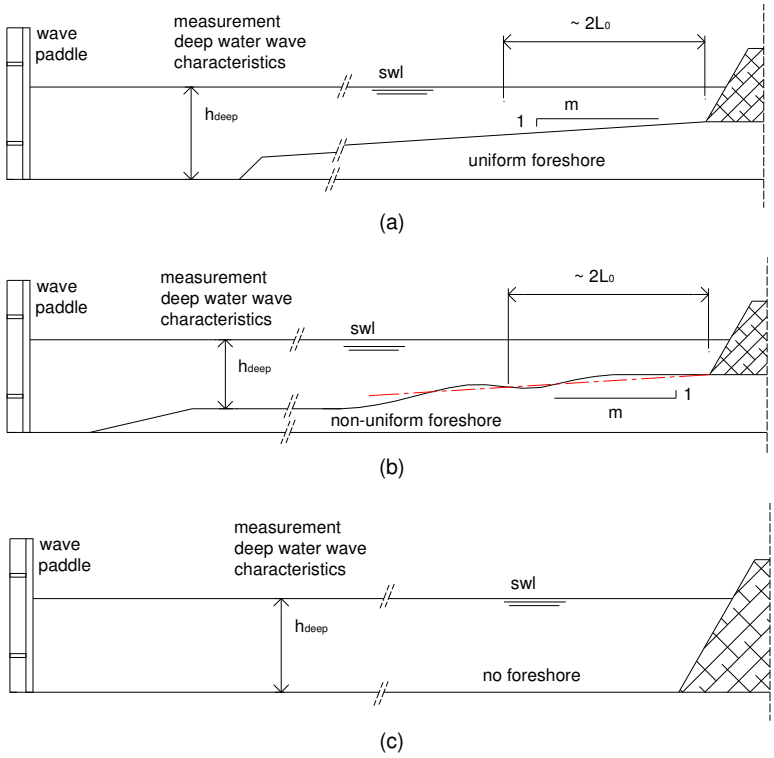

Figure 3.9 Determination of h_{deep} [m] and m [-]

3.6.3.3 h [m]

The value of h refers to the water depth just in front of the toe of the structure (figure 3.10). It is often referred to as the water depth 'at the toe of the structure'. In case of a flat flume bottom, the value of h is equal to the value of h_{deep}.

3.6.3.4 h_t [m], B_t [m]

These are the water depth on the toe respectively the width of the toe (figure 3.10). The value of h_t is measured in the middle of the toe. The value of B_t is measured on top of the toe.

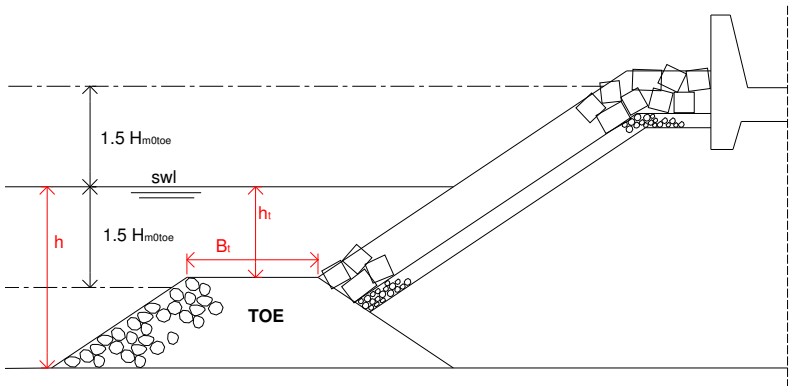

Figure 3.10 Determination of h [m] , h_t [m] and B_t [m]

The front slope of the toe is not included in the database, because it seems a less important parameter in view of the overall low position of the toe regarding to the water level. Moreover, the front slope of a structure toe is in many cases ≈ 1: 2. An extra restriction for the definition of a toe could therefore be that the front slope should approximate 1: 2.

If the structure has no toe, the value of the water depth on the toe, h_t , equals the value of the water depth at the toe of the structure, h. In this case the width of the toe, B_t , is equal to zero, e.g. figure 3.11.

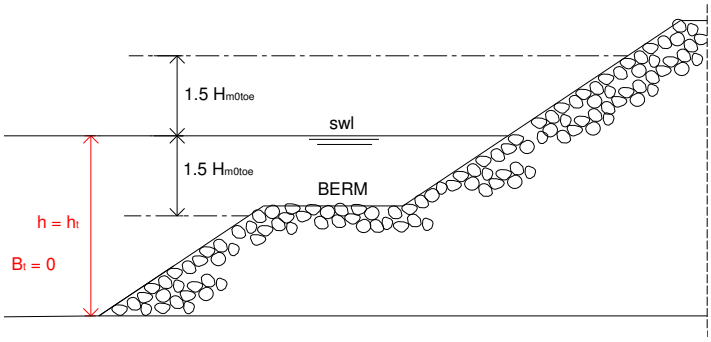

Figure 3.11 Determination of h [m] , h_t [m] and B_t [m] in case no toe is present

3.6.3.5 B [m], h_b [m], $tan\alpha_B$ [-], B_h [m]

These are four parameters to describe the berm of an overtopping structure (figure 3.12).
The value of B represents the berm width and is measured horizontally.

h_b is the water depth on the berm, measured in the middle of the berm. If the berm is situated above swl, the value of h_b is negative.
Tanα_B is the tangent of the angle that a (sloping) berm makes with a horizontal. If the berm is horizontal, tanα_B = 0.
The value of B_h refers to the width of the horizontally schematised berm. In case of a horizontal berm (i.e. tanα_B = 0) the value of B_h = B, but for a sloping berm, B_h < B. The value of B_h is obtained by extending the upper and lower slope of the structure up to the level of the middle point of the berm. By connecting these two points, the horizontal schematisation of the berm is obtained.

Figure 3.12 (c) consists of the enlarged box of figure 3.12 (b), explaining the difference between B_h and B.

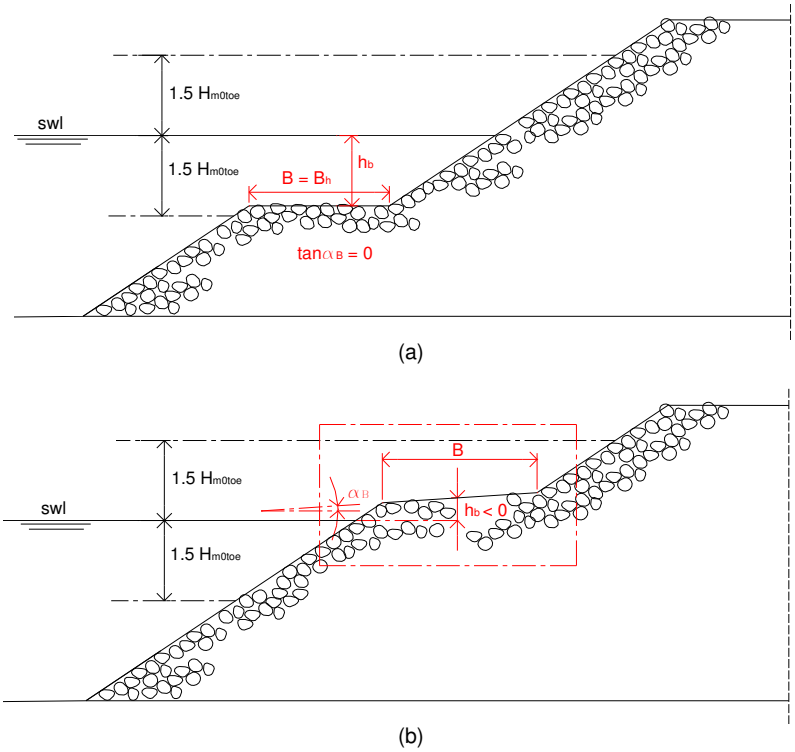

Figure 3.12 Determination of B [m], B_h [m], tanα_B [-], h_b [m]

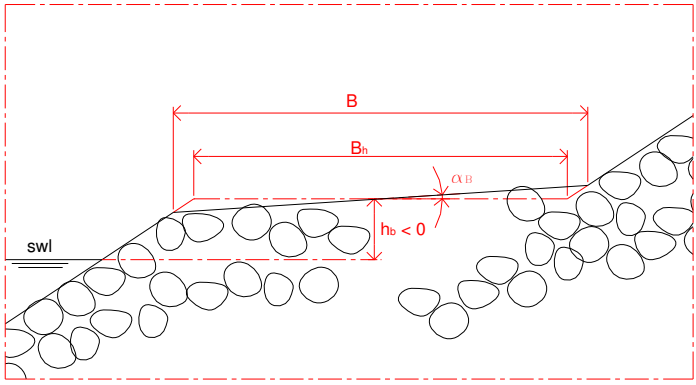

(c)

Figure 3.12 (continued) Determination of B [m], B_h [m], $tan\alpha_B$ [-], h_b [m]

If the structure has no berm, the values of B, B_h , $tan\alpha_B$ and h_b are all equal to zero, except for a composite slope.

In case of a composite slope (i.e. a structure consisting of subsequent different slopes without a horizontal part in between), h_b is defined as the transition depth between two successive slopes. Although no berm is present in this case, the value of h_b does not equal zero. Defining h_b as the transition depth between two successive slopes, amounts to defining a berm at this location with a berm width and slope equal to zero (figure 3.13). The schematisation of the composite slope is described in section 3.6.3.7.

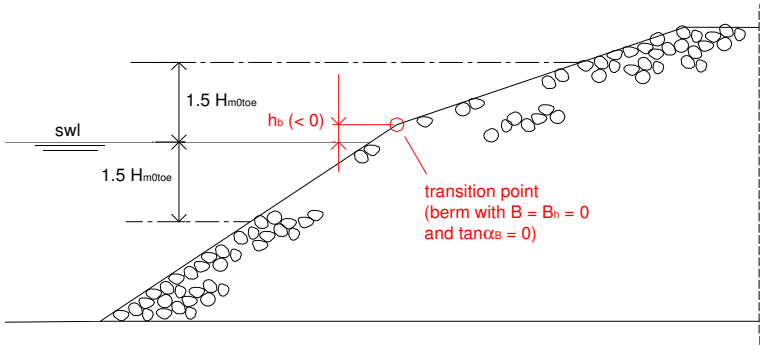

Figure 3.13 Determination of the transition depth h_b [m] in case of a composite slope

3.6.3.6 R_c [m], A_c [m], G_c [m]

These parameters describe the upper part of an overtopping structure (figure 3.14).
R_c is the crest freeboard of the structure. It is the distance, measured vertically, from swl to the point of the structure where overtopping is measured. This is not always the highest point of the structure, e.g. figure 3.14 (d).
A_c is called the armour crest freeboard of the structure. In case of armoured structures it is the distance, measured vertically from swl to the upper limit of the armour layer. In case of structures without armour, e.g. vertical structures or smooth slopes, A_c may be used together with R_c and G_c , to describe the crest of the structure more detailed, e.g. figure 3.14 (e). In many cases, $A_c = R_c$.
G_c represents the crest width.

Figure 3.14 gives several examples of crest structures with an indication of the corresponding parameters. As shown on the different figures, R_c can adopt a value larger, smaller or equal to A_c.

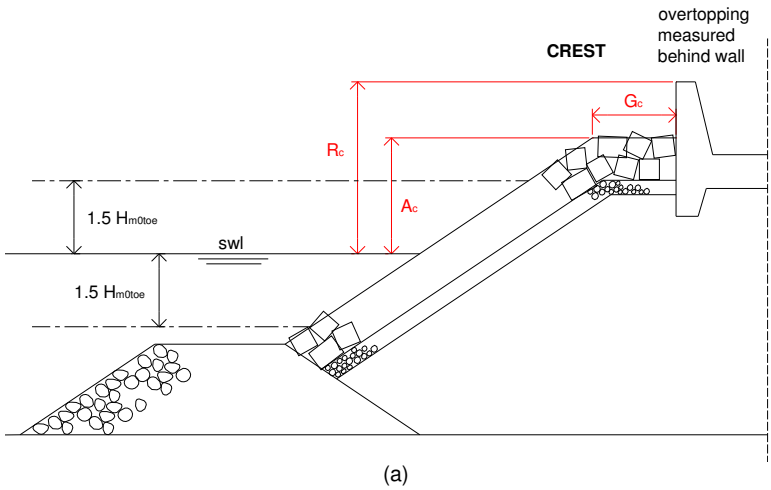

Figure 3.14 Determination of R_c [m], A_c [m] and G_c [m]

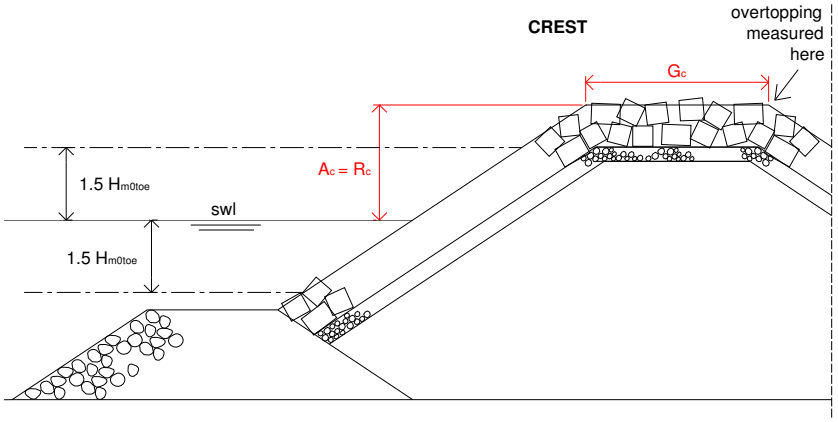

(b)

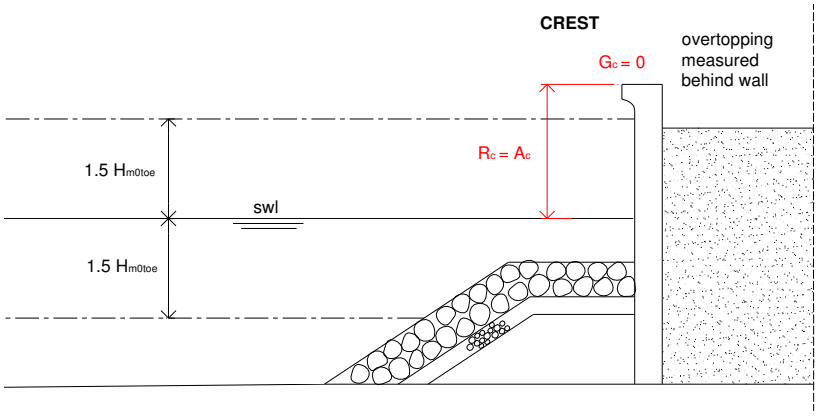

(c)

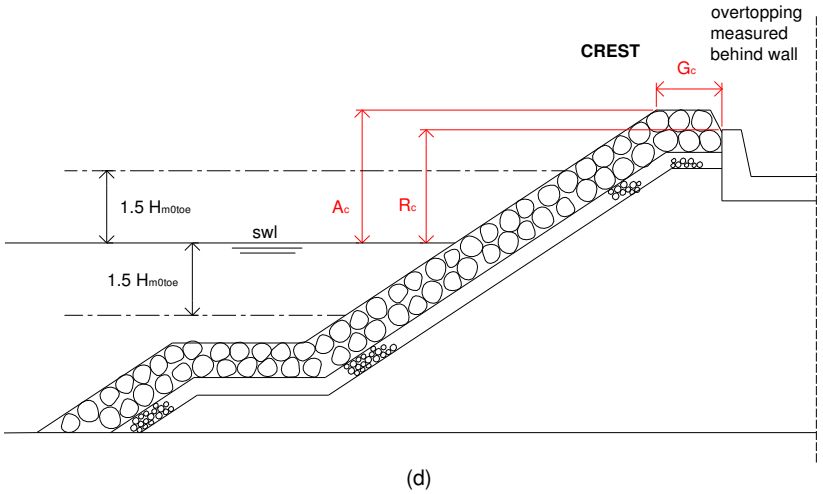

(d)

Figure 3.14 (continued-1) Determination of R_c [m], A_c [m] and G_c [m]

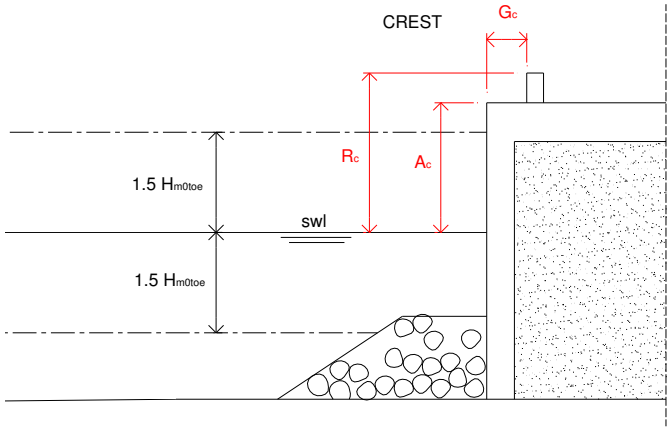

(e)

Figure 3.14 (continued-2) Determination of R_c [m], A_c [m] and G_c [m]

It should be mentioned that the parameter G_c only includes the *permeable* horizontal part of the crest when no wave return wall is present, as it is assumed that overtopping water just passes an impermeable surface when it reaches it. An example is given in figure 3.15 (a): as the crest consists of a horizontal impermeable surface, the value of G_c equals zero. Logically, if the crest consists of an impermeable horizontal road and overtopping is measured behind a wall located at the landside of the road, the crest width G_c will be equal to the width of the road, as only the water which passes the wall itself will be measured. An example is given in figure 3.15 (b).

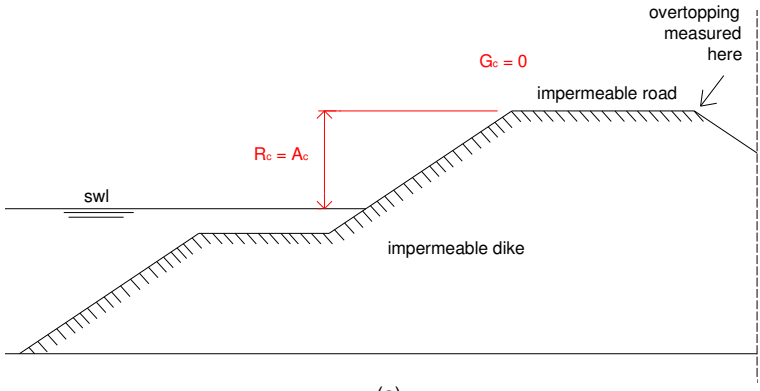

(a)

Figure 3.15 Determination of G_c [m]

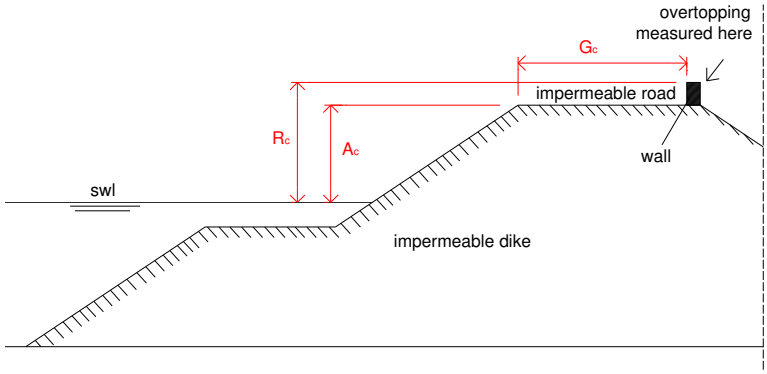

(b)

Figure 3.15 (continued) Determination of G_c [m]

3.6.3.7 cotα$_d$ [-], cotα$_u$ [-], cotα$_{excl}$ [-], cotα$_{incl}$ [-]

These parameters describe the slope(s) of the overtopping structure (figures 3.16 to 3.20). It has to be stressed that the toe and the crest of the structure are not included in these four slope parameters, as these are already described by separate parameters.

The four parameters provide three ways to describe the overtopping structure:

- with cotα$_d$ and cotα$_u$ or
- with cotα$_{excl}$ or
- with cotα$_{incl}$

Cotα$_d$ and cotα$_u$ are the cotangent of the angle that the structure part in the centre area below (cotα$_{\mathbf{down}}$) respectively above (cotα$_{\mathbf{up}}$) the berm makes with a horizontal.

Cotα$_{excl}$ and cotα$_{incl}$ refer to calculated 'mean' slopes. Cotα$_{incl}$ is the cotangent of the mean angle that the structure makes with a horizontal, where the berm (if located in the centre area of the structure) is included in this mean value (cotα$_{\mathbf{inclusive\ berm}}$). Cotα$_{excl}$ is the cotangent of the mean angle that the structure makes with a horizontal, where the present berm is not taken into account (cotα$_{\mathbf{exclusive\ berm}}$). If the structure has no berm, cotα$_{incl}$ = cotα$_{excl}$.

The slope angles are presented by means of their cotangent instead of their tangent (which was used for the slope of the berm), as the slope angles can adopt values up to and even larger than 90° (see section 3.6.4 for this last case). A value of 90° results in a zero value of the cotangent of the slope angle (instead of an infinite value for the tangent of the slope angle). A value larger than 90° results in a negative value of the cotangent of the slope angle (instead of a positive value of the tangent of the slope angle, indistinguishable from the tangent of a slope angle of 90°- α). The other way around, the cotangent of the slope angle of a horizontal

berm results in an infinite value, explaining the use of the tangent for the berm slope angle.

How the four slope parameters are determined exactly, is explained below (figures 3.16 and 3.17).

The upper slope angle of the structure, α_u , refers to the slope above the berm, which is determined by taking the point of the structure at a level of $1.5H_{m0\ toe}$ above swl and connecting it with the leeside endpoint of the berm. If the crest of the structure is situated in the centre area of the structure (this implies that the crest is situated less than $1.5H_{m0\ toe}$ above swl), then the starting point of the crest has to be used instead of the point at a level $1.5H_{m0\ toe}$ above swl to determine α_u .
The lower slope angle of the structure, α_d , refers to the slope below the berm, which is determined by taking the point of the structure at a level of $1.5H_{m0\ toe}$ below swl and connecting it with the seaside endpoint of the berm. If the toe of the structure is situated in the centre area of the structure (this implies that the toe is situated less than $1.5H_{m0\ toe}$ below swl), then the starting point of the toe has to be used instead of the point at a level $1.5H_{m0\ toe}$ below swl to determine α_d .
The mean slope angle, α_{incl} , is determined by taking the point on the upper slope at a level of $1.5H_{m0\ toe}$ above swl and connecting it with the point on the lower slope at a level of $1.5H_{m0\ toe}$ below swl. The subscript 'incl' refers to the fact that if there is a berm, it is included in the value of $\cot\alpha_{incl}$. If the toe and/or the crest of the structure are situated into the centre area, the lowest and/or the highest point which determine $\cot\alpha_{incl}$ are determined by the starting point of the toe (instead of by swl - $1.5H_{m0\ toe}$) and/or the starting point of the crest (instead of by swl + $1.5H_{m0\ toe}$).
The mean slope angle, α_{excl} , is determined by subtracting the horizontal width of the berm, B_h , from the horizontal distance between the two points which determine α_{incl} , and dividing this value by the vertical distance between the two points which determine α_{incl} .

In figure 3.16 the four slope angles are indicated, in graph (a) for a simple rubble mound structure without berm, in graph (b) for a rubble mound structure with a horizontal berm and in graph (c) for a rubble mound structure with a sloping berm.

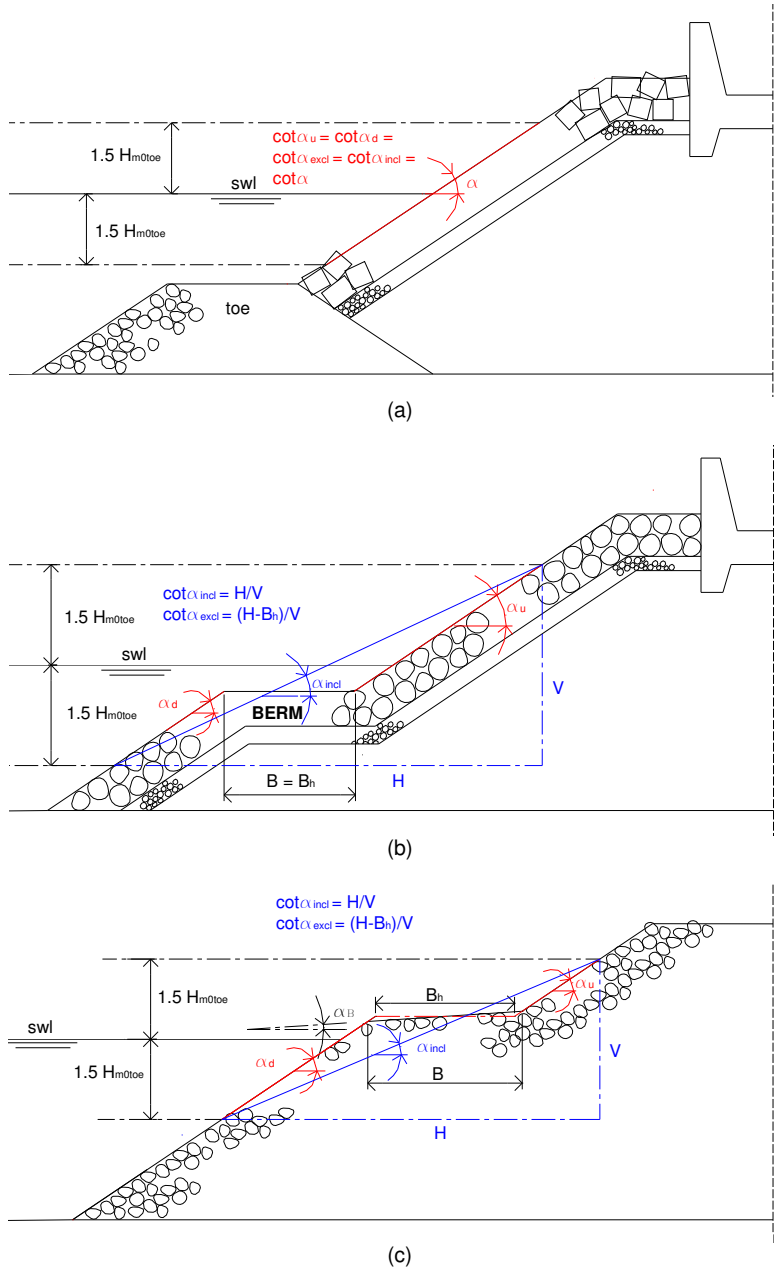

Figure 3.16 Determination of the structure slope parameters

In figure 3.17 two extra examples regarding the determination of the structure slope parameters are given. In graph (a) the toe is situated in the centre area of the structure. As shown in the figure, the starting point of the toe is used to determine α_d instead of the point at a level $1.5H_{m0\ toe}$ below swl. In graph (b) the crest is

situated in the centre area of the structure. Analogous the starting point of the crest is used to determine α_u instead of the point at level $1.5H_{m0\ toe}$ above swl.

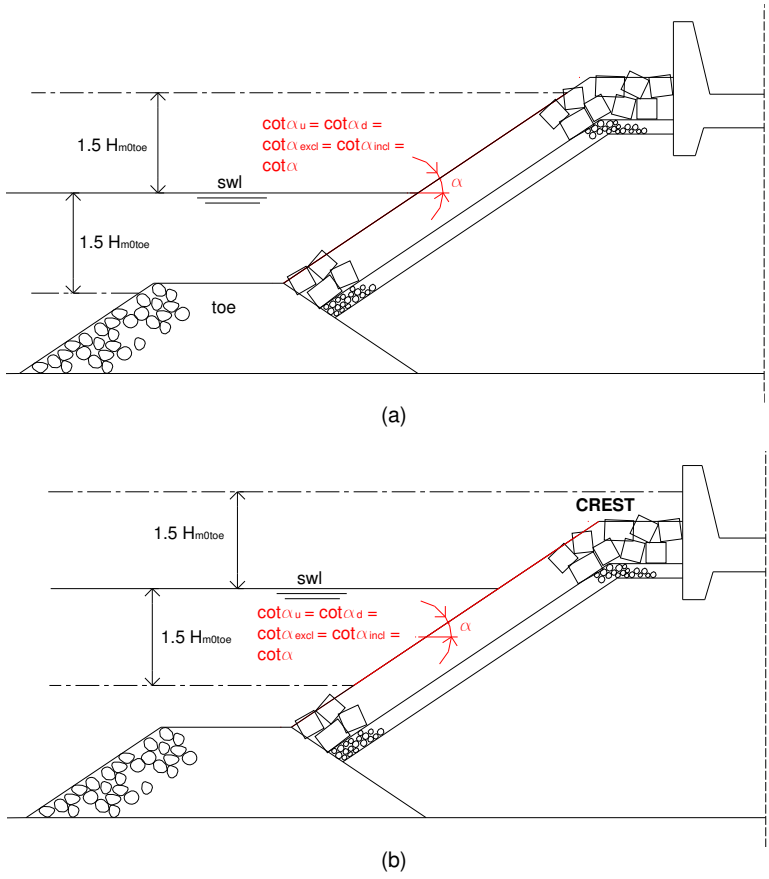

Figure 3.17 Determination of the structures slope parameters, extra examples

The use of the two parameters $\cot\alpha_u$ and $\cot\alpha_d$ often allows a better schematisation than the use of only one of the mean parameters $\cot\alpha_{excl}$ or $\cot\alpha_{incl}$. An example of a structure type for which the use of a mean slope leads to a bad schematisation is given in figure 3.18.

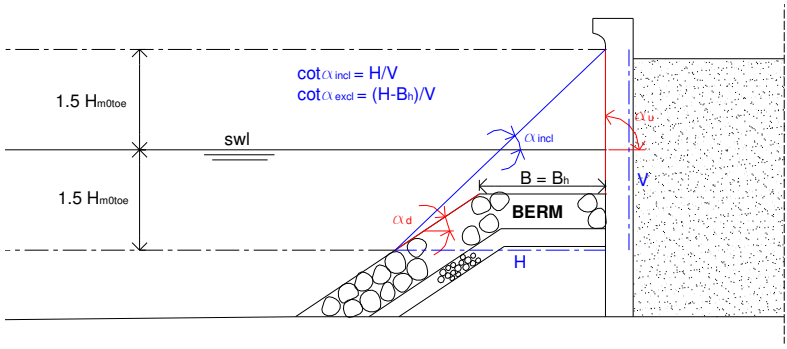

Figure 3.18 Structure type for which at least two slope parameters are requested

The use of the two slope parameters cotα$_u$ and cotα$_d$ also allows to schematise very well composite slopes. As mentioned in section 3.6.3.5 the position of the transition point of a composite slope is indicated by h_b . The slope upward respectively downward the transition point is defined now by cotα$_u$ and cotα$_d$.
For composite slopes composed of more than two subsequent different structure slopes (and consequently more than one transition point), a rougher schematisation is needed, even with two parameters cotα$_d$ and cotα$_u$.
Figure 3.19 shows a composite slope with only one transition point. By using cotα$_d$ and cotα$_u$, the structure is schematised very well.

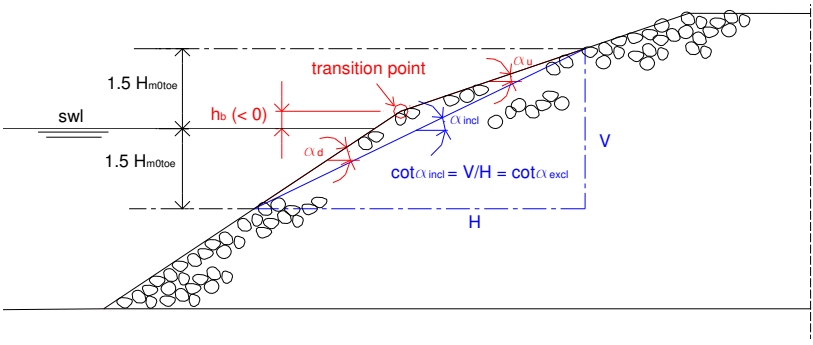

Figure 3.19 Schematisation of a composite slope composed of 2 subsequent slopes

Figure 3.20 shows a composite slope consisting of more than 2 subsequent slopes. Graph (a) and (b) give two possible schematisations, determined by the choice of the transition depth h_b . As can be seen in the figures, the schematisation in graph (b) fits the structure best.

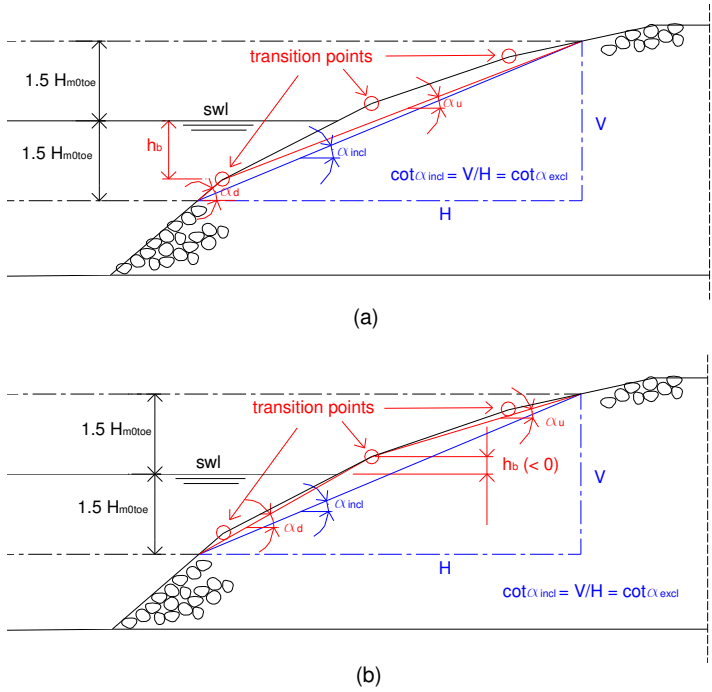

Figure 3.20 Schematisation of a composite slope composed of more than 2 subsequent slopes

3.6.3.8 γ_f [-]

The parameter γ_f gives an indication of the roughness and the permeability of the structure. The rougher and more permeable a structure, the lower the overtopping will be, as more energy is dissipated. This is incorporated in a lower value of the parameter γ_f.

The introduction of a reduction factor for the roughness for various types of revetments originates from Russian investigations performed in the 1950's with regular waves, and concerns a value derived for wave run-up. More recent values for γ_f for several revetment types are presented by TAW (2002), resulting from new run-up tests with irregular waves, also performed on large scale, from 1974 up to 2002. TAW (2002) prescribes a value of 1 for γ_f in case of an impermeable smooth structure, and a value of 0.7 respectively 0.55 in case of 1 respectively 2 layers of rock on an impermeable core.

As mentioned so far, within the CLASH project extensive research was performed to examine the roughness and permeability of rubble mound structures with different armour layers, especially with the aim of providing new information on the γ_f-value of these structures for the set-up of the overtopping database (see Pearson et al., 2004b). Within this study, 426 small scale overtopping tests were performed with several types of armour units, for each type of unit starting from a standard test situation and a standard cross-section. Equal hydrodynamic stability

was the starting point. The measured mean overtopping discharges were examined. At the same time the results of the overtopping tests performed by Aminti and Franco in 1988 (Aminti et al., 1988) were re-analysed. Eq. (2.5b) prescribed by TAW (2002) for surging wave conditions on a slope (see chapter 2) was used to assign γ_f -values to the structures. This CLASH research resulted in slightly adapted γ_f -values for rock slopes, and additionally, in new γ_f -values for rubble mound structures with various artificial armour units. Table 3.4 gives a summary of the obtained γ_f -values for the tested armour layers (see Pearson et al., 2004b).

Table 3.4 Newly derived values for γ_f (see Pearson et al., 2004b)

Type of armour layer	γ_f
Smooth impermeable surface	1.00
Rocks (1 layer, impermeable core)	0.60
Rocks (1 layer, permeable core)	0.45
Rocks (2 layers, impermeable core)	0.55
Rocks (2 layers, permeable core)	0.40
Cubes (1 layer, random positioning)	0.50
Cubes (2 layers, random positioning)	0.47
Antifers	0.47
HARO's	0.47
Accropods	0.46
X-blocks	0.45
Core-locs	0.44
Tetrapods	0.38

It should be remarked that in this case the γ_f -values are related only to the type of armour. Although they also contribute to the permeability of the structure, the exact design of the underlayers was not further considered. During the CLASH tests the filter and the core layer gradings were chosen in relation to the weight of the corresponding armour unit (filter: 1/5 to 1/15 W; core: < 1/50 W).

A rubble mound structure with an armour layer consisting of 2 layers of cubes or antifers performs somewhat worse than a 2 layered permeable rock slope: γ_f = 0.47 instead of 0.40. Tetrapods, with a γ_f -value of 0.38, seem to be the best of the tested armour units regarding roughness and permeability.

In addition to table 3.4, values of γ_f for structures with other types of armour layers were estimated based on data included in the database. Table 3.5 gives an overall view of the estimated values of γ_f . This table is not supported by extensive research and should therefore be considered as a provisional table.

Table 3.5 Estimated values for γ_f based on included overtopping tests

Type of armour layer	γ_f
SHEDS	0.55
Seabeas	0.50
Berm breakwater (reshaping)	0.40
Dolosse	0.43
Icelandic berm breakwater (not reshaping)	0.35

More types of armour layers than mentioned above are represented in the database. Some armour layers consist of very specific armour units which are not mentioned here, others consist of impermeable coverings with an energy-dissipating geometry, e.g. stepped slopes. For these types of armour layers, a well-considered estimation of the roughness/permeability factor γ_f was made.

For composite structures such as vertical walls with a rubble mound protection, a kind of 'mean value' has to be determined for γ_f.
As the influence of the roughness/permeability of the part of the structure which is situated below swl is found to be low (see TAW, 2002), the value of γ_f is determined only by the structure part situated above swl. This implies that in case of a vertical wall with a rubble mound protection situated entirely below swl, a value of $\gamma_f = 1$ is assigned to the structure.
In case two different types of roughness/permeability appear above swl, a weighed mean value is taken for the γ_f -value over the height of $1.5H_{m0\,toe}$ above swl, taking into account the width of the eventually present berm.

In order to distinguish the estimated values of γ_f (a.o. table 3.5) from the derived values of γ_f from model tests (only table 3.4), all estimated values of γ_f are marked in the database with the colour red, see section 3.8.

It should be remarked that the γ_f -values determined within CLASH concern small scale roughness/permeability -values, based on small scale testing with wave heights $H_{m0\,toe} < 0.15$m. This is in contrast with the γ_f -values proposed by TAW (2002), which are related to values of $H_{m0\ toe} > 0.75$m. In addition, the CLASH γ_f -values are determined for values of the breaker parameter ξ_{0p} in between approximately 3 and 5, whereas the previously determined γ_f -values by TAW (2002) are related to values of the breaker parameter $\xi_{0p} < 2$.
The implication on the γ_f -values in table 3.4 is dual. When only considering the effect of the small scale tests, smaller values of γ_f are obtained compared to TAW (2002), as a larger hydraulic roughness is felt by the waves. However, the value of ξ_{0p} also influences the γ_f -values. In TAW (2002) is mentioned that the influence of

roughness on impermeable slopes decreases for values of ξ_{0p} larger than 2, where no roughness is felt anymore for values of ξ_{0p} larger than 8. Van der Meer describes that for rough, permeable slopes the influence of roughness also decreases for values of ξ_{0p} larger than 2, but no reduction is found anymore for values of ξ_{0p} larger than approximately 5 (see Pearson et al., 2004b). Consequently, the γ_f -values proposed in table 3.4 apply for values of the breaker parameter ξ_{0p} = 3 to 5 whereas for smaller/larger values of ξ_{0p} a slightly smaller respectively larger γ_f -value may be expected.
The γ_f -values mentioned in table 3.5 also correspond to small scale tests. Although no specific attention was given to the value of ξ_{0p} , it is estimated that table 3.5 is also related to values of ξ_{0p} = 3 to 5, which leads to comparable γ_f -values for the entire database.

It should be remarked that besides the roughness and permeability, the absolute porosity of the structure (i.e. total volume of pores = porosity * volume) also contributes to the γ_f -value. A larger pore volume relative to the amount of water which is hitting and rushing up the slope leads to a lower γ_f -value due to the larger storing capacity of the structure. This 'reservoir effect' depends on the slope of the structure and the wave length (both incorporated in the value of ξ_0): long waves on steep slopes (i.e. a large value of ξ_0) feel this effect less compared to short waves on shallow slopes (i.e. a small value of ξ_0).

3.6.4 Influence of a recurve wave wall

Quite a lot of coastal structures are equipped with a (small or large) recurve wave wall with the aim of reducing the phenomenon of wave overtopping. A recurve wave wall 'turns' the waves at the top of the structure back seawards resulting to some extend in a lower overtopping quantity, depending on the relative height and the dimensions of the recurved part of the wave wall. At the moment of writing this thesis (end of 2004 - beginning of 2005), studies on the influence of a recurve wave wall are ongoing (see Pearson et al., 2004a), but the exact influence of its presence on the overtopping quantity is not yet known. In expectation of more detailed knowledge on this subject, the influence of a recurve wave wall is assessed as described in this section.

For the set-up of the database, a distinction is made between large and small recurve wave walls (figure 3.21), leading to a different way of schematising the corresponding tests.
A large recurve wave wall is defined within this work as a recurve wave wall having a dominant effect on the structure geometry. A small recurve wave wall on the other hand is defined as a minor construction part, such as an extra curve which is given to a small wall on top of a rubble mound structure.

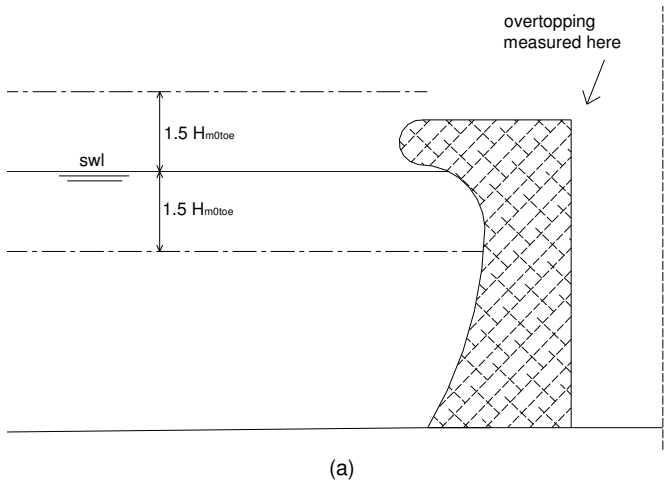

Figure 3.21 Distinction between a large (a) and a small (b) recurve wave wall

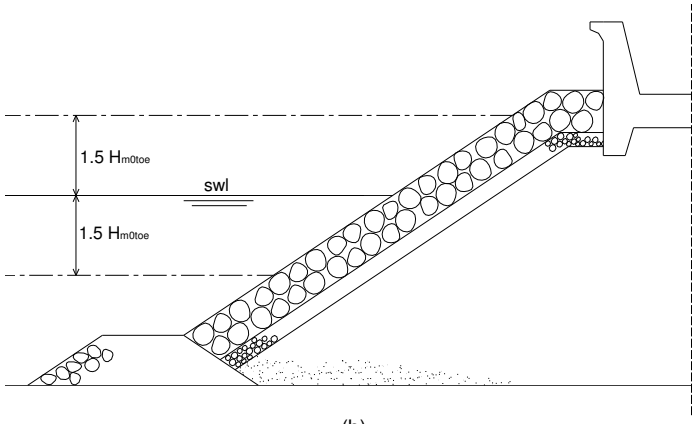

(b)

Figure 3.21 (continued) Distinction between a large (a) and a small (b) recurve wave wall

How each of these recurve wave walls is incorporated in the schematisation of the structure for the database is explained below.

3.6.4.1 Case (a): large recurve wave wall

As a large recurve wave wall influences the entire structure shape, it seems most adequate to include it in the main parameters describing the structure section (figure 3.21 (a)). In this way, the recurve wave wall can be considered as a composite slope consisting of two different slopes separated by a transition point at depth h_b . The upper slope leans back seaward introducing a negative value for its cotangent.

In figure 3.22 the same recurve wave wall as in figure 3.21 (a) is represented with a possible schematisation. The schematisation parameters describing the recurve wave wall are given in the figure.
The transition point is chosen rather arbitrary, providing upper and down slope with a good fitting to the structure.

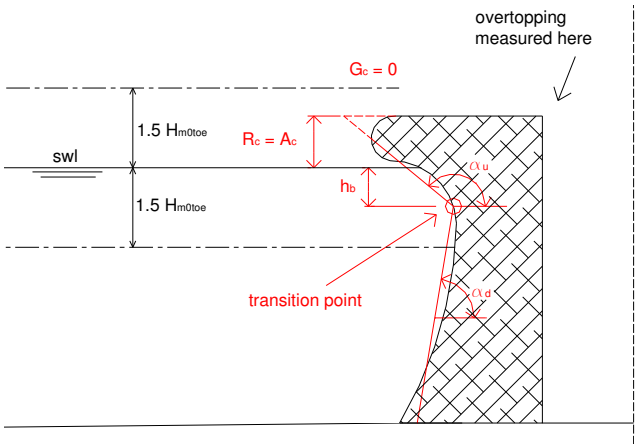

Figure 3.22 Schematisation of a large recurve wave wall

3.6.4.2 Case (b): small recurve wave wall

Compared to the previous case, a small recurve wave wall is much less dominant regarding the overall structure geometry (figure 3.21 (b)). It is clear that in case of a small recurve wave wall its description by means of the structure slope is not adequate.

The methodology for a small recurve wave wall which is used here, is based on the method proposed in TAW (2003) for vertical walls, in which the effect of a recurve wave wall is accounted for as a higher roughness of the structure felt by the waves, resulting in a lower value of γ_f.

Determining the final value of γ_f for the database is therefore performed in two steps. In a first step, the γ_f -value for a structure is determined according to section 3.6.3.8, resulting in a γ_f -value accounting for the roughness and permeability of the structure. In a second step an eventually extra reduction for a recurve wave wall is carried out. How this extra reduction is determined, based on TAW (2003), and extended for rough structure types, is described below.

Eqs. (3.12) and (3.13) describe the applied reduction for a small recurve wave wall. '$\gamma_{f\ armour}$' refers to the value of the roughness/permeability factor obtained solely due to the effect of roughness and permeability of the structure. This corresponds to the value of γ_f which is obtained by applying the methodology described in section 3.6.3.8. The mentioned 'γ_f' in eqs. (3.12) and (3.13) refers to the final value of the roughness/permeability factor, including the effect of a small recurve wave wall. When further in this thesis the roughness/permeability factor 'γ_f' is mentioned, the effect of a small recurve wave wall is included.

In case of a **rough** structure, i.e. $\gamma_{f\ armour} < 0.9$:

$$\begin{aligned} &\text{for } R_c/H_{m0\ toe} \geq 0.5 \quad : \gamma_f = \gamma_{f\ armour} - 0.05 \\ &\text{for } R_c/H_{m0\ toe} < 0.5 \quad : \gamma_f = \gamma_{f\ armour} \end{aligned} \tag{3.12}$$

In case of a **smooth** structure, i.e. $\gamma_{f\ armour} \geq 0.9$:

$$\begin{aligned} &\text{for } R_c/H_{m0\ toe} > 1 \quad : \gamma_f = \gamma_{f\ armour} - 0.3 \\ &\text{for } R_c/H_{m0\ toe} \leq 0.5 \quad : \gamma_f = \gamma_{f\ armour} \\ &\text{for } 0.5 < R_c/H_{m0\ toe} \leq 1 \quad : \text{interpolation} \end{aligned} \tag{3.13}$$

As the effect of a recurve wave wall on the overtopping phenomenon is only significant for relatively high crests (for low crests the waves just pass the structure without 'feeling' the recurve wave wall), the reduction depends on the value of $R_c/H_{m0\ toe}$. The reduction due to the presence of a small recurve wave wall is limited for rough structures, in order to exclude unrealistic low values of γ_f .

Eqs. (3.12) and (3.13) are graphically represented in figure 3.23 (a) respectively figure 3.23 (b).
Although the discontinuity in the reduction factor for rough structure types at the value of $R_c/H_{m0\ toe} = 0.5$ cannot appear in reality (see figure 3.23 (a)), it was utilised as approximation for practical use.

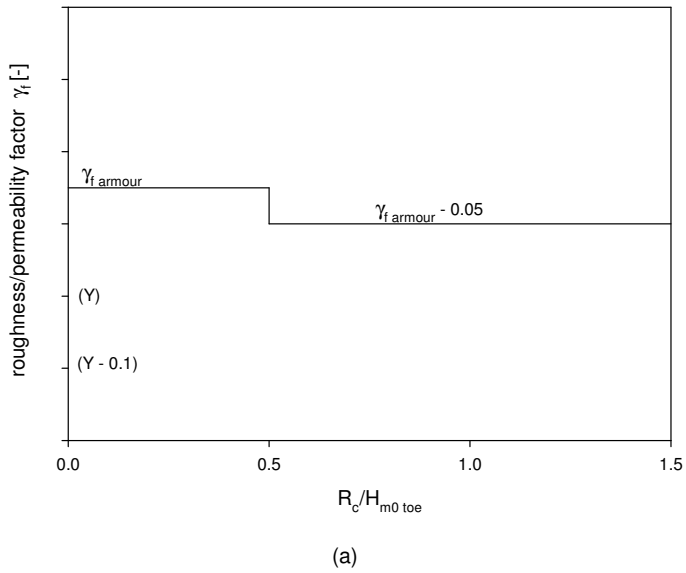

Figure 3.23 Roughness/permeability factor for (a) rough structures and (b) smooth structures

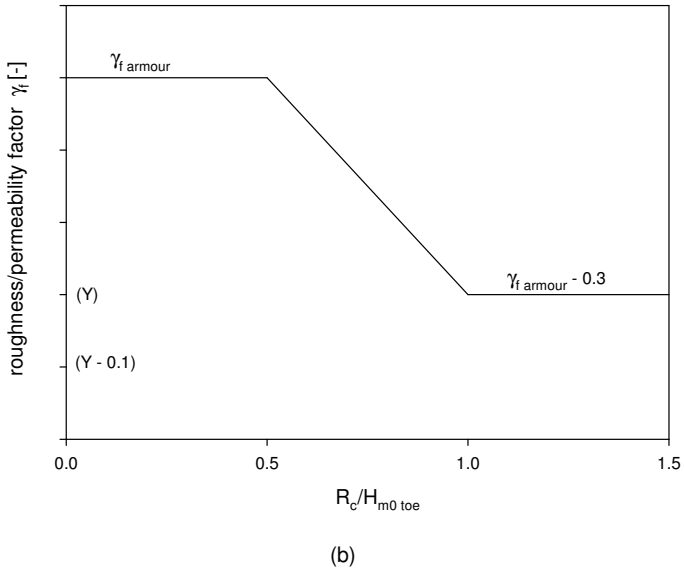

(b)

Figure 3.23 (continued) Roughness/permeability factor for (a) rough structures and (b) smooth structures

Figure 3.24 shows an example of a structure with a small recurve wave wall. The value of $\gamma_{f\ armour}$ is equal to 1 as the rubble mound structure is situated below swl. Regarding the level of the recurve wave wall (R_c /$H_{m0\ toe}$ > 1), eq. (3.13) and figure 3.23 (b) lead to a value of γ_f equal to 1 - 0.3 = 0.7.

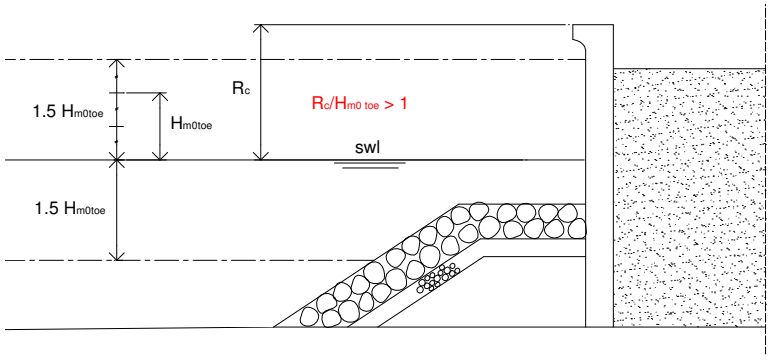

Figure 3.24 Influence of a small recurve wave wall on γ_f

As the reduction of γ_f to account for the presence of a small recurve wave wall concerns an estimation of γ_f , these reduced values are also marked in red in the database (see section 3.8).

3.6.5 Schematisation of difficult overtopping sections

The 17 structural parameters of the database do not allow to describe all overtopping sections evenly well. Some overtopping tests concern quite complicated structure sections which are schematised rather roughly by these 17 parameters. A minority of structure sections is assessed as too difficult to schematise with the available parameters, implicating that an unreliable representation of the structure section is obtained if doing so, i.e. too much information on the structure section is lost when only the 17 structural parameters are considered.

In this section five examples of rather complex overtopping structures are given as well as a possible schematisation, leading to an acceptable representation of the structure section. In some cases several solutions are possible.

- Example 1: Structure with a horizontal part with width > L_0 (figure 3.25)

Within a structure section, a horizontal (or slightly sloping) part with a length of more than one wave length L_0 can not be considered as a berm. In these cases the structure part is preferably considered as a part of the foreshore (see section 3.6.2). Consequently, the parameter m is approximated, leading to a rather rough schematisation of the foreshore slope. Another consequence is that the toe of the structure moves to the right (see figure 3.25) and SWAN calculations are needed to determine the wave characteristics at that location.

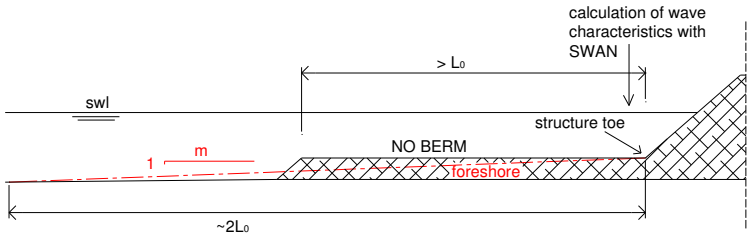

Figure 3.25 Example 1

- Example 2: Structure consisting of more than 2 subsequent slopes (figure 3.26)

Figure 3.26 shows a structure section consisting of three subsequent sloping parts. As stated in section 3.6.2 the slope 1:5 is too steep to be considered as a berm. The problem can be solved by considering the structure as a composite slope. The lowest transition point is included in the schematisation by considering the part of

the structure below as a structure toe with B_t = 0m. The upper transition point is defined as the transition depth h_b in between the upper and lower slope. The schematisation parameters are marked in figure 3.26.

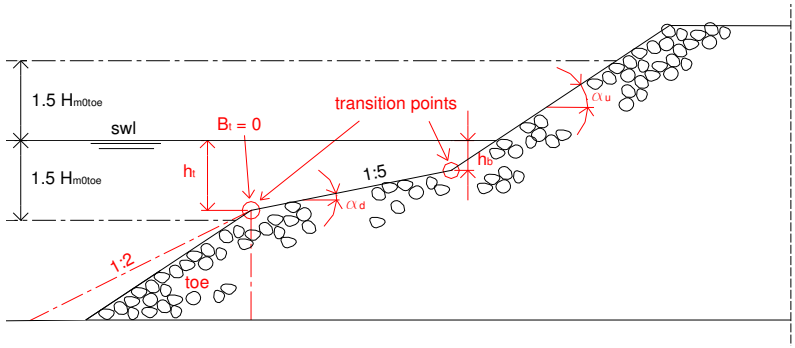

Figure 3.26 Example 2

- Example 3: Structure with more than one berm (figure 3.27)

The possibility exists that a structure is composed of several slightly sloping and horizontal parts. Figure 3.27 shows a structure consisting of two horizontal parts (two 'berms'), as well as a possible schematisation.

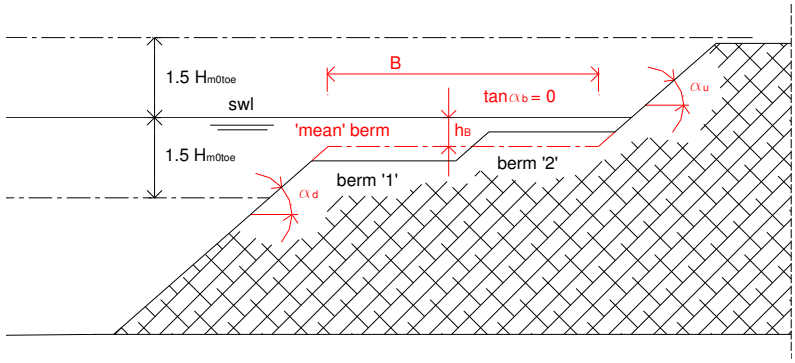

Figure 3.27 Example 3

As the difference in level between the two berms is quite small, the two horizontal parts can be schematised by means of one larger berm, with a mean berm level. The berm width is determined here by lengthening the upper and lower slope up to the level of the mean berm.

If the width of the two berms differs a lot (in this example they are almost equal), a weighed mean level for the mean berm can be taken.
Another possible schematisation could include a sloping berm, described by means of a value of $\tan\alpha_B$ different from zero and $B_h < B$.

- Example 4: A complicated toe configuration (figure 3.28)

In figure 3.28 the lower part of a structure is represented, consisting of a composite toe. The thin part at the left side in the figure can be ignored as it is situated relatively low compared to the rest of the toe. The two remaining parts of the toe are incorporated into a mean toe.

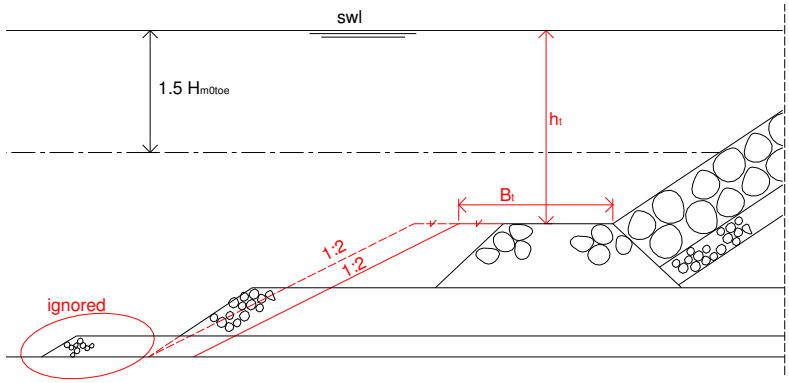

Figure 3.28 Example 4

As mentioned in section 3.6.3.4, it is assumed that the slope of a structure toe is approximately 1:2. By starting at the beginning of the toe (left in the figure below, at the intersection of the extended lower part with the bottom), assuming a slope of 1:2, and taking a 'mean' toe width, the value of B_t can be determined. The depth of the toe is taken equal to the depth of the highest part of the toe.
Other schematisations can be thought of, e.g. the toe level can be determined as the mean value of the levels of the two main toe parts. An argument to perform the schematisation as shown in figure 3.28 is the fact that the highest part of the toe is the part which is mostly felt by the waves.

- Example 5: Structure with a sloping crest (figure 3.29)

Figure 3.29 shows a structure containing a sloping crest configuration. As the sloping part is situated in the upper part of the structure, it should be schematised as a part of the crest.

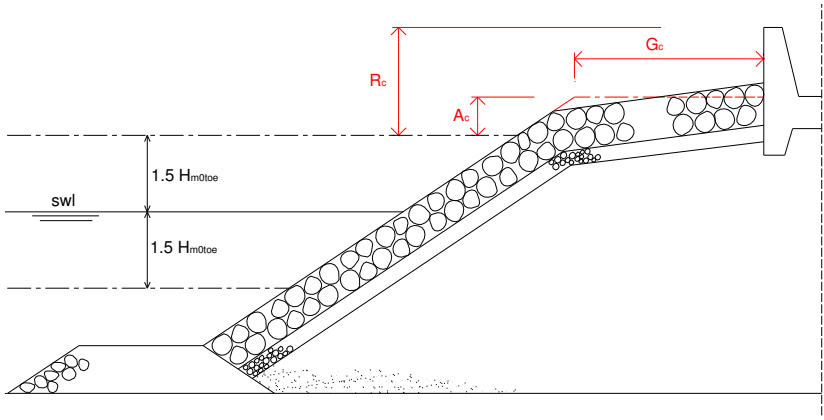

Figure 3.29 Example 5

The upper sloping part is schematised horizontally by drawing a horizontal line through the middle of the crest. Extending the slope of the structure results in the value for G_c.

3.7 Determination of the general parameters

The database contains for each overtopping test three general parameters: Name, RF and CF. This section explains how these parameters are assigned a value.

3.7.1 Name of the test

The first parameter, Name, assigns a unique name to each test. It consists of a basic test series number, which is the same for all the tests within the same test series, followed by a unique number for each test. The parameter Name is always composed of 6 characters. E.g. test 36 from test series 178 has the unique code: 178-036.

This parameter is only meant to recognise each test but has no further meaning.

3.7.2 The complexity factor CF

The complexity factor CF gives an indication of the complexity of the overtopping structure. The factor refers to the degree of approximation which is obtained by describing a test structure by means of structural parameters in the database. It should be mentioned that only the structure section itself is considered, i.e. an approximation of the foreshore is not accounted for in the value of CF.

Table 3.6 gives an overall view of the values the complexity factor CF can adopt. For each value a short explanation is given.

Table 3.6 Values of the complexity factor CF

CF	Meaning
1	simple section: the structural parameters describe the section exactly or as good as exactly
2	quite simple section: the structural parameters describe the section very well, although not exactly
3	quite complicated section: the structural parameters describe the section appropriate, but some difficulties and uncertainties appear
4	very complicated section: the section is too complicated to describe with the structural parameters, the representation of the section by these is unreliable

3.7.3 The reliability factor RF

The reliability factor RF gives an indication of the reliability of the considered overtopping test.

Table 3.7 gives an overall view of the values the reliability factor RF can adopt. For each value a short explanation is given.

Table 3.7 Values of the reliability factor RF

RF	Meaning
1	very reliable test: all needed information is available, measurements and analysis were performed in a reliable way
2	reliable test: some estimations/calculations had to be made and/or some uncertainties about measurements/analysis exist, but the overall test can be classified as 'reliable'
3	less reliable test: some estimations/calculations had to be made and/or some uncertainties about measurements/analysis exist, leading to a classification of the test as 'less reliable'
4	unreliable test: no acceptable estimations/calculations could be made and/or measurements/analysis include faults, leading to an unreliable test

The reliability factor RF is determined by several factors:

- the precision of the measurements/analysis of the researcher who performed the overtopping test
- the restrictions/possibilities of the test facility used to perform the test
- the estimations/calculations which had to be made because of missing parameter values

Table 3.8 gives a detailed overall view of the qualifying factors of RF and the corresponding value assigned to it, as determined for all overtopping tests included in the overtopping database.

Table 3.8 Determination of the reliability factor RF

- absorption system of the test facility:

→ active wave absorption is available: RF = 1
→ only passive wave absorption is available: RF = 2
→ no wave absorption system is available:
if low reflective structure: RF = 2
if high reflective structure: RF = 3

- wave generation system of the test facility:

→ regular waves are generated: RF = 4
→ irregular waves are generated:
if short-crested: RF = 1
if long-crested:
RF dependent on angle of wave attack:
if $\beta = 0°$: RF = 1
if $0 < \beta \leq 30°$: RF = 2
if $30 < \beta \leq 45°$: RF = 3
if $\beta > 45°$: RF = 4

- wave measurements:

→ reflection analysis is performed (separation of incident from reflected waves): RF = 1
→ no reflection analysis is performed (only total waves): RF = 3

- water depth at the toe of the structure:

→ if $h \leq 0$ (implicating that no wave characteristics at the toe are known or possible to calculate): RF = 4
→ if h is very small and no wave characteristics at the toe are available (no accurate calculations with SWAN are possible): RF = 4

- reliability of estimated wave periods at the toe of the structure if no calculations with SWAN (reliability dependent on degree of wave breaking):

→ if wave heights are known at deep water and at the toe of the structure:
- if $H_{m0\ toe}/H_{m0\ deep} > 0.6$: RF = 1
  (little breaking waves; spectral shape at the toe of the structure ≈ spectral shape at deep water; reliable estimation)
- if $H_{m0\ toe}/H_{m0\ deep} < 0.4$: RF = 3
  (breaking waves; spectral shape at the toe of the structure ≠ spectral shape at deep water; breaking = more energy for the low frequent components; no reliable estimation)
- if $0.4 \leq H_{m0\ toe}/H_{m0\ deep} \leq 0.6$: RF = 2
  (partially breaking waves; less reliable estimation)

→ if wave heights are only known at the toe of the structure:
- if $H_{m0\ toe}/h < 0.73$: RF = 1
  (little breaking waves)
- if $H_{m0\ toe}/h > 1$: RF = 3
  (breaking waves)
- if $0.73 \leq H_{m0\ toe}/h \leq 1$: RF = 2
  (partially breaking waves)

Table 3.8 (continued) Determination of the reliability factor RF

• calculations with Battjes and Groenendijk (2000)
RF = 2
• calculations with SWAN:
→ reliability dependent on the dimension of the situation: ➢ if two-dimensional situation (model test in wave flume): RF = 2 ➢ if three-dimensional situation (model test in wave basin or prototype measurement): RF = 3 → reliability dependent on the degree of wave breaking ($T_{m-1,0\ toe}$ always estimated): ➢ if $H_{m0\ toe}/H_{m0\ deep} > 0.6$: RF = 2 (little breaking waves) ➢ if $H_{m0\ toe}/H_{m0\ deep} < 0.4$: RF = 4 (breaking waves) ➢ if $0.4 \leq H_{m0\ toe}/H_{m0\ deep} \leq 0.6$: RF = 3 (partially breaking waves) ➢ if $H_{m0\ toe}/h < 0.73$: RF = 2 (little breaking waves) ➢ if $H_{m0\ toe}/h > 1$: RF = 4 (breaking waves) ➢ if $0.73 \leq H_{m0\ toe}/h \leq 1$: RF = 3 (partially breaking waves) → reliability dependent on the foreshore steepness: ➢ if foreshore slope 1/30 or less steep: RF = 2 ➢ if foreshore slope steeper than 1:30: RF = 3

It should be pointed out that the indicated RF -values in table 3.8 are minimum values. This means that if more than one of the mentioned influencing factors appeared within one test, at least the highest value of RF (lowest reliability) was restricted and eventually even a higher value of RF was assigned to the corresponding test.

3.8 Lay-out of the overtopping database

The final database consists of 10532 overtopping tests which are represented by an equal number of rows in a spreadsheet.

All tests are included in the database on the scale on which the measurements were performed, i.e. laboratory data are included with corresponding model values and prototype data with real, prototype values.

It could be important for researchers using the overtopping database to know which parameter values concern real measured values, which ones concern calculated values and which ones concern estimated values. This can not be checked by the value of RF as this factor only gives an overall indication of the reliability of the test.
To distinguish such cases from each other, colours were used to mark the calculated and estimated values:

- blue for wave characteristics at the toe of the structure calculated with SWAN
- green for wave heights at the toe of the structure calculated from $H_{1/3}$ with the method of Battjes and Groenendijk (2000)
- red for estimated wave period parameters from other period parameters
- red for estimated values of the roughness/permeability factor γ_f (which is the case for all structures with armour layers not present in table 3.4, and if a reduction for a small recurve wave wall is included)

Beside the 31 columns already mentioned (resulting from 11 hydraulic parameters, 17 structural parameters and 3 general parameters), 2 more columns are added to the spreadsheet (table 3.9).

The first added column, column 32, is called 'Remark' and contains a remark additional to the test, mainly bearing in mind a neural network application of the database.
As model and scale effects may affect small scale overtopping measurements in specific cases, prototype measurements should be left out from a neural network development. In chapter 4 section 4.4.2, more background information will be given on this subject. Further also laboratory measurements performed with artificial wind generation should not be considered for a neural network development. The fact that wind is no parameter of the database can be mentioned as reason for this. Finally, a part of the laboratory tests concerns test sections not appearing in reality (i.e. a synthetic test set-up in the laboratory), and should consequently also be left out from a neural network application.

Column 32 marks the three mentioned types of tests, and advises against using these for the development of a neural prediction method. For the laboratory tests with artificial wind generation, the generated wind velocity is mentioned as well.
The total number of prototype tests is 132, whereas a number of 223 laboratory tests is performed with artificial wind generation. Finally, 154 tests concern synthetic laboratory test sections. These last tests were given a CF -value equal to 4, which automatically implicates that these tests will not be used for the development of the neural prediction method in this thesis (see definition of weight factor in chapter 4, section 4.3.3).

Table 3.9 Information summarised in the database

Column number	Contents	Nature of parameter
1	Name	general
2	$H_{m0\ deep}$ [m]	hydraulic
3	$T_{p\ deep}$ [s]	hydraulic
4	$T_{m\ deep}$ [s]	hydraulic
5	$T_{m-1,0\ deep}$ [s]	hydraulic
6	h_{deep} [m]	structural
7	m [-]	structural
8	β [°]	hydraulic
9	h [m]	structural
10	$H_{m0\ toe}$ [m]	hydraulic
11	$T_{p\ toe}$ [s]	hydraulic
12	$T_{m\ toe}$ [s]	hydraulic
13	$T_{m-1,0\ toe}$ [s]	hydraulic
14	h_t [m]	structural
15	B_t [m]	structural
16	γ_f [-]	structural
17	$\cot\alpha_d$ [-]	structural
18	$\cot\alpha_u$ [-]	structural
19	$\cot\alpha_{excl}$ [-]	structural
20	$\cot\alpha_{incl}$ [-]	structural
21	R_c [m]	structural
22	B [m]	structural
23	h_b [m]	structural
24	$\tan\alpha_B$ [-]	structural
25	B_h [m]	structural
26	A_c [m]	structural
27	G_c [m]	structural
28	RF	general
29	CF	general
30	q [m^3/s/m]	hydraulic
31	P_{ow} [%]	hydraulic
32	Remark	extra information column
33	Reference	extra information column

A second added column, column 33, is called ‘Reference’. For public tests, column 33 contains a reference to a report or paper describing the tests. This allows interested researchers to find more information on specific tests or test series.

3.9 Contents of the overtopping database

In this section an overall view is given of the contents of the database, i.e.:

- the included range, mean value and standard deviation of the parameters
- the distribution of single parameter values within their range
- possible relationships between parameters

Not all parameters will be studied one by one in this section, but the reader should get an idea of what the contents of the database looks like on the basis of figures.

3.9.1 Reliability of the data

Not all tests included have equal reliability. This aspect is included in the database by means of 2 parameters: the reliability factor RF and the complexity factor CF as described in the previous chapter.
Table 3.10 gives an overall view of the number of tests present in the database with a specific combination of values of RF and CF.

Table 3.10 Overall view of reliability

reliability factor RF	complexity factor CF	number of tests in database
1	1	2631
1	2	210
1	3	341
1	4	204
2	1	2901
2	2	315
2	3	371
2	4	11
3	1	1753
3	2	757
3	3	124
3	4	8
4	1	704
4	2	123
4	3	48
4	4	31
	TOTAL:	10532

As can be deduced from table 3.10, the number of tests in the database with RF = 4 and/or CF = 4 is 1129. These concern ‘unreliable’ tests. The tests with RF = 4 (906 tests) refer to non-reliable tests regarding the measured values of the wave parameters. The tests with CF = 4 (254 tests, of which 223 with RF ≠ 4) refer to tests with a non-reliable representation of the structure section by the included

structural parameters. The tests with CF = 4 and RF ≠ 4 have to be considered therefore not really as unreliable tests, but as tests which could not be included in the database in a reliable way. Public data with CF = 4 and RF ≠ 4 can still be useful for further research, supposing that the corresponding report of the data is tracked, and correct information about the test section is considered.
In this context, the data in the database which are not useful for further research, so the data with only RF = 4, correspond with 906 tests, constituting approximately 8.60% of the total database. An extra 2.12% data with CF = 4 corresponds to possible useful data on condition that further information is found (CF = 4, and RF ≠ 4).

For tests with RF = 4 or CF = 4 sometimes values of parameters are missing in the database. Those tests will be excluded from the analysis in next sections. This implies that the number of tests which are considered in the analysis is 10532-1129 = 9403.

3.9.2 Measured overtopping discharges

To get an idea of the contents of the database, focussing on the measured wave overtopping discharges, one can make some commonly used graphs.

In figure 3.30 the dimensionless wave overtopping discharge $\frac{q}{\sqrt{gH_{m0\ toe}^3}}$ is represented versus the dimensionless crest freeboard $R_c / H_{m0\ toe}$. Figure 3.30 (a) shows all data, whereas figure 3.30 (b) zooms in on the area with most results, i.e. $R_c / H_{m0\ toe} \leq 5$.

To get an idea of the position of the data, two extra lines are represented in the figures: the overtopping formula of TAW (2002), set up for surging conditions at smooth dikes (see chapter 2, eq. (2.5b)), and the formula of Franco et al. (1994), for overtopping at vertical walls in relatively deep water (see chapter 2, eq. (2.13)).

Wave overtopping tests where no overtopping occurred, i.e. tests which are included in the database with a value for q of 0 $m^3/s/m$, are represented in the figures with a value of $\frac{q}{\sqrt{gH_{m0\ toe}^3}} = 10^{-8}$.

This fictive low dimensionless overtopping discharge is used to get an idea of the crest heights of the tests where no overtopping occurred.

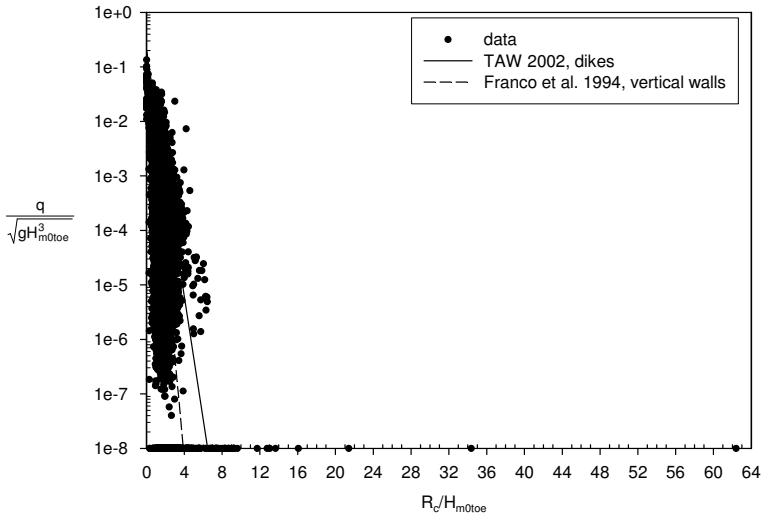

(a)

Figure 3.30 Dimensionless overtopping discharge versus dimensionless crest freeboard

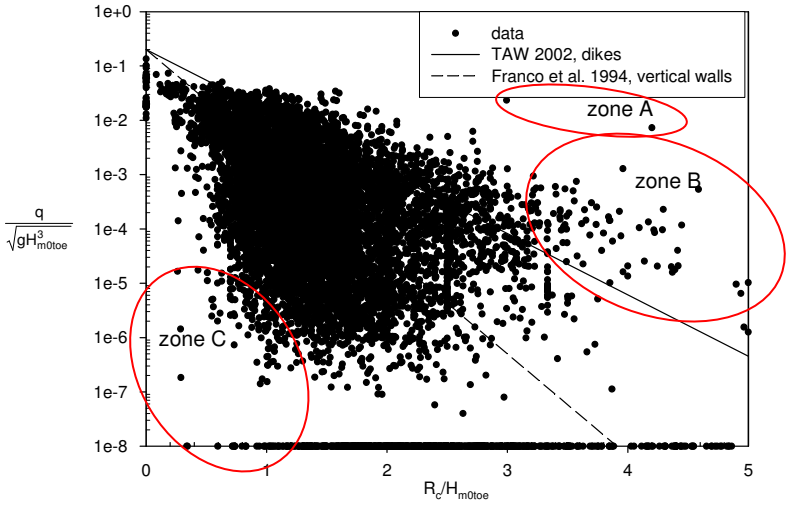

(b)

Figure 3.30 (continued) Dimensionless overtopping discharge versus dimensionless crest freeboard

The data on the right side of figure 3.30 (a) correspond to overtopping tests with very low values for $H_{m0\ toe}$, resulting in high values of $R_c/H_{m0\ toe}$.
In figure 3.30 (b), some zones with data are marked. Each of these correspond to a specific type of test structure and/or wave action.
Zone A contains 2 remarkable data points, giving high values for the dimensionless overtopping discharge, for relative high values of $R_c/H_{m0\ toe}$. These data correspond to tests where very heavy wave breaking occurred on a shallow foreshore, introducing effects of surf beat. The broken wave height in these tests is only 0.02m in a water depth of h = 0.033m, in combination with a value of $T_{m-1,0\ toe}$ = 10s.
Zone B often refers to tests with a structure section consisting of a vertical wall on a steep foreshore slope or a berm, where impacting waves occurred at the structure location. It should be noticed that in such test situations, relatively high overtopping values are measured (see position of data relative to the TAW -line).
Finally, zone C marks data with rather low values for the dimensionless overtopping discharge in combination with low values for $R_c/H_{m0\ toe}$. These points often refer to tests on a rubble mound structure. Specific structure characteristics such as a wide crest (high value of G_c) and/or a high crest (high value of A_c), are causing rather low values here for the dimensionless overtopping discharge.

3.9.3 Study of single parameters

3.9.3.1 Single parameter ranges

In table 3.11 an overall view is given of the range (minimum and maximum value), the mean value and the standard deviation of each parameter included in the database. As the tests included in the database contain small scale laboratory tests as well as prototype tests, in most cases the minimum (dimensional) values correspond with small scale model tests and the maximum (dimensional) values with prototype measurements.

Table 3.11 Parameter characteristics of database parameters

Parameter	Minimum	Maximum	Mean	Standard Deviation
$H_{m0\ deep}$ [m]	0.003	5.920	0.178	0.374
$T_{p\ deep}$ [s]	0.722	15.000	1.910	1.160
$T_{m\ deep}$ [s]	0.592	12.500	1.591	0.966
$T_{m-1,0\ deep}$ [s]	0.657	13.636	1.742	1.045
h_{deep} [m]	0	100.000	1.617	9.055
m [-]	6.000	1000.000	454.316	464.918
β [°]	0	80.000	3.517	11.218
h [m]	0.029	9.320	0.498	0.647
$H_{m0\ toe}$ [m]	0.003	3.765	0.155	0.263
$T_{p\ toe}$ [s]	0.727	16.400	1.959	1.334
$T_{m\ toe}$ [s]	0.606	11.781	1.574	0.939
$T_{m-1,0\ toe}$ [s]	0.661	10.640	1.769	1.059
h_t [m]	0.025	7.780	0.441	0.607
B_t [m]	0	10.000	0.115	0.511
γ_f [-]	0.330	1.000	0.697	0.274
$\cot\alpha_d$ [-]	0	7.000	1.943	1.446
$\cot\alpha_u$ [-]	-5.000	9.706	1.859	1.723
$\cot\alpha_{excl}$ [-]	-1.533	8.144	1.944	1.494
$\cot\alpha_{incl}$ [-]	-1.533	12.821	2.158	1.710
R_c [m]	0	8.345	0.245	0.548
B [m]	0	8.000	0.081	0.295
h_b [m]	-0.208	1.175	0.012	0.096
$\tan\alpha_B$ [-]	0	0.101	0.002	0.010
B_h [m]	0	8.000	0.074	0.271
A_c [m]	0	7.870	0.226	0.496
G_c [m]	0	5.000	0.155	0.480
RF	1.000	3.000	1.942	0.784
CF	1.000	3.000	1.314	0.627
q [m^3/s/m]	0	$1.653*10^{-1}$	$6.709*10^{-4}$	$5.716*10^{-3}$
P_{ow} [%]	0	81.000	11.352	14.745

To exclude the influence of the scale of the data, all dimensional parameters can be scaled by the Froude model law. This is done here by taking the wave height at the toe of the structure $H_{m0\ toe}$ as scaling parameter, which equals to scaling all tests to the same wave height $H_{m0\ toe}$ = 1m. In chapter 4, section 4.4, more detailed information will be given on this scaling process.

Table 3.12 gives the same characteristics as table 3.11, but this after scaling all parameters according to Froude as mentioned. To avoid confusion with the original parameter values, the scaled parameters are preceded by an 's' in superscript (see also chapter 4). As the dimensionless parameters have a scaling parameter of 1, these parameters remain the same, whether scaled or not.

Table 3.12 Parameter characteristics after scaling to $H_{m0\ toe}$ = 1m according to Froude

Parameter	Minimum	Maximum	Mean	Standard Deviation
${}^{s}H_{m0\ deep}$ [m]	0.692	6.304	1.119	0.333
${}^{s}T_{p\ deep}$ [s]	2.948	94.868	5.373	2.363
${}^{s}T_{m\ deep}$ [s]	2.494	79.057	4.477	1.954
${}^{s}T_{m-1,0\ deep}$ [s]	2.721	86.244	4.904	2.129
${}^{s}h_{deep}$ [m]	0	77.211	6.743	5.056
${}^{s}m$ [-]	6.000	1000.000	454.316	464.918
${}^{s}\beta$ [°]	0	80.000	3.517	11.218
${}^{s}h$ [m]	0.904	64.476	3.900	3.311
${}^{s}H_{m0\ toe}$ [m]	1.000	1.000	1.000	0
${}^{s}T_{p\ toe}$ [s]	2.847	108.138	5.595	3.927
${}^{s}T_{m\ toe}$ [s]	2.105	79.057	4.449	1.940
${}^{s}T_{m-1,0\ toe}$ [s]	2.721	86.244	5.070	3.134
${}^{s}h_{t}$ [m]	0.429	45.429	3.364	2.887
${}^{s}B_{t}$ [m]	0	50.000	0.923	2.057
${}^{s}\gamma_{f}$ [-]	0.330	1.000	0.697	0.274
${}^{s}\cot\alpha_{d}$ [-]	0	7.000	1.943	1.446
${}^{s}\cot\alpha_{u}$ [-]	-5.000	9.706	1.859	1.723
${}^{s}\cot\alpha_{excl}$ [-]	-1.533	8.144	1.944	1.494
${}^{s}\cot\alpha_{incl}$ [-]	-1.533	12.821	2.158	1.710
${}^{s}R_{c}$ [m]	0	62.390	1.571	1.152
${}^{s}B$ [m]	0	38.462	0.707	2.180
${}^{s}h_{b}$ [m]	-2.294	8.411	0.053	0.446
${}^{s}\tan\alpha_{B}$ [-]	0	0.101	0.002	0.010
${}^{s}B_{h}$ [m]	0	38.462	0.694	2.160
${}^{s}A_{c}$ [m]	0	62.390	1.470	1.168
${}^{s}G_{c}$ [m]	0	39.000	0.989	1.537
RF	1.000	3.000	1.942	0.784
CF	1.000	3.000	1.314	0.627
${}^{s}q$ [m^3/s/m]	0	$4.222*10^{-1}$	$7.248*10^{-3}$	$1.938*10^{-2}$
${}^{s}P_{ow}$ [%]	0	81.000	11.352	14.745

The scaled minima and maxima give a more comparable overall view of the tests, in which the distinction between small and large scale tests disappears. It gives an idea of the minima and maxima which would have appeared if all tests were performed with wave heights of 1m at the toe of the structure, keeping all other parameters in proportion.

It should be remarked that table 3.11 as well as table 3.12 give only little information on the distribution of each single parameter. The reader should be aware of the fact that the minimum and maximum values in the tables may be related to outlying data.

3.9.3.2 Single parameter values

In this section, the distribution of the values of some parameters is studied in more detail. This gives an idea of the presence or absence of certain single parameter ranges in the database. Successively the foreshore slope m, the incident wave angle β, the wave height at the toe of the structure $H_{m0\ toe}$, the roughness/permeability factor γ_f , the slope of the berm $\tan\alpha_B$ and the relative crest height R_c /$H_{m0\ toe}$ (which concerns in fact a combination of 2 parameters) are considered.

- **foreshore slope m**

Figure 3.31 (a) shows all values of m included in the database in an increasing order.
Values of m = 1000 refer to foreshores steepening very slowly, or even flat foreshores, e.g. model tests performed without foreshore in the laboratory. Almost 4000 tests, i.e. approximately 42% of the data, correspond to tests performed with a very shallow or flat foreshore. Other frequently appearing values for m are 100 and 50, respectively corresponding to approximately 10% and 7% of the data.
Looking at figure 3.31 (b), which focuses on steep foreshores (corresponding with small values of m), one can see that the number of tests with a foreshore steeper than or equal to 1:10 is about 450, corresponding to almost 5% of the data.

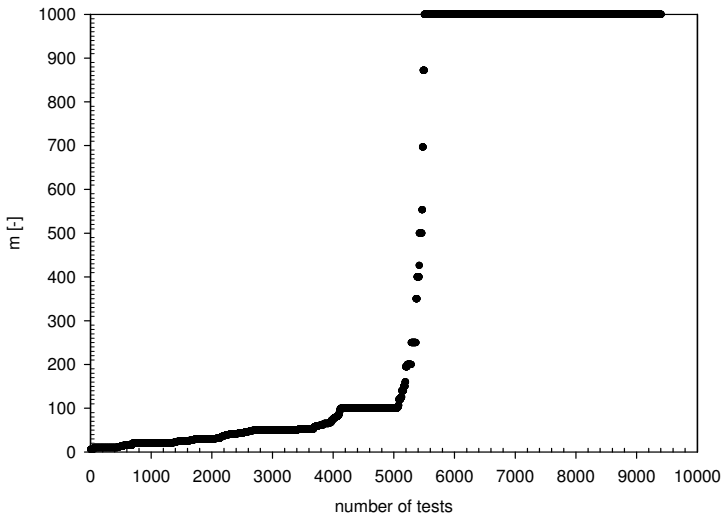

(a)

Figure 3.31 Values of m

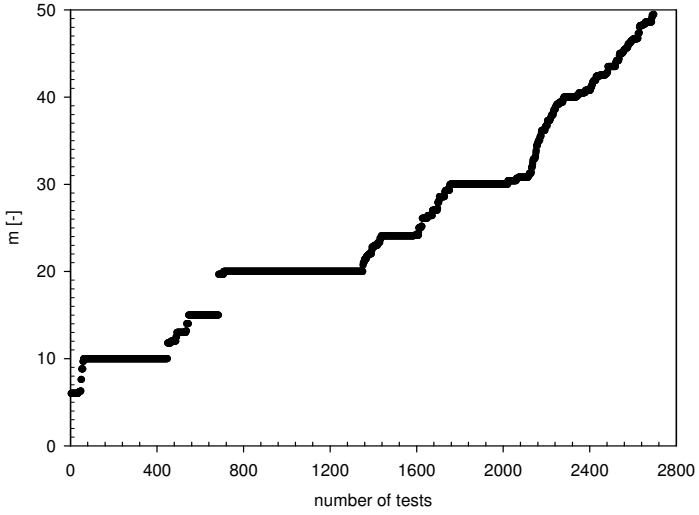

(b)

Figure 3.31 (continued) Values of m

- **Incident wave angle β**

The majority of the included overtopping data concerns 2D tests performed in a wave flume. This implies that for most tests a value of zero is assigned to β, corresponding to wave attack perpendicular to the structure. These tests constitute almost 88% of the data, or more precisely 8260 tests. The remaining 12% of the tests show values of β ranging up to 80 degrees. These last tests concern wave attack almost parallel to the structure.
Figure 3.32 shows the values of β different from zero, corresponding to 1143 tests. It should be remarked that the tests with values of β larger than 45° concern or prototype measurements, or model tests performed with short-crested waves, as model tests with long-crested waves and angles larger than 45° are ranked as unreliable (see section 3.7.3).

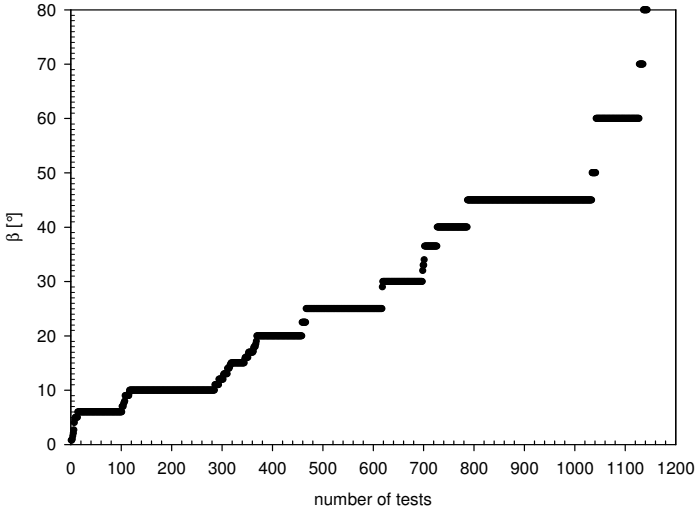

Figure 3.32 Values of β > 0°

Almost half of the tests included in the database with a value of β larger than zero, originate from the white spot tests which were performed within CLASH (see section 3.2). Tests with wave angles of 10°, 25°, 45° and 60° were performed in this context.

- **Incident wave heights $H_{m0\ toe}$**

As the database consists of data originating from small scale tests, large scale tests and even prototype measurements, the wave heights measured at the toe of the structure included in the database adopt values from some millimetres up to a few meters.
Figure 3.33 (a) shows the values of $H_{m0\ toe}$ included in the database, arranged from small to large. About 97% of the tests consists of tests with a wave height $H_{m0\ toe}$ up to 0.5m, see figure 3.33 (b). The majority of these data originate from small scale tests. For the remaining 3% of the data larger values of $H_{m0\ toe}$ are included, see figure 3.33 (c). These data concern large scale of prototype measurements.

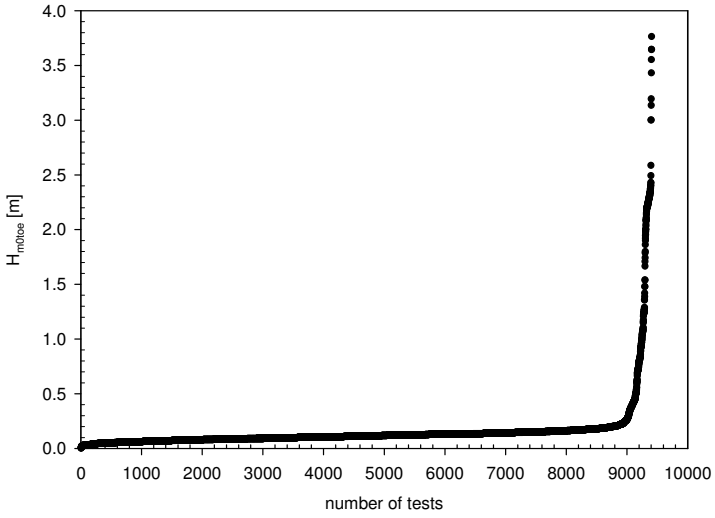

(a)

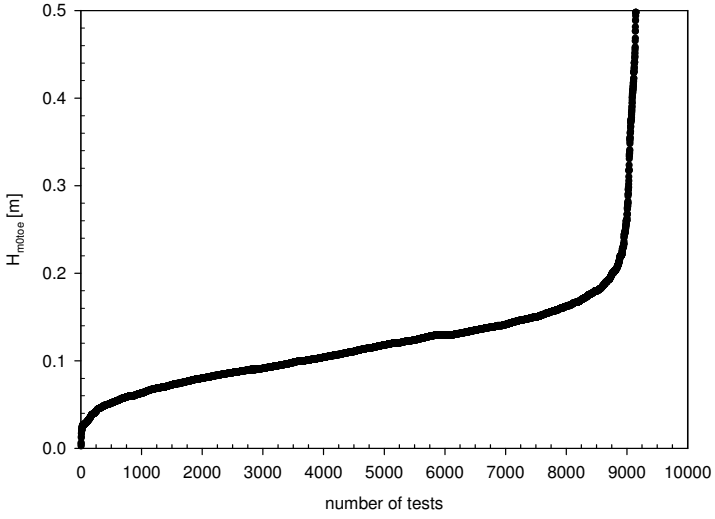

(b)

Figure 3.33 Values of $H_{m0\ toe}$

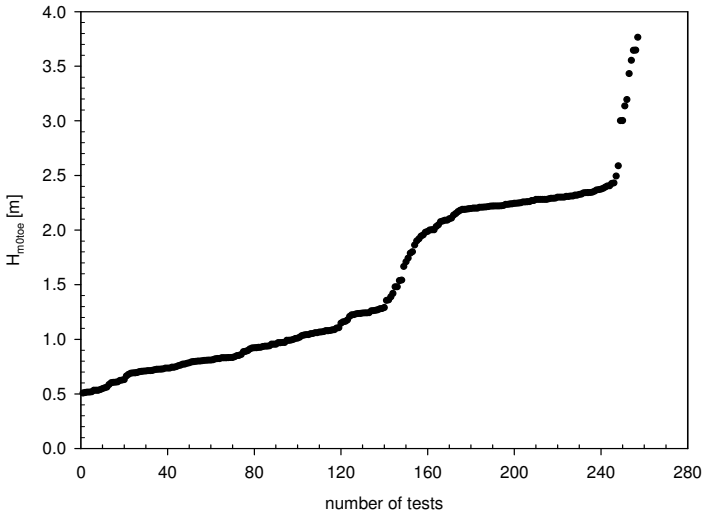

(c)

Figure 3.33 (continued) Values of $H_{m0\ toe}$

- **roughness/permeability factor γ_f**

Figure 3.34 gives an overall view of the values of γ_f included in the database. The values are ranked from small to large.

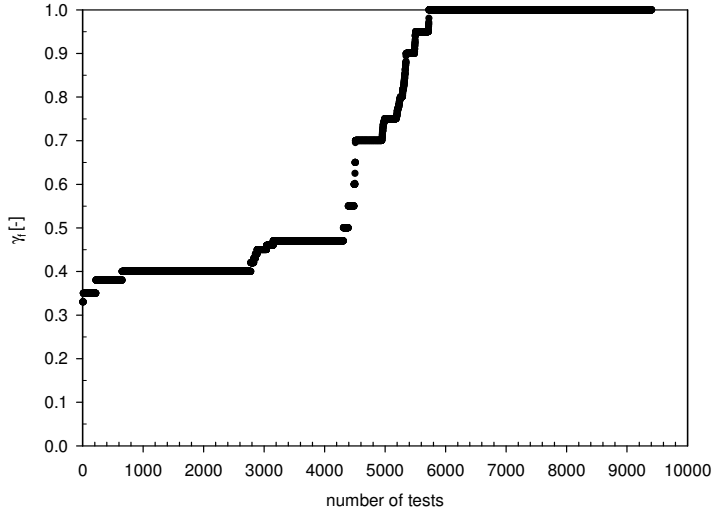

Figure 3.34 Values of γ_f

One can remark that the most appearing value of γ_f is 1, referring to smooth structure types (without influencing recurve wave wall). It concerns about 39% of the data.
A value of γ_f = 0.4 is also frequently included: approximately 23% of the data are assigned a value of 0.4. Most of these data concern tests on rubble mound breakwaters with 2 layers of rock. However, also tests on e.g. reshaping berm breakwaters belong to these tests.
Approximately 12% of the data have a γ_f -value of 0.47, corresponding to tests on rubble mound structures with cubes (2 layers), antifers or HARO's.
The lowest values of γ_f originate from (Icelandic) berm breakwaters and from structures with very rough armour layers such as tetrapods. Structures with a double layer of rocks, including a small recurve wave wall on top, also result in values of γ_f smaller than 0.4.
The values of γ_f = 0.7 up to 1 often originate from smooth vertical walls with a small recurve wave wall, but other structure types such as structures with a smooth but stepped surface are included as well.

- **slope of the berm $\tan\alpha_B$**

To provide the possibility to include a sloping berm in the database, the parameter $\tan\alpha_B$ is included. As stated before, the slope of a berm is preferably restricted to 1/15 and always restricted to 1/10.
In case of a horizontal berm, or in absence of a berm, the value of $\tan\alpha_B$ = 0. The number of tests with $\tan\alpha_B$ = 0 corresponds to over 96% of the data, resulting in only 338 tests with a sloping berm. The values of $\tan\alpha_B$ different from zero present in the database are given in an increasing order in figure 3.35. The steepest berm consists of a slope of 1/10, which is in accordance with the definition of a berm.

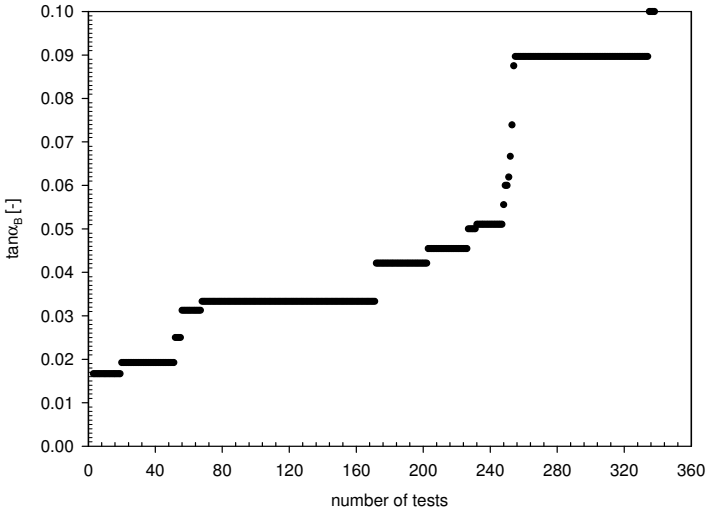

Figure 3.35 Values of $\tan\alpha_B > 0$

As the values of $\tan\alpha_B > 0$ are rather small (by definition) and taking into account the small number of data with $\tan\alpha_B > 0$ (only about 3.5%), it seems most relevant, especially with regard to the development of a neural prediction method, to describe all berms by means of their horizontal schematisation.

- **relative crest height $R_c / H_{m0\ toe}$**

The relative crest height $R_c / H_{m0\ toe}$ is known to be one of the most important factors governing the overtopping phenomenon. Generally, one can state that the mean overtopping discharge decreases if the relative crest height increases.
The value of the relative crest height can adopt high values in case of small values of $H_{m0\ toe}$.
Figure 3.36 (a) shows the relative crest height for all tests included in the database, in increasing order. The largest value of $R_c / H_{m0\ toe}$ is 62.39, corresponding to a test with $H_{m0\ toe}$ = 0.003m, which is the smallest wave height included in the database.
Figure 3.36 (b) zooms in on the dimensionless crest heights between 0 and 5, still corresponding to over 99% of the tests. The smallest value of $R_c / H_{m0\ toe}$ included in the database is zero, corresponding to a test in which the water level equals the structure height.

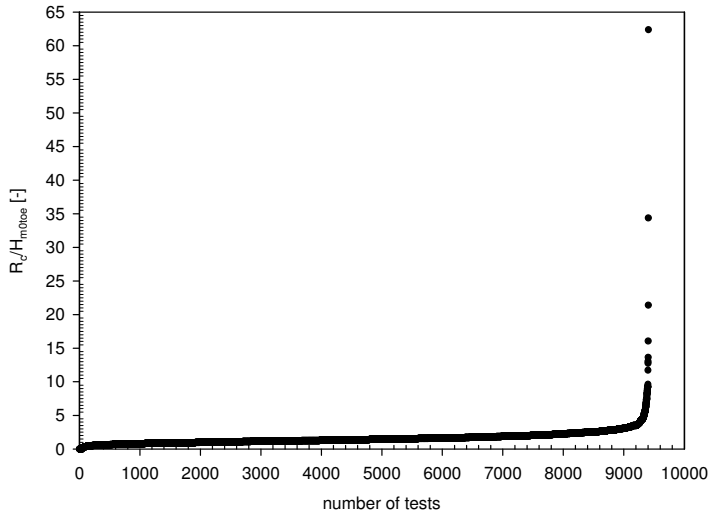

(a)

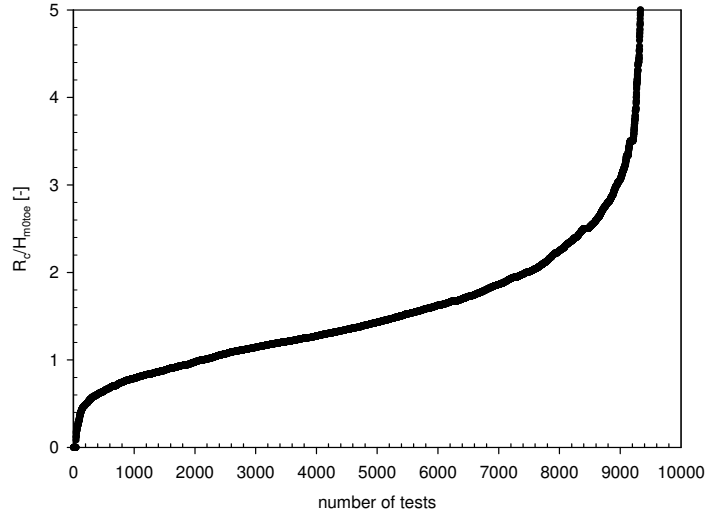

(b)

Figure 3.36 Values of R_c /$H_{m0\ toe}$

3.9.4 Study of combinations of parameters

In the previous section, figures focussed on the possible values of one single parameter (in the last case a dimensionless one) in the database.
In this section the aim is to look at certain combinations of parameter values. In order to exclude the scale of the tests from these figures, the (dimensional) parameters are all non-dimensionalised by $H_{m0\ toe}$.

Four parameter combinations are studied here:

- the relationship between structure slope parameters,
- the relationship between level and width of toe, berm and crest,
- the relationship between crest height and armour height, and between crest width and armour height, and
- the relationship between width of the real berm and width of the horizontally schematised berm.

3.9.4.1 Structure slope parameters

In figure 3.37 the value of $\cot\alpha_u$ is plotted versus the value of $\cot\alpha_d$. A distinction is made between structures with a value of $B_h \neq 0$m and structures with a value of $B_h = 0$m.

Approximately 17% of the data concern structures with a value of $B_h > 0$m (represented by circles in figure 3.37). These concern structures with a berm. About 26% of these data have an equal slope above and below the berm. These points are situated on the diagonal line in figure 3.37. The remaining 74% of these data have different values for the slope above and below the berm. As shown in figure 3.37 the values of $\cot\alpha_d$ may be higher or lower than the values of $\cot\alpha_u$ (below or above the diagonal line in figure 3.37). Data on the horizontal axis correspond to structures with a vertical part above the berm, e.g. a vertical wall with a rubble mound structure in front of it. Data on the vertical axis correspond to structures with a vertical part below the berm, e.g. a vertical wall combined with a sloping dike, separated from each other by a road.

The remaining 83% of the data are structures with a value of $B_h = 0$m (represented by triangles in figure 3.37). These concern structures without a berm. Within this group of tests one can distinguish composite slopes, which have different values for $\cot\alpha_u$ and $\cot\alpha_d$. $\cot\alpha_u$ and $\cot\alpha_d$ stand for the slope above respectively below the transition point here. They are represented by the triangles in figure 3.37, which are *not* situated on the diagonal line. The composite slopes take about 11% of the data with $B_h = 0$m. One can see that a part of the composite slopes have a negative value for $\cot\alpha_u$. These concern structure types with a large (seaward) overhanging upper structure part. The other 89% of the data with $B_h = 0$m

concerns structures schematised by only one single slope angle, i.e. $\cot\alpha_u = \cot\alpha_d$. The latter data are represented by the triangles on the diagonal line.

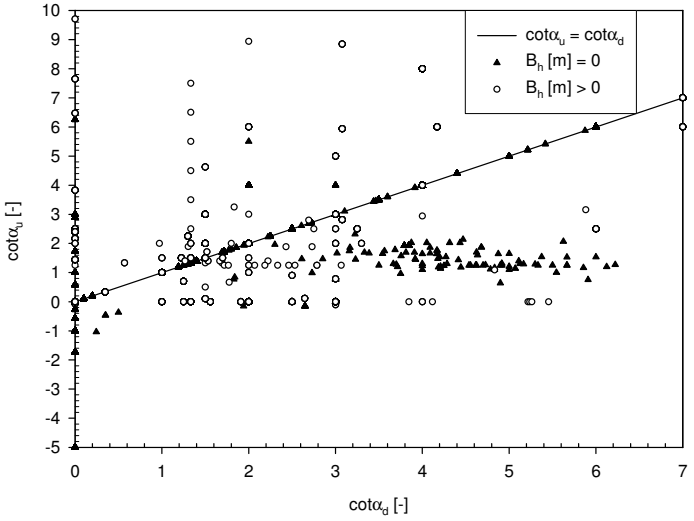

Figure 3.37 Relationship between structure slope parameters

3.9.4.2 Level versus width

Figure 3.38 gives an overall view of the relative level and width of toe, berm and crest of all structures in the database. A positive value is assigned to 'level' if the concerning structure part is situated above swl, a negative value if the concerning structure part is situated below swl.

This implicates that, regarding the definitions of the parameters h_t, h_b and A_c , the value of 'level/$H_{m0\ toe}$' on the Y-axis corresponds to:

- '$-h_t / H_{m0\ toe}$' for a toe,
- '$-h_b / H_{m0\ toe}$' for a berm and
- '$A_c / H_{m0\ toe}$' for a crest.

The value of 'width/$H_{m0\ toe}$' on the X-axis corresponds to:

- '$B_t / H_{m0\ toe}$' for a toe,
- '$B_h / H_{m0\ toe}$' for a berm and
- '$G_c / H_{m0\ toe}$' for a crest.

It should be remarked that the value of '$-h_b/H_{m0\ toe}$' in case of B_h = 0m (points on the vertical axis in figure 3.38), corresponds to the level of the transition point of the composite slope instead of the berm level, as a berm is not present in these cases.

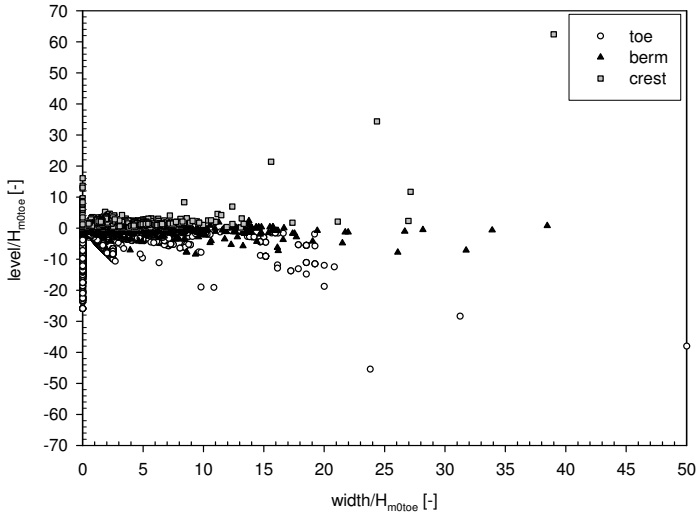

(a)

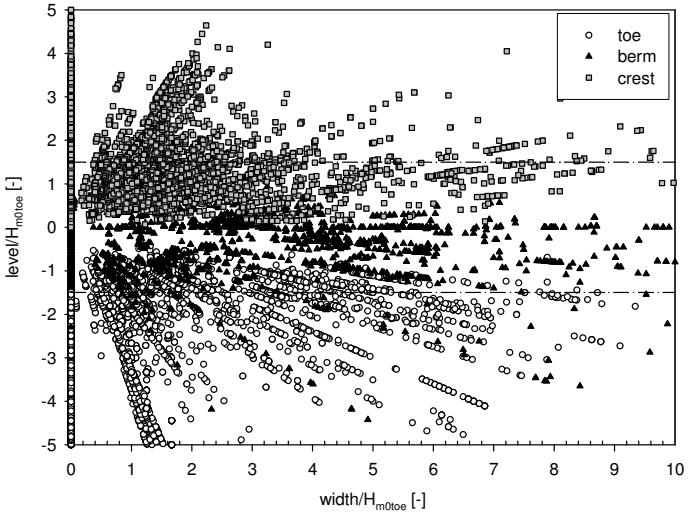

(b)

Figure 3.38 Relationship between toe, berm and crest parameters

In figure 3.38 (a) all data are represented, figure 3.38 (b) zooms in on the area where most points are located. Outliers in figure 3.38 (a) result from tests with very low values for $H_{m0\ toe}$.

Figure 3.38 clearly shows that the crest level is generally located higher than the berm level, which on its turn is located higher than the toe level. In most cases the berms are located within the range of $1.5H_{m0\ toe}$ around swl, corresponding to the

two horizontal lines in figure 3.38 (b) (values +1.5 and -1.5 on the Y-axis). This is in accordance with the definition of a berm (see section 3.6.2).
The majority of the data lies within the range of $-5 < \text{level}/H_{m0\ toe} < +5$ and $0 < \text{width}/H_{m0\ toe} < 10$.

3.9.4.3 Crest height and width versus armour crest height

In figure 3.39 and figure 3.40 the relative crest height $R_c / H_{m0\ toe}$ respectively crest width $G_c / H_{m0\ toe}$ is plotted versus the relative armour height $A_c / H_{m0\ toe}$.
In graph (a) of both figures again some outliers resulting from tests with small wave heights $H_{m0\ toe}$ can be seen. Figures 3.39 (b) and 3.40 (b) zoom in on the areas with most data.

Figure 3.39 shows that in a lot of cases the crest height R_c equals the armour crest height A_c. Values of R_c both lower and higher than A_c are represented in the database as well.
Rubble mound structures with a small wall on the crest for example may have values of R_c larger than, equal to or smaller than A_c, depending on the height of the armour relative to the top of the wall. Figure 3.39 shows that structures with values of R_c larger than A_c are more frequently included than the other way around.

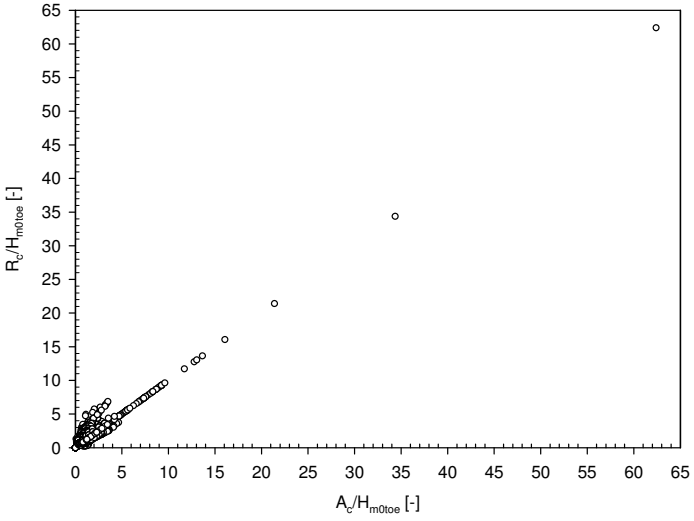

(a)

Figure 3.39 Relationship between crest height and armour crest height

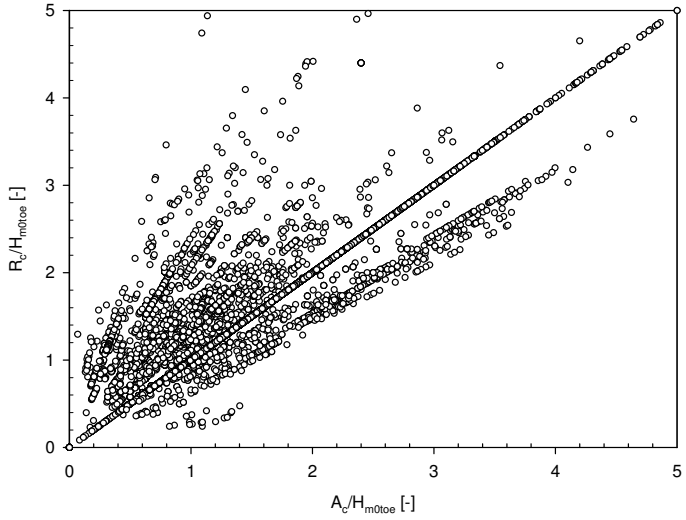

(b)

Figure 3.39 (continued) Relationship between crest height and armour crest height

Values of R_c and A_c equal to zero appear only simultaneously in the database (point on the intersection of X-axis and Y-axis in figure 3.39). This refers to structure types where the water level equals the crest level of the structure.

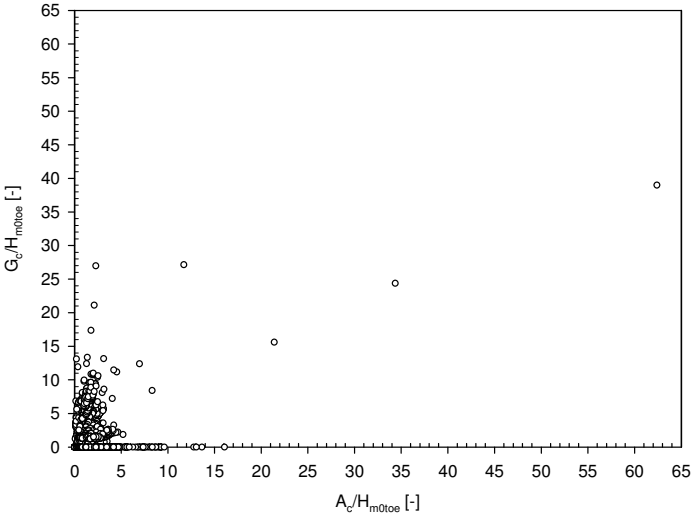

(a)

Figure 3.40 Relationship between crest parameters

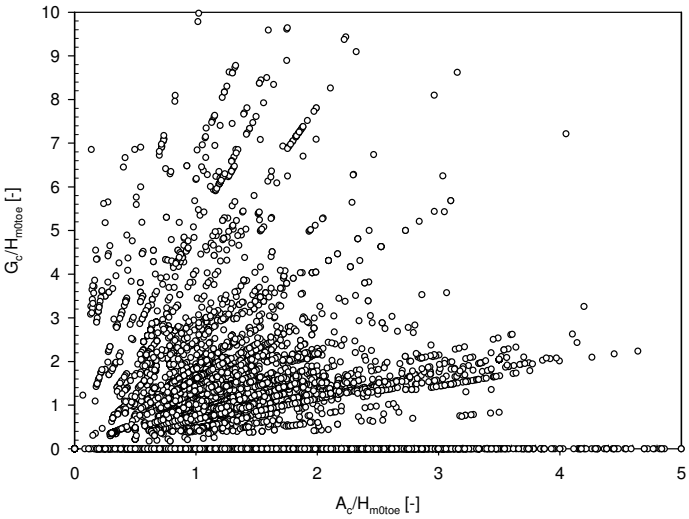

(b)

Figure 3.40 (continued) Relationship between crest parameters

Figure 3.40 shows a great number of data located on the X-axis, referring to structure types with a value for the crest width G_c = 0m. This indicates that overtopping was measured immediately behind the crest, except in case of a crest composed of an impermeable horizontal plane (see section 3.6.3).

3.9.4.4 Berm characteristics

In figure 3.41 the relative berm width B /$H_{m0\ toe}$ is plotted versus the relative width of the horizontally schematised berm B_h /$H_{m0\ toe}$. It is clear that in most cases both parameters are equal. This is in accordance with the conclusion which was made in section 3.9.3.2: for most tests included in the database the present berm is horizontal or almost horizontal.

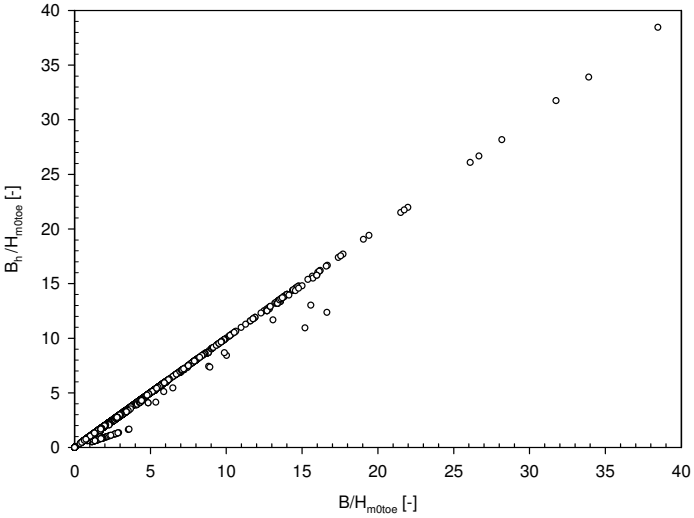

Figure 3.41 Relationship between berm parameters

In case of a sloping berm, the width of the horizontally schematised berm B_h is always smaller than (or exceptionally equal to) the horizontally measured width of the sloping berm B. Structures with $B \neq B_h$ are represented by the points below the diagonal line in figure 3.41.

CHAPTER 4
DEVELOPMENT OF A NEURAL PREDICTION METHOD FOR WAVE OVERTOPPING

4.1 Neural networks: an introduction

This introduction is mainly based on Suykens (2001), Efron and Tibshirani (1993), Rojas (1996) and http://www.faqs.org/faqs/ai-faq/neural-nets/.

4.1.1 What are neural networks

Some definitions of 'neural network' (NN) found on the World Wide Web are:

- *'A simplified emulation of the connections of the human brain, used for investigating learning and self-organisation within an artificial environment.'*
  (www.calresco.org/glossary.htm)

- *'A processing architecture derived from models of neuron interconnections of the brain. Typically different from computers by incorporating learning rather than programming and parallel rather than sequential processing.'*
  (www.bannerengineering.com/literature_resources/reference/glossary_pplus.html)

- *'A real or virtual device, modelled after the human brain, in which several interconnected elements process information simultaneously, adapting and learning from past patterns.'*
  (http://www.answers.com/topic/neural-network)

When the author talks about neural networks in this work this refers to 'artificial' neural networks. Artificial NN's fall within the field of artificial intelligence, and can in this context be defined as systems that simulate intelligence by attempting to reproduce the structure of human brains.
One estimates that human brains contain over 10^{11} neurons and 10^{14} synapses in the human nervous system. These biological neurons consist of three main parts (see figure 4.1): the neuron *cell body* branching extensions called *dendrites* for receiving input, and *axons* that carry the neuron's output to dendrites of other neurons via synapses.

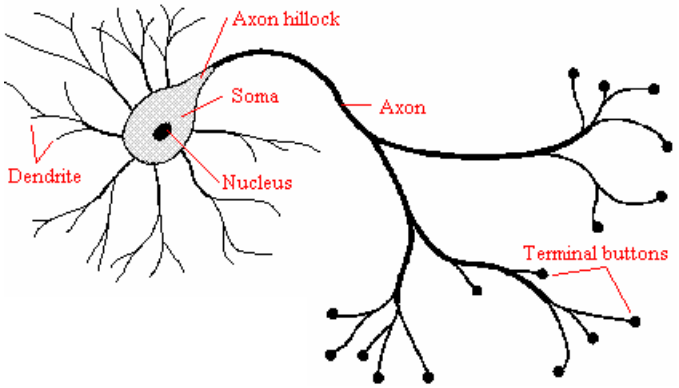

Figure 4.1 Schematic representation of a biological neuron (from Jain et al., 1996)

Artificial NN's are developed based on these biological neurons, and can be trained on given input-output patterns. Typically, artificial NN's consist of many inputs and outputs what makes these attractive for modelling multivariable systems and establishing nonlinear relationships between several variables in databases.

An important quality of NN's is that they are 'universal approximators': NN's are able to approximate any continuous nonlinear function arbitrary well on a compact interval, even with only one hidden layer (Hornik, 1989). An additional quality of NN's is that they can be used with a high dimensional input space. Barron (1993) has shown that NN's can avoid the curse of dimensionality in the sense that the approximate error becomes independent of the dimension of the input space (under certain conditions), which is not the case for polynomial expansions.

Although NN's are powerful models, one should be aware of the fact that they do not provide a miraculous solution for any problem. The choice of the number of neurons, learning and generalisation issues, how to deal with noise, avoiding bad local minima solutions … can be mentioned as important and critical design issues, which contribute to or may harm the reliability of the solution.

Two important groups of feedforward NN models which may be distinguished are multilayer perceptrons (MLP's) and radial basis functions (RBF's). 'Feedforward' refers to the movement of information in forward direction, i.e. no connections are present which bring information back to previous layers or which make exchange of information within one layer possible. Networks which do have such connections are called 'recurrent' networks.

The networks further used in this work concern MLP's, which are the most frequently used NN's in practical regression problems. Two classes of problems for which MLP's often are applied concern regression problems and classification problems.

4.1.2 Topology of feedforward neural networks

The most simple neural model concerns the McCulloch-Pitts model, consisting of one simple neuron (figure 4.2).

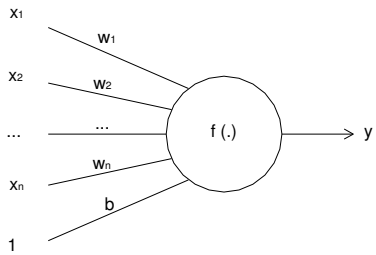

Figure 4.2 McCulloch-Pitss model

The McCulloch-Pitss model is a very strong mathematical abstraction of reality. The neuron corresponds to a simple static nonlinear element. The incoming signals x_i are each multiplied by their corresponding interconnection weights w_i, and added up. After adding an additional bias term b, this signal is sent through a static nonlinearity f(.) yielding the output y. This can be summarised as follows:

$$y = f\left(\sum_i w_i x_i + b\right) \tag{4.1}$$

The nonlinearity f(.), called the 'activation function', is typical of the saturation type, e.g. tanh(.). Biologically, this corresponds to the firing of a neuron in case the weighed sum of inputs exceeds a certain threshold value.

A multilayer perceptron is an extension of the simple McCulloch-Pitts model, in which several neurons are organised in multiple layers, each consisting of multiple neurons.
Figure 4.3 shows an MLP with one hidden layer. As one single hidden layer is sufficient to have a universal approximator (Hornik, 1989), this is a frequently used MLP-configuration.

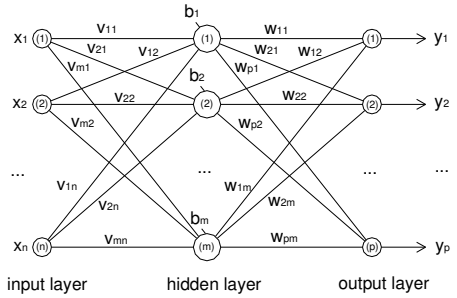

Figure 4.3 Multilayer perceptron with one hidden layer

In matrix-vector notation the proposed MLP can be described as:

$$Y = W\, f\,(V\,X + \beta) \tag{4.2}$$

where input $X \in \Re^n$, output $Y \in \Re^p$, interconnection matrices $W \in \Re^{p \times m}$, $V \in \Re^{m \times n}$ and bias vector $\beta \in \Re^m$, and where n is the dimension of the input space, p the dimension of the output space, m the number of neurons in the hidden layer and $\Re$ the set of real numbers.

Elementwise notation gives:

$$y_i = \sum_{r=1}^{m} w_{ir}\; f\left(\sum_{j=1}^{n} v_{rj}\, x_j + b_r\right) \qquad\qquad i = 1\,, ...,\, p \tag{4.3}$$

In this example a linear activation function is assumed for the output layer. Depending on the application one might choose other functions as well. However, for problems of nonlinear function estimation and regression a linear activation function in the output layer is most frequently applied.

The neural models applied in this work concern MLP's as presented in figure 4.3. Detailed information on how these networks are calibrated is given in next section.

The second important group of feedforward NN's are radial basis functions. RBF's make use of localised basis functions, typically with Gaussian activation functions, organised within one hidden layer. The saturation type nonlinearities of the MLP's have disappeared here.

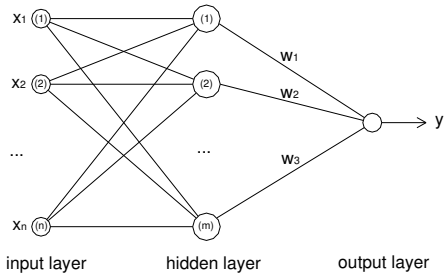

Figure 4.4 Radial basis function network

The network in figure 4.4 is described by:

$$y = \sum_{i=1}^{m} w_i h\left(\|X - C_i\|\right) \tag{4.4}$$

and with Gaussian activation functions this becomes:

$$y = \sum_{i=1}^{m} w_i \, exp\left(-\|X - C_i\|^2 \Big/ \sigma_i^2\right) \tag{4.5}$$

where input X Є $\Re^n$, output y Є $\Re$, output weights W Є $\Re^m$, centres C_i Є $\Re^n$ and widths σ_i Є $\Re$ (i = 1,…,m), and where n is the dimension of the input space, m the number of neurons in the hidden layer and $\Re$ the set of real numbers, and where h(.) refers to the activation function of the neurons and $\|A\|$ to the norm of the vector A.

As this kind of network is not used in this work, RBF's are not further considered here. More information can be found in specialised literature.

4.1.3 Learning process of the MLP

Starting from a certain model structure, the NN problem is reduced to the determination of the unknown interconnection weights and biases. These 'parameters' are established during the so-called training process or learning process (sometimes also called calibration process).

By presenting the network examples of input with corresponding output, the network 'learns' the relationship between both. This is represented in the values of the interconnection weights and biases.

A distinction can be made between two types of learning: unsupervised learning and supervised learning. In case of the former learning type, the network is only provided with inputs. No desired outputs are presented to the network during the training process. The network itself must then decide how to group the input data. This principle is often referred to as 'self-organisation' or 'adaptation'.
A more common technique, which is used in this work, is the supervised learning technique. Here both the inputs and the outputs are provided to the network. Starting from small random initialisation values of the weights and biases, the network processes the inputs. The resulting output of the network generally differs from the desired output. The goal of the training process is to iteratively adapt the weights and biases in order to reduce the difference between the desired and calculated output or target values.

Several algorithms have been developed for the training process of NN's.
The first algorithm which was invented for the supervised training of MLP's (and feedforward networks in general) is the backpropagation method. It was basically developed by Paul Werbos in 1971, but only in 1986 Rumelhart (see Rumelhart et. al., 1986) succeeded in making the method widely known.
After a random initialisation, the weights and biases are iteratively updated, based on the error obtained with the values of the weights and biases present at that moment. The iterative adaptation is performed in a backward direction, which is on the origin of the name of the so-called backpropagation algorithm. Iteratively adapting the weights and biases is performed so that the error ('cost') is minimised.

If one considers an MLP network and K input patterns with corresponding output patterns (index k = 1, …, K), the backpropagation algorithm adapts the weights of the network as follows:

$$\Delta w_{ij,k} = \eta\ \delta_{i,k}\ o_{j,k} \tag{4.6}$$

where

$\delta_{i,k} = \left(T_{i,k} - o_{i,k}\right) f_i'\left(o_{i,k}\right)$ if i concerns an output neuron

$\delta_{i,k} = \left(\sum_a \delta_{a,k}\ w_{ai}\right) f_i'\left(o_{i,k}\right)$ if i concerns a hidden neuron

and where

$\Delta w_{ij,k}$ = the correction of the weight value w_{ij} from neuron j to neuron i, for input pattern k

η = the 'learning rate'

$o_{j,k}$ = the output value of neuron j, corresponding to input pattern k

$T_{i,k}$ = the target value of output neuron i, corresponding to input pattern k
= output i of output pattern k

$f_i'(.)$ = the derivative of the activation function f(.) of neuron i

a = the index number of a neuron in the layer following on the layer of the considered neuron

By defining the error for pattern k as follows:

$$E_k = \frac{1}{2}\sum_i \left(T_{i,k} - o_{i,k}\right)^2 \tag{4.7}$$

the correction of the weight value $\Delta w_{ij,k}$ may also be written as:

$$\Delta w_{ij,k} = -\eta\ \frac{\partial E_k}{\partial w_{ij}} \tag{4.8}$$

and the objective function which is minimised is the mean squared error on the trainingset of patterns, E:

$$\min_{w_{ij}} E = \min_{w_{ij}} \left(\frac{1}{K}\sum_k E_k\right) \tag{4.9}$$

The backpropagation algorithm is an elegant method to obtain analytic expressions for the gradient of the cost function defined on a feedforward network with many layers.

It should be mentioned that 'batch training' as well as 'incremental training' can be applied. The batch training method, which is used in this work, only updates the interconnection weights after processing the entire trainingset. One iteration step, which corresponds to presenting all input patterns once to the NN, is called one 'epoch'. During incremental training, an update of weights is performed after each single training pattern.

The backpropagation algorithm (= steepest descent algorithm) has some important disadvantages, such as the fact that it converges quite slowly. To speed up the method, a momentum term may be added. The interconnection weights are then adapted as follows:

$$\Delta w_{ij}(s+1) = \eta\ \delta_{i,k}\ o_{j,k} + \alpha\ \Delta w_{ij}\ (s) \tag{4.10}$$

where the same notations as in eq. (4.6) are used, where s is the iteration step and $0 < \alpha < 1$. Often an adaptive learning rate η is applied.

Considering batch training, the problem may be approached as a nonlinear optimisation problem:

$$\min_x f(x) \tag{4.11}$$

where x and f(x) correspond to the unknown interconnection weights and the cost function E respectively.
The most simple optimisation algorithm is the steepest descent algorithm:

$$x_{s+1} = x_s - \alpha_s \nabla f(x_s) \tag{4.12}$$

where the index s refers to the iteration step.
This is exactly the backpropagation method without momentum term as described above.

However, many other algorithms, which are much faster, to solve the optimisation problem have been developed. It is not the aim to describe all these algorithms in detail in this work. The author restricts to mentioning some of them.
A first example of a faster algorithm is the *Newton method*, converging quadratically. However, the Newton method may lead to numerical problems if the Hessian matrix has zero eigenvalues. In addition, very complicated computations arise due to the need of the second order derivatives of the cost function.
The *Levenberg-Marquard method* deals with these problems, and converges still faster than the steepest descent method. By adding an additional constraint, the

Hessian matrix is replaced by a matrix which is always positive definite. A Jacobian matrix is often used to approximate the Hessian matrix.
Quasi-newton methods may also be mentioned as algorithms which are faster than the backpropagation algorithm. In these methods an approximation for the Hessian matrix is built up based upon gradient information only during the iterative learning process. Unfortunately, for large NN's with many interconnection weights, it becomes hard to store the matrices in computer memory.
Conjugate gradient algorithms present a solution here.
Detailed information on various training algorithms can be found in specialised literature.

In this work the Levenberg-Marquard method is applied as training algorithm. The algorithm is adapted in this way that it produces a network that generalises well (see section 4.1.4).

4.1.4 Generalisation performance

When training a NN, one has to keep in mind that the goal of this training process is to model the underlying generator of the data, and not to memorise the data itself. This implicates that one aims to develop a network which produces not only small errors on the trainingset, but also on novel inputs: one prefers the network to 'generalise' well.

The problem is often referred to as the 'bias-variance trade off'. When training a NN, one is minimising the error on the training data, which may lead to a network which predicts the training data very well, but which has a bad generalisation performance. This typically leads to a result with small or zero bias, but with large variance, implicating that the network has learned the individual data instead of the underlying model.

In order to assess the final performance of a developed network, often a so-called 'testset' is used. The testset concerns a random part of the available dataset of which the data were not included in the trainingset, and which only serves to 'test' the performance of the network. The network is assessed on the performance of the model for the testset. By doing so, one assumes that the trainingset as well as the testset are both good representatives of the entire input space.

To avoid so-called 'overtraining' of a network, various methods have been proposed. Initially, a larger dataset is always favourable for the generalisation performance of the model. However, as datasets are often restricted to a specific number of available items, increasing the dataset is no real option to improve generalisation. Methods such as regularisation, early stopping and cross-validation are alternatives to control the generalisation performance of the network.

Training a network with regularisation implies that an extra term E_W is added to the cost function. This results in a new cost function F which is minimised during the training process:

$$F = \alpha E_D + \beta E_W \tag{4.13}$$

where E_D is the sum of squared errors of the trainingset (i.e. corresponding to the previous cost-function), E_W the sum of squares of the network weights, and α and β objective function parameters.

The aim of adding this weight decay term to the cost-function is to keep the interconnection weight values small, which leads to a smoother model. If $\alpha << \beta$, the emphasis is put on the reduction of the errors during training of the network. If $\alpha >> \beta$, the emphasis is put on the weight size reduction, implicating that a smoother network will be obtained at the expense of the accuracy. With

regularisation, any modestly oversized network should be able to sufficiently represent the true function.
The main difficulty in regularisation is choosing the correct values for the objective function parameters.
David MacKay performed extensive research on the application of Bayes' theorem (Thomas Bayes, 1702-1761) to NN training and to optimise regularisation. Detailed information on this subject can be found in MacKay (1992a and 1992b), but will not be treated here in detail.
Foresee and Hagan (1997) propose a Levenberg-Marquard based approach to Bayesian learning. The Levenberg-Marquard algorithm, implemented with a Gauss-Newton approximation of the Hessian matrix, provides the Hessian matrix which is required for Bayesian optimization of the regularisation parameters. The additional computation required for optimisation of the regularisation is minimal. This leads to a new training algorithm, which consistently produces networks with a good generalisation, see Foresee and Hagan (1997). Within this work, the training algorithm proposed by Foresee and Hagan (1997) is used.

Instead of adding an extra term to the cost function, early stopping may be applied to avoid overtraining of the network. The available dataset has to be split up into three sets in this case: a trainingset, a validationset and a testset. The training process is stopped at the moment the error on the (independent) validationset becomes minimal. The testset serves to assess the performance of the network.
A disadvantage of this method is that one can not use the entire available dataset for the training of the network. A part of the data should be left out for the early stopping process of the network (and a part for testing of the network, but this is always the case). Moreover, the results can be influenced by the specific data belonging to the validationset.
It is possible to show that early stopping is closely related to regularisation (Bishop, 1995).

A procedure which avoids the problem of splitting up the data is cross-validation. When cross-validation is applied the trainingset is split up in S parts. The same network lay-out is now trained several times, with S-1 parts of the trainingset, each time leaving out another part. An estimation of the generalisation error of the network is determined as the mean of the generalisation errors obtained for each testset (which is determined as the part of the dataset which was left out). It is demonstrated by Goutte (1997) and in reply by Zhu and Rohwer (1996) that for small datasets cross-validation is superior to the use of a single testset.

4.1.5 The bootstrap resampling technique in neural network applications

Instead of analysing subsets of the dataset (e.g. cross-validation), in the bootstrap method subsamples of the dataset are analysed, where a subsample is a random sample *with replacement* from the full dataset. Sampling *with replacement* implicates that when a data point is sampled from the full dataset, it does not disappear from the full dataset, i.e. it is 'replaced' for the sampling of the next data point. Consequently, a subsample of N data may (theoretically) be composed of N equal data.

Comparable to cross-validation, the bootstrap resampling technique may be used to determine the generalisation error of the NN while using all available data for the calibration of the model. The bootstrap technique seems to works better than cross-validation in many cases (Efron, 1982). However, the bootstrap technique has many more applications. The technique may for example be used for estimation of confidence bounds for network outputs (Efron and Tibshirani, 1993).

In this section the bootstrap resampling technique is briefly described, both general and more specifically in order to determine the generalisation error, to determine percentile confidence intervals and to determine a better ensemble network prediction.

4.1.5.1 General

The bootstrap method is a computer-based method for assigning measures of accuracy to statistical estimates. Originally, the bootstrap technique was introduced by Efron in 1979 for determining the standard error of an estimator $\hat{\theta}$ (Efron, 1982).

The method tries to imitate the situation in the real world by sampling randomly, *with replacement*, from the original dataset. The obtained 'bootstrap sets' are each supposed to be a fair representative of a trainingset, extracted from the input space.

Suppose e.g. a random sample $\mathbf{x} = (x_1, x_2, \ldots, x_n)$ from an unknown probability distribution *F* has been observed, and one is interested in a parameter $\theta = f(F)$. The available dataset **x** is considered as a fair representative of the whole input space from which the data are extracted, so it is assumed that $\hat{\theta} = s(\mathbf{x})$, calculated on the basis of the dataset **x**, is a good approximation of the real value of θ. By sampling B bootstrap sets $\mathbf{x_{(b)}}$ (with b = 1, … , B) from the original dataset **x,** where each bootstrap set $\mathbf{x_{(b)}}$ consists of n data, and is sampled *with replacement* from the original dataset **x**, the parameter θ can be calculated for each bootstrap set, i.e. $\hat{\theta}_{(b)} = s\left(\mathbf{x_{(b)}}\right)$. This procedure can be repeated many times

with many randomly generated datasets (B large). The calculated standard error of $\hat{\theta}_{(b)}$ is considered to be an approximation of the standard error of $\hat{\theta}$.

The idea behind the bootstrap technique is that the distribution of the available dataset **x** is a fair approximation of the actual probability distribution *F* of the input space. By sampling randomly *with replacement*, the data situated in regions where the distribution is dense will be selected more than the data situated in regions where the distribution is sparse. Thus for the computations, not the unknown probability distribution *F* is used, but an approximation of it, $\hat{F}$. This idea is also known as the 'plug-in principle': the empirical distribution $\hat{F}$ is an estimation of the true distribution *F*.

The following section describes how the bootstrap technique can be applied for functional approximation including NN's.

4.1.5.2 Determining the generalisation error with the bootstrap method

The bootstrap method may be applied in a similar way to estimate the generalisation error of a developed NN approximating a function.
Suppose the NN model is developed on the basis of n data which are available in the original dataset. By generating B different bootstrap trainingsets, a good estimation of the expected mean squared error (mse) can be calculated. Each bootstrap set is generated by sampling n data, randomly and *with replacement*, from the original dataset. Starting from the same model structure and the same stop criterion for the training process, the B bootstrap sets are used to train B NN's. For each bootstrap network b, the mean squared error for the corresponding bootstrap set, mse_b, as well the mean squared error for the original dataset mse_b^* can be determined.
The standard deviation of the mse_b -values can be considered as an approximation of the true standard deviation of the function fit. However, as the values of mse_b are based on the data on which the bootstrap network b is trained, this value will be too optimistic. The 'optimism O' in the computation of the expected error is defined as:

$$O = \frac{1}{B}\sum_{b=1}^{B}(mse_b^* - mse_b) \tag{4.14}$$

The optimism 'O' is a measure for the degree of underestimation present in the mean squared error originally computed for a trainingset.

It should be mentioned that NN's have many local minima, which has an influence on this bootstrap estimation of the mse. When training a NN several times, the possibility exists that for different training processes (with different trainingsets), various local minima are reached. This may lead to several completely different solutions regarding the values of the weights, where the mse of two bootstrap networks are actually not comparable.
The method proposed by Moody and Utans may be used to assure that the different networks converge to similar local minima of the error function (Moody, 1994). They propose for each bootstrap model to start training with values for the initial weights equal to the weight values of the original trained network.
However, if the aim of the study is to analyse what happens in general when the given network is trained with data coming from the input space, the method of Moody and Utans (Moody, 1994) should not be applied as it is not known at which local minimum training stopped.

In addition, it should be remarked that the several developed bootstrap networks may be used to provide a better predictor than the original network.
The combination of different NN's to reach one prediction is often called 'committees of networks'. If f_b refers to the model obtained by one bootstrap training b, then the prediction of the committee of networks, f(x), is defined as:

$$f(x) = \frac{1}{B}\sum_{b=1}^{B} f_b(x) \tag{4.15}$$

The rationale is here that if each bootstrap network is biased for a particular part of the input space, the mean prediction over the ensemble of networks can reduce the prediction error significantly.
Further in this work, such committee of networks is applied to reach a good final neural quantifier.

4.1.5.3 Confidence intervals based on bootstrap percentiles

The bootstrap technique allows to determine confidence intervals for the neural approximation. Efron and Tibshirani (1993) describe several methods to approximate confidence intervals with the bootstrap method.
In this work bootstrap confidence intervals based on percentiles of the distribution of the bootstrap replications are considered. These confidence intervals are preferred over standard normal intervals derived from the bootstrap replications, as especially when the bootstrap distribution of $\hat{\theta}_{(b)}$ deviates from the normal distribution (which may be the case for a rather small number of bootstrap sets), percentile intervals provide better results.

If one starts again from the bootstrap replications $\mathbf{x}_{(b)}$ (with b = 1, …, B) to calculate $\hat{\theta}_{(b)} = s\left(\mathbf{x}_{(b)}\right)$, the cumulative distribution of $\hat{\theta}_{(b)}$ can be noted as $\hat{G}$. The (1 - α) percentile interval is defined now by the $\frac{\alpha}{2}$ and $1-\frac{\alpha}{2}$ percentiles of $\hat{G}$:

$$\left[\hat{\theta}_{\%,lower}, \hat{\theta}_{\%,upper}\right] = \left[\hat{G}^{-1}\left(\frac{\alpha}{2}\right), \hat{G}^{-1}\left(1-\frac{\alpha}{2}\right)\right] \tag{4.16}$$

Expression (4.16) refers to the ideal bootstrap situation where the number of bootstrap calculations B is infinite. In practise, the number of bootstrap calculations will be finite. By ordering the values of $\hat{\theta}_{(b)}$ from small to large, the $B.\frac{\alpha}{2}^{\text{th}}$ value in the list and the $B.\left(1-\frac{\alpha}{2}\right)^{\text{th}}$ value form the (1 - α) percentile interval. Logically, if $B.\frac{\alpha}{2}$ and $B.\left(1-\frac{\alpha}{2}\right)$ differ from integer values, these should be rounded off to the upper or lower integers (e.g. so that the widest percentile interval is restrained).
If $\hat{\theta}^{B}_{(\alpha)}$ is the $(B.\alpha)^{\text{th}}$ value of the ordered values of $\hat{\theta}_{(b)}$, then the (1 - α) percentile interval also can be written as:

$$\left[\hat{\theta}_{\%,lower}, \hat{\theta}_{\%,upper}\right] = \left[\hat{\theta}^{B}_{(\alpha/2)}, \hat{\theta}^{B}_{(1-\alpha/2)}\right] \tag{4.17}$$

Starting from a histogram of the bootstrap replications, several percentiles can be determined, leading to the so-called bootstrap percentile confidence intervals.

4.1.5.4. Assessing errors in bootstrap estimates

Bootstrap estimates, like all statistics, have inherent errors. Typically bootstrap estimates are nearly unbiased, but they can have a substantial variance (Efron and Tibshirani, 1993). Two sources contribute to this variance: sampling variability, due to the fact that the starting point is only a sample n instead of the entire population, and bootstrap resampling variability, due to the fact that only B bootstrap resamples are considered instead of an infinite number.
Efron and Tibshirani (1993) show that the variance of bootstrap estimates is lower if the sample size n increases and if the number of bootstrap samples B increases.
As the sample size n depends on the available dataset, it is often a fixed value which can not be raised by the researcher.

The number of bootstrap sets B needed for bootstrap estimations of reliability depends on the statistic which is considered. Efron and Tibshirani (1993) state that the variance of the bootstrap estimate of the standard error for $\hat{\theta} = s(\mathbf{x})$ does not reduce substantially anymore for values of B larger than 20 or 50. For percentile estimations more bootstrap sets are needed because the percentile depends on the distribution where fewer samples occur. For an optimum result, one suggests to increase the value of B up to 500 or 1000 for the percentile estimation (Efron and Tibshirani, 1993). Generaly speaking, bootstrap statistics that depend on the extreme tails of the distribution of $\hat{\theta} = s(\mathbf{x})$ require a larger number of bootstrap calculations to achieve an acceptable accuracy than bootstrap statistics not depending on these extreme tails.
In this work, the number of bootstrap calculations from which percentile confidence intervals are estimated is B = 100. Although this number is lower than advised for an optimum result, the percentile confidence intervals are reasonably good, which is confirmed further in this work.

4.1.6 Practical implementation of neural networks within this work

Within this work NN's form the basis of a prediction method for wave overtopping at coastal structures. Although one single network providing the prediction method is the most straightforward option, it was found that a significantly better prediction method is obtained if 2 subsequent NN's are considered, i.e.:

- one NN for the classification of overtopping discharges, the so-called 'classifier' and
- a second NN for the determination of the quantity of overtopping, the so-called 'quantifier'.

The classifier predicts whether overtopping occurs or not, i.e. $q = 0$ $m^3/s/m$ or $q > 0$ $m^3/s/m$. *If* the classifier predicts overtopping discharges $q > 0$ $m^3/s/m$, *then* the quantifier is used to determine a value of the mean overtopping discharge q. Consequently, the classifier may be considered as a filter for the application of the quantifier.

The use of 2 subsequent NN's for the final overtopping prediction method instead of 1 single network originates in fact from the previously found approximately exponential relationship between the measured overtopping discharge and the crest freeboard of a structure (see chapter 2): measured overtopping discharges increase approximately exponential for decreasing crest freeboards (when remaining parameters are kept constant). Consequently, if a network is trained with non-preprocessed q -values as output, the network only performs well for the largest q -values ($q \approx 10^{-1}$ $m^3/s/m$ - 10^{-2} $m^3/s/m$). The network is not able to distinguish the smaller overtopping discharges from each other, as during the training process differences between $q_{measured}$ (= measured q -value) and q_{NN} (predicted q -value) are minimised.
It is found that a much better result is obtained when the output value q is preprocessed to its logarithm during training. Such network is also able to distinguish the smaller overtopping discharges, with equal relative errors for small and large overtopping discharges (see further). Keeping into account the importance of these smaller overtopping values (referring to the tolerable overtopping limits mentioned in chapter 2) this last approach is preferred.
Training a network with the logarithm of the overtopping discharge as output resulted in the quantifier in the first phase of the network development. However, as the logarithm of zero is minus infinity, training on this preprocessed output suppressed the inclusion of zero overtopping data in the trainingdata of the quantifier. As will be shown further in this work, the consequence was found to be that the quantifier does not generalise well for small and zero overtopping discharges. This finding resulted in the development of the classifier in a second phase of the network development. This also explains why the quantifier is discussed first further in this chapter.

For both the classification model (i.e. the classifier) and the regression model (i.e. the quantifier), MLP's with 1 hidden layer are trained. If the universal approximation quality of NN's is relied on (Hornik, 1989), this single hidden layer should be sufficient.
The use of an MLP for the classification model requires the replacement of the output of the network by two discrete values, to guide the network to two classes of outputs. More information on this subject is given further in this chapter.

The starting point for the development of the neural models is the extensive overtopping database which has been described in the previous chapter. Not all of the information included in the database is used for the training of the models, i.e. not all parameters are used, and not all data are used. Which parameters and data are used for each model and why, is described further in this chapter.

The training of the models is performed with updating of the weights and biases according to the Levenberg-Marquard algorithm (see section 4.1.3). To assure a good generalisation performance, Bayesian regularisation is applied (Foresee and Hagan, 1997, see section 4.1.4).

In a first attempt an optimal network configuration is determined for both neural classifier and neural quantifier. In both cases the available dataset is split up in a trainingset (85%) and a testset (15%) for each network configuration. The trainingset is used to train the various models, whereas the performance of the developed models is compared on the basis of the testset.

In a second attempt, the bootstrap technique is applied to the restrained optimal classifier and quantifier model configurations. The advantage of this resampling technique is that the entire dataset can be used for the development of the final model.
For the development of the final classifier, 61 bootstrap models are trained, whereas for the development of the final quantifier, 100 bootstrap models are trained. The bootstrap models allow to optimise the decision boundary for the classifier. For the quantifier the bootstrap models provide a committee of networks to predict the overtopping discharge q. In addition, percentile confidence intervals can be calculated for the obtained point prediction of q.

For the development of the neural models within this work, the computer program Matlab (MATLAB®, Version 6.0, Release 12), supported with a NN toolbox (neural network toolbox 4.0), is used.

4.2 Neural network applications in coastal engineering

Recently, NN's have been applied successfully in various fields of coastal engineering research. The following NN studies concern research related to coastal structures:

- analysis of the stability of rubble mound breakwaters by Mase et al. (1995)
- prediction of wave forces on vertical structures by Van Gent and Van den Boogaard (1998)
- prediction of wave run-up and overtopping by Medina (1999) and Medina et al. (2002)
- prediction of wave transmission by Panizzo et al. (2003)

Mase et al. (1995) analysed the applicability of NN's for predicting the stability of rubble mound breakwaters.
An MLP with 1 hidden layer was calibrated with a dataset consisting of 100 data, originating from Van der Meer's experimental data (Van der Meer, 1988). A modified momentum method was applied for the learning process. Seven input parameters concerning the stability of rock slopes were proposed. For a first NN the damage level S (= $A/(D_{n50})^2$, where A = the eroded area of the breakwater cross-section and D_{n50} = the nominal diameter of the stone) was used as output parameter, whereas for a second NN the stability number N_s (= $H_s /(\Delta D_{n50})$, where H_s = the significant wave height and Δ = the relative density of the rocks) was used as output parameter.
The predicted damage levels by the NN agreed satisfactorily well with the measured damage levels of a part of the Van der Meer data which were not used for the training process, and of Smith et al.'s data (Smith et al., 1992). The agreement between the predicted stability numbers by the NN and the measured stability numbers was also found to be good, but not better than the stability formula of Van der Meer (1988) itself.

Van Gent and Van den Boogaard (1998) used NN's to predict horizontal forces on vertical structures. The horizontal force exceeded by 99.6% of the waves, $F_{h\text{-}99.6\%}$, was considered. A dataset composed of 612 data resulting from model tests performed in 5 different laboratories was used. An MLP with 1 hidden layer was calibrated with the standard backpropagation method. The network consisted of 9 input parameters corresponding to the main factors determining the total horizontal wave force on vertical structures.
Comparison of the performance of the neural model with the formula of Goda (1985) showed for the considered data a better performance of the neural model. In addition, a method to describe the reliability of the prediction was developed. Van Gent and Van den Boogaard showed that inconsistencies in the database may largely influence the prediction method.

Medina (1999) and Medina et al. (2002) studied NN modelling of run-up and overtopping.
Medina (1999) used an Evolutionary Strategy (ES) to optimise the parameters and the topology of two NN's. It concerned MLP's with 1 hidden layer predicting run-up of regular waves at a conventional rubble mound breakwater and at a dissipating basin breakwater. Three, respectively 5, input parameters were proposed. The experimental data described by Medina (1998) and González and Medina (1999) were used for the calibration of the models, i.e. 826 tests with regular waves on a conventional breakwater and 1250 tests with regular waves on a dissipating basin breakwater. A part of the tests was performed with artificial wind generation in laboratory. The predictions obtained with the NN for the conventional breakwater were found to be reasonably accurate. The predictions obtained with the NN for the dissipating basin breakwater were poorer. No further comparison with existing formulae was performed.
In Medina et al. (2002) the same ES was used to calculate a chain of two pruned neural models able to detect significant overtopping (i.e. $q > 10^{-4.5}$ l/m/s) and to estimate overtopping discharges at a rubble mound breakwater. Two MLP's with each 1 hidden layer and 4 input parameters were proposed. A number of 113 tests with irregular waves, of which a part was performed with wind generation, (see Medina et al., 2001) served for the calibration of the models. The models proved to be efficient for the considered data. Here as well no comparison with existing empirical formulae was performed.
It should be mentioned that, comparable to the final approach of the overtopping prediction method in this work, Medina et al. (2002) proposed already two subsequent neural models to predict overtopping, where the first one 'classified' overtopping and where the second one 'quantified' significant overtopping. However, the neural models developed in this thesis concern far more complicated neural models (i.e. more and other input parameters, and more hidden neurons) and are moreover based on almost 100 times more available overtopping data. Also the training of the neural models, for which Medina et al. (2001) used an ES, is performed in a different way in this thesis.

Panizzo et al. (2003) calibrated a neural model with experimental data on wave transmission over rubble mound low-crested structures. The reference datasets used were the data gathered within the EC project DELOS, from which 5 subsets of data were defined (total number of data ≈ 2143). An MLP with 1 hidden layer was calibrated using the Levenberg-Marquard algorithm. Six dimensionless parameters, related to hydraulic as well as structural parameters, were proposed as input.
A good performance of the developed neural model for the transmission coefficient K_t was found. Comparison with existing empirical formulae showed that the neural model results were more accurate.

Many other NN applications in coastal engineering can be referred to. More examples of recent NN research performed in various fields of coastal engineering are:

- tidal level forecasting (Tsai et al., 1999)
- prediction of the occurrence of impact wave force (Mase et al., 1999)
- analysis of wave directional spreading (Deo et al., 2002),
- prediction of storm-built beach profile parameters (Tsai et al., 2000),
- prediction of scour depths at culvert outlets (Liriano et al., 2001),
- prediction of wind induced water levels (Westra et al., 2002),
- prediction of sedimentation in the Maasmond (Bierens, 2002),
- prediction of the breaker depth and breaking height of breaking waves (Deo et al., 2003),
- …

These references are definitely not meant to give a complete overall view of performed NN research in coastal engineering during the last years. The aim is rather to give an idea of the various subjects for which NN's may be used.

Simultaneously with this research, a neural prediction method for wave overtopping at coastal structures has been developed within the CLASH project (Pozueta et al., 2004a and 2004b). The largest difference between the prediction method developed in this thesis, and the CLASH prediction method is that in this thesis a sequence of 2 neural networks is proposed, whereas the CLASH prediction method is only composed of 1 single network. The single CLASH network is comparable to the quantifier developed in this thesis. As will be shown further in this thesis, the use of 2 subsequent neural networks has a clear surplus value versus the use of only 1 single neural network.

The studies mentioned in this section show that NN's have applications in very different research domains. Complex relationships in various research fields may be modelled with NN's, on condition that enough measurements are available to calibrate the neural model. NN's are often used if the derivation of reliable empirical relations on the basis of measurements is difficult due to the complex relationships. It has been proved that the prediction capacity of a NN is largely dependent on the quality of the data on which it was trained (e.g. Van Gent and Van den Boogaard, 1999). As mentioned in the studies above, existing empirical design formulae are often used to give an idea of the prediction capacity of the developed network.

4.3 Parameters used for the neural network development

The extensive overtopping database described in chapter 3 provides the data for the development of the two neural models, i.e. the classifier and the quantifier. As mentioned before, more information on the overtopping measurements than strictly needed for the development of the neural prediction method has been included in the database.

By selecting in a first approach 18 of the 31 database parameters for the development of the neural prediction method (see table 4.1), all characteristics assessed as possibly relevant for the overtopping phenomenon are restricted from the overtopping database. Sometimes a 'best choice' is made between equivalent or closely related parameters. The 18 selected parameters are used either as input, as output or as part of the weight factor (see further), and consist of 5 hydraulic parameters, 11 structural parameters and 2 general parameters.
Table 4.1 shows the 18 parameters as well as their function in the development of the neural models.

Table 4.1 Database parameters selected for NN development

Nature		Parameter	Function
hydraulic	1	$H_{m0\ deep}$ [m]	input
	2	$H_{m0\ toe}$ [m]	input
	3	$T_{m\ -1,0\ toe}$ [s]	input
	4	β [°]	input
	5	q [m^3/s/m]	output
structural	1	h [m]	input
	2	h_t [m]	input
	3	B_t [m]	input
	4	γ_f [-]	input
	5	$\cot\alpha_d$ [-]	input
	6	$\cot\alpha_u$ [-]	input
	7	R_c [m]	input
	8	h_b [m]	input
	9	B_h [m]	input
	10	A_c [m]	input
	11	G_c [m]	input
general	1	RF [-]	weight factor
	2	CF [-]	weight factor

In a first phase of the creation of the neural prediction method the quantifier is developed. The final selection of appropriate input parameters is performed in this first phase, where a sensitivity-analysis showing the relative importance of the chosen input parameters will ultimately lead to the omission of 1 input parameter

(see further). In a second phase the input parameters found to be relevant during the development of the quantifier are used to develop the classifier.

Figure 4.5 shows a cross-section of a rubble mound structure with a berm. The 16 restricted input and output parameters are marked. Chapter 3 is referred to for detailed information on each parameter.

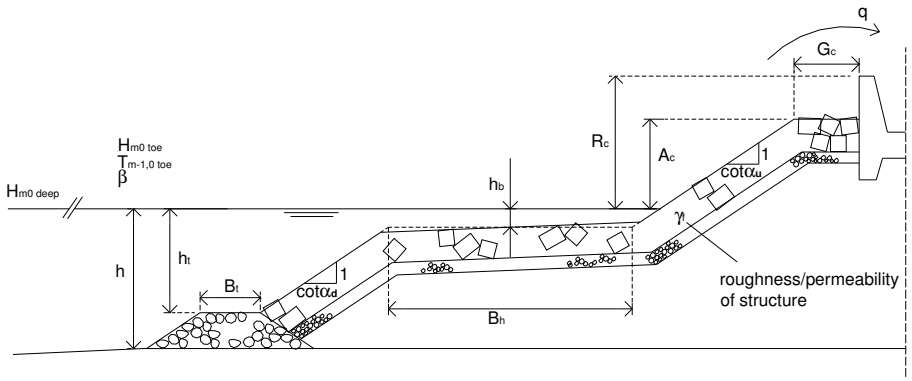

Figure 4.5 Database input/output parameters selected for NN development

The reason why the above mentioned 18 parameters are selected for the NN development is explained in the following section. A distinction is made between input parameters, output parameters and general parameters.

4.3.1 Input parameters

From the four deep water wave parameters present in the database ($H_{m0\ deep}$, $T_{m\ deep}$, $T_{p\ deep}$ and $T_{m\ -1,0\ deep}$), only the parameter $\mathbf{H_{m0\ deep}}$ is restrained.

Basically, the intention was to include only wave parameters determined at the toe of the structure in the neural prediction method. However, as described by Van der Meer et al. (2005b), by only considering the incident wave characteristics, one has little information on the 'history' of the waves. Nevertheless, the latter may be important for the overtopping phenomenon.

Previous studies have proved that wave overtopping in case of gentle foreshores and heavy wave breaking is often much higher than for the same wave heights concerning non-breaking waves in deeper water (Smith, 1999, Van Gent, 1999). The question is if such situations, where effects as surf beat are introduced, can be distinguished by only considering the wave characteristics at the toe of the structure. Although the degree of wave breaking may be retrieved from the proportion of $H_{m0\ toe}$ to the water depth, this parameter does not provide information on the amount of energy decay, whereas the proportion of $H_{m0\ toe}$ to $H_{m0\ deep}$ does.

In addition, overtopping tests performed within the framework of the VOWS project (www.vows.ac.uk) on vertical or almost vertical walls, preceded by steep foreshores, have shown that due to wave breaking on the wall, significant overtopping may occur. Also here the parameter $H_{m0\ deep}$ might be thought of as containing important additional overtopping information.

Taking the above considerations into account, the parameter $H_{m0\ deep}$ is included as input parameter in a first approach of developing the quantifier. In section 4.6.5 is studied if this parameter indeed contains additional information.

The wave height $\mathbf{H_{m0\ toe}}$ as well as the wave period $\mathbf{T_{m-1,0\ toe}}$ and the angle of wave attack $\boldsymbol{\beta}$ refer to the wave characteristics of the 'incident' waves.

From all wave period parameters at the toe of the structure present in the database ($T_{m\ toe}$, $T_{p\ toe}$ and $T_{m-1,0\ toe}$), the wave period $T_{m-1,0\ toe}$ is assessed as characteristic period parameter to describe the phenomenon of wave overtopping (Van Gent, 2001a). Due to combinations of swell and sea or due to processes on the foreshore, wave energy spectra at the toe of coastal structures are often double or multi-peaked. Sometimes the wave spectrum is completely flattened so that no real peaks can be distinguished, e.g. in case of heavy wave breaking on a shallow foreshore. It is shown by Van Gent (2001a) that, on the contrary to $T_{m-1,0\ toe}$, the values of $T_{p\ toe}$ and $T_{m\ toe}$ are not sufficient to describe the energy spectrum in these cases. The parameter $T_{m-1,0\ toe}$ focuses on the longer wave periods in the wave climate, performing better for describing phenomena as run-up and overtopping. As $T_{m-1,0\ toe}$ is a spectral parameter, its value can be easily determined by spectral analysis.

The water depth **h** just in front of the structure is a first structural input parameter. In addition, the parameters included in the database describing the toe of the structure, i.e. $\mathbf{h_t}$ and $\mathbf{B_t}$, are thought to be relevant for the overtopping phenomenon. The same applies to the combined effect of roughness and permeability of the structure, which is included in the value of the parameter $\boldsymbol{\gamma_f}$.

From the four parameters describing the structure slope ($\cot\alpha_u$, $\cot\alpha_d$, $\cot\alpha_{excl}$, $\cot\alpha_{incl}$), the parameters $\mathbf{\cot\alpha_u}$ and $\mathbf{\cot\alpha_d}$, describing the structure slope above respectively below the berm (or transition point in case of a composite slope), are restricted for the NN development. The remaining 2 slope parameters concern calculated mean slopes and are not further used.

The database contains four parameters describing the berm of the structure, i.e. B, B_h, $\tan\alpha_B$ and h_b. Only the water depth on the berm, $\mathbf{h_b}$, and the horizontally schematised width of the berm, $\mathbf{B_h}$, are selected for the NN development. The single parameter B_h is preferred over the use of the two parameters B and $\tan\alpha_B$, as the (small number of) sloping berms included in the database concerns only slightly inclined structure parts (see section 3.9.3.2), and as an extra input parameter concerns a substantial increase of the neural model complexity.

Finally, the 3 structural database parameters describing the crest of a structure, i.e. $\mathbf{R_c}$, $\mathbf{A_c}$ and $\mathbf{G_c}$, are also selected for the NN development.

4.3.2 Output parameter

Within this work mean overtopping discharges, q in $m^3/s/m$, are studied. The value of **q** logically serves as output parameter for the neural models.
The database parameter P_{ow} , referring to the percentage of waves resulting in overtopping, is not further used within this work. It concerns an additional parameter which is usually not recorded during overtopping tests, leading to many blank values in the database.

The output parameter q is only used in its present form (although preprocessed) for the development of the quantifier. For the development of the classifier, the output should be guided to two classes. For this reason the output parameter q is replaced for the classifier by 2 possible values, referring to two 'classes' of overtopping:

- the value of q is replaced by '+1' if the overtopping discharge q is assessed significant and
- the value of q is replaced by '-1' if the overtopping discharge q is equal to zero or assessed as negligible.

Section 4.5.4 and further section 4.7.1 explain which overtopping values are assessed as significant and which overtopping values are assessed as negligible.
As already mentioned in section 4.1.6 the output value q is preprocessed for the development of the quantifier by taking the logarithm of it. This implicates that the quantifier predicts values of log(q) instead of q. What exactly are the implications of this preprocessing for the neural prediction method is described in section 4.6.2.

4.3.3 Parameters used as weight factor

The reliability of each test is enclosed in the database by means of two parameters, i.e. the reliability factor **RF** and the complexity factor **CF**, standing for the reliability of the wave parameters, respectively the complexity of the structure section (see chapter 3). Values of 1 (RF: very reliable test; CF: simple section) to 4 (RF: unreliable test, CF: very complicated section) were assigned to these parameters.

For the development of the neural models, the parameters RF and CF are combined into one factor, called the 'weight factor' of the test. The weight factor may be considered as giving an indication of the overall reliability of the test. According to Pozueta et al. (2004b) the weight factor is determined as:

$$\text{weight factor} = (4 - RF) * (4 - CF) \tag{4.18}$$

Table 4.2 shows the values of the weight factor for all possible combinations of RF and CF.

Table 4.2 Determination of the weight factor

weight factor		Value of CF			
		1	2	3	4
Value of RF	1	9	6	3	0
	2	6	4	2	0
	3	3	2	1	0
	4	0	0	0	0

The value of the weight factor is linked to the number of times the corresponding test is used as input during the training and testing process of both the quantifier and the classifier. The more the same test is used as input during the training process, the more the final neural model will be focussed on the corresponding test. This implies that the NN is forced to draw attention to the fact that tests with high reliability and low complexity are more important than tests with low reliability and high complexity. If one supposes that the weight factor is a good indication of the overall reliability of the test, the prediction of the trainingdata with high overall reliability by the final model will be on average better than the prediction of the trainingdata with low overall reliability. It will be demonstrated in section 4.6.7 that this is indeed the case for the quantifier.

Table 4.2 shows that a part of the tests included in the database will not be used for the development of the neural models (weight factor = 0), others even nine times. If each test is considered as many times as the value of its weight factor, then 52267 test results are counted in the 'weighted database' instead of the original 10532 tests.

By using a weight factor, one can avoid that the network focuses on less reliable values, which would result in a worse prediction method. By applying the proposed method with the weight factor, less reliable data are not excluded from the dataset, but they are just given less influence.

The author is aware of the fact that the use of the weight factor for the development of the neural models may have a side effect. One can imagine that specific structures types may be under-represented in the group of overall very reliable data (weight factor = 9), leading to a final quantifier/classifier which predicts/classifies overtopping worse for these specific structure types, although these may be included as many times as others in the original database.
However, this side effect is weakened as the number of data included in the original database is rather large.

4.4 Implications of scale models

The overtopping database is composed of model tests performed on different model scales as well as of prototype measurements.
The first important question is how to deal with these different scales regarding the NN development. In section 4.4.1 this problem is treated in detail. In addition, attention should be given to model and scale effects which were found to influence small scale overtopping tests under specific circumstances. This problem is reflected upon in section 4.4.2.

4.4.1 Dealing with different scales

4.4.1.1 Rationale

A small part of the overtopping data included in the database concerns prototype measurements at real sites. The remaining data are laboratory tests, performed on various model scales. The laboratory tests are all models of (real or fictive) prototype situations, obtained by scaling the prototype situations according to the widely used Froude model law in coastal engineering.

To facilitate comparison of all tests within the database, two possible approaches can be distinguished:

- replace all considered parameters by commonly used dimensionless variables
  e.g. $R_c \rightarrow R_c / H_{m0\ toe}$; $T_{m-1,0\ toe} \rightarrow s_0$; etc., or
- use a specific length scale 'N_L', characteristic for each test, to scale all parameters to a comparable situation
  e.g. $R_c \rightarrow R_c / N_L$; $T_{m-1,0\ toe} \rightarrow T_{m-1,0\ toe} / N_L^{0.5}$; etc.

The second approach relies on the Froude model law, and results in comparable parameters as obtained with the first approach. Which approach is used has little influence on further results, for both approaches the values of the obtained parameters are independent of the scale of the test. The author opted for the second approach, as in this approach the input parameters are maintained in their present form. This easily can be seen by considering the scaling process as a scaling to a fictive situation in which the value of the scaling parameter N_L is equal to unity.

4.4.1.2 Froude model law

Froude modelling is applied for modelling flows in which the inertial forces are balanced primarily by the gravitational forces. The forces associated with surface tension, elastic compression and viscosity in these cases are supposed to be of

minor importance. The majority of hydraulic models in coastal engineering are scaled according to the Froude model law.

The Froude Number expresses the relative influence of inertial and gravitational forces in a hydraulic flow, and is given by the square root of the ratio of inertial to gravitational forces, i.e.:

$$\sqrt{\frac{inertial\ force}{gravity\ force}} = \sqrt{\frac{\rho L^2 v^2}{\rho L^3 g}} = \frac{v}{\sqrt{gL}} \tag{4.19}$$

where ρ is the fluid density in kg/m^3, L is the length in m, v is the velocity in m/s and g is the gravitational acceleration in m/s².

If one requires that the Froude Number is the same in the model as in prototype, one comes to the Froude model criterion, i.e.:

$$\frac{N_v}{\sqrt{N_g . N_L}} = 1 \tag{4.20}$$

where N refers to a 'scale ratio' (or briefly 'scale'), i.e. the ratio of the value of a parameter in prototype to the value of the same parameter in the model. N_L stands for the scale of the length, N_v for the scale of the velocity and N_g for the scale of the gravitational acceleration.

For all practical applications the gravitational scale is the unity, i.e. $N_g = 1$, and the Froude model criterion is simplified to the following relationship:

$$\frac{N_v}{\sqrt{N_L}} = 1 \tag{4.21}$$

Starting from a given model scaling criterion, the scale ratio for any physical property can be set up by dimensional considerations and/or Newton's 2nd Law.
In table 4.3 the scale ratios for common physical flow parameters are listed for the Froude model criterion. As the gravitational scale N_g is equal to unity, all ratios can be expressed as a function of the length scale N_L and the scale of the mass density N_ρ.

Table 4.3 Scale ratios for the Froude model criterion

Characteristic	Dimension	Scale ratio
Geometric		
Length	[m]	N_L
Area	[m²]	N_L^2
Volume	[m³]	N_L^3
Kinematic		
Time	[s]	$N_L^{0.5}$
Velocity	[m/s]	$N_L^{0.5}$
Acceleration	[m/s²]	1
Discharge	[m³/s]	$N_L^{2.5}$
Kinematic viscosity	[m²/s]	$N_L^{1.5}$
Dynamic		
Mass	[kg]	$N_L^3.N_\rho$
Force	[kg.m/s²]	$N_L^3.N_\rho$
Mass density	[kg/m³]	N_ρ
Specific weight	[kg/(m².s²)]	N_ρ
Dynamic viscosity	[kg/(m.s)]	$N_L^{1.5}.N_\rho$
Surface tension	[kg/s²]	$N_L^2.N_\rho$
Volume Elasticity	[kg/(m.s²)]	$N_L.N_\rho$
Pressure and stress	[kg/(m.s²)]	$N_L.N_\rho$
Momentum, Impulse	[kg.m/s]	$N_L^{3.5}.N_\rho$
Energy, Work	[kg.m²/s²]	$N_L^4.N_\rho$
Power	[kg.m²/s³]	$N_L^{3.5}.N_\rho$

If the same fluid is used in the model as in prototype, $N_\rho = 1$. In this case all scales in table 4.3 may be expressed in function of the length scale N_L only.

4.4.1.3 Preprocessing data according to Froude

The parameter $H_{m0\ toe}$ is known to be one of the most important parameters regarding the overtopping phenomenon, and is in addition always larger than zero. These features are on the basis of the choice of $H_{m0\ toe}$ as scaling parameter N_L. Scaling all tests with $H_{m0\ toe}$ as scaling parameter can be considered as scaling all tests to a fictive situation in which the value of $H_{m0\ toe}$ = 1m. In chapter 3, section 3.9.3.1, Froude scaling with $H_{m0\ toe}$ as scaling parameter has already been applied to give an overall view of the parameter ranges included in the database, independently of the scale of the tests.

Other scaling parameters than $H_{m0\ toe}$ may be thought of, e.g. R_c or h.
However, the comparison of a neural quantifier developed with $H_{m0\ toe}$ as scaling parameter with neural quantifiers developed with R_c respectively h as scaling parameters, learned that $H_{m0\ toe}$ is by far the best choice. The choice of R_c as scaling parameter led to difficulties for tests with small and zero values of R_c. Tests with zero values of R_c could not be used (division by zero) leading to a model

where no overtopping predictions for tests with zero R_c -values could be made. Moreover, such model showed a bad performance for small values of R_c. Also the choice of h as scaling parameter gave bad results. The fact that for large values of h the influence of h on the overtopping phenomenon becomes negligible may be a reason for this.
These findings explain the use of the parameter $H_{m0\ toe}$ as scaling parameter further in this work.

A consequence of scaling the parameters of all tests to a value of $H_{m0\ toe}$ = 1m is that the dimension of the input space of the neural prediction method reduces with one parameter: the parameter $H_{m0\ toe}$ disappears as an independent input parameter, whereas it is included as scaling parameter in the majority of the remaining input parameters.
The influence of the parameter $H_{m0\ toe}$ on the overtopping phenomenon may be tested after the development of the neural prediction method by altering the value of $H_{m0\ toe}$ for constant values of the remaining non-scaled input parameters.

Starting from the Froude scale ratios listed in table 4.3, new (scaled) values of input and output parameters for the neural prediction method are obtained, see table 4.4. Four parameters remain the same after scaling according to Froude, i.e. the three dimensionless input parameters γ_f , $\cot\alpha_d$ and $\cot\alpha_u$, and the parameter β.

Table 4.4 Scaled database input /output parameters selected for NN development

	input	Output
1	$H_{m0\ deep} / H_{m0\ toe}$	
2	$T_{m-1,0\ toe} / (H_{m0\ toe})^{0.5}$	
3	β	
4	$h / H_{m0\ toe}$	
5	$h_t / H_{m0\ toe}$	
6	$B_t / H_{m0\ toe}$	
7	γ_f	$q / (H_{m0\ toe})^{3/2}$
8	$\cot\alpha_d$	
9	$\cot\alpha_u$	
10	$R_c / H_{m0\ toe}$	
11	$h_b / H_{m0\ toe}$	
12	$B_h / H_{m0\ toe}$	
13	$A_c / H_{m0\ toe}$	
14	$G_c / H_{m0\ toe}$	

When referring in the following sections to input/output parameters of the neural model which are Froude scaled to $H_{m0\ toe}$ = 1m, the parameters are marked with an 's' in superscript before the parameter, i.e. ${}^{s}H_{m0\ deep}$ (= $H_{m0\ deep}$ / $H_{m0\ toe}$), ${}^{s}T_{m-1,0\ toe}$ (= $T_{m-1,0\ toe}$ / $H_{m0\ toe}^{0.5}$), etc.
For input parameters β, γ_f , $\cot\alpha_d$ and $\cot\alpha_u$, the value of the scaled parameter equals the original parameter, i.e. ${}^{s}\beta = \beta$, ${}^{s}\gamma_f = \gamma_f$, ${}^{s}\cot\alpha_u = \cot\alpha_u$ and ${}^{s}\cot\alpha_d = \cot\alpha_d$.

The output parameter ${}^{s}q$ only differs a factor 3.1 (= $g^{1/2}$) from the often used dimensionless q -value in literature: $\frac{q}{\sqrt{gH_{m0\ toe}^3}}$, with g = the acceleration due to gravity.

4.4.2 Model and scale effects

The presumption that model and scale effects may affect (small scale) overtopping measurements, resulted a.o. from a conclusion of the EC project OPTICREST (De Rouck et al., 2001). Within this project wave run-up $Ru_{2\%}$, i.e. the run-up exceeded by 2% of the waves, measured on a prototype rubble mound slope, was found to be about 20% higher than measured in small scale test facilities.

During the CLASH project extensive research on model and scale effects for overtopping measurements was performed. The presumption that model and scale effects do affect wave overtopping measurements in laboratory under certain conditions was confirmed, and model and scale effects were quantified, resulting in a 'CLASH scaling procedure' to apply to overtopping measured during small scale testing (see Kortenhaus et al., 2005).

In section 4.4.2.1 the CLASH results on model and scale effects are summarised. Further in section 4.4.2.2 the practical application of the CLASH scaling procedure within this work is discussed.

4.4.2.1 CLASH scaling procedure

Kortenhaus et al. (2005) summarise the CLASH research on model and scale effects. The origin of differences when comparing hydraulic model tests with large scale and prototype tests is described in detail. Three sources of possible errors are distinguished:

- model effects, also called 'laboratory effects',
- scale effects, and
- effects of measurement techniques.

Model effects are described as originating from the incorrect reproduction of the prototype situation due to the inability to model exactly the structure, geometry, and waves and currents, or due to the boundary conditions of the wave flume. Examples of model effects are wind effects, currents … appearing in prototype and not in the model. Also side wall effects of the wave flume, reflection of waves in the flume … may be mentioned.

Scale effects are described as resulting from the incorrect reproduction of a prototype water-structure interaction in the scale model. It is believed that scale effects can not be avoided when performing scaled model tests (Oumeraci, 1999a and 1999b). The influence of surface tension on wave run-up and overtopping, the influence of viscosity on wave propagation ... may be mentioned in this context.

Finally, effects of measurement techniques originating from different measurement equipment used for sampling the data in prototype and model situation are described. These effects may originate from the resolution of the measuring devices, the position of the measuring devices, etc.

In a first step of this CLASH research the minimum combined effect of measurement techniques and model effects is studied, i.e. the minimum spread which is always present in data obtained from hydraulic model tests regardless how accurately the tests were performed. It is shown that various measurement uncertainties and model effects may have a considerable effect on overtopping measurements in laboratories.
In this context the accuracy of the overtopping measurements gathered in the database should be considered during the set-up of the neural prediction method. How and to which extent the accuracy of the overtopping measurements influences the final prediction method is discussed in section 4.5.

In a second step Kortenhaus et al. (2005) propose a CLASH scaling procedure. The procedure basically consists of a 'scaling map' which helps to identify model and scale effects and which proposes in addition correction factors to account for these.
The CLASH scaling procedure should be applied to wave overtopping results originating from small scale model tests *which have been scaled to prototype results* using Froude, referred to as q_{ss} ($q_{\mathbf{s}small\_\mathbf{s}cale}$) in the text below. The corrected, final overtopping result is referred to as q_{scale_wind}, q_{scale_nowind} and q_{wind}, depending on the correction which has been applied (see figure 4.6). Small scale overtopping tests are defined in this CLASH procedure as model tests with a measured wave height $H_{m0\ toe}$ *smaller than 0.5m*. This also implicates that the scaling procedure should only be applied if *the corresponding wave height $H_{m0\ toe}$ in the scale where the final overtopping result is needed, is larger than 0.5m*. For all other situations, the CLASH scaling procedure proposes a scaling factor equal to 1, i.e. no correction factor should be applied.

Figure 4.6 shows the CLASH scaling map. A distinction is made between rough sloping structures and other structure types. Opposite to what the name may suggest, the map accounts besides for scale effects, also for the model effect of wind (i.e. wind which is present in prototype and not in laboratory).

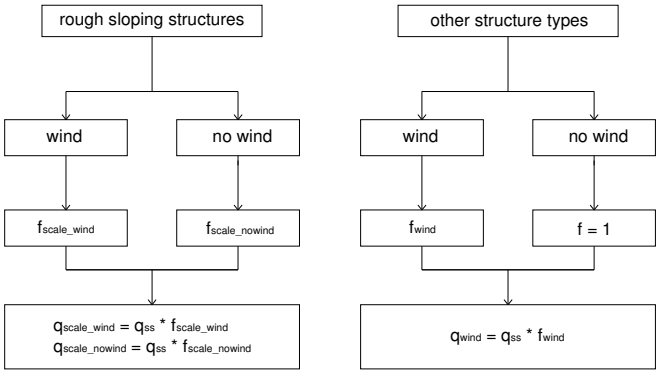

Figure 4.6 CLASH scaling map

The CLASH scaling map presents three possible outputs:

- q_{scale_wind}: relevant for rough sloping structures and accounting for both possible scale and wind effects
- q_{scale_nowind}: relevant for rough sloping structures and accounting only for possible scale effects; the main interest of this output is to predict wave overtopping discharges for large scale tests without wind
- q_{wind}: relevant for vertical structures and smooth (sloping) structures, accounting for possible wind effects

The correction factors f_{wind} , f_{scale_nowind} and f_{scale_wind} , proposed in figure 4.6 are defined in table 4.5.

Table 4.5 CLASH correction factors

Value of q_{ss}	f_{wind}	f_{scale_nowind}	f_{scale_wind}
$q_{ss} < 1.10^{-5}$ m^3/s/m	4	16	24
1.10^{-5} m^3/s/m ≤ q_{ss} ≤ 1.10^{-2} m^3/s/m	$1+3.\left(\frac{-\log q_{ss}-2}{3}\right)^3$	$1+15.\left(\frac{-\log q_{ss}-2}{3}\right)^3$	$1+23.\left(\frac{-\log q_{ss}-2}{3}\right)^3$
$q_{ss} > 1.10^{-2}$ m^3/s/m	1	1	1

Two additional remarks to the CLASH scaling procedure should be made:

- The rough sloping structures present at the left side of the CLASH scaling map in figure 4.6, are defined as sloping structures with a value of $\gamma_{f\ armour} \leq 0.7$, where $\gamma_{f\ armour}$ is the roughness/permeability factor of the

structure without taking into account the possible influence of a small recurve wave wall (see chapter 3). Smooth sloping structures are defined as sloping structures with a value of $\gamma_{f\ armour} \geq 0.9$, and are subject to the scaling procedure proposed at the right side of the CLASH scaling map in figure 4.6.

To avoid an abrupt transition from rough to smooth sloping structures, a linear interpolation for the correction factors is suggested for $0.7 < \gamma_{f\ armour} < 0.9$, i.e.:

$f_{scale\_wind\_inter} = 5\ (1 - f_{scale\_wind})\ \gamma_{f\ armour} + 4.5\ (f_{scale\_wind} - 1) + 1$ and

$f_{scale\_nowind\_inter} = 5\ (1 - f_{scale\_nowind})\ \gamma_{f\ armour} + 4.5\ (f_{scale\_nowind} - 1) + 1$

- The CLASH scaling map can not be applied to small scale measurements q equal to zero. In Kortenhaus et al. (2005) a method is described to predict large scale or prototype overtopping values in these cases as well. The rationale is that the zero is obtained through the limited measurement accuracy present at small scale.

  The method uses available non-zero q -values of the same test series (i.e. identical structure geometry) with comparable wave characteristics, to estimate small non-zero q -values corresponding to the zero small scale results.

  The starting point is a graph with the dimensionless overtopping discharge $\frac{q}{\sqrt{gH_{m0\ toe}^3}}$ versus the dimensionless crest height $R_c / H_{m0\ toe}$ (or armour height $A_c / H_{m0\ toe}$, depending on the structure geometry) where an empirical formula is fitted through the non-zero q -values. Starting from the value of $R_c / H_{m0\ toe}$ (or $A_c / H_{m0\ toe}$) of the test with q = 0 $m^3/s/m$, the empirically predicted value $\frac{q_{est}}{\sqrt{gH_{m0\ toe}^3}}$ is determined, resulting in a (small) estimated value of q, i.e. q_{est}.

  The CLASH scaling map is then applied, starting from this small non-zero estimation q_{est}.

As within the CLASH project the time for validation of the CLASH scaling procedure was limited, it might be expected that the coefficients of the correction factors will be finetuned in the near future. In addition, further validation of the CLASH scaling procedure with newly available prototype measurements may lead to improvements of the procedure in future.

4.4.2.2 Practical application within this work

As the majority of overtopping tests included in the database concern small scale overtopping tests, a prediction method for small scale overtopping tests is developed within this work. To avoid confusion of the neural models, large scale tests (including prototype measurements), which would possibly be affected by model and scale effects if performed on a small scale, are excluded from the development of the neural models.

Table 3.2 (chapter 3, section 3.2) shows that the database only contains 'large scale tests' on rough sloping structures which refer to prototype measurements. 'Large scale tests' refers to the definition given to this expression within the CLASH scaling procedure, i.e. tests with $H_{m0\ toe} > 0.5$m.
This implicates that only the 132 prototype measurements should be left out for the development of the neural models. The model tests with values of $H_{m0\ toe} > 0.5$m concern all structure types other than rough sloping, so no other results are expected if these tests are performed on a small(er) scale. Consequently, all model tests included in the overtopping database could be used for the development of the neural models, independently of the size of the scale on which the test was performed.

In addition to the prototype measurements, small scale tests subject to specific (model) effects which are not taken into account into the neural prediction method also had to be excluded for the development of the neural models. The minority of model tests performed with artificial wind generation are such tests. As wind is not included as an input parameter in the neural models, the neural prediction method will not be able to distinguish these tests from others.

As mentioned in chapter 3, section 3.8, column 32 of the database contains remarks advising against the use of prototype measurements and model tests performed with artificial wind generation for the development of a NN.

Table 4.6 gives an overall view of the number of data which are excluded respectively included for the NN development. The values are given for the original database as well as for the extended, i.e. weighted database, where the overall reliability of the tests is taken into account.

Table 4.6 Number of data available for NN development

	original database	weighted database
Total # data in database	10532	52267
of which		
# prototype measurements	132	564
# model tests performed with wind simulation	223	840
Remaining data available for NN	10177	50863
of which		
# with RF and CF both ≠ 4	9071	50863

The CLASH scaling procedure may be applied to estimate prototype overtopping discharges corresponding to the obtained small scale predictions with the neural prediction method. In section 4.6.9.1 and section 4.7.6.1 the combination neural model - CLASH scaling procedure is checked, by subsequently undertaking the following steps:

- simulation of the prototype situations with the developed neural prediction method
- application of the CLASH scaling procedure to these small scale predictions
- comparison of the estimated prototype discharges with the available measured prototype discharges

In contrast to the prototype measurements, the model tests performed with artificial wind generation are not further considered in this thesis.

The author draws the attention to the fact that some model effects and effects of measurement techniques, not accounted for in the CLASH scaling procedure, are accounted for in the data itself, more specifically in the value of the reliability factor RF assigned to the tests. The model effect of wave reflection in a flume is e.g. accounted for by assigning a higher value to RF if no active wave absorption system was present in the flume. An example of accounting for measurement accuracy is the higher RF which has been assigned to tests where waves were measured in breaking wave zones.

4.5 Small and zero overtopping measurements

In the previous section, besides model and scale effects, effects of measurement techniques on overtopping measurements have been mentioned. This section focuses on the specific effect of the measurement accuracy of the q -values on the neural prediction method. As will be shown, special attention should be given to small and zero overtopping measurements.

4.5.1 Rationale

Data with various values for the mean overtopping discharge q are included in the database. The largest values of q are in the range of 1.10^{-1} $m^3/s/m$, the smallest values in the range of 1.10^{-9} $m^3/s/m$. Also zero values for situations where no overtopping occurred are included. Logically, the differences in q partly originate from the different scales of the tests included in the database. However, also scaled values of q, i.e. ${}^{s}q$, leading to more comparable test situations, cover a range of different values.

Suppose the accuracy of an overtopping measurement system in laboratory is 1.10^{-7} $m^3/s/m$. A measurement of $q_1 = 1.10^{-3}$ $m^3/s/m$ is relatively more accurate than a measurement of $q_2 = 1.10^{-6}$ $m^3/s/m$, i.e. a relative error of ±0.01% for q_1 versus a relative error of ±10% for q_2. Depending on the accuracy of the overtopping measurement system, the relative errors may be larger or smaller, but in general the relative error on the small q -values is higher than the relative error on the large q -values.
The relative errors on the q -values are considered here, as the output of the quantifier is preprocessed to its logarithm for the training process: studying the relative errors on q, corresponds exactly to studying the absolute errors on log(q), which are aimed to investigate in this section. The following transformations show this:

$\log(q_1 \pm 10^{-7}) = \log[q_1(1 \pm 0.0001)] = \log(q_1) + \log(1 \pm 0.01\%) = -3 \pm 4.34*10^{-5}$ and
$\log(q_2 \pm 10^{-7}) = \log[q_2(1 \pm 0.1)] = \log(q_2) + \log(1 \pm 10\%) = -6 \pm 0.04$

The accuracy of $\log(q_1)$ is clearly higher than the accuracy of $\log(q_2)$.
As all input and output parameters of a test are scaled to the situation $H_{m0\ toe} = 1m$, the accuracy of $\log({}^{s}q)$ should actually be considered. The relative accuracy of the values of $H_{m0\ toe}$ also has a significant influence, which is shown in eq. (4.22):

$$\log({}^{s}q) = \log(q/H_{m0\ toe}{}^{1.5}) = \log(q) - 1.5*\log(H_{m0\ toe}) \qquad (4.22)$$

How the differences in accuracy of the $\log({}^{s}q)$ -values due to the differences of measurement accuracy of q -values (and $H_{m0\ toe}$ -values) are taken into account for the development of the quantifier is explained in detail in section 4.5.3.

The accuracy of an overtopping measurement system also affects zero overtopping measurements in laboratories. Apart from possible model and scale effects, it may be expected that a part of the zero values in the database do not correspond with zero overtopping discharges in prototype situations. The overtopping discharges in laboratories are in some cases just too small to measure with the available measurement system. Consequently, the zero values are in a certain sense dependent on the considered test series. In section 4.5.4 it is explained how this effect of measurement accuracy is taken into account for the development of the classifier.

A problem which arises is that, for the majority of tests, the accuracy of the overtopping measurement system is simply not given, even not in the report describing the overtopping tests. Consequently, it is difficult to assess the accuracy of the overtopping measurements. In addition, even for the reader of the overtopping report, it is sometimes not possible to retrieve if a zero q -value in the report corresponds to no overtopping or to an overtopping volume too small to measure with the available measurement system. In section 4.5.2 the mean accuracy of overtopping measurements at various scales is estimated through several examples.

4.5.2 Overtopping measurement accuracies

The accuracy of overtopping measurements mainly depends on the measurement system. Weighing systems for example, where the overtopping box is connected to an accurate balance, are more accurate than systems where changes in water levels are measured by wave gauges in the overtopping box. Through the following examples, an idea of the accuracy of common measurement systems is obtained, see also Van der Meer et al. (2005b).

Imagine a small scale test, with following characteristics:

- overtopping box with surface area of 0.04m²
- width of overtopping tray = 0.1m
- test duration = 30min
- measurement of water level changes with wave gauges

Measurement accuracies of the wave gauges of 5 respectively 1mm result in limit discharges of:

$(5mm*0.04m^2)/(30min*0.1m) = 1.1*10^{-6}$ $m^3/s/m$ and

$(1mm*0.04m^2)/(30min*0.1m) = 2.2*10^{-7}$ $m^3/s/m$.

Larger overtopping boxes with the same width of the overtopping tray, result in larger limit values of q. A surface area of e.g. 0.1m² results in limit discharges of $2.8*10^{-6}$ $m^3/s/m$ and $5.6*10^{-7}$ $m^3/s/m$.

In case of using a weighing system with weighing accuracy of 5 respectively 1 gram, limit discharges of $2.8*10^{-8}$ $m^3/s/m$ and $5.6*10^{-9}$ $m^3/s/m$ are obtained.

This example shows that the accuracy of small scale overtopping measurements may vary in between about 10^{-6} $m^3/s/m$ for the less accurate systems and even smaller values than 10^{-8} $m^3/s/m$ for the most accurate systems. A large difference in accuracy is obtained when comparing weighing systems with wave gauge systems. Early overtopping tests (tests performed before ~1990) are often performed by measuring water levels with wave gauges whereas more recent tests use weighing systems leading to more accurate results.

A large scale test, e.g. in the Large Wave Flume (Groβen Wellen Kanal) at Hannover, is approximately characterised by:

- overtopping tank with surface area of 8m²
- width of overtopping tray = 1m
- test duration = one and a half hour
- measurement of water level changes with wave gauges

Measurement accuracies of the wave gauges of 5 respectively 1mm result in limit discharges of $7.4*10^{-6}$ $m^3/s/m$ and $1.5*10^{-6}$ $m^3/s/m$.

Finally, for prototype measurements, the overtopping measurements at a rubble mound breakwater in Zeebrugge, Belgium, are mentioned:

- overtopping tank with surface area of 14.8m²
- width of tank = 7.4m
- measurement duration = two hours
- measurement of water level changes with pressure sensors

The pressure sensors have an accuracy of about 3.5mm, resulting in a limit discharge of $1.9*10^{-6}$ $m^3/s/m$.

Summarised, it can be estimated that measurement accuracies of small scale tests are most frequently in between 10^{-6} $m^3/s/m$ and 10^{-8} $m^3/s/m$. Recent overtopping measurements (with a weighing system) incline to an accuracy of 10^{-8} $m^3/s/m$ or even more accurate. Large scale test accuracies may be estimated to be about 10^{-5} $m^3/s/m$ - 10^{-6} $m^3/s/m$, whereas prototype measurements may have limit values of even larger than 10^{-6} $m^3/s/m$.

In table 4.7 the estimated measurement accuracies are scaled to prototype values. As the prototype values depend on the length scale of the model test, some examples for specific length scales are given.

Table 4.7 Prototype overtopping discharges corresponding with estimated overtopping measurement accuracies in various test situations

Estimated overtopping measurement accuracy	**Corresponding prototype overtopping discharge**	
small scale test	if length scale = 1:50	if lenght scale = 1:25
10^{-6} $m^3/s/m$	$3.5*10^{-4}$ $m^3/s/m$	$1.3*10^{-4}$ $m^3/s/m$
10^{-7} $m^3/s/m$	$3.5*10^{-5}$ $m^3/s/m$	$1.3*10^{-5}$ $m^3/s/m$
10^{-8} $m^3/s/m$	$3.5*10^{-6}$ $m^3/s/m$	$1.3*10^{-6}$ $m^3/s/m$
large scale test	if length scale = 1:5	if length scale = 1:2
10^{-5} $m^3/s/m$	$1.1*10^{-4}$ $m^3/s/m$	$2.8*10^{-5}$ $m^3/s/m$
10^{-6} $m^3/s/m$	$1.1*10^{-5}$ $m^3/s/m$	$2.8*10^{-6}$ $m^3/s/m$
prototype measurement	(length scale = 1:1)	
10^{-6} $m^3/s/m$	10^{-6} $m^3/s/m$	

The largest prototype discharge in table 4.7, i.e. the lowest corresponding prototype accuracy, is obtained for rather inaccurate small scale tests on a small model scale (1:50): a prototype overtopping discharge of $3.5*10^{-4}$ $m^3/s/m$ is obtained. Also for the least accurate large scale tests a prototype discharge of ~10^{-4} $m^3/s/m$ is found. However, considering the more accurate model tests as well as the prototype measurements, it can be stated that the measurement accuracies generally correspond to prototype overtopping discharges in between 10^{-5} $m^3/s/m$ and 10^{-6} $m^3/s/m$.

These prototype discharges may be compared with tolerable overtopping limits prescribed in literature, see chapter 2, table 2.9 and table 2.10.
In table 2.9 overtopping discharges of 10^{-5} $m^3/s/m$ - 10^{-6} $m^3/s/m$ are assessed as unsafe for vehicles driving at high speed. The limit of comfort for pedestrians is fixed on $4*10^{-6}$ $m^3/s/m$, but values of 10^{-5} $m^3/s/m$ are still not assessed as dangerous. For buildings the overtopping range of 10^{-5} $m^3/s/m$ - 10^{-6} $m^3/s/m$ results in minor damage whereas no structural damage at all is expected for the defending structures itself (seawalls, dikes and revetments).
In table 2.10 limit discharges in the range 10^{-5} $m^3/s/m$ - 10^{-6} $m^3/s/m$ are suggested only for unaware pedestrians ($3*10^{-5}$ $m^3/s/m$) and vehicles driving at moderate or high speed (1 à $5*10^{-5}$ $m^3/s/m$).
Consequently, when performing overtopping tests in laboratories or prototype overtopping measurements, on average measurement accuracies allow to measure overtopping discharges even in the range of small tolerable overtopping limits, which are assessed as not or little dangerous for people and structures.

4.5.3 Influence of (in)accuracies of small q -values on the development of the quantifier

Due to the preprocessing of the q -values to the logarithm of these values for the training of the quantifier, only non-zero overtopping data can be included in the training process. Consequently only the correctness of non-zero data plays a role here.

Eq. (4.22) shows that the relative error on $H_{m0\ toe}$ has a larger impact on the accuracy of the log(^{s}q) -values than the relative error on q (factor 1.5).
It is difficult to quantify the possible error on the measurement of $H_{m0\ toe}$. Although it is not the aim to study the measurement accuracies of wave parameters in detail, a rough estimation of the measurement accuracy of $H_{m0\ toe}$ is needed to assess the accuracy of the preprocessed output of the quantifier.
It seems reasonable to assume that in general the wave height $H_{m0\ toe}$ will be determined with a relative error lower than 5%. Considering the many small scale tests in the database, this corresponds to an accuracy of minimum 0.005m on a wave height $H_{m0\ toe}$ of 0.1m. In many (small scale) laboratories, a measurement accuracy of 0.001m water level is reached. This corresponds with only 1% relative error on total wave heights of 0.1m. However, these errors may increase due to e.g. reflection analysis (additional inaccuracies) and breaking waves complicating the measurements. Also for smaller wave heights $H_{m0\ toe}$ the relative error will increase. From this point of view a relative error in general lower than 5% seems reasonable for measurements of $H_{m0\ toe}$.

If one supposes the measurement accuracy of q in small scale tests is ~10^{-7} m^3/s/m (see table 4.7), relative errors larger than 5% on q may be expected for measurements of q smaller than $2*10^{-6}$ m^3/s/m. For values of q smaller than $2*10^{-6}/1.5$, the inaccuracy of q disturbs the value of log(^{s}q) more than the inaccuracy on the value of $H_{m0\ toe}$ itself under the mentioned assumptions.

One could try to remove the values of log(^{s}q) for which the largest inaccuracies are expected from the development of the quantifier by excluding data with low values of q, e.g. data with q < 10^{-6} m^3/s/m. In this way 'confusion' of the network by many of these probably less reliable data is avoided.
In figure 4.7 values of ^{s}q are plotted versus values of q for all data which may be considered for the development of the quantifier, i.e. the zero data, plus the data which would confuse the quantifier regarding model and scale effects, plus the data with weight factor = 0 are excluded. A total number of 8195 data is represented in the figure. This corresponds to the mentioned 9071 data in table 4.6 minus 876 zero overtopping measurements with weight factor > 0.

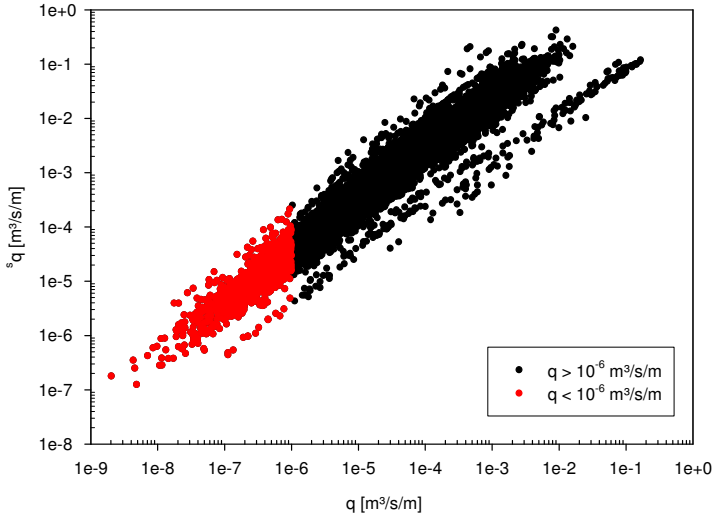

Figure 4.7 Values of ^{s}q versus q for all data which may be considered for the development of the quantifier (8195 data)

The large scale data can be clearly distinguished in figure 4.7, resulting in lower values of ^{s}q due to larger values of $H_{m0\ toe}$. Approximately 13% of the data represented in figure 4.7 concern data with an overtopping measurement $q < 10^{-6}$ $m^3/s/m$ (at any scale in the database), i.e. 1028 data.

It can be suspected that the prediction limit of a quantifier only trained on values of q larger than 10^{-6} $m^3/s/m$ will be situated around the corresponding ^{s}q -value of 10^{-5} $m^3/s/m$ (see figure 4.7), as a network is only able to predict values on which it has been trained. In addition, it may be expected that the prediction of values of ^{s}q near this limit will be less accurate due to the vicinity of the limit of applicability of the network.

The corresponding prototype overtopping discharge depends on the value of $H_{m0\ toe}$ in the prototype situation. For a prototype measurement with $H_{m0\ toe}$ = 3m, a prototype discharge of $q = {}^{s}q * (H_{m0\ toe})^{3/2} = 10^{-5} * (3)^{3/2} \approx 5*10^{-5}$ $m^3/s/m$ is obtained. A prototype measurement of $H_{m0\ toe}$ = 5m corresponds to a prototype discharge of $q \approx 10^{-4}$ $m^3/s/m$. The comparison with the tolerable overtopping limits mentioned in table 2.9 and table 2.10 (see chapter 2), shows that prototype discharges of 10^{-4} $m^3/s/m$ correspond to:

- dangerous situations for pedestrians on vertical wall breakwaters and structural damage to buildings (table 2.9)
- tolerable overtopping limit for aware pedestrians (table 2.10)

This implicates that by not considering measurements of q (at any scale in the database) smaller than 10^{-6} $m^3/s/m$, the prediction capacity of the quantifier will be

restricted up to these limits, i.e. smaller prototype discharges, corresponding to safer situations, especially for pedestrians, will not be predictable.

To lower the quantifier prediction limit to smaller prototype discharges, one could include the data for which the largest inaccuracies are expected (i.e. in accordance to previous example, the data with values of $q < 10^{-6}$ $m^3/s/m$ in the database) for the development of the quantifier. Supposed the scatter on the output of the quantifier is normally distributed around the correct values, then the training of the quantifier with all available data (i.e. 8195 data) should result in a good 'mean' prediction method, also for values of ${}^{s}q < 10^{-5}$ $m^3/s/m$.
Referring to figure 4.7, the prediction limit of the quantifier should be extended in this way to values of ${}^{s}q = 10^{-6}$ $m^3/s/m$ or even to slightly smaller values. Estimated corresponding prototype overtopping discharges are at least a factor 10 smaller, i.e. a limit value of ${}^{s}q = 10^{-6}$ $m^3/s/m$ corresponds in prototype to $q \approx 5*10^{-6}$ $m^3/s/m$ and $q \approx 10^{-5}$ $m^3/s/m$ for a measured prototype value of $H_{m0\ toe}$ = 3m respectively 5m. As mentioned before (see section 4.5.2) these prototype discharges correspond to tolerable overtopping limits which are not or little dangerous for people and structures.
It should be mentioned that due to the preprocessing to $\log({}^{s}q)$ the scatter on the output of the quantifier is probably not normally distributed. Starting from the plausible assumption that the scatter on the measured q and $H_{m0\ toe}$ -values is normally distributed, large errors on the values of q and $H_{m0\ toe}$ have a different impact on the values of $\log({}^{s}q)$ if these errors concern too large or too small values. This can be easily seen in figure 4.8, where the logarithmic function is represented. The steep curve for values of x lower than 1 causes negative values log(1-a) with a larger absolute value than the positive values log(1+a), where a > 0. Consequently the larger the expected errors on q and $H_{m0\ toe}$, the larger the difference will be between the absolute value of the errors on log(q) for too small and too large measurements.

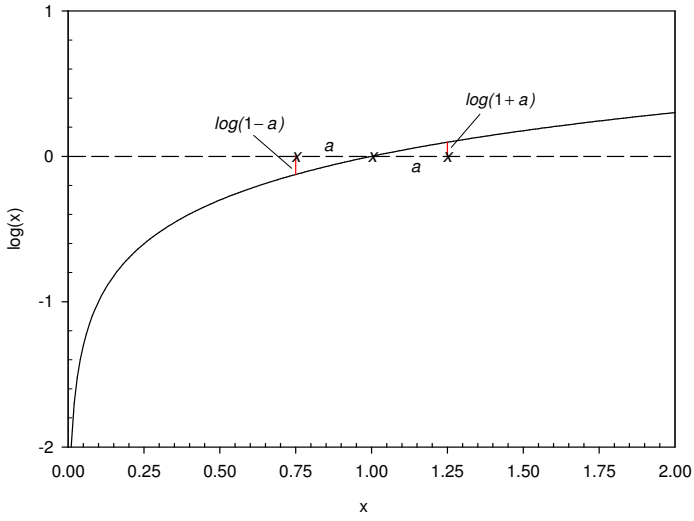

Figure 4.8 Logarithmic function log(x) for 0 < x < 2

A large error of e.g. 25% on q, results in an error on the logarithm of q of log(1+0.25) = 0.097 if the measurement is too high versus log(1-0.25) = -0.125 if the measurement is too low. This corresponds to a deviation of (0.097-0.125)/2 = -0.014 of the error on log(q) inclined to the negative side, which is a deviation of -3.2% on the corresponding q -value, as -0.014 = log(1-0.032). However, for relatively small errors on q the absolute value of the error on the logarithm of q will be almost equal for too high or too low q-measurements. A relative measurement error of e.g. 5% on q, results in log(1+0.05) = 0.021 and log(1-0.05) = -0.022, which corresponds to a deviation of (0.021-0.022)/2 = -0.0005 of the error on log(q) inclined to the negative side. This is only a deviation of 0.1% on the corresponding q -value, which is negligible. The expected maximum relative error of 5% on the value of $H_{m0\ toe}$ results in a comparable, negligible deviation on the q -value.

As it is assumed that only a minority of the low q -values will be disturbed by large relative errors such as 25%, the training of the quantifier on all values of q should lead to a model which is able to find an acceptable 'mean' value. Some underprediction of q may be the consequence of the deviation of the scatter on the log(^{s}q) -values, although this effect is expected to be small.

4.5.4 Influence of incorrect zero q -values on the development of the classifier

To avoid confusion of the classifier, which is only trained on 2 possible values, i.e. +1 and -1, it is important to assure a more or less consequent zero-boundary of the data included in the training process. As mentioned before, different measurement accuracies of laboratories result in a dependency of zero q -values of the test series. The intention is to select only 'precise' zero overtopping data for the development of the classifier, where 'precise' stands for zero data originating from tests with an accurate measurement system, assuring that zero overtopping measurements really concern zero or al least negligible discharges.
However, the number of available zero data in the database is rather low, i.e. 876 data of the 9071 data which were assessed as useful for the NN development (see table 4.6). Consequently, the more zero data are excluded, the smaller the domain will be the zero overtopping data constitutes, which is worse for the development of the classifier.

Finally, the 'precise' zero data for the development of the classifier were selected as follows:

- Each test series containing zero values for the measured overtopping discharge was studied in detail. Zero data which seemed unreliable were excluded. When for example within one test series two tests with comparable input parameters were included, where the overtopping discharge for one test concerned zero and for the other a rather high overtopping discharge, the zero was considered as unreliable and consequently excluded. Also the zero data from test series for which an inaccurate measurement system for overtopping was described in the overtopping report were not considered.
- In addition, all test series from before 1990 of which the measurement system was unknown, were assumed to be performed with less accurate measurement systems (see section 4.5.2). Moreover, the zero data originating from these test series were not considered for the development of the classifier.
- To further reduce the probability that the same overtopping situation was included once as a zero value and once as a non-zero value, a strict zero-border was set on ${}^{s}q = 10^{-6}$ $m^3/s/m$. Consequently, the (small number of) data with values of ${}^{s}q$ lower than 10^{-6} $m^3/s/m$ were assigned to class -1, i.e. considered as insignificant overtopping.

4.6 Development of a neural quantifier for q ≠ 0 $m^3/s/m$, for all structure types

In this section the development of a neural 'quantifier' for overtopping is described. The aim of the quantifier is to predict mean overtopping discharges which will occur under certain wave conditions at a specific structure, and this for any structure type.

Only non-zero data are used for the training of the quantifier. Section 4.6.1 describes the methodology followed in this work for the selection of the data. The preprocessing of the output of the quantifier, which is on the origin of the use of only non-zero data, is discussed in section 4.6.2.

In a first attempt of searching an optimal network configuration for the quantifier, the available data are split up in a trainingset (85%) and a testset (15%). The trainingset is used to train various models, whereas the performance of the models is compared on the basis of the testset. The criterion which is used to assess the performance of the models is discussed in section 4.6.3. Starting from a basic network architecture, an optimal network configuration is determined (sections 4.6.4, 4.6.5 and 4.6.6).

In a second attempt the bootstrap method is applied (section 4.6.7) resulting in a final quantifier network, for which ranges of applicability are set up (section 4.6.8). Finally, the performance of the developed quantifier is studied in section 4.6.9.

4.6.1 Selection of data

In section 4.5.3 the influence of inaccuracies of small q -values on the development of the quantifier has been considered. Two approaches to develop the neural quantifier were distinguished (see also figure 4.7):

- Only the data with a measured overtopping discharge q larger than 10^{-6} $m^3/s/m$ are considered for the development of the quantifier, i.e. 8195 - 1028 = 7167 data.
  In this first approach data with large errors on $\log({}^s q)$ are removed. It is expected that due to the lacking of these data, the corresponding model will not be able to predict small overtopping discharges in the magnitude of ${}^s q < 10^{-5}$ $m^3/s/m$.
- All data available for the development of the quantifier are considered, i.e. 8195 data.
  In this second approach also the data with q smaller than 10^{-6} $m^3/s/m$ are used. Values of $\log({}^s q)$ with more scatter are included, but the network prediction area is extended. It is expected that a model with an acceptable mean prediction will be obtained.

In table 4.8 for both approaches the number of data selected from the total number of 8195 available data for the development of the quantifier is represented.

Table 4.8 Number of data selected for the development of the quantifier

	# data in original database (with RF and CF ≠ 4)	# data in weighed database
first approach ($q < 10^{-6}$ $m^3/s/m$ excluded)	7167	40262
second approach (all data included)	8195	46328

The development of the neural quantifier is dealt with within this work by starting with the first approach, i.e. only data with $q \geq 10^{-6}$ $m^3/s/m$ are considered. The obtained results are described in sections 4.6.4 and 4.6.5. The influence of including also data with measured values of $q < 10^{-6}$ $m^3/s/m$ is studied in section 4.6.6, corresponding to the second approach. This second approach is found to give the best results for the quantifier, (see section 4.6.6) so this approach is restricted for further development of the final neural quantifier with the bootstrap method.

4.6.2 Preprocessing the output of the network

In order to improve the prediction capacity of the quantifier, the output is preprocessed before starting the training process. This is done by taking the logarithm of ^{s}q, i.e. $\log(^{s}q)$, as the output value instead of ^{s}q.
The exclusion of the zero data from the development of the quantifier originates from this preprocessing, as log(0) equals minus infinity.

Figure 4.9 shows a histogram of all values of ^{s}q available for the development of the quantifier (i.e. 8195 data). Figure 4.10 shows a histogram of the corresponding values of $\log(^{s}q)$. It is clear that the logarithm of ^{s}q is more evenly distributed than the raw ^{s}q -values. This explains the better performance of a quantifier trained on the $\log(^{s}q)$ -values over the performance of a quantifier trained on the raw ^{s}q -values, which was already mentioned in section 4.1.6.

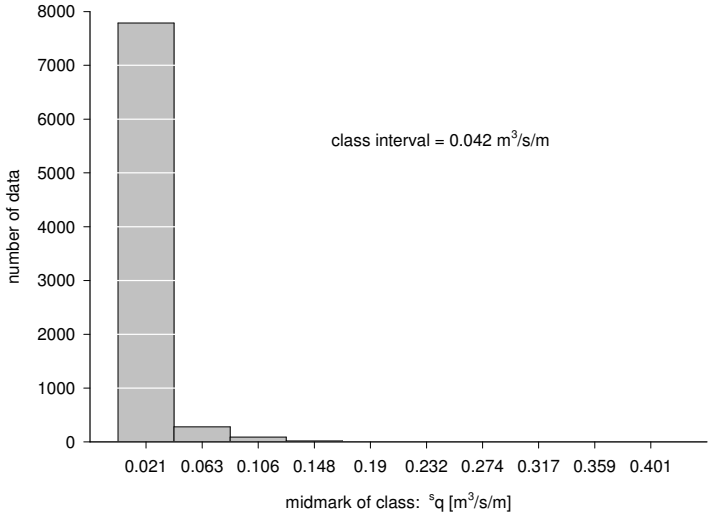

Figure 4.9 Histogram of ^{s}q -values

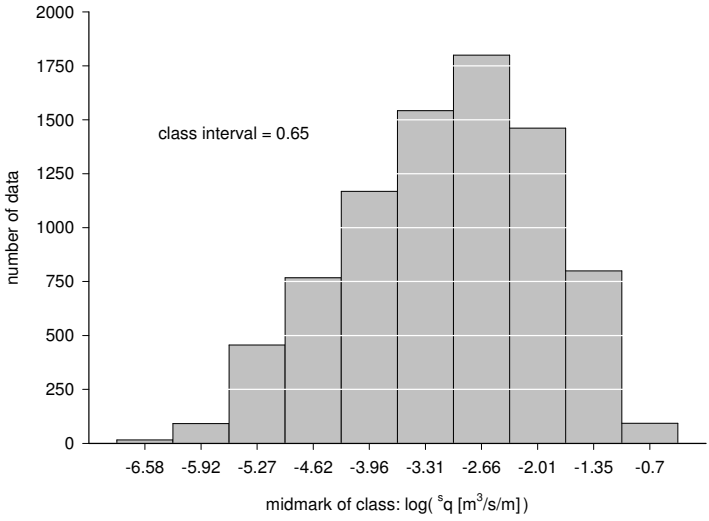

Figure 4.10 Histogram of log(^{s}q) -values

By taking the inverse of the logarithm of the predicted network output, i.e. $\log^{-1}(\text{output}) = 10^{\text{output}}$, the predicted scaled discharge $^sq_{NN}$ is easily found.

A consequence of using log(^{s}q) as output is that the quantifier is forced to draw more attention to the small overtopping discharges during the training process. This is explained by the fact that minimising the absolute error on log(^{s}q) (what happens during the training process) corresponds to minimising the relative error on ^{s}q , resulting in smaller absolute errors on small values of ^{s}q compared to large values of ^{s}q (see before, section 4.5.1).

Developing a quantifier on log(^{s}q) also implicates that a zero overtopping prediction is not possible, as this would require a network prediction of minus infinity. Further in this work it will be shown that for measured zero overtopping values the prediction by the quantifier is even not necessarily a small overtopping discharge (see section 4.6.9.2). This finding was on the basis of the development of a second NN, the classifier, to distinguish significant from negligible overtopping.

4.6.3 Evaluating the quantifier performance

The performance of a specific network configuration is studied on the basis of the predictions obtained for the testset.

It should be mentioned that the multiplication of the available data according to their weight factor (see section 4.3.3) is only performed after splitting up the data in training- and testset, to avoid that the same data are included in both sets. This procedure leads to a completely independent testset, which is necessary to asses the network performance.

After training a specific network configuration on the (weighed) trainingset, the independent (weighed) testset is used to assess the behaviour of the developed network. This is done based on the root-mean-square error (rms-error or rmse) of this independent testset, which is defined as follows:

$$rmse\_test = \sqrt{\frac{1}{N_{test}} \sum_{n=1}^{N_{test}} \left[log({}^{s}q_{measured})_n - log({}^{s}q_{NN})_n \right]^2} \qquad (4.23)$$

where N_{test} equals the (weighed) number of testdata, $log({}^{s}q_{measured})$ refers to the logarithm of the desired output and $log({}^{s}q_{NN})$ refers to the logarithm of the predicted output by the NN. The values of ${}^{s}q_{measured}$ and ${}^{s}q_{NN}$ are both expressed in $m^3/s/m$.

The lower the value of rmse_test, the better the overall prediction capacity of the considered network.

4.6.4 Architecture of the network

At this moment all information for the development of the quantifier is available. The architecture of the basic overtopping quantifier is shown in figure 4.11.
The network consists of:

- one input layer with 14 input parameters, all scaled according to Froude, with the value of $H_{m0\ toe}$ as scaling parameter (see table 4.4, section 4.4.1.3)
- one hidden layer with a certain number of hidden neurons, m, and
- one output layer with the preprocessed, scaled according to Froude, overtopping discharge, $\log({}^{s}q)$, as output parameter

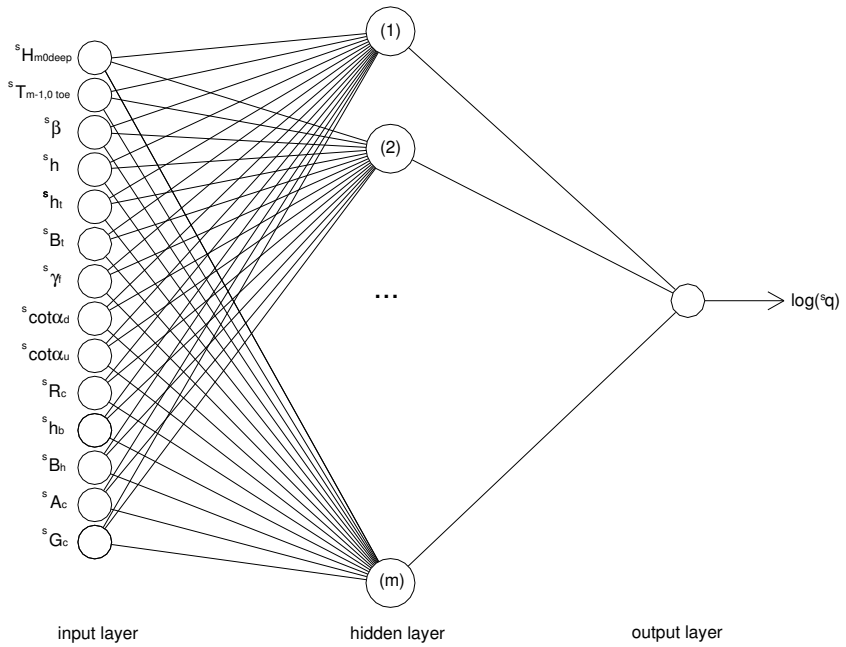

Figure 4.11 Basic network architecture of overtopping quantifier

The number of hidden neurons is determined by training several models, where the number of hidden neurons is varied. An acceptable number of hidden neurons is chosen by comparing the performance of the models for their testset.
One should be aware that one extra hidden neuron corresponds to a significant increase of the network complexity. In case of 14 input parameters and 1 output parameter, 16 additional parameters have to be determined during the training process for one extra hidden neuron:

- 14 interconnection weights between the 14 input parameters and the new hidden neuron,
- 1 bias value of the new hidden neuron and
- 1 interconnection weight between the new hidden neuron and the output parameter

Figure 4.12 shows the value of rmse_test for trained models with a number of hidden neurons varying from 15 up to 33. As the training- and testset are chosen arbitrary, for each model a different testset is used. Besides the division in training- and testset, also the initialisation of the weights and biases is arbitrary for each model. Consequently, the final result as well as the value of rmse_test depend on these random choices. This explains the slightly fluctuating curve of figure 4.12.

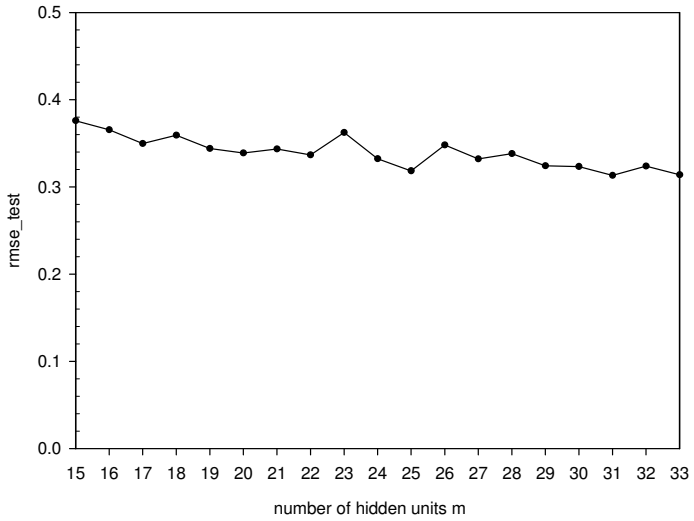

Figure 4.12 Values of rmse_test for different numbers of hidden neurons for the quantifier

The higher the number of hidden neurons, the lower the value of rmse_test, although no significant improvement is noticed for a number of hidden neurons larger than 25. As simplicity is preferred over needless complexity, the number of hidden neurons is chosen on 25.

4.6.5 Importance of each input parameter

In this section the importance of the 14 input parameters of the quantifier are studied. Special attention is given to the importance of the input parameter $^{s}H_{m0\ deep}$ in section 4.6.5.1. In addition, the relative importance of the 14 input parameters is studied in section 4.6.5.2. In section 4.6.5.3 the obtained conclusions on the input parameters are summarised and implications for the development of the final quantifier are given.

4.6.5.1 Influence of $H_{m0\ deep}$

As described in section 4.3.1, it may be expected that the parameter $^{s}H_{m0\ deep}$ is necessary to obtain good overtopping predictions. Especially in some specific situations such as when waves are heavily breaking on a shallow foreshore or when waves are breaking on a vertical wall, the parameter $^{s}H_{m0\ deep}$ may contain important overtopping information.
Whether the parameter $^{s}H_{m0\ deep}$ is important or not is checked by comparing the performance of two models:

- a model with $^{s}H_{m0\ deep}$ as one of the input parameters (network configuration as shown in figure 4.11) versus
- a model where the input parameter $^{s}H_{m0\ deep}$ is left out, leading to a reduced number of 13 input parameters (network configuration as shown in figure 4.11, without the input parameter $^{s}H_{m0\ deep}$)

Both models are developed with a number of 25 hidden neurons.
To simplify the comparison of the prediction capacity of the models, the same training- and testset is used for both. This implicates that only the random initialisation of the parameters (i.e. weights and biases) differs in both models.

Initially, the performance of the two models is compared based on the obtained values of rmse_test. In addition, the rms-error obtained for a restricted number of testdata, originating from specific test series for which an influence of the parameter $^{s}H_{m0\ deep}$ on the measured overtopping discharge q may be expected, is studied for both models.

Following values for rmse_test are obtained:

- network with parameter $^{s}H_{m0\ deep}$: rmse_test = 0.3184
- network without parameter $^{s}H_{m0\ deep}$: rmse_test = 0.3206

One can see that the obtained rms-errors for the testset are approximately equal for both models, i.e. rmse_test ≈ 0.32.

In addition, the rms-errors for the testset of the following five test series are studied:

- Test series 226 and 227 describe tests with very heavy breaking waves, introducing effects of surf beat on the gentle foreshore. It concerns smooth dikes (slopes 1:6, 1:4, 1:3 and 1:2.5) combined with foreshore slopes 1:100, 1:250 and 1:1000.
- Test series 502, 503 and 504 describe tests with breaking waves on a vertical or almost vertical wall (i.e. battered wall: slope 10:1 or 5:1). The corresponding foreshore slopes are steep, i.e. 1:10 or 1:50, leading to breaking waves on the structure.

The results of the testset for these five test series are given in figure 4.13 and figure 4.14 for the network with, respectively without $^{s}H_{m0\ deep}$ as input parameter. Predicted values of ^{s}q, $^{s}q_{NN}$, are represented versus measured values of ^{s}q, $^{s}q_{measured}$. At the right side of the figures the rms-errors for the five considered test sets are shown.

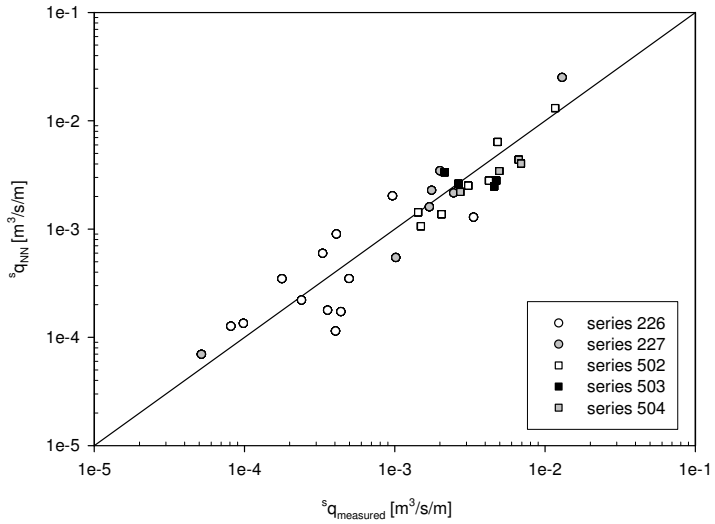

series	rmse testset
226	0.3133
227	0.1848
502	0.1244
503	0.1996
504	0.1749

Figure 4.13 Performance of a model composed of 14 input parameters (i.e. with $^{s}H_{m0\ deep}$), for 5 specific test series

Figure 4.13 shows that the testset of series 226 gives a clearly higher rms-error than the other testsets, i.e. a value larger than 0.30, whereas for the other testsets values lower than 0.20 are obtained. However, also for the testset of series 226 the data approach the diagonal line quite well. If the error factor of a prediction is defined as $^{s}q_{NN}$ / $^{s}q_{measured}$ if $^{s}q_{NN} > {}^{s}q_{measured}$ (overprediction), and as $^{s}q_{measured}$ / $^{s}q_{NN}$

if ${}^{s}q_{NN} < {}^{s}q_{measured}$ (underprediction), then the largest error factor concerns 2.2 for an overprediction and 3.5 for an underprediction of the considered overtopping tests. Both values are obtained for data from the testset of series 226.

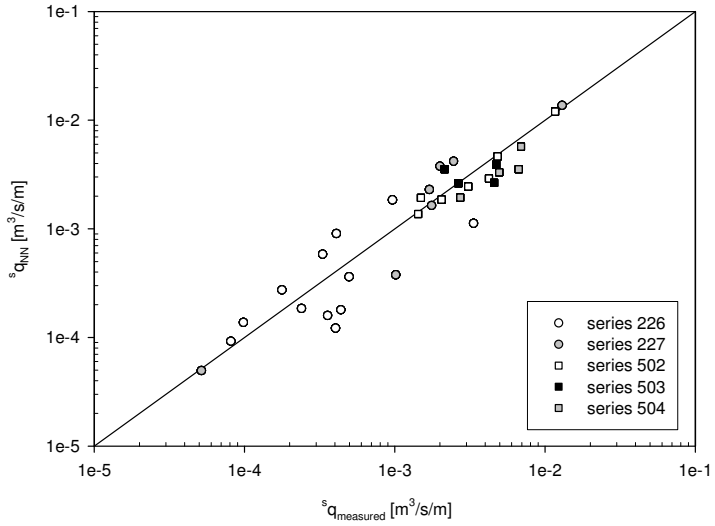

series	rmse testset
226	0.3055
227	0.2262
502	0.0854
503	0.1664
504	0.1838

Figure 4.14 Performance of a model composed of 13 input parameters (i.e. without ${}^{s}H_{m0\ deep}$), for 5 specific test series

Figure 4.14 shows that for the network trained without ${}^{s}H_{m0deep}$ as input parameter as well, the largest value of the rms-error is obtained for the testset of series 226. The values of the rms-error for the testset of series 226, 502 and 503 are slightly lower compared to figure 4.13, whereas the values of the rms-error for the testset of series 227 and 504 are slightly higher. Also here all points approach the diagonal line quite well. The largest error factor corresponding with an overprediction is 2.2 (${}^{s}q_{NN} / {}^{s}q_{measured}$), versus 3.3 corresponding with an underprediction (${}^{s}q_{measured} / {}^{s}q_{NN}$). Both of the largest values are obtained for data from series 226.

It may be concluded that the performance of both networks is approximately evenly well. As comparable rms-errors are found for the entire testset as well as for the testdata of the 5 specific series for which an influence of ${}^{s}H_{m0\ deep}$ might be expected, it is shown that no significant improvement of the quantifier is obtained by including the value of ${}^{s}H_{m0\ deep}$ as an extra input parameter.

4.6.5.2 Relative influence of the input parameters

The relative importance of the 14 input parameters ($^{s}H_{m0\ deep}$ is still restrained as input parameter) is studied by developing 14 neural models. Each model is trained with only 13 input parameters, i.e. each time one of the 14 input parameters is left out. All models are trained and tested with the same training- respectively testset.

The results are summarised in table 4.9, which contains the values of rmse_test for the 14 developed models. As a reference the value of rmse_test for the original network considering all 14 input parameters is given. This reference value as well as the value of rmse_test obtained when the parameter $H_{m0\ deep}$ is omitted were already given in the previous section.

Table 4.9 Values of rmse_test showing the relative influence of the input parameters

input parameter left out	# input parameters	rmse_test
-	14	0.3184
$^{s}H_{m0\ deep}$	13	0.3206
$^{s}T_{m\ -1,0\ toe}$	13	0.3899
$^{s}\beta$	13	0.3357
^{s}h	13	0.3435
$^{s}h_{t}$	13	0.3429
$^{s}B_{t}$	13	0.3335
$^{s}\gamma_{f}$	13	0.4093
$^{s}\cot\alpha_{d}$	13	0.3348
$^{s}\cot\alpha_{u}$	13	0.3516
$^{s}R_{c}$	13	0.3939
$^{s}h_{b}$	13	0.3219
$^{s}B_{h}$	13	0.3484
$^{s}A_{c}$	13	0.3323
$^{s}G_{c}$	13	0.3641

The same results are represented in figure 4.15, where the values of rmse_test are plotted on the y-axis, versus the input parameter left out on the x-axis. The horizontal line corresponds to rmse_test = 0.3184, which is obtained for the network considering all 14 input parameters.

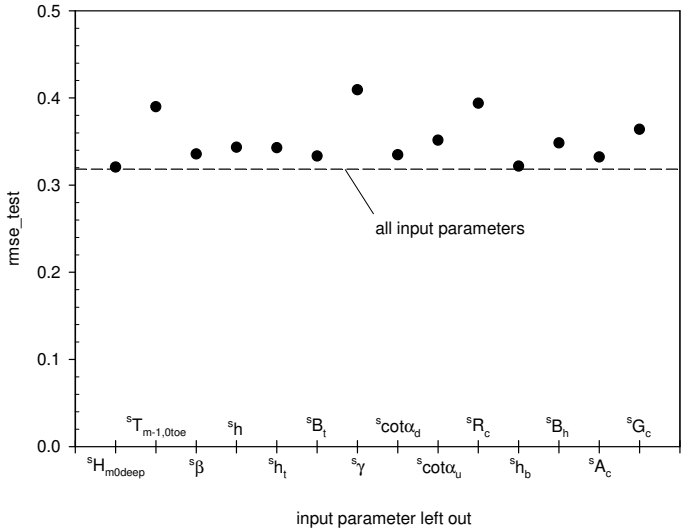

Figure 4.15 Graphical representation of values of rmse_test showing the relative influence of the input parameters

From table 4.9 and figure 4.15 the parameters which contribute most to the overtopping prediction can be easily detected. A significantly higher value of rmse_test when an input parameter is left out compared to the reference value of rmse_test = 0.3184, refers to a parameter containing essential overtopping information.
Three input parameters can be clearly distinguished from the others, i.e. $^{s}T_{m-1,0\ toe}$, $^{s}\gamma_{f}$ and $^{s}R_{c}$. One can conclude that these parameters concern the three most important input parameters of the quantifier.
However, one should be aware of the fact that some parameters may be connected to each other and therefore influence the obtained result. The influence of the parameter $^{s}R_{c}$ e.g. may be underrepresented. When leaving out the parameter $^{s}R_{c}$, the parameter $^{s}A_{c}$ still remains in the input space. As the parameters $^{s}R_{c}$ and $^{s}A_{c}$ are in a lot of cases equal or almost equal to each other, the increase of rms-error by leaving out $^{s}R_{c}$ is probably lower than the increase which should be obtained if the parameter $^{s}A_{c}$ was not present as input parameter.

In contrast to what might be expected, the parameter h_{b} , standing for the berm level, seems to have little importance: the obtained value of rmse_test when the parameter h_{b} is omitted, is comparable to the reference value of rmse_test. A possible explanation for this is the restriction of the berm level to swl ± $1.5H_{m0\ toe}$ for the majority of the overtopping tests included in the database. The fact that the value of h_{b} is often equal to zero (if no berm is present) may also contribute to the impression that the influence of this parameter is rather small.

Mathematically the lowest value of rmse_test is obtained for the original network containing 14 input parameters, i.e. rmse_test = 0.3184. However, a comparable value for rmse_test is obtained for the models where ${}^{s}H_{m0\ deep}$ and ${}^{s}h_{b}$ is left out.

4.6.5.3 Conclusion on the input parameters

In section 4.6.5.1 it has been found that the parameter ${}^{s}H_{m0\ deep}$ does not contain additional information to predict overtopping, even not in situations where heavy wave breaking on shallow foreshores or wave breaking on vertical walls occurs. It may be concluded that also for these specific situations the parameters ${}^{s}T_{m-1,0\ toe}$ and ${}^{s}h$ contain enough information on the influencing characteristics of the waves on the overtopping phenomenon.

In section 4.6.5.2 the relative influence of all input parameters has been compared by leaving out each input parameter one by one. It has been found that the parameters ${}^{s}T_{m-1,0\ toe}$, γ_f and ${}^{s}R_c$ are the most important input parameters. Parameters resulting in rather small increases of the value of rmse_test when omitting these, do not necessarily correspond to useless input parameters, as the influence of these parameters may be restricted to a rather small number of data included in the testset. The parameter ${}^{s}h_{b}$ can be mentioned as a good example in this context.

As the parameter ${}^{s}H_{m0\ deep}$ does not contain additional overtopping information, and as in small scale tests, this parameter is often not available and difficult to determine, it was decided to exclude this parameter from the input space for further development of the quantifier. The influence of the remaining 13 input parameters is believed to be significant, at least for specific overtopping situations. Consequently the quantifier will be developed further on the basis of these 13 input parameters.

4.6.6 Influence of small overtopping discharges

The quantifier developed at this moment consists of 13 input parameters and has 25 neurons in the hidden layer. It has been trained on data with a measured overtopping discharge q larger than 10^{-6} $m^3/s/m$, i.e. the 'first approach' mentioned in table 4.8 has been applied. The general performance of the model is represented by a value of rmse_test = 0.3206.

As explained in section 4.5.3, by leaving out the data with $q < 10^{-6}$ $m^3/s/m$, a better general performance of the quantifier is probably obtained, as data for which a lot of scatter on the $\log(^s q)$ -values is expected, are omitted. The other side of the picture is that this quantifier will not be able to predict such low values sufficiently well.

In this section the 'second approach' mentioned in table 4.8 is studied. Starting from the same network architecture, a new model is developed, where all available data are used. The number of available data increases in this case to 8195 (corresponding to 46328 data in the weighed database). The performance of this new model is compared to the performance of the existing model. Special attention is given to the prediction of small overtopping discharges by both models.

The first, existing model is referred to as 'net_existing', the second, newly developed model, also including data with measured values of $q < 10^{-6}$ $m^3/s/m$ is referred to as 'net_new'.

The value of rmse_test of the existing network has been determined before, and may be compared to the value of rmse_test of the new network:

- net_existing : rmse_test = 0.3206
- net_new : rmse_test = 0.4055

The value of rmse_test of the new network, including the data with low overtopping discharges, is indeed larger than the value of rmse_test of the existing network developed without these data.
If the performance of the new model is only studied for these testdata of which the measured q -values are larger than 10^{-6} $m^3/s/m$ (i.e. only comparable data as used for the development of the existing model are considered), the value of rmse_test is equal to 0.3647. This value is lower than the value of 0.4055 obtained for the entire testset, although the performance is still worse than the performance of the existing net. It may be concluded that by including the additional data (i.e. data with measured values of $q < 10^{-6}$ $m^3/s/m$), the remaining part of the network is also disturbed in a certain sense, leading to a slightly worse result for this part of the network.

In figure 4.16 and figure 4.17 the general performance of both models is graphically represented. Values of ${}^{s}q_{NN}$ are represented versus values of ${}^{s}q_{measured}$. The black dots refer to the trainingdata, the grey triangles to the testdata.

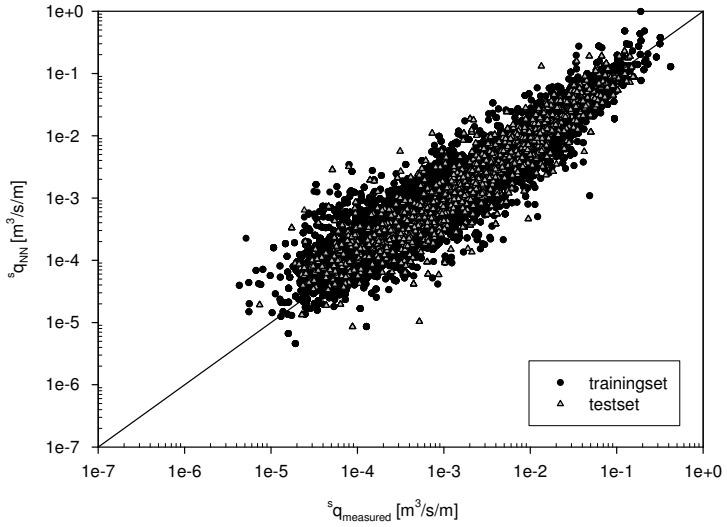

Figure 4.16 General performance of net_existing

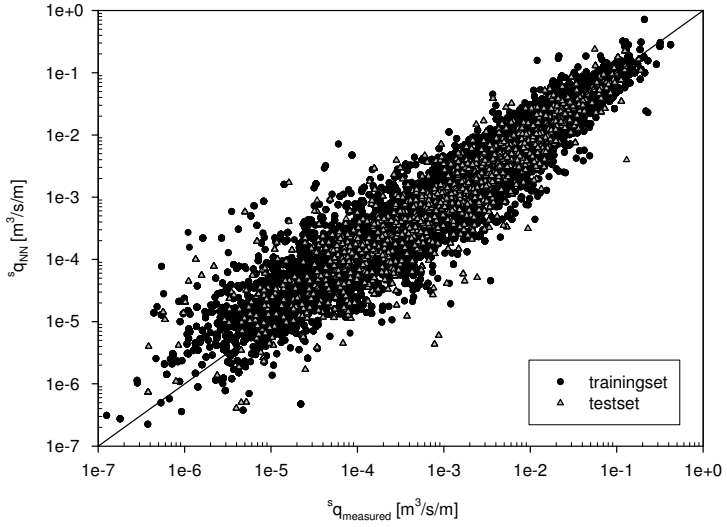

Figure 4.17 General performance of net_new

The extra data included in 'net_new' can be clearly distinguished in figure 4.17: these fill up the gap in the left lower corner. The scatter on the result for the new network is clearly higher than for the existing network.

Further the performance of both models for small overtopping discharges may be studied.
A can be seen in figure 4.16 training the existing model with measured values of $q > 10^{-6}$ $m^3/s/m$ corresponds approximately to training this model with values of ${}^{s}q_{measured} > 10^{-5}$ $m^3/s/m$. To study the prediction performance of the existing model for low overtopping discharges, a simulation with this network is performed for the testdata of the new model with a value of ${}^{s}q_{measured} < 10^{-5}$ $m^3/s/m$. The obtained rms-error is compared with the corresponding rms-error for the new model for this subset of the entire testset.

Figure 4.18 and figure 4.19 show values of ${}^{s}q_{NN}$ versus ${}^{s}q_{measured}$ for the mentioned testdata, and this for the existing model respectively the new model. The data in figure 4.19 are easily found as a part of the data in figure 4.17.

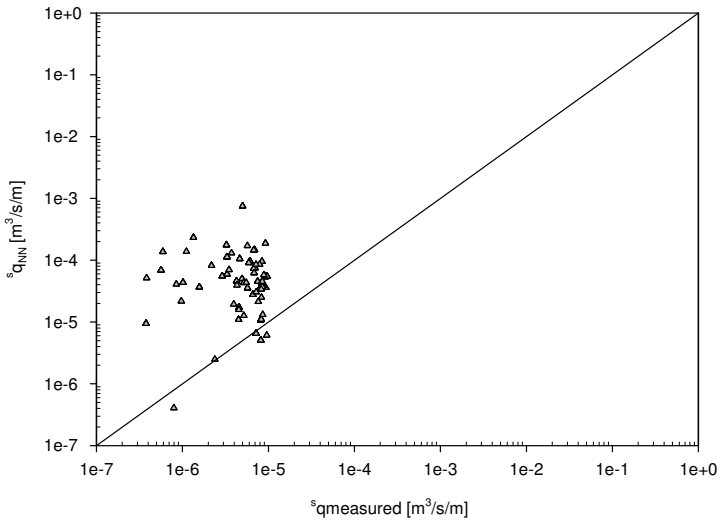

Figure 4.18 Performance of net_existing for testdata of net_new with ${}^{s}q_{measured} < 10^{-5}$ $m^3/s/m$

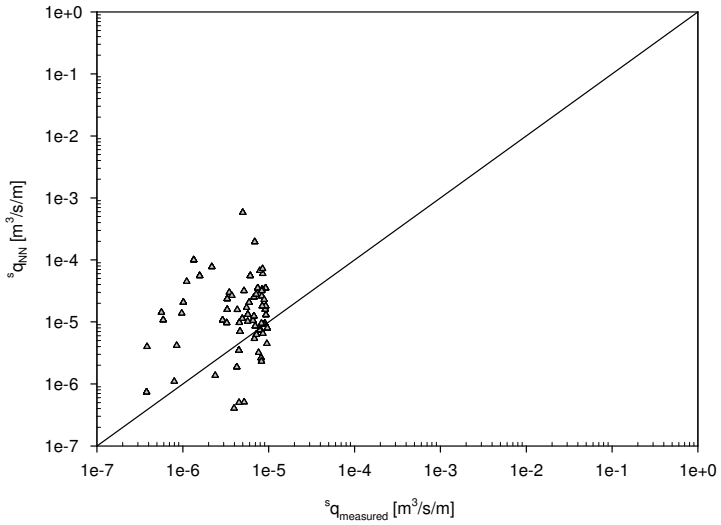

Figure 4.19 Performance of net_new for testdata of net_new with $^sq_{measured} < 10^{-6}$ m^3/s/m

The corresponding rms-errors are:

- net_existing :
  data with $^sq_{measured} < 10^{-5}$ m^3/s/m: rmse = 1.1404
- net_new :
  data with $^sq_{measured} < 10^{-5}$ m^3/s/m: rmse = 0.7750

And for the smallest values of $^sq_{measured}$ only:

- net_existing :
  data with $^sq_{measured} < 10^{-6}$ m^3/s/m: rmse = 1.7833
- net_new :
  data with $^sq_{measured} < 10^{-6}$ m^3/s/m: rmse = 0.9631

The performance of the existing model is clearly worse for these low overtopping data than the performance of the new model for these data.
Figure 4.18 shows that the existing model has a tendency to overpredict such low overtopping discharges, which is logical as the model was only trained on higher discharges. Although the scatter is still quite large, the performance of the new model is significantly better for these low values (figure 4.19).
The presence of the scatter on the results for the new model may be explained by the fact that for the data with low values of $^sq_{measured}$ quite some scatter on the values of log($^sq_{measured}$) is expected. Moreover, these low values are situated near the limit of applicability of the new model.

It may be concluded that although the performance of the new model becomes slightly worse compared to the existing model for values of ${}^{s}q_{measured} > 10^{-5}$ $m^3/s/m$, the new model is found to perform significantly better for values of ${}^{s}q_{measured} < 10^{-5}$ $m^3/s/m$. As it is important that the quantifier is also able to predict these low overtopping discharges, the new model, i.e. the model developed also taking into account the tests with ${}^{s}q_{measured} < 10^{-5}$ $m^3/s/m$, is restricted for the development of the final quantifier.

4.6.7 Application of the bootstrap method

4.6.7.1 Methodology

In previous sections an optimal quantifier configuration has been searched for by comparing various models developed with a training- and a testset. As training- and testset are randomly determined from the entire dataset, the possibility exists that a 'bad' division of the data in training- and testset occurs. This could lead to the fact that specific information is only included in the testset and not in the trainingset, with the result that the network is not able to learn and consequently predict this particular information.

The bootstrap method (Efron, 1982) deals with this problem of the optimal use of the available data, and allows to use the available data to train the network, and to determine the generalisation error at the same time.
In addition, applying the bootstrap technique for the final development of the quantifier allows the use of a so-called 'committee of networks' to determine a better, ensemble network prediction (see section 4.1.5.2). Further bootstrap percentile intervals may be calculated, providing an estimation of the reliability of the prediction (see section 4.1.5.3).
Background information regarding the bootstrap method is to be found in section 4.1.5, where the method and its possibilities are described in detail.
In this section the specific steps to perform bootstrap resampling for the development of the final quantifier are explained.

As no division of the data in training- and testset is required for the bootstrap method, the **first step** consists of multiplying all data according to their weight factor, resulting in an extended, weighed dataset. This implicates an increase in data from 8195 to 46328 (see table 4.8).
The distribution of the data in the weighed dataset reflects two things:

- the distribution of the real input world (which corresponds to the basic assumption of the bootstrap technique) and
- the reliability of the data (overall very reliable data are included more than overall less reliable data, resulting in a local denser distribution)

In the **second step** various bootstrap datasets are generated. Each bootstrap set is generated by randomly sampling 46328 data *with replacement* from the 46328 available data in the weighed database. In the **third step** each bootstrap set serves as a trainingset for the development of a bootstrap network. The total number of bootstrap networks developed in this work is 100.

In the **fourth step** the prediction by the committee of networks is used as better ensemble prediction, i.e. for each data point the mean prediction of the 100

bootstrap networks is considered as final quantifier prediction (see eq. (4.15)). The restriction of the ensemble prediction as final result relies on the better prediction capacity of a combination of networks over the prediction performance of a single network.

The predictions of the various bootstrap networks allow to derive information on the reliability of the prediction. The bootstrap percentile intervals are defined in the **fifth step**. The extent of a percentile interval of a prediction gives an idea of the location of this data point in the input space. Wide percentile intervals correspond to a place in the input space with low density, leading to a high uncertainty on the prediction. Small percentile intervals refer to a place in the input space with high density, with a consistent prediction as result.

4.6.7.2 Result

Figure 4.20 shows the final result of the committee of networks for the original dataset. Predicted values ${}^{s}q_{NN}$ are represented versus measured values ${}^{s}q_{measured}$. Each value of ${}^{s}q_{NN}$ on the figure concerns a mean value of 100 predictions obtained with the same number of bootstrap networks.

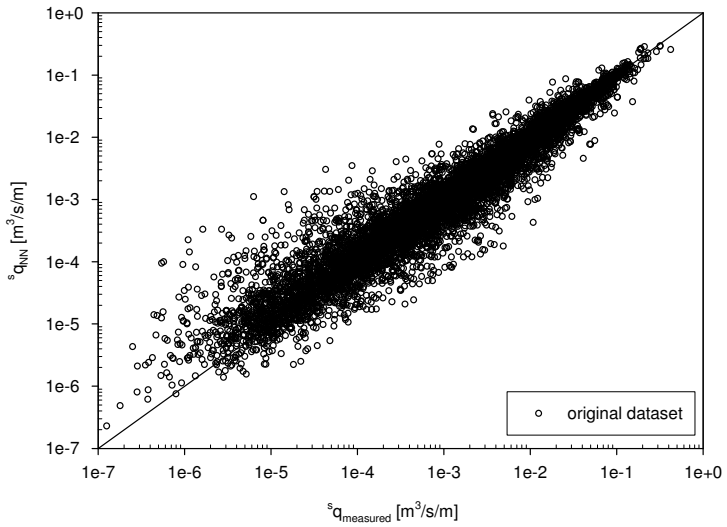

Figure 4.20 Prediction by the committee of networks for the original dataset (8195 data)

The rms-error of the original dataset is 0.3409 without considering the overall reliability of the data, and 0.3100 taking the overall reliability of the data into account (i.e. the rms-error for the weighed dataset).

The analysis of the results of the committee of networks for groups of data with the same weight factor shows that the most reliable data are on average predicted best. On the other hand, least reliable data are on average predicted worst. This is exactly what was expected, as the committee of networks has been forced to focus on the reliable data.
Figure 4.21, figure 4.22 and figure 4.23 illustrate the above stated. Figure 4.21 shows the results of the data with values of the weight factor = 9 and 6. Figure 4.22 shows the results of the data with values of the weight factor = 4 and 3 and finally figure 4.23 shows the results of the data with weight factor = 2 and 1. In general, more scatter is present for the overall less reliable data.

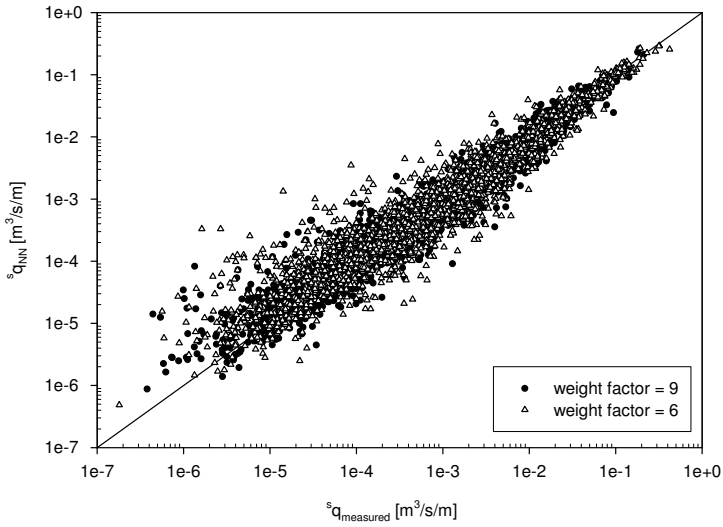

Figure 4.21 Prediction by the committee of networks for original data with weight factor = 9 and 6 (5064 data)

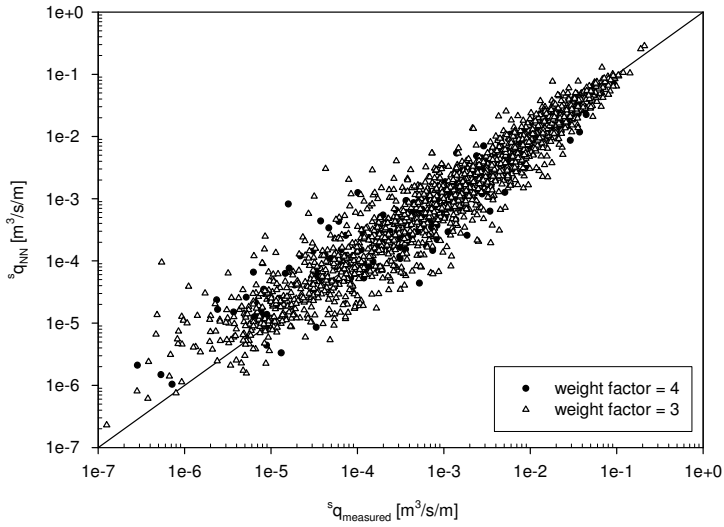

Figure 4.22 Prediction by the committee of networks for original data with weight factor = 4 and 3 (1997 data)

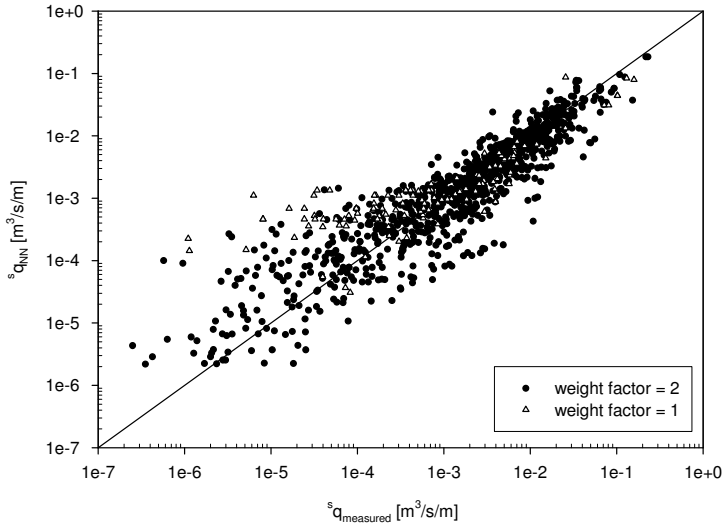

Figure 4.23 Prediction by the committee of networks for original data with weight factor = 2 and 1 (1134 data)

In addition to these figures, table 4.10 gives an overall view of the rms-errors for the corresponding groups of data. As the weight factor within each group is equal, the rms-error with and without taking the overall reliability of the data into account

is the same. It is confirmed that the prediction is indeed better for the most reliable data.

Table 4.10 Values of rmse for the original data grouped according to weight factor (WF)

	rmse	# data
WF = 9	0.2546	2503
WF = 6	0.3404	2561
WF = 4	0.3249	296
WF = 3	0.3611	1701
WF = 2	0.4212	1014
WF = 1	0.7108	120

Besides studying the rms-error of the original dataset (or of groups of data within the original dataset), other ways to assess the general performance of the developed committee of networks can be thought of.
One can look for example at the values of the error factor for each data point. The error factor was already defined in section 4.6.5.1 as ${}^{s}q_{NN}$ / ${}^{s}q_{measured}$ if ${}^{s}q_{NN} > {}^{s}q_{measured}$ (overprediction), and as ${}^{s}q_{measured}$ / ${}^{s}q_{NN}$ if ${}^{s}q_{NN} < {}^{s}q_{measured}$ (underprediction), and represents the number of times a measured value is overpredicted respectively underpredicted.

Table 4.11 shows the maximum error factors obtained when a specified percentage of outliers is not considered. Overpredictions are distinguished from underpredictions. The values are determined taking the reliability of the tests into account.
The maximum error factors obtained for the entire dataset (100% -value in table 4.11) are given in brackets. These extreme values refer to outliers and are therefore not representative for the performance of the committee of networks. Considering only 99% of the dataset (i.e. the 0.5% highest overprediction factors and the 0.5% highest underprediction factors are not considered), reduces the maximum error factors to 31.35 (overprediction) and 10.21 (underprediction). Further reducing the dataset to 95% or 90% results in even smaller error factors, i.e. 5.35 and 3.62, respectively 3.34 and 2.78.

Table 4.11 Maximum error factors for the original dataset (weighed values)

% of dataset considered	(100%)	99%	95%	90%
maximum overprediction factor	(203.55)	31.35	**5.35**	3.34
maximum underprediction factor	(27.48)	10.21	**3.62**	2.78

The maximum error factors obtained when 5% outliers are omitted are marked in bold in table 4.11. These values may be considered as a good indication of the general performance of the committee of networks.

4.6.7.3 Bias of the network?

Looking at figure 4.20, one could have the impression that the committee of networks tends to overpredict the small overtopping discharges. It may seem that the best matching curve through the points is not the wanted diagonal line, but a curve which inclines to higher values of ${}^{s}q_{NN}$ for low values of ${}^{s}q_{measured}$. If it can be proved that this is not only an impression, this would implicate that the committee of networks is biased for small overtopping values. An improvement of the final prediction method would be obtained in this case by correcting the committee of networks' output with the quantified bias.

By plotting the values of $\log({}^{s}q_{NN}) - \log({}^{s}q_{measured})$ versus the predicted values $\log({}^{s}q_{NN})$, a possible bias can easily be detected by fitting a (smooth) curve through the data, see figure 4.24. The fitted line (a polynomial with three degrees of freedom) is marked in red. The value of $\log({}^{s}q_{NN})$ should be taken as a reference on the X-axis and not the value of $\log({}^{s}q_{measured})$, as the bias should be a function of the output of the committee of networks to allow a correction to it. In contrast to what might be expected, figure 4.24 shows that the fitted curve approximately coincides with the horizontal line for which $\log({}^{s}q_{NN}) = \log({}^{s}q_{measured})$. Only for very small values of ${}^{s}q_{NN}$ the fitted curve deviates slightly from the horizontal line.

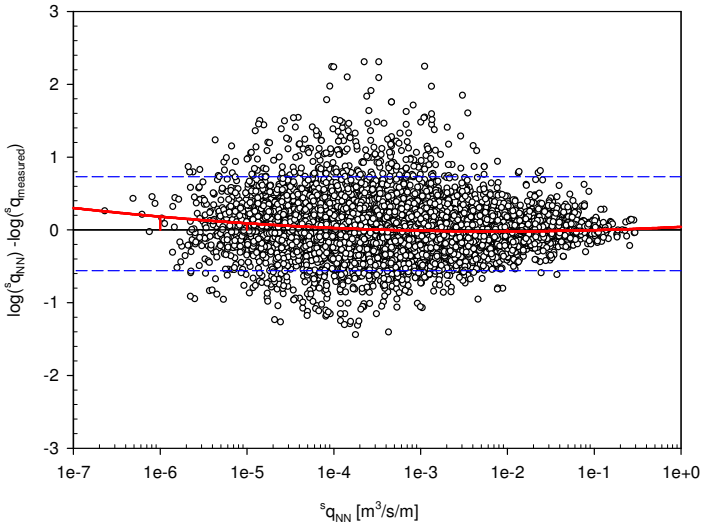

Figure 4.24 Detection of possible bias of the committee of networks

The fact that the fitted curve in figure 4.24 does not correspond with significant bias is confirmed by the low values of the error factors ${}^{s}q_{NN}$ / ${}^{s}q_{measured}$ corresponding with the red curve. For values of ${}^{s}q_{NN}$ larger than 10^{-4} $m^3/s/m$ the error factor is ≈ 1. For a value ${}^{s}q_{NN} = 10^{-5}$ $m^3/s/m$ the error factor is ≈ 1.2 and for a value of ${}^{s}q_{NN} = 10^{-6}$ $m^3/s/m$ the error factor is ≈ 1.5. The distances corresponding to these error factors are also marked in red in figure 4.24.
It should be remarked that, due to the rather scarce number of data in the domain of ${}^{s}q_{NN} < 10^{-5}$ $m^3/s/m$, the fitted curve may even be too pronounced.
As the mentioned bias factors are very low, and taking into account the small number of data with ${}^{s}q_{NN} < 10^{-5}$ $m^3/s/m$, it is concluded that the committee of networks' output should not be corrected for the presence of bias.

The error factors mentioned in table 4.11 correspond to horizontal lines in figure 4.24. Not considering 5% outliers as explained in section 4.6.7.2, an overprediction factor ${}^{s}q_{NN}$ / ${}^{s}q_{measured}$ of 5.35 was found. This corresponds to a horizontal line at a value of y = log(5.35) = 0.73. The underprediction factor ${}^{s}q_{measured}$ / ${}^{s}q_{NN}$ of 3.62 corresponds to a horizontal line at y = -log(3.62) = -0.56. Both lines are represented as blue dashed lines in figure 4.24. The lines mark out the interval in which 95% of the data are situated: $-0.56 < \log({}^{s}q_{NN}) - \log({}^{s}q_{measured}) < 0.73$.

It can be remarked that the impression that the committee of networks is biased, originates from the fact one is inclined to look in the vertical direction in figure 4.20, i.e. one is inclined to consider the error on $\log({}^{s}q)$ for fixed values of ${}^{s}q_{measured}$ instead of for fixed values of ${}^{s}q_{NN}$. To illustrate this, a plot is made in which the value of $\log({}^{s}q_{NN}) - \log({}^{s}q_{measured})$ is represented versus the value of $\log({}^{s}q_{measured})$, see figure 4.25. The fitted line deviates indeed more significantly from the horizontal line for which $\log({}^{s}q_{NN}) = \log({}^{s}q_{measured})$.

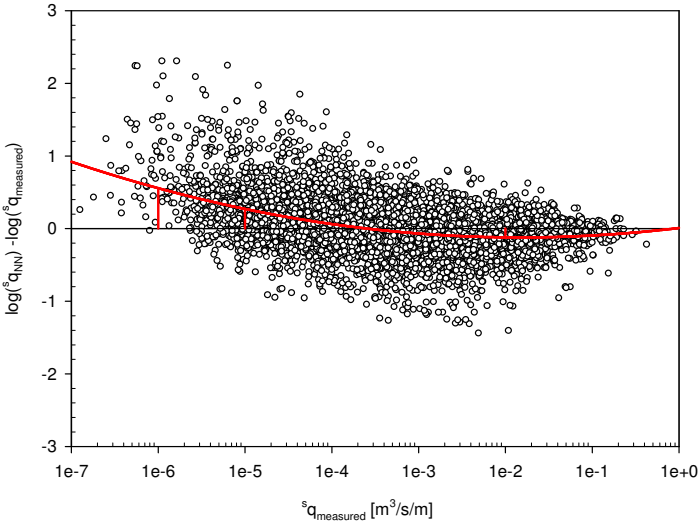

Figure 4.25 Increase of relative errors for small values of $^{s}q_{measured}$

For a value of $^{s}q_{measured} = 10^{-5}$ m^3/s/m an error factor of $^{s}q_{NN} / {}^{s}q_{measured} = 1.9$ is found and for a value of $^{s}q_{measured} = 10^{-6}$ m^3/s/m even a larger error factor of $^{s}q_{NN} / {}^{s}q_{measured} = 3.6$ is found. For larger values of $^{s}q_{measured}$ the fitted curve goes below the horizontal line, corresponding to mean underpredictions of the committee of networks. For $^{s}q_{measured} = 10^{-2}$ m^3/s/m an error factor of $^{s}q_{measured} / {}^{s}q_{NN} = 1.3$ is found.

4.6.8 Limits of application of the quantifier

The committee of networks or briefly the 'quantifier' developed in section 4.6.7, has been trained on a dataset which is supposed to be representative for the existent input space, or at least for the input space in which researchers are commonly interested.

As a NN is only able to predict well within the ranges of the data on which it was trained, and as in addition extrapolation of a network outside these ranges can lead to pointless results, it is very important to indicate ranges of applicability of the quantifier.

The input space of the quantifier is a 13-dimensional input space. New input for the quantifier should be located within the cloud of data on which the network has been trained in this 13-dimensional space. It is quite complicated to examine the distribution of data in a 13-dimensional input space. Therefore, the limits of application of the quantifier are set up in two phases.
Basic limits for the input parameters are obtained by studying the values of each of the 13 input parameters individually in section 4.6.8.1. By studying in a second phase all possible combinations of 2 input parameters (section 4.6.8.2), an idea of the spreading of the input within the 13-dimensional space is obtained, resulting in additional restrictions for the input parameter values. The final ranges of applicability for the quantifier are summarised in section 4.6.8.3.

4.6.8.1 Limit values of individual input parameters

Table 4.12 gives an overall view of the 13 input parameters as well as the corresponding minimum and maximum values of the data used for the development of the final quantifier. Also the minimum and maximum values of the 99% interval are given, where the 99% interval concerns the parameter interval obtained when the 0.5% largest and 0.5% smallest values of the parameter are omitted.

Table 4.12 Extreme parameter values of the input of the data used for the development of the final quantifier (weighed dataset, i.e. 46328 data)

	input parameter	min	max	min of 99% interval	max of 99% interval
1	${}^{s}T_{m\text{-}1,0\ toe}$ [s]	2.72	69.94	2.89	15.29
2	${}^{s}\beta$ [°]	0	80.00	0	60.00
3	${}^{s}h$ [m]	0.90	32.22	1.05	15.56
4	${}^{s}h_t$ [m]	0.43	25.93	0.64	14.93
5	${}^{s}B_t$ [m]	0	19.19	0	8.22
6	${}^{s}\gamma_f$ [-]	0.33	1.00	0.35	1.00
7	${}^{s}\cot\alpha_d$ [-]	0	7.00	0	6.00
8	${}^{s}\cot\alpha_u$ [-]	-5.00	9.71	-5.00	8.00
9	${}^{s}R_c$ [m]	0	6.44	0.08	3.78
10	${}^{s}h_b$ [m]	-1.21	7.83	-0.99	1.82
11	${}^{s}B_h$ [m]	0	38.46	0	13.27
12	${}^{s}A_c$ [m]	0	6.24	0.07	3.54
13	${}^{s}G_c$ [m]	0	13.17	0	7.37

Parameters for which the minimum and/or maximum values are very different from the 99% values refer to parameters which contain outliers, i.e. extremely high or low values compared to the mean values. As can be seen in table 4.12 examples which can be mentioned in this context are ${}^{s}T_{m\text{-}1,0\ toe}$ and ${}^{s}h_b$.
For sure new input data should be situated within the minimum and maximum value of each parameter. Additionally, one could say that the 99% interval is preferred for new data to be situated in, as predictions at the limit of the range of a parameter, have a larger probability to be less reliable. Final conclusions on the limits of application for the quantifier are given in section 4.6.8.3.

4.6.8.2. Limit values of combined input parameters

Plots of combinations of 2 input parameters give an idea of the distribution of the input in the 13-dimensional space. In annex a matrix plot of the input on which the quantifier has been trained is available. In a matrix plot all parameters are plotted versus each other, resulting in a grid of 13 x 13 plots in this work. On the diagonal line, the histograms of the input parameters are represented.
As it was found in section 4.6.5 that the three parameters which are most important in the prediction method are ${}^{s}T_{m\text{-}1,0\ toe}$, ${}^{s}\gamma_f$ and ${}^{s}R_c$, special attention should be given to these parameters.

Analysis of the matrix plot confirms that for some parameters outliers are present. By reducing the limits of application of each individual parameter to the 99% interval values (see table 4.12), the majority of these outliers will be excluded, resulting in a more homogeneous distribution.

However, it is remarkable that for a value of $\gamma_f = 1$ often different parameter limits of the remaining input parameters occur compared to a value of $\gamma_f < 1$. The different behaviour of smooth structure types such as vertical walls and dikes versus rough structure types such as rubble mound structures is on the origin of this phenomenon. Different limits of the parameter ${}^{s}R_c$ may for example be explained as due to larger energy dissipation on a rough sloping structure compared to a smooth dike, a lower crest freeboard is needed for the former structure type. Also for vertical walls, the relative crest height is often higher in the design than for a rubble mound structure.
The value of ${}^{s}R_c$ is mentioned as an example, but comparable differences are found for the minimum or maximum values of other input parameters.

Based on this finding, the final limits of application of the quantifier in next section are split up for values of $\gamma_f = 1$ or $\gamma_f < 1$.

4.6.8.3. Ranges of applicability for the quantifier

Table 4.13 shows the final ranges of applicability determined for the quantifier. Structure types with a value of $\gamma_f = 1$ are distinguished from structure types with a value of $\gamma_f < 1$. Parameters containing noticeable outliers are restricted so that the outliers are excluded.
The distinction between $\gamma_f = 1$ and $\gamma_f < 1$ corresponds approximately to the distinction between smooth structure types and rough structure types. However, some smooth structure types are assigned a value of $\gamma_f < 1$ (see chapter 3). For these structures the ranges of applicability set up in the right part of table 4.13 should be applied.

Table 4.13 Ranges of applicability for the quantifier

		$\gamma_f = 1$			$\gamma_f < 1$	
1	3.00	$\leq {}^{s}T_{m\text{-}1,0\ toe}$ [s] $\leq$	22.00	3.00	$\leq {}^{s}T_{m\text{-}1,0\ toe}$ [s] $\leq$	12.00
2	0	$\leq {}^{s}\beta$ [°] $\leq$	60.00	0	$\leq {}^{s}\beta$ [°] $\leq$	60.00
3	1.00	$\leq {}^{s}h$ [m] $\leq$	20.60	1.00	$\leq {}^{s}h$ [m] $\leq$	13.30
4	1.00	$\leq {}^{s}h_t$ [m] $\leq$	20.50	0.65	$\leq {}^{s}h_t$ [m] $\leq$	13.30
5	0	$\leq {}^{s}B_t$ [m] $\leq$	11.40	0	$\leq {}^{s}B_t$ [m] $\leq$	5.00
6	1.00	$\leq {}^{s}\gamma_f$ [-] $\leq$	1.00	0.35	$\leq {}^{s}\gamma_f$ [-] $\leq$	0.95
7	0	$\leq {}^{s}\cot\alpha_d$ [-] $\leq$	7.00	0	$\leq {}^{s}\cot\alpha_d$ [-] $\leq$	5.30
8	-5.00	$\leq {}^{s}\cot\alpha_u$ [-] $\leq$	6.00	0	$\leq {}^{s}\cot\alpha_u$ [-] $\leq$	8.00
9	0	$\leq {}^{s}R_c$ [m] $\leq$	5.00	0.25	$\leq {}^{s}R_c$ [m] $\leq$	2.80
10	-1.00	$\leq {}^{s}h_b$ [m] $\leq$	3.60	-1.00	$\leq {}^{s}h_b$ [m] $\leq$	1.20
11	0	$\leq {}^{s}B_h$ [m] $\leq$	16.20	0	$\leq {}^{s}B_h$ [m] $\leq$	6.20
12	0	$\leq {}^{s}A_c$ [m] $\leq$	4.00	0.10	$\leq {}^{s}A_c$ [m] $\leq$	2.90
13	0	$\leq {}^{s}G_c$ [m] $\leq$	7.60	0	$\leq {}^{s}G_c$ [m] $\leq$	5.40

The neural quantifier should only be used for situations of which the input parameters fall within the ranges of table 4.13. For all situations where at least one input parameter falls outside these ranges, the neural quantifier should not be used as no reliable prediction can be guaranteed.

It should be remarked that probably for specific parameter combinations further parameter restrictions are needed. However, it may be expected that the limits set up in table 4.13 exclude the majority of situations which were not included in the training process. In addition, the quantifier is only meant to function well for real structure types, which may be supposed to be represented mostly within the cloud of data on which the quantifier has been developed.

4.6.9 Simulations with the developed quantifier

In this section, the results of some simulations obtained with the developed quantifier are studied. Only data which were not used for the development of the neural model are available as new input for the network, i.e. prototype data and data with zero overtopping measurements. In addition, the performance of the quantifier may be studied (although restricted) through synthetic datasets.

As the neural quantifier predicts overtopping discharges for small scale situations, the prototype simulations have to be subjected to the CLASH scaling procedure (see section 4.4.2.1) before comparison with the prototype overtopping measurements is possible. As described in section 4.4.2.2 this implicates that in fact the combination quantifier - CLASH scaling procedure is checked. Detailed information on this subject is given in section 4.6.9.1.

Other data which were not used for the development of the quantifier are the data with zero overtopping measurements. The quantifier is not able to predict the value 'zero', as it is trained on the logarithm of the overtopping discharge q. However, if the quantifier is able to generalise from small to zero overtopping, then the predictions of the quantifier for zero overtopping situations should equal small discharges. In section 4.6.9.2 the predictions of the quantifier for the zero measurements are studied.

Finally, one can generate synthetic datasets of which the corresponding overtopping discharge can be assessed relying on previous knowledge on overtopping. Examples are e.g. the prediction of overtopping at a smooth dike or a vertical wall. In addition, influences of parameters such as the roughness/permeability factor γ_f may be studied. The results are given in section 4.6.9.3.

4.6.9.1 Prototype simulations

The overtopping database contains 132 prototype measurements, of which 111 measurements are assessed as overall reliable (i.e. weight factor ≠ 0). As the test descriptions of the remaining 21 measurements are assessed as not giving a reliable overall view of the tests, these measurements are not further considered.
The 111 reliable data all originate from the prototype measurements performed within the CLASH project. It concerns three test series: test series 044 (a vertical wall with a rubble mound toe protection, 23 data), 381 (a rubble mound breakwater armoured with rocks, 77 data) and 957 (a rubble mound breakwater armoured with antifers, 11 data).
For each prototype site the predictions obtained by the quantifier, ${}^{s}q_{NN}$, are corrected to account for model and scale effects according to the CLASH scaling

procedure. The corrected quantifier results, ${}^{s}q_{NN\_corr}$, are compared to the prototype measurements, ${}^{s}q_{measured}$.

4.6.9.1.1 Test series 044

The test structure consists of a vertical wall with a rubble mound toe protection composed of rocks in front of it, and is situated at Samphire Hoe, near Dover (United Kingdom). Depending on the water level, the mound is schematised as a berm (low water level) or a toe (high water level).
Figure 4.26 shows a picture of the front view of the prototype structure. For detailed information on this prototype site and the corresponding overtopping measurements is referred to Pullen (2004a).

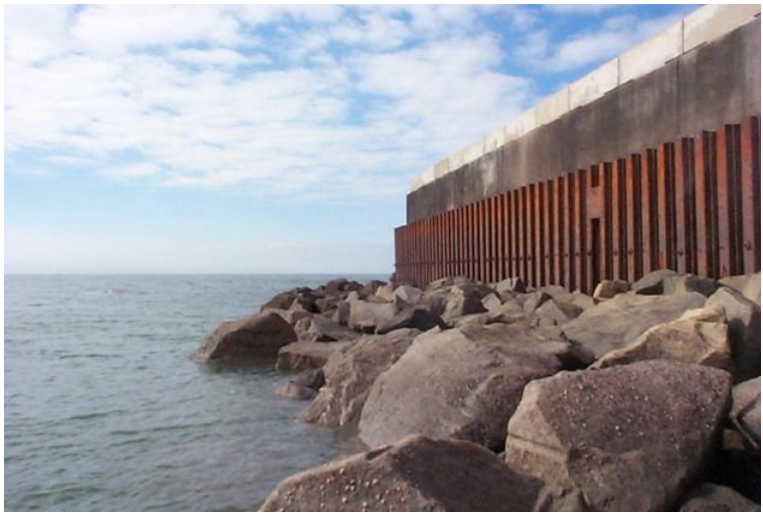

Figure 4.26 Samphire Hoe measurement site

In all, 23 data are available, originating from 2 measured storms (1-2 May 2003), of which the overtopping results are processed per half an hour. It should be remarked that this processing time is rather short. With a mean wave period of the incident waves $T_{m\ toe} \approx 5$ - 6s during the measured storm, this corresponds to approximately 1800s/5s = 360 à 1800s/6s = 300 waves. As overtopping is very unevenly distributed in time and in space (see chapter 2), this short processing time may significantly influence the measured discharges. However, the processing time was chosen to allow for changes in water level and changes in wave conditions (see Pullen, 2004a).

Schematisation of these 23 tests results in the following ranges of the input parameters for the neural quantifier:

${}^{s}T_{m-1,0\ toe}$ [s]	: 4.13 - 5.85
${}^{s}\beta$ [°]	: 0.78 - 30.00
${}^{s}h$ [m]	: 1.66 - 2.40
${}^{s}h_t$ [m]	: 0.63 - 2.00
${}^{s}B_t$ [m]	: 0 - 4.47
${}^{s}\gamma_f$ [-]	: 1.00
${}^{s}\cot\alpha_d$ [-]	: 0 - 1.00
${}^{s}\cot\alpha_u$ [-]	: 0
${}^{s}R_c$ [m]	: 2.33 - 6.16
${}^{s}h_b$ [m]	: 0 - 0.69
${}^{s}B_h$ [m]	: 0 - 5.90
${}^{s}A_c$ [m]	: 0.66 - 3.19
${}^{s}G_c$ [m]	: 0.41 - 0.74

A comparison of these test ranges with the ranges of applicability of the quantifier (see table 4.13) shows that the input parameters ${}^{s}h_t$ and ${}^{s}R_c$ exceed the allowable values. Seven of the 23 data fall outside the ranges of applicability of the quantifier, implicating that no reliable prediction can be guaranteed with the quantifier. These 7 data are not further considered.

For the remaining 16 data a quantifier simulation is performed and the corresponding scaling factors to obtain prototype predictions are determined. As the structure concerns a smooth vertical structure, only the model effect of wind has to be accounted for, i.e.: $q_{proto} = q_{ss} * f_{wind}$ (see CLASH scaling map in section 4.4.2.1). Depending on the presence of wind during the prototype storm, the factor f_{wind} may be equal or larger than one. As described by Pullen (2004a), during the second storm wind speeds had become insignificant by the time that overtopping measurements started. A value of $f_{wind} = 1$ is consequently adopted for these measurements. During the first storm significant wind was present, but according to Pullen (2004a) less overtopping was measured than what might have been captured in the absence of wind. The fact that the overtopping water was blown over a wide area is mentioned as a reason for this. It is therefore decided to also adopt a value of $f_{wind} = 1$ for the first measured storm.

Figure 4.27 shows the obtained results. The predicted overtopping discharges are represented versus the measured overtopping discharges. As the scale factor for the model effect of wind is assumed to be equal to 1, no correction of the ${}^{s}q_{NN}$ -values had to be performed, i.e. ${}^{s}q_{NN\_corr} = {}^{s}q_{NN}$. Figure 4.27 shows also the 90% percentile intervals of the quantifier predictions.

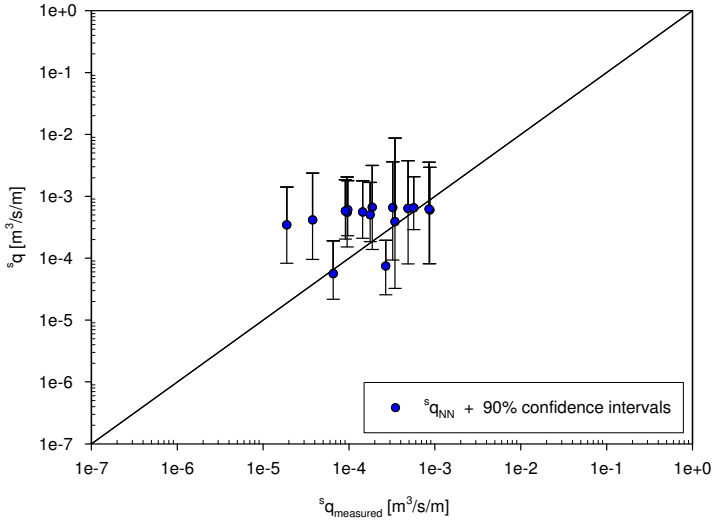

Figure 4.27 Quantifier simulation of Samphire Hoe measurements

Comparing the quantifier simulations ${}^{s}q_{NN}$ to the prototype measurements ${}^{s}q_{measured}$ gives an rms-error of 0.6050.
One can see that the values of ${}^{s}q_{NN}$ are for a part of the measurements too high. Other values are near the diagonal line. The overpredictions seem to be larger for the lower values of ${}^{s}q_{measured}$.
It may be remarked that the network predicts for many data about the same overtopping discharge, whereas these originate from various measured overtopping discharges. This is reflected in figure 4.27 by a series of data approximately on a horizontal line. Analysis showed that these points are related to the larger water depths, with only a slight variation of the wave characteristics and the water levels. The network seems to have difficulties to distinguish these differences. However, it should be remarked that the possibility exists that the rather short processing time of the measurements leads to some scatter on the measurements itself.

4.6.9.1.2 Test series 381

The test structure consists of a rubble mound breakwater armoured with rocks, situated at Ostia, near Rome (Italy). The breakwater protects a marina. The crest of the breakwater is kept low in order to avoid ‘visual pollution’.
In figure 4.28 a picture of overtopping at the Ostia breakwater is represented. Detailed information on the Ostia prototype site and the corresponding measurements is given in Franco et al. (2004).

Figure 4.28 Ostia measurement site

The 77 available data of Ostia originate from 7 measured storms (2003 - 2004), of which the overtopping results are processed per hour. For the measured mean wave periods $T_{m\ toe} \approx 6$ - 9s, this corresponds to processing overtopping events per 600 à 400 waves. Especially for the longer waves ($T_{m\ toe} \approx 9$s) this processing time is rather short.
Schematisation of the tests results in following input ranges for the neural quantifier:

${}^{s}T_{m-1,0\ toe}$ [s]	: 4.57 - 6.66
${}^{s}\beta$ [°]	: 1.00 - 40.00
${}^{s}h$ [m]	: 1.74 - 2.32
${}^{s}h_t$ [m]	: 1.74 - 2.32
${}^{s}B_t$ [m]	: 0
${}^{s}\gamma_f$ [-]	: 0.40
${}^{s}\cot\alpha_d$ [-]	: 4.00
${}^{s}\cot\alpha_u$ [-]	: 4.00
${}^{s}R_c$ [m]	: 1.72 - 2.56
${}^{s}h_b$ [m]	: 0
${}^{s}B_h$ [m]	: 0
${}^{s}A_c$ [m]	: 1.72 - 2.56
${}^{s}G_c$ [m]	: 2.00 - 2.75

Comparison of the test ranges with the ranges of applicability of the quantifier (see table 4.13) shows that the values of the input parameters all fall within these ranges.
Quantifier simulations of all measurement points are performed, and the corresponding scaling factors to obtain prototype predictions are determined. For

rough sloping structures such as the Ostia breakwater, significant model and scale effects are expected: $q_{proto} = q_{ss} * f_{scale\_wind}$ (see CLASH scaling map in section 4.4.2.1).
In figure 4.29 the small scale results predicted by the quantifier ${}^{s}q_{NN}$, as well as the corrected values to account for model and scale effects ${}^{s}q_{NN\_corr}$ are represented. In addition, the 90% percentile intervals for the corrected values ${}^{s}q_{NN\_corr}$ are shown. The 90% percentile intervals are calculated by correcting the 90% percentile values obtained for the original results ${}^{s}q_{NN}$ for the expected model and scale effects.

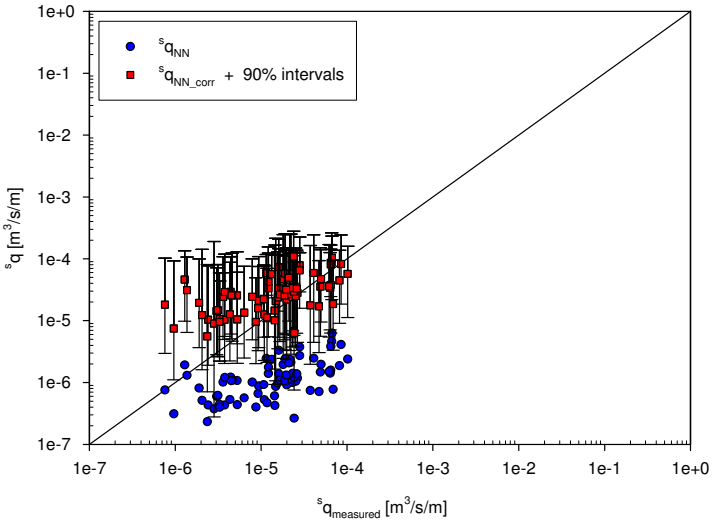

Figure 4.29 Quantifier simulation of Ostia measurements

Figure 4.29 shows that the final values of ${}^{s}q_{NN\_corr}$ result in a rather good match between the predictions and the prototype measurements, although for small values of ${}^{s}q_{measured}$, the corrected result seems to overpredict the measured discharges. An rms-error of 0.5258 is obtained.
It is suspected that the overpredictions for small values of ${}^{s}q_{measured}$ are due to the fact that the data are situated in the vicinity of the limit of applicability. If the CLASH scaling map provides appropriate correction factors, the network should predict for the lowest values of ${}^{s}q_{measured}$, values of ${}^{s}q_{NN}$ near 10^{-7} - 10^{-8} $m^3/s/m$. Figure 4.7 in section 4.5.3 shows that this value is below the ${}^{s}q$ -values on which the quantifier has been trained, i.e. the minimum value in figure 4.7 concerns ${}^{s}q \approx 10^{-7}$ $m^3/s/m$.

4.6.9.1.3 Test series 957

Test series 957 concerns a rubble mound breakwater armoured with antifers, situated at Zeebrugge (Belgium). A picture of overtopping at the Zeebrugge breakwater is given in figure 4.30. Detailed information on the Zeebrugge prototype site and the corresponding measurements is summarised in Troch et al. (1998) and Geeraerts et al. (2004a).

Figure 4.30 Zeebrugge measurement site

The 11 available data of Zeebrugge originate from 9 measured storms (1999 - 2004) of which the overtopping results are processed per 1 hour (3 data) or per 2 hours (8 data). For the measured mean wave periods $T_{m\,toe} \approx 5.5$ - 6.5s, this corresponds to processing overtopping events per 550 à 600 waves for the 1 hour measurements versus per 1100 à 1300 waves for the 2 hour measurements.

Schematisation of the 11 tests results in the following ranges of the input parameters for the neural quantifier:

${}^{s}T_{m-1,0\ toe}$ [s]	: 3.60 - 3.77
${}^{s}\beta$ [°]	: 0
${}^{s}h$ [m]	: 2.28 - 3.65
${}^{s}h_t$ [m]	: 1.87 - 3.04
${}^{s}B_t$ [m]	: 2.66 - 4.01
${}^{s}\gamma_f$ [-]	: 0.47
${}^{s}\cot\alpha_d$ [-]	: 1.40
${}^{s}\cot\alpha_u$ [-]	: 1.40
${}^{s}R_c$ [m]	: 1.37 - 2.30
${}^{s}h_b$ [m]	: 0
${}^{s}B_h$ [m]	: 0
${}^{s}A_c$ [m]	: 1.89 - 3.01
${}^{s}G_c$ [m]	: 1.33 - 2.01

The value of ${}^{s}A_c$ is for one data point slightly too large, i.e. 3.01m whereas a maximum value of 2.90m is prescribed for the application of the quantifier (see table 4.13). Consequently, this one point is left out further in this section.

Similar to test series 381 the prototype structure concerns a rough sloping structure for which significant model and scale effects are expected: $q_{proto} = q_{ss} * f_{scale\_wind}$ (see CLASH scaling map in section 4.4.2.1)
The results are given in figure 4.31, where in addition the 90% intervals for the corrected values ${}^{s}q_{NN\_corr}$ are shown. Also here the 90% percentile intervals are calculated by correcting the 90% percentile values obtained for the original results ${}^{s}q_{NN}$ for the expected model and scale effects.

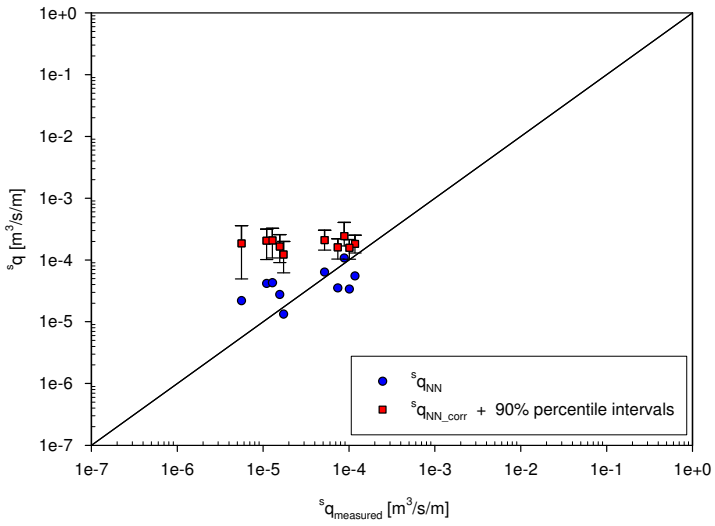

Figure 4.31 Quantifier simulation of Zeebrugge measurements

The corrected values seem to be conservative, and especially for low overtopping discharges ^{s}q, overpredictions of more than a factor 100 occur! The overprediction results in a rather large value for the rms-error, i.e. rmse = 0.8893. It is not yet clear at this moment what lies on the origin of these overpredictions. As the largest overpredictions occur for the lowest values of $^{s}q_{measured}$, the vicinity of the limit of applicability may be noticeable. However, the overpredictions are clearly present for larger values of $^{s}q_{measured}$ as well, which raises the question whether the CLASH scaling procedure is not too conservative for this structure.
It should be mentioned that the 90% percentile intervals for the corrected results $^{s}q_{NN\_corr}$ are much smaller than for the two previous prototype sites. This is largely due to the CLASH scaling procedure, which leads to different scaling factors for the upper 90% border compared to the lower 90% border, due to the dependency of the scaling factors of the value of q_{ss} (see section 4.4.2.1).

4.6.9.1.4 Conclusion

In the previous sections the performance of the combination neural quantifier - CLASH scaling procedure has been studied for the available CLASH prototype measurements. Values of the rms-error equal to 0.6050 (Samphire Hoe), 0.5258 (Ostia) and 0.8893 (Zeebrugge) are obtained. Especially for the Ostia case a rather good match between prototype measurements and corrected quantifier predictions is noticed.
As for the Samphire Hoe case it is assumed that no wind effect has to be taken into account, the quantifier results can be compared directly to the prototype measurements. For larger water depths the quantifier seems to have difficulties to distinguish different overtopping situations, although it is noticed that due to the rather short processing time some scatter on the measurements may be expected.
For the two sloping rubble mound structures overpredictions are found for the smallest values of $^{s}q_{measured}$. Especially for the Ostia case it may be expected that the vicinity of the limit of applicability of the quantifier contributes to these overpredictions. For the Zeebrugge case rather large overpredictions, also for higher values of $^{s}q_{measured}$, are noticed. No direct reason is found for this phenomenon. It may be concluded that the deviations of the corrected predictions from the real measurements may be due to the performance of the quantifier itself as well as due to the CLASH scaling procedure. However, it is difficult to assess only on the basis of these results whether the quantifier prediction is too high or if the CLASH scaling map provides too high scaling factors. Within this work, the performance of the quantifier will be further studied. Additional prototype measurements in the future should be used to further check the CLASH scaling procedure.

4.6.9.2 Simulation of data with zero measured overtopping

The data with zero overtopping measurements may be used to check if the quantifier is able to generalise for the trend of zero overtopping. If this is indeed the case, low values for ${}^{s}q_{NN}$ should be obtained, i.e. preferably lower than approximately 10^{-6} $m^3/s/m$.

The number of data with a value of q = 0 $m^3/s/m$ in the original database, which are considered as 'reliable' zero measurements in this work is 657, corresponding to 3521 data in the weighed database (see further table 4.15 in section 4.7.1). Of these 3521 data, 43.06% have at least one of the 13 input parameters outside the ranges of applicability of the quantifier, implicating that these can not be simulated by the quantifier. This is not so strange, as zero measurements are caused by specific combinations of parameters on which the quantifier has not been trained. However, still 56.94% of the zero measurements, i.e. 2005 weighed data, corresponding to 348 original data, do fall within the ranges of applicability which are set up for the quantifier. The simulation of these data is considered in this section.

The results are shown in figure 4.32, where the values of ${}^{s}q_{NN}$ are plotted in descending order. For each prediction the 90% percentile intervals are represented.

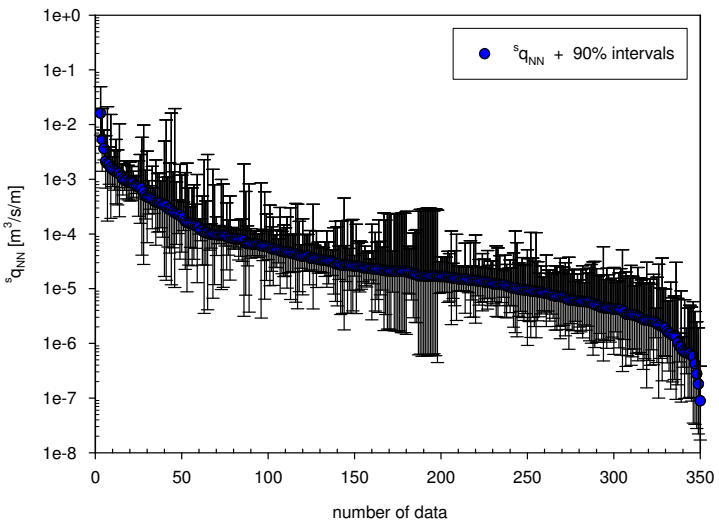

Figure 4.32 Quantifier simulation of zero overtopping measurements

In contrast to what might be expected, figure 4.32 shows that the majority of the quantifier simulations of zero overtopping situations results in quite high overtopping predictions. Values of ${}^{s}q_{NN}$ even larger than 10^{-3} $m^3/s/m$ occur.

Table 4.14 gives an overall view of the values of ${}^{s}q_{NN}$ for the zero measurements. The percentages concern weighed values, i.e. the overall reliability of each of the 348 data is taken into account. The numbers are expressed in percentages of the simulated zero data as well as in percentages of the total number of zero data.

Table 4.14 Values of ${}^{s}q_{NN}$ for 348 simulated zero measurements

	% of simulated zero data (2005 weighed zero data)	% of all zero data (3521 weighed zero data)
(1 wrong zero measurement with ${}^{s}q_{NN} > 10^{-2}$ $m^3/s/m$)	(0.15)	(0.09)
10^{-2} $m^3/s/m \geq {}^{s}q_{NN} > 10^{-3}$ $m^3/s/m$	2.69	1.53
10^{-3} $m^3/s/m \geq {}^{s}q_{NN} > 10^{-4}$ $m^3/s/m$	12.92	7.36
10^{-4} $m^3/s/m \geq {}^{s}q_{NN} > 10^{-5}$ $m^3/s/m$	49.88	28.40
10^{-5} $m^3/s/m \geq {}^{s}q_{NN} > 10^{-6}$ $m^3/s/m$	30.07	17.12
10^{-6} $m^3/s/m \geq {}^{s}q_{NN}$	4.29	2.44
TOTAL :	100.00	56.94

As shown in table 4.14 only 4.29% of the simulated zero data concerns values of ${}^{s}q_{NN} \leq 10^{-6}$ $m^3/s/m$, and approximately $2/3^{th}$ of the zero measurements is predicted as ${}^{s}q_{NN} > 10^{-5}$ $m^3/s/m$. One of the 348 zero measurements is found to concern an erratic data point, i.e. the value of ${}^{s}q_{measured}$ certainly should be > 0 $m^3/s/m$ instead of the included zero value. It concerns an overtopping measurement at a vertical structure with a rubble mound protection in front of it. The water depth on the rubble mound protection ${}^{s}h_t$ equals 5.36m, whereas the value of ${}^{s}R_c$ is only 0.60m. Combined with a wave steepness s_0 of 0.04 this should certainly result in wave overtopping as the waves will just flow over the wall. This erratic zero measurement is not further considered in this work.

Looking at the 90% percentile intervals of the data in figure 4.32, large, extended intervals can be distinguished from rather small intervals.
It is known that extended intervals correspond to a position in the input space which is sparsely occupied, leading to uncertain predictions. A large extent of the reliability intervals in figure 4.32 is an indication of the uncertain prediction, even though the mean value predicted by the committee of networks is higher than zero (whereas it is known that the measurement was zero in the laboratory).
Small percentile intervals, especially with high values of ${}^{s}q_{NN}$, are of much more concern. It indicates that all bootstrap networks predict consequently a large value

of ${}^{s}q_{NN}$ for a zero overtopping measurement. Although the possibility exists that an erratic zero q -value is included in the database (such as the one mentioned in table 4.14), the risk of wrong data may be supposed low as the zero data were thoroughly screened before using them. As it is supposed that the majority of considered zero data really concern zero overtopping discharges, it can be concluded that the prediction capacity of the quantifier for negligible or zero overtopping is poor. Moreover, in the majority of cases the (small) percentile intervals show that consistently too high overtopping is predicted, i.e. a false impression of a reliable prediction is obtained.

The fact that a network is only able to perform well within the cloud of points on which the model has been trained may be mentioned as the main reason why the quantifier is not able to predict zero overtopping well. On the other hand, the simulated data all fall within the ranges of applicability which were set up for the quantifier. However, as mentioned in section 4.6.8, it might be expected that the ranges of table 4.13 still enclose certain 'gaps' in the 13-dimensional input space where no input data for the development of the quantifier were situated. Probably the majority of the simulated 56.94% of 657 'reliable' zero data are situated in such 'gaps', resulting in extrapolation of the network with consequently bad results.
As the ranges of applicability set up for the quantifier are not able to exclude these data for simulation by the quantifier, another criterion is needed to distinguish significant from negligible overtopping discharges. The so-called classifier, described in section 4.7, deals with this problem.

4.6.9.3 Simulation of synthetic datasets

In this section four synthetic datasets are generated, and the predicted overtopping discharges by the quantifier are compared with existing deterministic formulae.
For all four datasets the same wave characteristics are used, i.e. ${}^{s}\beta = 0°$ (perpendicular wave attack) and ${}^{s}T_{m-1,0\ toe} = 4.91s$ (corresponding to a wave steepness $s_0 = 0.043$). Also the water depth is chosen equal for all datasets, i.e. ${}^{s}h = 7.14m$. Several data within one set are generated by altering the crest height of the structure.

The first synthetic dataset concerns overtopping at a smooth dike. No berms or toe are present, and the crest width is equal to zero. The slope of the dike is supposed to be 1:2 and the impermeable surface results in a value of $\gamma_f = 1$.

Figure 4.33 shows the quantifier predictions and the 90% percentile intervals for values of the dimensionless crest freeboard $\frac{R_c}{H_{m0\ toe}} = 0$ up to 4, or, as

$\frac{R_c}{H_{m0\ toe}} \cong {}^{s}R_c$, for values of ${}^{s}R_c$ (= ${}^{s}A_c$) = 0m up to 4m. The symbol '$\cong$' refers to the fact that, although the numerical value of both expressions is equal to each other, the interpretation of the expressions is slightly different: $\frac{R_c}{H_{m0\ toe}}$ refers to a dimensionless crest freeboard, whereas ${}^{s}R_c$ refers to a dimensional crest freeboard in a fictive situation where $H_{m0\ toe}$ = 1m. The limit of 4m corresponds to the limit of application of the quantifier, see table 4.13.

On the y-axis the commonly used dimensionless overtopping discharge $\frac{q}{\sqrt{gH^3_{m0\ toe}}}$ is represented. It can be easily seen that $\frac{q}{\sqrt{gH^3_{m0\ toe}}} = \frac{{}^{s}q}{\sqrt{g}}$. In addition to the quantifier prediction, the overtopping formula of TAW (2002) set up for surging conditions at smooth dikes (see chapter 2, eq. (2.5b)) is represented.

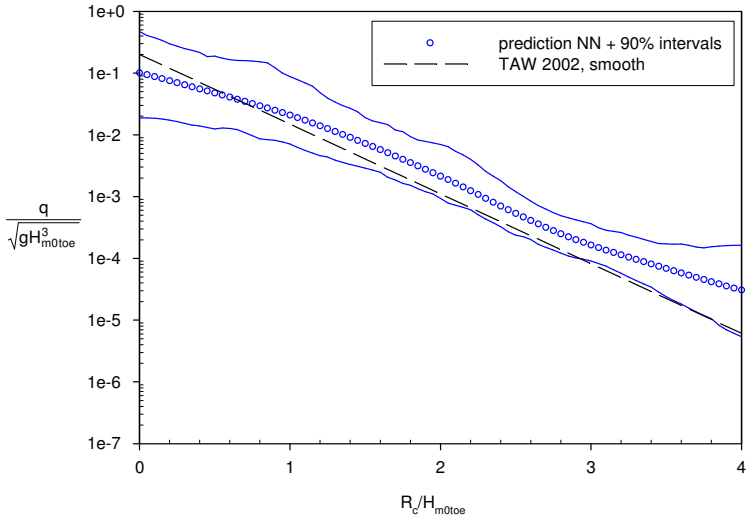

Figure 4.33 Quantifier prediction of overtopping at dike

The predicted overtopping discharge by the quantifier is slightly higher for values of ${}^{s}R_c$ > 1m than the values obtained with the TAW -formula. For values of ${}^{s}R_c$ < 0.5m the quantifier predicts slightly lower values than obtained with the TAW -formula.

It can be mentioned that the 'curve' of the quantifier prediction line for $0 < \frac{R_c}{H_{m0\ toe}} < 2.5$ corresponds to early findings on overtopping at dikes, presented in the Dutch 'Guidelines for design of river dikes' (see TAW, 1985 and 1989),

where a quadratic relationship between the logarithm of a dimensionless mean overtopping discharge and a dimensionless crest freeboard is proposed.

The 90% percentile intervals are smallest for values of ${}^{s}R_c$ = 2 à 3m. The percentile intervals show that the quantifier encounters more uncertainties for the smallest and largest values of ${}^{s}R_c$, corresponding to ${}^{s}R_c$ -values in the vicinity of the limit of applicability.

In order to study the influence of the roughness/permeability of the surface, an analogous dataset is generated, where a rubble mound structure is considered instead of a smooth dike. The armour is supposed to consist of 2 layers of rock, i.e. γ_f = 0.4 (see chapter 3, table 3.4). As a rubble mound structure always has a certain crest width (corresponding to 2 or 3 armour units), the value of ${}^{s}G_c$ is supposed to be equal to 0.9m. The remaining structure geometry is chosen equal to the dike in the previous dataset.
The result is shown in figure 4.34. To facilitate comparison, in figure 4.34 (a) the same axes ranges as in figure 4.33 are represented. Figure 4.34 (b) zooms in on the results. As it concerns a rough structure, the maximum value of ${}^{s}R_c$ is 2.8m and the minimum value of ${}^{s}R_c$ = 0.25m (see table 4.13). Besides the TAW -line for smooth dikes, also the TAW -line for rough structure slopes with γ_f = 0.4 is represented (TAW, 2002, see chapter 2, eq. (2.5b)).

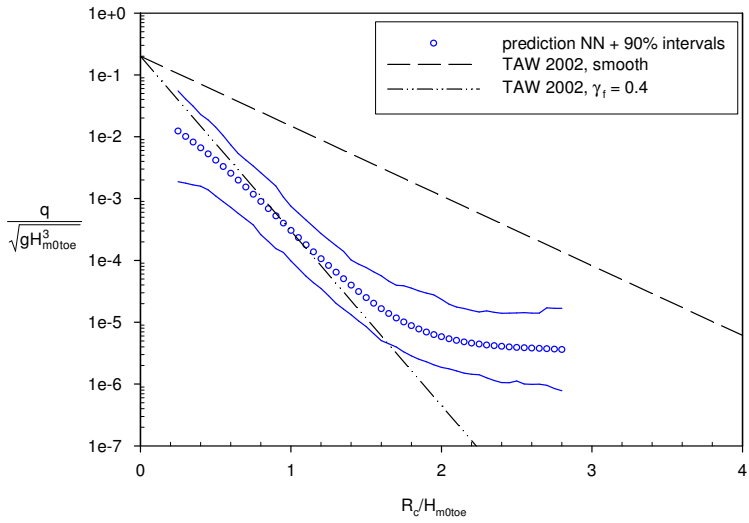

(a)

Figure 4.34 Quantifier prediction of overtopping at rubble mound structure with rocks

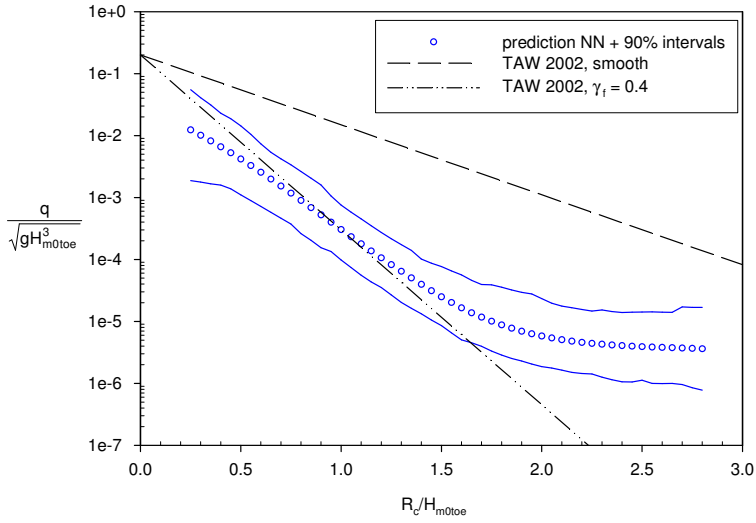

(b)

Figure 4.34 (continued) Quantifier prediction of overtopping at rubble mound structure with rocks

As expected the overtopping curve descends on the figure. The same slightly varying trend of the 90% percentile intervals as noticed for the smooth dike is observed, i.e. slightly more extended intervals for the largest and smallest values of ${}^{s}R_c$. The smallest intervals occur for values of ${}^{s}R_c$ = 0.5 à 1.5m (which are lower ranges than for the prediction at the smooth dike). Figure 4.34 also shows that for the largest considered ${}^{s}R_c$ values, the quantifier keeps predicting quite high values of the dimensionless overtopping discharge, whereas a trend to zero overtopping is expected (comparable to the predictions by the TAW -formula). One gets the impression that the quantifier has difficulties to predict dimensionless overtopping discharges $\frac{q}{\sqrt{gH_{m0\ toe}^3}}$ lower than ≈ 10^{-5} - 10^{-6}. In a prototype situation with $H_{m0\ toe}$ = 3 or 5m the value of 10^{-5} corresponds to q ≈ 1.5*10^{-4} m^3/s/m respectively q ≈ 3.5*10^{-4} m^3/s/m.

The third synthetic dataset is related to overtopping at a vertical wall. Again starting from the same wave characteristics and water depth, figure 4.35 is generated. The formulae of Franco et al. (1994) (see chapter 2, eq. (2.13)), and of Allsop et al. (1995) (see chapter 2, eq. (2.16)) are represented for comparison. Both formulae are set up for overtopping at vertical walls in relatively deep water, which is in

accordance with the considered synthetic dataset. As the value of γ_f = 1, the limit value of ${}^sR_c$ is 4m (see table 4.13).

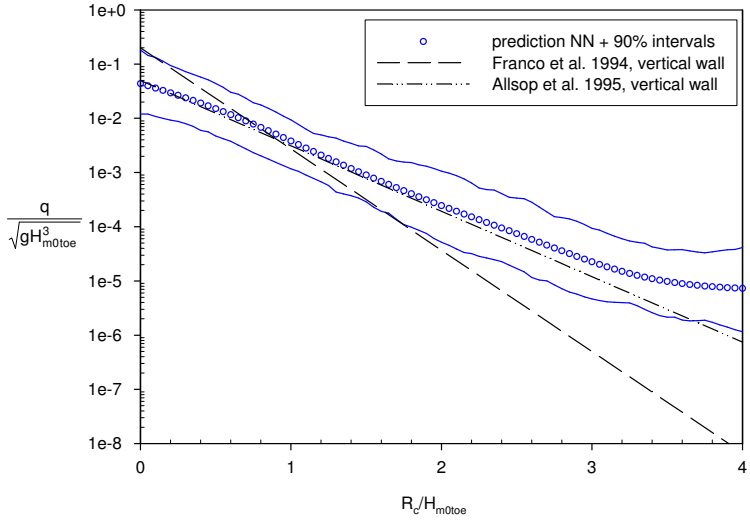

Figure 4.35 Quantifier prediction of overtopping at vertical wall

The quantifier prediction follows the line proposed by Allsop et al. (1995) very well for values of ${}^sR_c$ < 3m. For larger values of ${}^sR_c$ the quantifier predicts slightly higher overtopping discharges. The same remark as for the previous dataset can be made here, i.e. the quantifier seems to have difficulties predicting low overtopping discharges.
In contrast to the previous sloping structures, also small or very small 90% percentile intervals are obtained for values of ${}^sR_c$ = 0m. The availability of overtopping tests with vertical walls where ${}^sR_c$ = 0m in the database explains this.

The last synthetic dataset concerns the same vertical wall as in the previous dataset, but it has a small recurved part on top. This is reflected in the synthetic dataset by means of the parameter γ_f , see chapter 3, section 3.6.3.8. The small recurved part is only felt by the waves if ${}^sR_c$ > 0.5m. For lower crest freeboards the waves just flow over the low wall. Consequently, exactly the same data as in the previous dataset are obtained for values of ${}^sR_c$ < 0.5m. For values of ${}^sR_c$ larger than 1m, a reduction of 0.3 is applied to γ_f , i.e. γ_f = 0.7 instead of 1. For values of 0.5m ≤ ${}^sR_c$ ≤ 1m linear interpolation in between γ_f = 1 and 0.7 is performed.
As the value of γ_f is smaller than 1 for the largest ${}^sR_c$ -values, the calculations are restricted to values of ${}^sR_c$ smaller than 2.80m.

It should be mentioned that data with $\gamma_f < 1$ (data with ${}^{s}R_c > 0.5$m) only fall within the ranges of applicability of the quantifier if the γ_f -value is smaller than 0.95 (see table 4.13). Consequently no reliable prediction is possible for values of 0.5m < ${}^{s}R_c$ < 0.5833m. Within this range no simulation is performed.

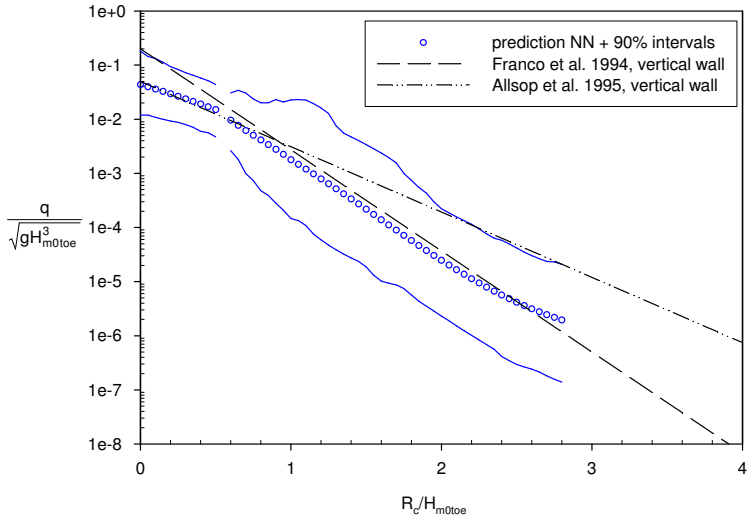

(a)

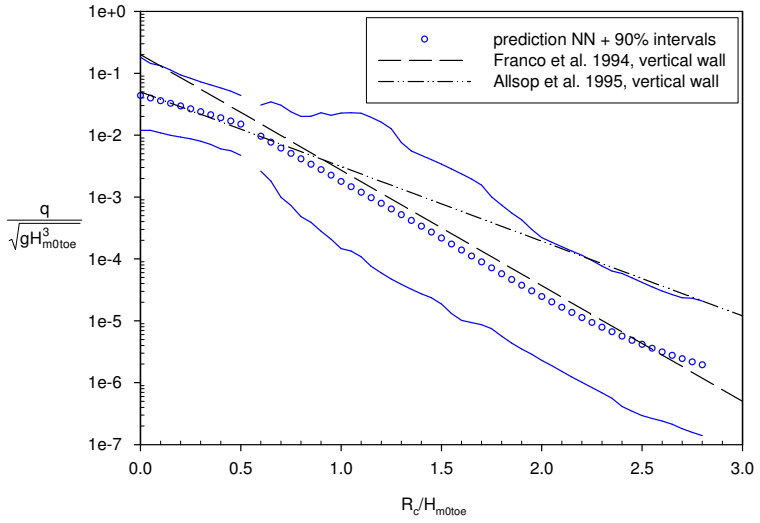

(b)

Figure 4.36 Quantifier prediction of overtopping at recurved vertical wall

The result is shown in figure 4.36. The same empirical formulae as for the previous dataset are represented. In order to simplify comparison with the previous figure, figure 4.36 (a) represents the same ranges of the axes as figure 4.35. In figure 4.36 (b) is zoomed in on the results.
The 90% percentile intervals are clearly wider for this structure type. This is due to the fact that fewer overtopping results for such structure types are available in the database than for simple vertical walls. However, it may be clear that the quantifier learned that the presence of a recurved part has a reducing effect on the phenomenon of overtopping. In contrast to the behaviour of the quantifier for the considered rubble mound structure with rocks (see figure 4.34), the decreasing overtopping prediction trend also holds for the largest values of ${}^{s}R_c$, up to $\frac{q}{\sqrt{gH_{m0\ toe}^3}} \approx 10^{-6}$.
It is rather surprising that the quantifier prediction of overtopping at a recurve wave wall for values of ${}^{s}R_c$ > 1m coincides with the curve given by Franco et al. (1994) for overtopping at a simple vertical wall.

As far as the correctness of the results obtained for the four synthetic datasets can be assessed on the basis of existing deterministic formulae, the quantifier performs very well for dimensionless overtopping discharges larger than approximately 10^{-5} - 10^{-6}. For large values of ${}^{s}R_c$, for which an overtopping trend to zero is expected, the quantifier has more difficulties. Especially for the prediction of overtopping at a rubble mound structure with rocks, an overprediction for larger values of ${}^{s}R_c$ is noticed.

4.7 Development of a neural classifier for q, for all structure types

In section 4.6.9.2 it was found that the quantifier is not able to generalise for zero overtopping discharges, i.e. the quantifier does not necessarily predict small overtopping discharges for zero overtopping measurements. In addition, it was noticed in section 4.6.9.3 that the quantifier has problems in the vicinity of its limit of applicability, i.e. dimensionless discharges lower than 10^{-6} are rarely predicted.
The consequences are sometimes large overpredictions of the overtopping discharge, where the user of the network is not aware of. On the contrary, in these cases often small percentile intervals give a false impression of a reliable prediction.
These findings were on the basis of the development of a 'classifier' for overtopping. The goal of this classifier is to avoid large overpredictions of overtopping, by excluding data for which zero overtopping occurs from simulation by the quantifier. Without predicting the exact overtopping discharges, the classifier has to distinguish situations where overtopping occurs from situations where no or negligible overtopping occurs. The classifier consequently functions as filter for the quantifier: only the data assessed by the classifier as significant overtopping, should be simulated by the quantifier.

In this section the development of the neural classifier is described. As the final classifier and quantifier are meant to function in series, the lay-out of both models should be similar. This implicates that the input parameters present in the final quantifier are used for the classifier. The output parameter is logically different and also the number of hidden neurons is not necessarily equal.

In section 4.7.1 the methodology followed for the selection of the data for the development of the classifier is described. The criterion to study the performance of a classifier model is given in section 4.7.2, on the basis of which an optimal network configuration is determined (section 4.7.3). The development of the final classifier by means of the bootstrap method is described in section 4.7.4. Comparable to the quantifier ranges of applicability are set up for the classifier in section 4.7.5. Finally, section 4.7.6 shows that the performance of the combination classifier - quantifier is significantly better compared to the performance of the single quantifier.

4.7.1 Selection of data

The classifier is developed by training a NN on only two possible output values, i.e. +1 and -1, standing for significant overtopping and zero or negligible overtopping respectively.

The importance of a well-considered selection of zero data to be used for the development of the classifier has been explained in section 4.5.4 and a methodology to select the 'reliable' zero data has been proposed. Summarised, by screening all zero data per test series, zero data evaluated as probably unreliable were excluded. In addition, all zero data from test series performed before 1990 were not considered. Finally, all data with ${}^{s}q$ - values lower than 10^{-6} $m^3/s/m$ were assessed as data with negligible overtopping, and thus belonging to class -1.

As non-zero overtopping discharges are replaced by the value +1 for the development of the classifier, the accuracy of the measurements is not important. Except for the small number of data with ${}^{s}q < 10^{-6}$ $m^3/s/m$ (which are assigned to class -1), all data with $q \neq 0$ $m^3/s/m$ which were available for the development of the quantifier, are assigned to class +1 for the development of the classifier.

Table 4.15 gives an overall view of the total number of data available for the development of the classifier. The original number of data as well as the weighed number of data are represented.

Table 4.15 Number of data available for the development of the classifier

	# data in original database (with RF and CF ≠ 4)	# data in weighed database
Total # zero data	876	4535
of which		
# with low accuracy	21	90
# from before 1990	198	924
(# remaining 'reliable' data)	(657)	(3521)
Total # non-zero data	8195	46328
of which		
# with ${}^{s}q < 10^{-6}$ $m^3/s/m$	41	189
(# remaining data)	(8154)	(46139)
Results in:		
Total # data for available for class -1	698	3710
Total # data for available for class +1	8154	46139

Table 4.15 shows that the number of data available for class +1 is much higher than the number of data available for class -1. To force the classifier to pay as much attention to the negligible or zero overtopping data as to the significant overtopping data, an equal number of data from both classes should be used to develop the model (see Medina et al., 2002). This implicates that, starting from the data mentioned in table 4.15, only 698/8154 = 8.6% of the data from class +1 can be used. It is clear that the choice of these 8.6% data out of class +1, will largely influence the development of the classifier.

Two reasons may be quoted for the fact that the number of zero data is quite low compared to the non-zero data.
The first reason is that researchers performing overtopping tests are more interested in non-zero overtopping data (e.g. to compare with admissible overtopping rates) than in zero overtopping data. Many researchers even simply do not report their zero measurements.

The second reason can be attributed to the fact that many laboratories perform parametric tests, which are stopped at the moment no overtopping is measured anymore. In a parametric test series, the influence of one or some parameters is studied, keeping the remaining test configuration unchanged. Parametric tests to determine for example the influence of the dimensionless crest freeboard $R_c / H_{m0\ toe}$ on the overtopping phenomenon are often performed: for a fixed test structure the water levels and wave characteristics are varied. By lowering the water level, lower overtopping discharges are obtained for the same wave characteristics. The moment no significant overtopping is measured anymore, the test series is normally stopped, as the researcher knows for sure that lower water levels will result in other zero measurements. Few zero values in the overtopping results is an unavoidable consequence.
Varying structure characteristics, such as the crest width G_c of a structure, is another possibility for parametric tests. Overtopping tests with increasing crest width, stopped at the moment a first zero is measured, leads to the same result. Other less frequently performed tests can be thought of, e.g. increasing the width of a structure berm, increasing the roughness of the armour layer of a rubble mound structure…
The consequence of performing parametric tests in this way, is that only near the border of overtopping - no overtopping, zeros are included in the database, although it is known that for larger $R_c / H_{m0\ toe}$ -values, $G_c / H_{m0\ toe}$ -values, … also zero overtopping would be measured. It may be consequently expected that the data from class -1 only constitute a part of the entire 'negligible overtopping' -space, i.e. the data included in class -1 are not a representative sample for all possible zero or negligible overtopping measurements. By developing a classifier on these restricted zero values only,

classifying problems will rise for $R_c/H_{m0\ toe}$ -values, $G_c/H_{m0\ toe}$ -values, … which are slightly higher than the value corresponding to a zero measurement for a specific structure.

In order to solve the problem of the lack of zero data in the database on the one hand, and the problem of the bad distribution of the zero data within the entire 'negligible overtopping' -space on the other hand, artificial zero data are created. The available zero measurements are used as a starting point, and the zero space is extended in two directions:

- artificial data with higher values of ${}^sR_c$ are added and
- artificial data with higher values of ${}^sG_c$ are added.

By adding artificial data with higher ${}^sR_c$ and ${}^sG_c$ -values, the zero space is only filled in two single directions. As mentioned before more parameters can be thought of which could, by increasing or decreasing their value (depending on the parameter), result in an increase of the zero data. However, only the parameters ${}^sR_c$ and ${}^sG_c$ are used in this work, as these seem to be most relevant to the author. Moreover, the first class of artificial data will receive more attention than the second class, as the methodology of performing parametric tests with decreasing water level is frequently applied in laboratories. Section 4.7.3.1 describes how the artificial data are exactly created.

The creation of artificial zero data for the development of the classifier has a dual advantage, i.e.:

- filling of the 'negligible overtopping' -space in two directions, resulting in a better distribution of the zero or negligible data, and
- the increase of the number of zero data, which allows to use more of the available information of class +1.

4.7.2 Evaluating the classifier performance

The classifier model is trained on two possible outputs, i.e. +1 and -1, to which classifier predictions after developing the model are transposed as follows: all predictions smaller than zero, i.e. Є] -infinity, 0 [, are assigned a value -1 and all remaining predictions, i.e. Є [0, +infinity [, are assigned a value +1.

The performance of a classifier configuration is assessed on the basis of the rms-error obtained for an independent testset. This rms-error, rmse_test, has been defined for the quantifier in section 4.6.3, eq. (4.23). The same expression is used for the classifier, where the values of $\log({}^{s}q_{measured})$ and $\log({}^{s}q_{NN})$ are replaced by the output of the classifier. As the output of the classifier can only adapt the values +1 or -1, the following relationship can be derived:

$$(rmse\_test)^2 * 25 = perc\_wrong\_test \qquad (4.24)$$

where perc_wrong_test stands for the percentage of wrongly classified testdata.
It is clear that the lower the value of rmse_test, the better the overall prediction capacity of the classifier.
Similar to the quantifier, a weighing factor is applied to the data, where the multiplication of each test is only performed after the dataset is split up in training- and testset to strictly separate these.

4.7.3 Development of a neural classifier

4.7.3.1. Extension of the dataset

As explained in section 4.7.1 artificial data are created to improve the classifying capacities of the neural classifier. Artificial data with higher ${}^{s}R_c$ -values as well as artificial data with higher ${}^{s}G_c$ -values are generated. The available zero overtopping measurements are the starting point for the creation of the artificial zero data.

The first set of artificial zero data is created by copying the input parameters of the available zero measurements, except for the value of ${}^{s}R_c$, which is raised. Inextricably bound up with this is an increase of the value of ${}^{s}A_c$, see figure 4.37. If the value of ${}^{s}R_c$ is multiplied by (1+x), with x > 0, the value of ${}^{s}A_c$ increases by a factor [1+x* (${}^{s}R_c$ / ${}^{s}A_c$)]. Increasing the value of ${}^{s}A_c$ as well corresponds to extending the middle part of the structure, keeping the crest configuration unchanged. To avoid unrealistic cross-sections, it is important to also adapt the ${}^{s}A_c$ -value.

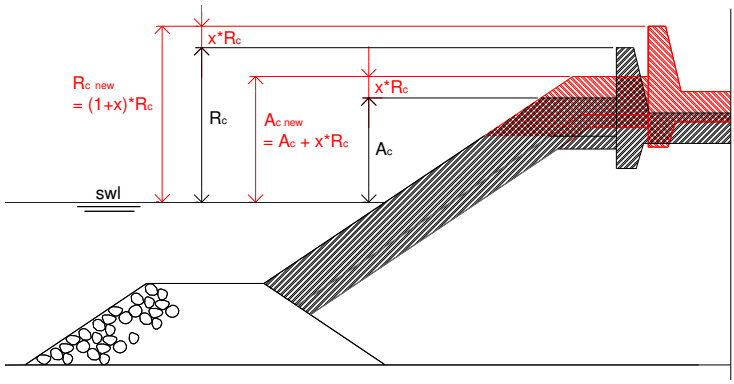

Figure 4.37 Creation of artificial data by raising the value of R_c (and A_c)

Several artificial data may be created from one available zero measurement by choosing various values for x, e.g. 0.1, 0.2, 0.5, 1, 2, …
In case a value of ${}^{s}R_c$ = 0m appears, the multiplication is impossible, but as data with zero crest freeboard always give overtopping, this is not relevant here.

The second set of artificial zero data is created by copying the input parameters of the original zero measurements once more, and raising only the value of ${}^{s}G_c$. Multiplying the ${}^{s}G_c$ -value with a factor (1+y), with y > 0, does not request changes to additional input parameters, see figure 4.38.

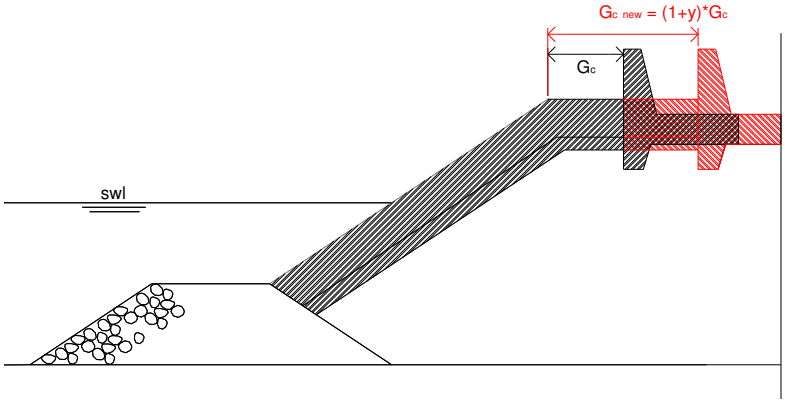

Figure 4.38 Creation of artificial data by raising the value of G_c

To avoid unrealistic cross-sections, the creation of artificial tests from a zero measurement is only performed when the original value of ${}^{s}G_c$ is larger than zero. Not only results multiplying a value of ${}^{s}G_c$ = 0m into the same zero value for ${}^{s}G_c$, but also unrealistic structure geometries would often occur in this way. Examples are simple vertical walls and impermeable dikes. Adding a certain crest width, keeping all other parameters unchanged, supposes an additional *permeable* horizontal part of the crest, which is not realistic.
Also here various values of y may lead to the creation of several artificial data from the same zero measurement.

The influence of the choice of the parameters x and y is analysed in next section.

4.7.3.2 Determination of multiplication factors

In order to determine the influence of the factors (1+x) and (1+y) on the performance of the classifier, a number of combinations of x and y is considered. Various classifiers are developed and the classifying performance of these classifiers is compared.

As the zero data, included in the database, are often related to the border of ${}^{s}R_c$-values leading to zero overtopping, the classifier will need zero data with higher values of ${}^{s}R_c$. However, it is the border of zero overtopping which is most important for the classifier, which implicates that extra data near to this border may be interesting. Starting from the same reasoning for the crest width ${}^{s}G_c$, some values and combinations for x and y are chosen.

Table 4.16 gives an overall view of the considered combinations as well as the new total number of data available for class -1. The mentioned numbers concern original numbers, i.e. not weighed.

Table 4.16 Considered combinations of artificial data

	Combination 1	Combination 2	Combination 3
value of x in (1+x)* $^{s}R_c$	0.5 / 1	0.1 / 0.5	0.1 / 0.2 / 0.3 / 0.5
value of y in (1+y)* $^{s}G_c$	1	0.2	0.2 / 0.5
new number of data (original) in class -1	2452	2452	4206

In combinations 1 and 2, two factors are considered for $^{s}R_c$ versus only one factor for $^{s}G_c$. More attention is given to the increase of the crest height compared to the increase of the crest width. The factors in combination 1 are larger compared to the factors in combination 2. Consequently combination 2 gives more attention to the zero border, which may be advantageous for the classifier's classifying capacity near this zero border. In combination 1 more attention is given to the further extension of the dataset in the two directions.
Finally, in combination 3 more factors are used, resulting in an increase of the number of artificial data. Combination 3 considers the same factors as in combination 2, but adds more data, with the advantage to use more data from class +1 at the same time.

The new number of data available for class -1 is lower than (number of factors +1) * 698, as the data from class -1 with $G_c = 0$m (340 tests), are not duplicated, i.e. 2452 = 4 * 698 - 340 and 4206 = 7 * 698 - 2 * 340.

Three classifiers are developed, corresponding to the three combinations listed in table 4.16. For each classifier the following procedure is passed through:

1) The originally available data in class -1 are extended with artificial data, using the factors of table 4.16, and the methodology as described in the previous section.
2) An equal number of non-zero data is randomly taken from the 8154 available data in class +1. As the number of data in class -1 in combination 3 is larger than in combination 1 and 2, the total number of data used for the development of the classifier is higher for the former combination.

3) 85% of the data is used for the training process, 15% for the test process. The division in training and testset is performed randomly over the assembled data from class -1 and +1.
4) The data in the trainingset and testset are each multiplied according to their weight factor.
5) Starting with the same 13 input parameters as used for the quantifier, a fixed number of 20 hidden neurons, and the randomly determined trainingset, the neural model is calibrated.

In a first attempt the prediction capacity of the classifiers is assessed on the basis of the performance for their corresponding testset, see table 4.17. Besides the rms-error also the percentage of wrongly classified data, obtained with eq. (4.24), is given. For each combination the results are split up for class +1 and class -1. Table 4.17 also shows the results for the so-called 'restset'. The restset contains all data from class +1 which were not used for the development of the classifier, and may consequently be considered as a kind of second testset. However, as the restset only contains data from class +1, it does not give any information on the performance of the classifiers for zero measurements.

Table 4.17 Performance of each classifier for corresponding (weighed) testset (and additionally weighed restset)

	Combination 1	Combination 2	Combination 3
testset:			
rmse	0.4426	0.5560	0.4496
% data wrongly classified	**4.90**	**7.73**	**5.05**
of which			
(# data in class -1)	(1904)	(1811)	(3467)
% of class -1 wrongly classified	6.25	4.80	5.13
(# data in class +1)	(2180)	(2135)	(3380)
% of class +1 wrongly classified	3.72	10.21	4.97
restset:			
rmse	0.4439	0.5435	0.4712
(# data in restset)	(32296)	(32568)	(22428)
% data wrongly classified	**4.92**	**7.38**	**5.55**

Table 4.17 shows that the total percentage of wrongly classified testdata is situated between ~5% and ~8% for all combinations.
Although the starting point of combination 1 and combination 2 was the same number of measured and artificial data, the number of data in the testset of combination 1 differs from the number of data in the testset of combination 2. This is due to the fact that the multiplication of the data according to their weight factor

has only been performed after the separation of training- and testset. For combination 3 the number of testdata is logically larger as more artificial data were generated.

It is difficult to compare the three classifiers only on the basis of the values in table 4.17, as for each combination other artificial data were generated, resulting in different artificial data in the corresponding testsets. Therefore, in a second attempt the performance for the weighed, original dataset, i.e. without artificial data, is studied for each combination. Table 4.18 gives an overall view of the results. As the percentages of wrongly classified data may give a better feeling of the performance, only these values are represented. However, with eq. (4.24) the corresponding rms-errors are easily obtained.

Table 4.18 Performance of each classifier for weighed original dataset

	Combination 1	Combination 2	Combination 3
% data wrongly classified	**5.11**	**6.78**	**5.22**
of which			
(# data in class -1)	----------	(3710)	----------
% of class -1 wrongly classified	15.31	5.93	11.29
(# data in class +1)	----------	(46139)	----------
% of class +1 wrongly classified	4.28	6.85	4.73

The comparison of the total percentages of wrongly classified data for the original dataset learns that combination 2 performs worst. However, the difference with the other combinations is small. When the results for the separate classes are studied, it can be noted that the prediction of class -1 is clearly better for combination 2 compared to combination 1 and 3 (only ~6% misclassifications versus ~15 and ~11%). The prediction of class +1 on the other hand is worse for combination 2 (almost 7% misclassifications versus ~4 and ~5%).

Finally, in a third attempt some new artificial datasets are created, with the aim of testing the zero generalisation capacity further away from the zero border of the classifiers (but still within the range of frequently occurring parameter values). Due to the fact that the zeros included in the original dataset are mainly situated near the zero border, table 4.18 does not give any information on the performance of the classifier for zero data further away from this zero border.
The artificial datasets are generated in the same way as described in section 4.7.3.1. Only new artificial data with higher values of ${}^{s}R_{c}$ are created. Two values of x are chosen so that the new artificial data are not yet present in the training- or testset of any of the developed classifiers, i.e. x = 0.15 and x = 1.5.
The results for the new, weighed artificial datasets are represented in table 4.19.

Table 4.19 Performance of each classifier for new weighed artificial datasets

	Combination 1	Combination 2	Combination 3
artificial data with x = 0.15 for class -1			
(# data)	----------	(3710)	----------
% of data wrongly classified	6.63	1.29	1.99
artificial data with x = 1.5 for class -1			
(# data)	----------	(3710)	----------
% of data wrongly classified	1.13	1.21	1.24

For the artificial dataset with x = 0.15, the classification of combination 1 is clearly worse than the classification of combination 2 and 3. This is explained by the factors on which the network has been trained: combination 1 has only been trained on extra data with as smallest factor (1+x) = 1.5. Combination 2 and 3 have both been trained on extra data containing the factor (1+x) = 1.1, with as a consequence that these combinations have been trained with more zero data at the border of zero overtopping.
The performance of the classifiers for the artificial dataset with x = 1.5 is comparable for the three combinations, implicating that the generalisation performance for large ${}^{s}R_{c}$ -values is approximately equal for all classifiers.

With reference to the obtained results, the following remarks should be made:

- The results are influenced by the random choice of the data which are used for the training and the test process, and in addition by the random initialisation of the weights and biases.
- The proportion of data from class -1 to data from class +1 in the trainingset (which is determined by the random choice of trainingdata), may have an influence on the better or worse prediction capacity for data from one class versus the other. Table 4.20 shows that for combination 2 the number of trainingdata in both classes is almost equal, versus the presence of slightly more trainingdata in class +1 compared to class -1 for combination 1 and 3. This might contribute to the observation that the combinations 1 and 3 seem slightly inclined to predict non-zero overtopping (see table 4.17 and table 4.18).

Table 4.20 Division of trainingdata

	Combination 1	Combination 2	Combination 3
# trainingdata in class -1	11226	11319	19083
# trainingdata in class +1	11663	11436	20331

- The assessment of erratic classified data may be different for the two classes, i.e. it may be worse if non-zero overtopping is classified as zero (i.e. unsafe overtopping prediction) than if zero overtopping is classified as non-zero (i.e. safe overtopping prediction). This consideration is treated further in this section in more detail.

Considering the results as well as the above mentioned remarks, the author assesses the classifier developed with combination 3 for the artificial data as the best classifier. The general performance of this classifier is found to be good, whereas the performance for data in class +1 is equal or better than for data in class -1. In addition, the generalisation performance for larger values of ${}^{s}R_{c}$ is good.
Combination 3 is consequently restricted for the further development of the final classifier.

4.7.3.3 Architecture of the network

The architecture of the overtopping classifier is similar to that of the quantifier. As both networks are meant to function in series, the input layer of the classifier consists of the same 13 input parameters as the input layer of the final quantifier is constituted of. The output of the classifier logically differs from the quantifier output, and can adapt only 2 possible values, i.e. +1 for significant overtopping and -1 for zero or negligible overtopping. The number of hidden neurons in the calculations of previous section was fixed on 20. This section studies if this number of neurons is acceptable or if it has to be increased or may be lowered. The combination 3 for the artificial data from previous section is further considered.

Figure 4.39 shows the value of 'perc_wrong_test', i.e. the percentage of wrongly classified data from the testset, for classifier models developed with a number of hidden neurons varying from 12 up to 27. Additionally, the value of 'perc_wrong_rest' is represented, standing for the percentage of wrongly classified data from the restset (which contains the data from class +1 not used for development of the classifier). Analogous to the curve in figure 4.12, where an acceptable number of hidden neurons for the quantifier was searched for, the fluctuating of the curves may be attributed to the random choices which are made for each model.

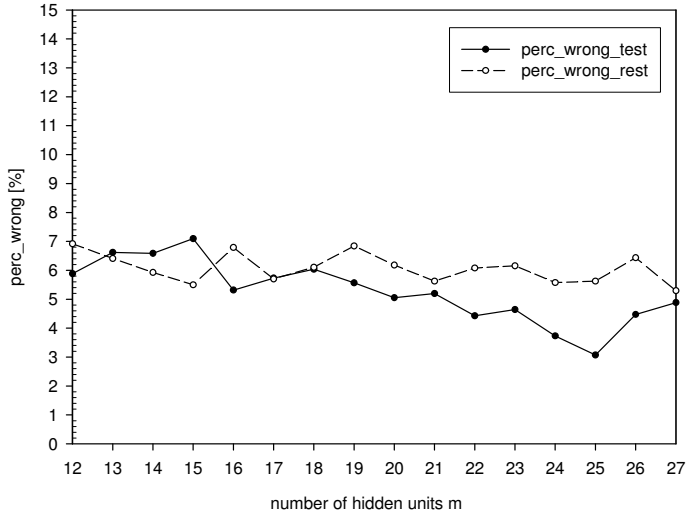

Figure 4.39 Values of perc_wrong_test and perc_wrong_rest for different numbers of hidden neurons for the classifier

For both curves a decrease of the percentage of wrongly classified data with an increasing number of hidden neurons is observed, although this decrease is not very pronounced. The figure shows that even a slightly lower number of hidden neurons than 20 does not lead to a significant increase of erratic classified data.

It may be remarked that a lower number of hidden neurons (20, compared to 25 for the quantifier) was originally chosen as the network only has to approach two possible output values, which implicates a simplification of the function to be predicted by the network. This is confirmed in figure 4.39, on the basis of which a number of 20 hidden neurons may be assessed as an acceptable choice.

4.7.4 Application of the bootstrap method

4.7.4.1 Methodology

The classifier developed at this moment is dependent on the random selection of the (restricted number of) data from class +1 as well as on the arbitrary choice of training- and testset. As for the quantifier, the bootstrap method (Efron, 1982) may be applied, allowing an optimal use of the available data.

The application of the bootstrap technique for a classifying problem does not result in the typical percentile intervals as obtained for a regression problem. Using the bootstrap technique for the classifier in a comparable way as for the quantifier, would lead to the following result:

- The final, ensemble classifier prediction is equal to the mean of the predictions obtained by the bootstrap models. This corresponds to assigning a data point to this class which is predicted by more than half of the bootstrap models.
- The 'degree of equivalence' of the bootstrap predictions is a measure for the reliability of the ensemble prediction. It should be clear that for a data point which is classified by all bootstrap models as +1, i.e. significant overtopping, it is more probable to indeed belong to this class compared to a data point which is only classified by $2/3^{th}$ of the bootstrap models as +1 (and by the remaining $1/3^{rd}$ of the bootstrap models as -1). The typical percentile intervals are substituted by an indication of the probability of correct classification.

As the probability of correct classification is a rather abstract value which is hardly of practical use for the user of the network, preference is given to interpret the obtained bootstrap results in an alternative way. Instead of using the latter results to represent the probability of correct classification, an alternative decision criterion to assign a point to one of both classes is defined based on the bootstrap predictions. The method allows to account for the difference in assessment of misclassifying a zero measurement versus misclassifying a non-zero measurement. How the bootstrap results are interpreted exactly is explained in detail in next section.

The bootstrap calculations, leading to the various bootstrap models, are performed in a comparable way as for the quantifier.
In a **first step** the data from class -1 as well as the data from class +1 are multiplied according to their weight factor. This results in two extended, weighed datasets consisting of 22550 data for class -1 (instead of 4206, see table 4.16), and 46139 data for class +1 (instead of 8154, see table 4.15).

In a **second step** various bootstrap datasets are generated. For each bootstrap dataset the following procedure is passed through:

1) 22550 data are randomly sampled *with replacement* from the 22550 available data in class -1
2) an identical number of data, i.e. 22550, is randomly sampled *with replacement* from the 46139 available data in class +1
3) the sampled data of the two classes are assembled to one bootstrap dataset consisting of 45100 data

The created bootstrap datasets serve in a **third step** as trainingsets for the development of an equal number of bootstrap models. The total number of performed bootstrap calculations is 61.

In a **fourth step** the corresponding 61 bootstrap results for each data point (61 values of -1 or +1) are used to assess the final classification of the data point (see next section).

4.7.4.2 Interpretation of the results

In this section an alternative way to interpret the bootstrap results is proposed. The fundamental reason for this is that one would like to punish a misclassification of a data point from class +1 more than the misclassification of a data point from class -1. The former situation leads to more dangerous design situations compared to the latter situation. Considering safety, it is clear that the number of misclassified non-zero overtopping measurements by the final classifier should be as low as possible. The misclassification of zero data only leads to a too conservative design of structures. Logically, keeping the number of misclassified zero data low is also preferred.

As mentioned in the previous section, the most comparable approach of the bootstrap method to a typical regression problem is to assign a data point to this class which is predicted by the majority of the bootstrap models. If at least 31 of the 61 bootstrap models predict a value of -1, or in other words, if the mean value of all bootstrap predictions is < 0, then the data point is assigned to class -1.
The mean value of all bootstrap predictions gives an indication of the probability of a data point to be correctly classified. A mean value near +1 or -1 corresponds with a data point which is classified consequently as +1 respectively -1 by the bootstrap models and consequently may be expected to be probably correctly classified. The other way around, a mean value near 0 corresponds with a data point for which approximately an equal number of bootstrap models predict +1 or -1, corresponding with a higher probability of misclassification.

Table 4.21 shows the performance of the classifier for the original dataset obtained with this classic approach.

Table 4.21 Results obtained for weighed original dataset with classic approach of the bootstrap method

% data wrongly classified	4.59
of which	
(# data in class -1)	(3710)
% of class -1 wrongly classified	10.44
(# data in class +1)	(46139)
% of class +1 wrongly classified	4.12

Table 4.21 shows that 10.44% of the measured zero or negligible overtopping discharges is classified as significant overtopping by the classifier. In addition, 4.12% of the measured overtopping discharges larger than zero are wrongly classified as zero by the classifier. This brings the total percentage of misclassifications to ~4.5%.

The percentage of misclassified non-zero data seems to be rather low, i.e. a mere 4.12%. However, looking in more detail to these tests shows that the corresponding values of ${}^{s}q_{measured}$ for these tests sometimes concern quite high overtopping discharges. Table 4.22 gives an indication of the corresponding values of ${}^{s}q_{measured}$ for this 4.12% of misclassified non-zero data.

Table 4.22 Values of ${}^{s}q_{measured}$ corresponding with wrongly classified data from class +1 (classic approach)

values of ${}^{s}q_{measured}$	% wrongly classified (of 46139 data)
${}^{s}q_{measured} > 10^{-2}$ m^3/s/m	0
10^{-2} m^3/s/m $\geq {}^{s}q_{measured} > 10^{-3}$ m^3/s/m	0.25
10^{-3} m^3/s/m $\geq {}^{s}q_{measured} > 10^{-4}$ m^3/s/m	0.75
10^{-4} m^3/s/m $\geq {}^{s}q_{measured} > 10^{-5}$ m^3/s/m	2.12
10^{-5} m^3/s/m $\geq {}^{s}q_{measured} > 10^{-6}$ m^3/s/m	1.01
TOTAL:	4.12

In contrast to what might be expected, table 4.22 shows that the misclassified non-zero data concern rather high values of ${}^{s}q_{measured}$: values up to > 10^{-3} m^3/s/m are present. The maximum value of ${}^{s}q_{measured}$ is $5.64*10^{-3}$ m^3/s/m.

As the classification of high overtopping discharges as zero is assessed as worse than the prediction of high overtopping discharges in case of zero q -values, one should try to reduce this number of 4.12% wrongly classified non-zero data, even

in spite of the fact that 10% misclassified zero -values is over double of the misclassified non-zero values.

In order to reduce the probability of misclassification of the non-zero data, the criterion that attributes a prediction to the class -1 can be made more strict: instead of considering the mean value 'zero' of all bootstrap predictions as the border between class -1 and +1, a lower (i.e. negative) value is chosen. This implicates that a data point is sooner classified as non-zero than as zero. The lower this border value, the lower the number of misclassified non-zero data will be. It is clear that an increase of the number of misclassified zero data goes hand in hand with the decrease of the number of misclassified non-zero data.

In table 4.23 different selection criteria are proposed, and the corresponding percentages of misclassified data are given. In the first column the selection criterion is expressed in terms of the value of $61*y_{NN\_mean}$, in which y_{NN_mean} stands for the mean value of the 61 bootstrap predictions. In column 2 the criterion is expressed by the corresponding number of bootstrap predictions obtained for class +1 (respectively -1). Columns 3, 4 and 5 finally show the obtained results, in general, and separately for both classes.

Table 4.23 Results obtained for weighed original dataset considering different selection criteria

Selection criterion for class +1: $61*y_{NN\_mean}$ …	# bootstrap models predicting class +1 (-1)	total % data wrongly classified (of 49849 data)	% data wrongly classified from class -1 (3710 data)	% data wrongly classified from class +1 (46139 data)
> 0 (crit A)	≥ 31 (≤ 30)	4.59	10.44	4.12
> -10	≥ 26 (≤ 35)	4.38	11.79	3.79
> -20	≥ 21 (≤ 40)	3.97	13.27	3.23
> -30	≥ 16 (≤ 45)	3.67	15.30	2.74
> -40	≥ 11 (≤ 50)	3.33	16.64	2.26
> -50 (crit C)	≥ 6 (≤ 55)	3.09	19.29	1.80
> -60 (crit B)	≥ 1 (≤ 60)	2.85	26.22	0.98

When moving downward in table 4.23, the selection criterion becomes more strict for class -1 (and consequently less strict for class +1). The first row of table 4.23, referred to as 'criterion A', corresponds to the classic approach of the bootstrap

method which has been considered until now. The last row of table 4.23, referred to as 'criterion B', is a selection criterion that only assigns a data point to class -1 if all bootstrap models attribute the point to class -1.
The general trend which can be derived from table 4.23 is that, if the selection criterion for the non-zero data (class +1) becomes less strict, the percentage of wrongly classified data from class -1 increases, while the percentage of wrongly classified data from class +1 decreases. Due to the larger number of non-zero data in the original dataset, this also corresponds to a decrease of the total number of wrongly classified data. The decrease of the percentage of wrongly classified data from class +1 is exactly that what is strived for, while the increase of the wrongly classified data from class -1 is an unavoidable consequence.

Before taking a decision on the selection criterion which will be used for the final classifier, one should look in more detail to the nature of the data which are misclassified by the classifier. The misclassifications obtained with the mentioned two most extreme selection criteria are studied in this context, i.e.:

- criterion A: prediction = +1 if $61*y_{NN\_mean} > 0$ (first row in table 4.23)
- criterion B: prediction = +1 if $61*y_{NN\_mean} > -60$ (last row in table 4.23)

In general, when changing from selection criterion A to selection criterion B, the percentage of wrongly classified data from class +1 has decreased from more than 4% to less than 1%, whereas the percentage of wrongly classified data from class -1 has increased from about 10% to about 26%.
In a first attempt, the nature of the misclassifications from class +1 for both criteria is compared. Afterwards the nature of the misclassifications from class -1 is compared.

- Data originating from class +1, i.e. data with $^{s}q_{measured} > 0$ $m^3/s/m$

The wrongly classified data from class +1 concern data with significant overtopping measurements, which are classified as zero.
It is quite logical that it is worse if high overtopping discharges, e.g. $^{s}q_{measured} = 10^{-2}$ $m^3/s/m$, are classified as zero than if rather low overtopping discharges, e.g. $^{s}q = 10^{-5}$ $m^3/s/m$, are classified as zero. In general, the measured value of ^{s}q is an indication of the magnitude of the error.
For criterion A, in table 4.22 an overall view was already given of the magnitude of the values of $^{s}q_{measured}$ for wrongly classified non-zero data. Table 4.24 is set up in the same way for criterion B.

Table 4.24 Values of $^{s}q_{measured}$ corresponding with wrongly classified data from class +1, criterion B

values of $^{s}q_{measured}$	% wrongly classified (of 46139 data)
$^{s}q_{measured} > 10^{-2}$ m^3/s/m	0
10^{-2} m^3/s/m ≥ $^{s}q_{measured} > 10^{-3}$ m^3/s/m	0.01
10^{-3} m^3/s/m ≥ $^{s}q_{measured} > 10^{-4}$ m^3/s/m	0.10
10^{-4} m^3/s/m ≥ $^{s}q_{measured} > 10^{-5}$ m^3/s/m	0.63
10^{-5} m^3/s/m ≥ $^{s}q_{measured} > 10^{-6}$ m^3/s/m	0.24
TOTAL:	0.98

The misclassified data still concern values of $^{s}q_{measured}$ up to > 10^{-3} m^3/s/m. However, the percentages of table 4.24 are significantly lower than those of table 4.22. The maximum value of $^{s}q_{measured}$ for criterion B is $1.25*10^{-3}$ m^3/s/m, compared to $5.64*10^{-3}$ m^3/s/m for criterion A.
Similar to criterion A, the largest percentage of misclassified non-zero data corresponds to values of 10^{-4} m^3/s/m ≥ $^{s}q_{measured} > 10^{-5}$ m^3/s/m for criterion B.

- Data originating from class -1, i.e. data with $^{s}q_{measured} = 0$ m^3/s/m

The wrongly classified data from class -1 concern data with zero or negligible overtopping measurements, assessed by the classifier as significant overtopping. As the goal of the classifier is to serve as filter for the data to be put into the quantifier, all data assessed by the classifier as +1, i.e. showing significant overtopping, should be simulated by the quantifier to obtain a prediction of the value of the overtopping discharge.
Logically, only data which are situated within the limits of application of the quantifier may be simulated by this last one.
For criterion A, 1.03 % of the 10.44% wrongly classified zero data fall outside the limits of application of the quantifier. This implicates that only 10.33% wrongly classified zero data can be simulated by the quantifier. For criterion B, 9.36 % of the 26.22% wrongly classified zero data are out of range, resulting in a quantifier simulation of 23.77% wrongly classified zero data. The wrongly classified zero data which are out of range of the quantifier are not further considered. No prediction can be obtained for these data with the developed neural model.
The quantifier simulations of the remaining wrongly classified zero data, $^{s}q_{NN}$, are represented in figure 4.40 (a) and figure 4.40 (b) for criterion A respectively B. The values of $^{s}q_{NN}$ are represented in the figures in descending order. It concerns 383 respectively 881 weighed data (corresponding to 60 respectively 160 different data, i.e. originating from the original non-weighed zero dataset).

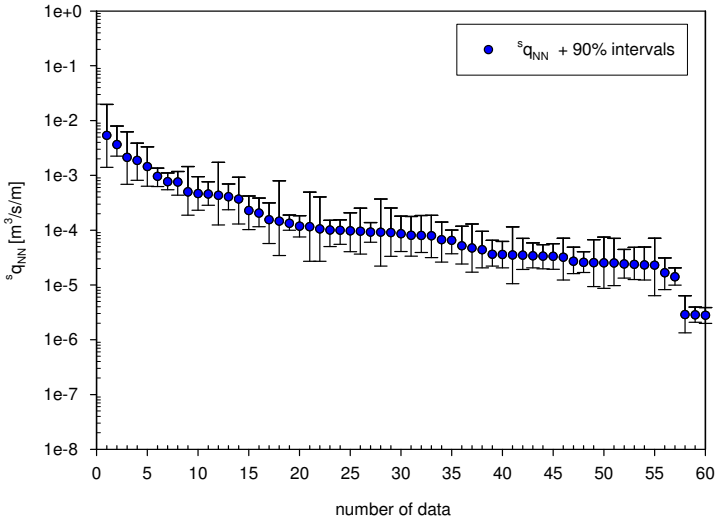

(a)

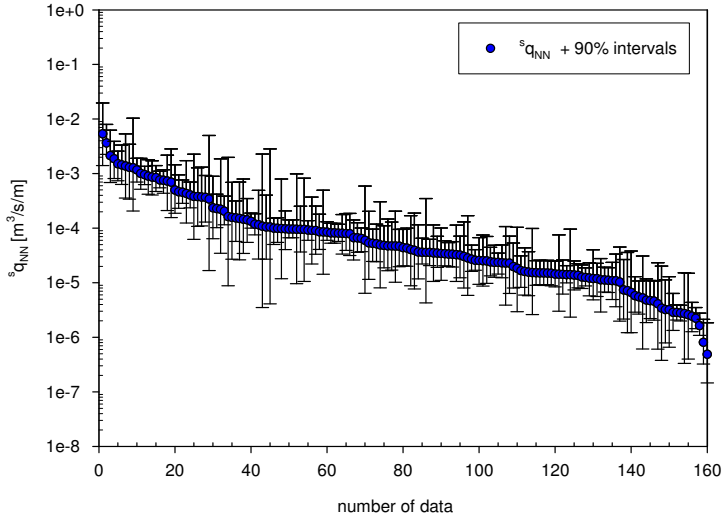

(b)

Figure 4.40 Quantifier simulation of wrongly classified data from class -1, (a) considering criterion A and (b) considering criterion B

The predicted value by the quantifier gives an idea of the magnitude of the error: high values of $^{s}q_{NN}$ are assessed as worse than low values of $^{s}q_{NN}$, as it is known that the real measured overtopping $^{s}q_{measured}$ was zero or negligible. Special attention should be given to the often small percentile intervals corresponding to

the quantifier simulations of the wrongly classified data, which give a false impression of a reliable prediction.

Table 4.25 shows the distribution of the values of ${}^{s}q_{NN}$ which are represented in figure 4.40. The numbers are expressed in percentages of the wrongly classified data of class -1 as well as in percentages of the total number of data from class -1. All numbers are related to weighed values.

Table 4.25 Values of ${}^{s}q_{NN}$ for wrongly classified data from class -1

values of ${}^{s}q_{NN}$	% of wrongly classified data from class -1		% data from class -1 (3710 data)	
	criterion A (387 data)	criterion B (972 data)	criterion A	criterion B
(input out of range)	(1.03)	(9.36)	(0.11)	(2.45)
${}^{s}q_{NN} > 10^{-2}$ m^3/s/m	0	0	0	0
10^{-2} m^3/s/m ≥ ${}^{s}q_{NN} > 10^{-3}$ m^3/s/m	5.43	4.32	0.57	1.13
10^{-3} m^3/s/m ≥ ${}^{s}q_{NN} > 10^{-4}$ m^3/s/m	31.27	18.31	3.26	4.80
10^{-4} m^3/s/m ≥ ${}^{s}q_{NN} > 10^{-5}$ m^3/s/m	57.11	54.84	5.96	14.38
10^{-5} m^3/s/m ≥ ${}^{s}q_{NN} > 10^{-6}$ m^3/s/m	5.17	12.24	0.54	3.21
10^{-6} m^3/s/m ≥ ${}^{s}q_{NN}$	0	0.93	0	0.24
TOTAL :	100	100	10.44	26.22

It is clear that by changing the selection criterion from A to B, the number of wrongly classified data from class -1 increases. The distribution of the obtained quantifier predictions ${}^{s}q_{NN}$ is similar for criterion A and B. For both criteria most quantifier predictions ${}^{s}q_{NN}$ are situated in between 10^{-4} m^3/s/m and 10^{-5} m^3/s/m.

One can conclude that for both criteria

- the wrongly classified data from class +1 concern values of ${}^{s}q_{measured}$ within the range 10^{-2} m^3/s/m ≥ ${}^{s}q_{measured} > 10^{-6}$ m^3/s/m, whereas the largest percentage of these data corresponds to values of 10^{-4} m^3/s/m ≥ ${}^{s}q_{measured} > 10^{-5}$ m^3/s/m
- a minority of the wrongly classified data from class -1 fall outside the limits of application of the quantifier and are consequently not further considered, so no overprediction can be obtained
- the remaining wrongly classified data from class -1 result in predictions of the quantifier within the range 10^{-2} m^3/s/m ≥ ${}^{s}q_{NN} > 10^{-6}$ m^3/s/m, most predictions ${}^{s}q_{NN}$ are situated in between 10^{-4} m^3/s/m and 10^{-5} m^3/s/m

Besides the fact that the number of misclassified data for class +1 decreases and for class -1 increases for criterion B compared to criterion A, the classifiers do not show differences in behaviour, i.e. the same ranges are occupied and similar

distributions are noticed for values of ${}^{s}q_{measured}$ respectively ${}^{s}q_{NN}$. It may be expected that for any selection criterion, the same behaviour will occur.

Based on the observation that the wrongly classified non-zero data concern rather high values of ${}^{s}q_{measured}$, and considering the important aspect of safety in overtopping design, a selection criterion which gives priority to minimise the number of wrongly classified non-zero data should be chosen. However, to avoid a too strict classifier for class -1, preference is given not to use criterion B, which only assigns a data point to class -1 if all bootstrap models predict class -1. The second most strict criterion for class -1 is therefore opted for. It concerns the criterion mentioned on the last but one row of table 4.23, referred to as 'criterion C': a data point is assigned to class +1 if more than 5 bootstrap models predict class +1. Criterion C is still much more strict for data from class -1 compared to data from class +1, but allows for some models to lead to bad predictions in some parts of the input space due to local scarce occupation, without causing consequent overprediction of overtopping.

Table 4.23 shows that the chosen selection criterion C corresponds to a misclassification of less than 20% of the zero data, versus a misclassification of only 1.80% of the non-zero data. Table 4.26, table 4.27 and figure 4.41 give an overall view of the nature of these misclassifications. The 718 wrongly classified (weighed) data from class -1 correspond to 120 different data in the original database, of which the quantifier prediction is represented in figure 4.41.

Table 4.26 Values of ${}^{s}q_{measured}$ corresponding with wrongly classified data from class +1 for final criterion C

values of ${}^{s}q_{measured}$	% wrongly classified (of 46139 data)
${}^{s}q_{measured} > 10^{-2}$ m^3/s/m	0
10^{-2} m^3/s/m ≥ ${}^{s}q_{measured} > 10^{-3}$ m^3/s/m	0.02
10^{-3} m^3/s/m ≥ ${}^{s}q_{measured} > 10^{-4}$ m^3/s/m	0.29
10^{-4} m^3/s/m ≥ ${}^{s}q_{measured} > 10^{-5}$ m^3/s/m	0.99
10^{-5} m^3/s/m ≥ ${}^{s}q_{measured} > 10^{-6}$ m^3/s/m	0.50
TOTAL:	1.80

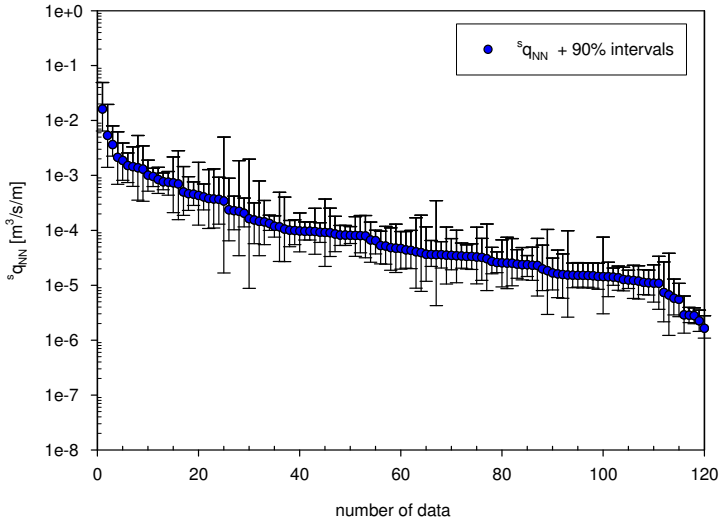

Figure 4.41 Quantifier simulation of wrongly classified data from class -1 for final criterion C

Table 4.27 Values of $^{s}q_{NN}$ for wrongly classified data from class -1 for final criterion C

values of $^{s}q_{NN}$	% of wrongly classified data from class -1 (718 data)	% data from class -1 (3710 data)
(input out of range)	(5.57)	(1.07)
$^{s}q_{NN} > 10^{-2}$ m^3/s/m	0	0
10^{-2} m^3/s/m ≥ $^{s}q_{NN} > 10^{-3}$ m^3/s/m	5.01	0.97
10^{-3} m^3/s/m ≥ $^{s}q_{NN} > 10^{-4}$ m^3/s/m	21.73	4.19
10^{-4} m^3/s/m ≥ $^{s}q_{NN} > 10^{-5}$ m^3/s/m	60.31	11.63
10^{-5} m^3/s/m ≥ $^{s}q_{NN} > 10^{-6}$ m^3/s/m	7.38	1.42
10^{-6} m^3/s/m ≥ $^{s}q_{NN}$	0	0
TOTAL :	100	19.29

Due to the choice of a strict selection criterion for class -1, it may be expected that data which are on the border of zero overtopping will be inclined to be classified as non-zero overtopping, (sometimes) leading to rather high overtopping discharges predicted by the quantifier.

However, compared to the single quantifier performance, the number of overtopping overpredictions is significantly reduced with the restricted selection criterion C for the classifier. One can compare the results represented in table 4.27 to the previously obtained results with the single quantifier, summarised in

table 4.14 (see section 4.6.9.2). Although the results represented in table 4.14 only consider the zero overtopping measurements, i.e. 3521 weighed data, whereas table 4.27 considers 3710 weighed negligible overtopping data, i.e. 189 (weighed) data with ${}^{s}q_{measured} < 10^{-6}$ m^3/s/m are additionally included in class -1, one gets an idea of the significantly better performance of the combination classifier - quantifier compared to the single quantifier performance for zero overtopping measurements. It has been found in table 4.14 that (56.94% - 2.44% - 0.09%) = 54.41% of the considered zero data are predicted by the quantifier as ${}^{s}q_{NN} > 10^{-6}$ m^3/s/m. The use of the classifier reduces the quantifier predictions ${}^{s}q_{NN} > 10^{-6}$ m^3/s/m to (19.29% - 1.07%) = 18.22% of the considered zero data (see table 4.27). This is a reduction of approximately a factor 3! In addition, the percentage of zero overtopping measurements for which no overtopping prediction can be given, decreases from 43.06% for the single quantifier, to only 1.07% if the classifier is used as filter for the quantifier. The classifier classifies (100% - 19.29%) = 80.71% of the considered zero overtopping measurements correctly as negligible or zero overtopping.
This noticeably better prediction of the zero overtopping measurements when using the classifier as a filter for the quantifier has as negative consequence the classification of 1.80% of the non-zero measurements as zero. However, this percentage is very low and is therefore considered as acceptable.

4.7.5 Ranges of applicability for the classifier

Analogous to the quantifier, ranges of applicability should be defined for the classifier. As the dataset on which the classifier has been trained, encloses the dataset on which the quantifier has been trained, the minimum/maximum-intervals for individual input parameter of the classifier will at least be evenly wide as these of the quantifier. The classifier has not only been trained on extra zero measurements, but especially the artificially created zero data will enlarge the ranges of applicability.

In table 4.28 ranges of applicability set up for the classifier are given. Comparison with table 4.13 shows that for the classifier only different limits of application are given for the input parameters ${}^{s}R_c$, ${}^{s}A_c$ and ${}^{s}G_c$. More specifically, the maximum values are multiplied with a factor 1.5. This factor originates from the methodology applied to create the artificial data, where the input parameters ${}^{s}R_c$ and ${}^{s}G_c$ were multiplied with a maximum factor of (1+0.5).

Table 4.28 Ranges of applicability for the classifier

		$\gamma_f = 1$			$\gamma_f < 1$	
1	3.00	$\leq {}^{s}T_{m\text{-}1,0\ toe}$ [s] $\leq$	22.00	3.00	$\leq {}^{s}T_{m\text{-}1,0\ toe}$ [s] $\leq$	12.00
2	0	$\leq {}^{s}\beta$ [°] $\leq$	60.00	0	$\leq {}^{s}\beta$ [°] $\leq$	60.00
3	1.00	$\leq {}^{s}h$ [m] $\leq$	20.60	1.00	$\leq {}^{s}h$ [m] $\leq$	13.30
4	1.00	$\leq {}^{s}h_t$ [m] $\leq$	20.50	0.65	$\leq {}^{s}h_t$ [m] $\leq$	13.30
5	0	$\leq {}^{s}B_t$ [m] $\leq$	11.40	0	$\leq {}^{s}B_t$ [m] $\leq$	5.00
6	1.00	$\leq {}^{s}\gamma_f$ [-] $\leq$	1.00	0.35	$\leq {}^{s}\gamma_f$ [-] $\leq$	0.95
7	0	$\leq {}^{s}\cot\alpha_d$ [-] $\leq$	7.00	0	$\leq {}^{s}\cot\alpha_d$ [-] $\leq$	5.30
8	-5.00	$\leq {}^{s}\cot\alpha_u$ [-] $\leq$	6.00	0	$\leq {}^{s}\cot\alpha_u$ [-] $\leq$	8.00
9	0	$\leq {}^{s}R_c$ [m] $\leq$	7.50	0.25	$\leq {}^{s}R_c$ [m] $\leq$	4.20
10	-1.00	$\leq {}^{s}h_b$ [m] $\leq$	3.60	-1.00	$\leq {}^{s}h_b$ [m] $\leq$	1.20
11	0	$\leq {}^{s}B_h$ [m] $\leq$	16.20	0	$\leq {}^{s}B_h$ [m] $\leq$	6.20
12	0	$\leq {}^{s}A_c$ [m] $\leq$	6.00	0.10	$\leq {}^{s}A_c$ [m] $\leq$	4.35
13	0	$\leq {}^{s}G_c$ [m] $\leq$	11.40	0	$\leq {}^{s}G_c$ [m] $\leq$	8.10

Analogous to the quantifier, new input for the classifier should always be situated within the given ranges of applicability.

4.7.6 Simulations with the developed classifier, as filter for the quantifier simulations

In this section, the predictions obtained with the developed classifier are studied for some specific test series. The chosen final classifier selection criterion from the previous section is used: data which are classified by more than 5 of the 61 bootstrap models as belonging to class +1, are assessed as data for which significant overtopping may be expected.

As the goal of the classifier is to function as filter for the quantifier, special attention is given to the filter -effect of the classifier, i.e. it is studied if the classifier results in additional restrictions for input for the quantifier.

Finally, the so-called 'combined classifier-quantifier predictions' are discussed for each studied test series, and compared to the single quantifier predictions. The combined classifier-quantifier predictions concern the final overtopping predictions within this work. It is shown that the performance of the combination classifier-quantifier is significantly better than the performance of the single quantifier.

In section 4.7.6.1 the results obtained for the prototype measurements are studied. Additionally, in section 4.7.6.2 the results obtained for the same synthetic test series as used to check the performance of the single quantifier (see section 4.6.9.3) are studied.

4.7.6.1 Prototype simulations

In this section the prototype measurements from the three prototype CLASH measurement sites are simulated with the classifier. Section 4.6.9.1 is referred to for detailed information on these three test series.

For each prototype site the final classifier-quantifier result is given. After accounting for model and scale effects according to the CLASH scaling procedure (see section 4.4.2), the final corrected results, $^{s}q_{NN\_corr\_final}$, are compared to the prototype measurements, $^{s}q_{measured}$.

4.7.6.1.1 Test series 044

In section 4.6.9.1.1 it was found that only 16 of the 23 prototype data can be simulated by the quantifier. Simulating these 16 measurements with the classifier results in 16 times a prediction of significant overtopping. This implicates that the obtained result with the quantifier for these tests in section 4.6.9.1.1 can be adopted as a part of the final classifier-quantifier result.

When the remaining 7 prototype data are considered, it is found that three of these fall within the less restricted ranges of applicability of the classifier. It concerns data with values of $^{s}R_c$ = 6.16m, 5.16m and 5.04m, which are smaller values than the maximum value of 7.50m (see table 4.28). The classifier simulation of these data

results each time in a significant overtopping prediction. However, no reliable quantification with the quantifier is possible.
For the other 4 prototype data no prediction can be obtained with the developed neural model, not even with the classifier.
The outcome of the combined classifier-quantifier network can consequently be summarised as follows, see figure 4.42:

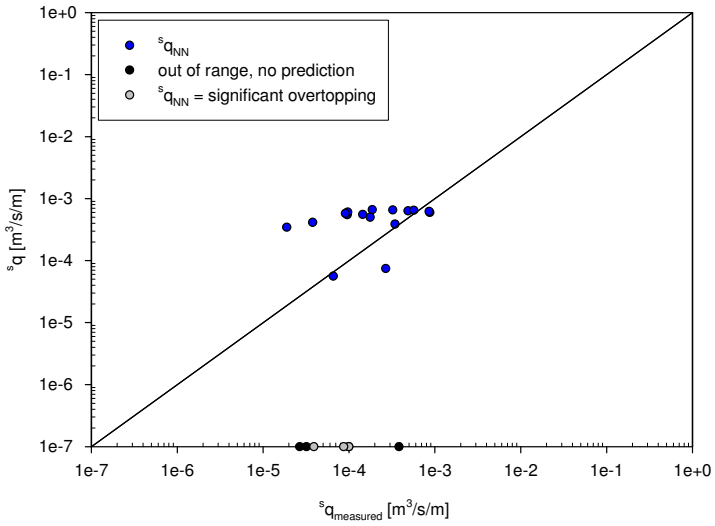

Figure 4.42 Combined classifier-quantifier prediction of Samphire Hoe measurements

- 19 of the 23 prototype data are assessed by the classifier as resulting in significant overtopping in small scale tests. The quantifier is only able to quantify 16 of these measurements. The corresponding prototype predictions, equal to the small scale predictions, were already given in section 4.6.9.1.1 (figure 4.27) and may be considered as final predictions. The rms-error was found to be 0.6050.
  The three prototype data assessed by the classifier as significant overtopping situations in small scale tests, though out of the ranges of applicability of the quantifier, correspond to values of $^sq_{measured} = 3.90*10^{-5}$ m^3/s/m, $8.68*10^{-5}$ m^3/s/m and $9.97*10^{-5}$ m^3/s/m, and are marked in figure 4.42 at a fictive value of $^sq = 10^{-7}$ m^3/s/m.
- 4 of the 23 prototype data are out of the ranges of applicability of both classifier and quantifier. No reliable prediction is obtained for these data. The corresponding values of $^sq_{measured}$ are also marked in figure 4.42 at a fictive value of $^sq = 10^{-7}$ m^3/s/m.

4.7.6.1.2 Test series 381

As all 77 data fall within the ranges of applicability of the quantifier (see section 4.6.9.1.2), all data can also be simulated with the classifier. Eight of the 77 data are assessed by the classifier as negligible or zero overtopping in small scale tests, versus 69 as significant overtopping. For the latter data, the obtained results with the quantifier in section 4.6.9.1.2 can be adopted as a part of the final classifier-quantifier result.

Figure 4.43 shows the quantifier results obtained in section 4.6.9.1.2, where the zero predictions by the classifier are crossed out.

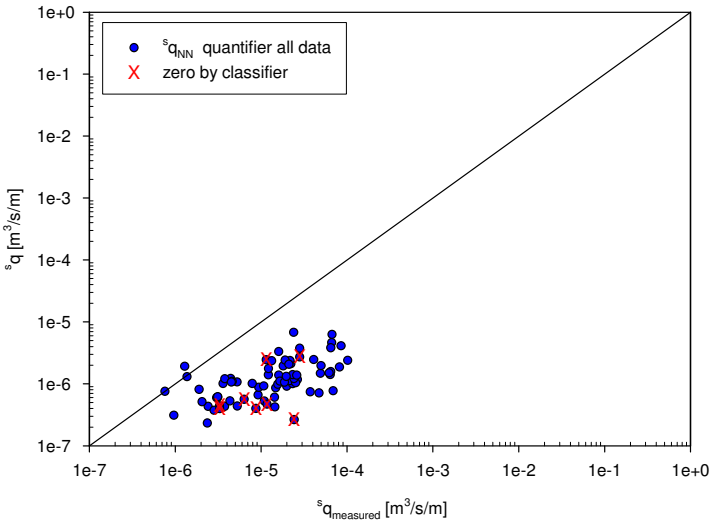

Figure 4.43 Classifier assessment of quantifier simulation of Ostia measurements

Figure 4.43 shows that the 8 zero predictions do not concern the lowest values of $^sq_{measured}$, which might be expected. However, taking into account the expected model and scale effects, the corresponding predictions for small scale situations are all expected to be quite low.

As the same test structure is on the basis of the data, and as the wave characteristics are comparable, the CLASH scaling procedure to determine the expected prototype discharges in case of zero predictions in laboratory can be applied (see section 4.4.2.1). The procedure to estimate a small non-zero overtopping value in small scale tests when a zero is measured, is worked out in figure 4.44.

The dimensionless overtopping discharge $\frac{q}{\sqrt{gH_{m0\,toe}^3}}$ is plotted versus the dimensionless crest freeboard $\frac{R_c}{H_{m0\,toe}} \cong {}^{s}R_c$. The quantifier predictions for non-zero classifier predictions are represented. The best matching TAW prediction line for rough slopes (TAW, 2002, see eq. (2.5b) in chapter 2) is fitted through these predictions, corresponding to a value of γ_f = 0.38. The data predicted by the classifier as insignificant overtopping are represented in figure 4.44 at a value of $\frac{q}{\sqrt{gH_{m0\,toe}^3}}$ = 10^{-8}. It may be expected that the zero predictions correspond to the small overtopping values on this best-matching line. Figure 4.44 shows the methodology used to determine the corresponding values of $\frac{q_{ss\_est}}{\sqrt{gH_{m0\,toe}^3}}$, where the $R_c/H_{m0\,toe}$ -values are the starting point.

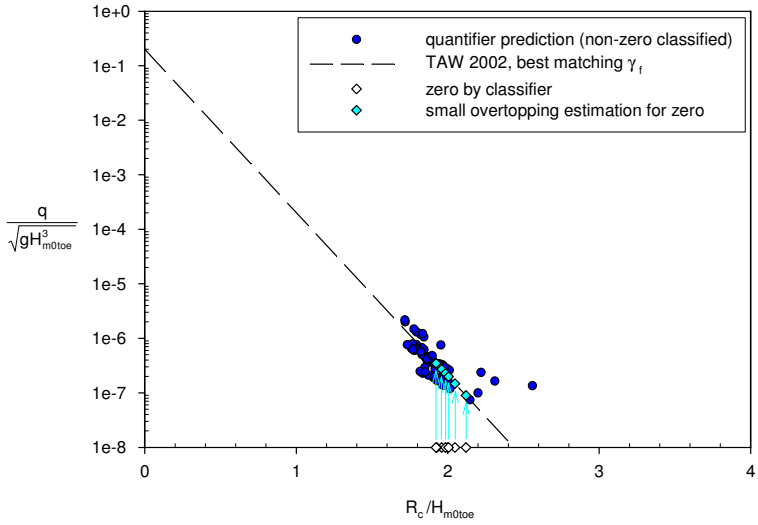

Figure 4.44 Non-zero estimation of zero classified Ostia measurements based on quantifier predictions of non-zero classified Ostia measurements

The obtained small non-zero overtopping estimations of the zero classified data, q_{ss_est} , are used to determine the corresponding prototype predictions, with the same scaling factor f_{scale_wind} as used in section 4.6.9.1.2.

The outcome of the combined classifier-quantifier network can be summarised as follows, see figure 4.45:

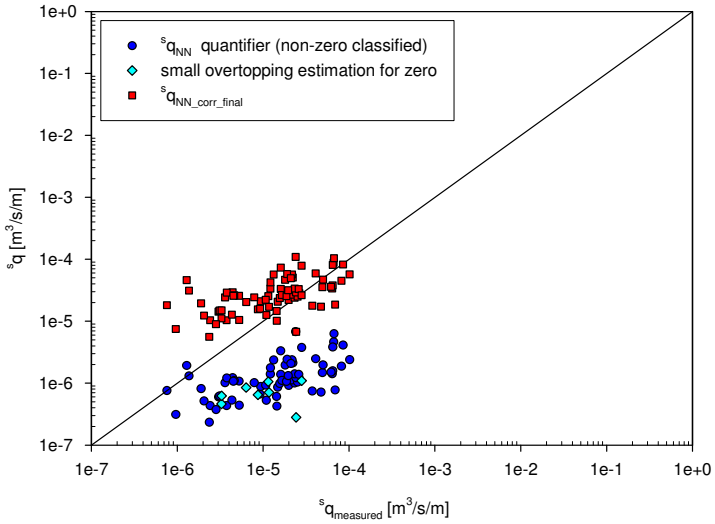

Figure 4.45 Combined classifier-quantifier prediction of Ostia measurements

- 8 of the 77 prototype data are assessed by the classifier as resulting in zero or negligible overtopping in small scale tests. As the aim of the simulation is to obtain a prototype prediction, a procedure to estimate prototype predictions from zero or insignificant small scale predictions is applied. The estimations for the zero predictions all concern values of ${}^{s}q_{ss\_est} \leq 10^{-6}$ m^3/s/m.
- Applying a scaling factor f_{scale_wind} to the 8 converted zero predictions q_{ss_est} combined with the previously determined values of ${}^{s}q_{NN\_corr}$ for the remaining 69 data, results in values of ${}^{s}q_{NN\_corr\_final}$ as represented in figure 4.45. The rms-error of the final corrected network prediction ${}^{s}q_{NN\_corr\_final}$ is found to be 0.5249 (versus an rms-error of 0.5258 for ${}^{s}q_{NN\_corr}$ in section 4.6.9.1.2).

4.7.6.1.3 Test series 957

In section 4.6.9.1.3 it was found that 10 of the 11 prototype measurements can be simulated by the quantifier. Simulating these 10 measurements with the classifier results in 10 times a prediction of significant overtopping. This implicates that the obtained result with the quantifier in section 4.6.9.1.3 can be adopted as a part of the final network result.

Studying the remaining single prototype measurement shows that this point falls within the ranges of applicability of the classifier, i.e. ${}^{s}A_c$ = 3.01m (see table 4.28). The classifier predicts zero or negligible overtopping for this point.
Similar to test series 381, the CLASH scaling procedure is applied to determine a corresponding overtopping discharge to be expected in prototype. Figure 4.46 shows the methodology. It should be noted that in figure 4.46 the dimensionless armour freeboard $\frac{A_c}{H_{m0\ toe}} \cong {}^{s}A_c$ is plotted on the x-axis instead of the dimensionless crest freeboard $R_c / H_{m0\ toe}$, as the maximum armour level is situated higher than the point determining the crest freeboard.

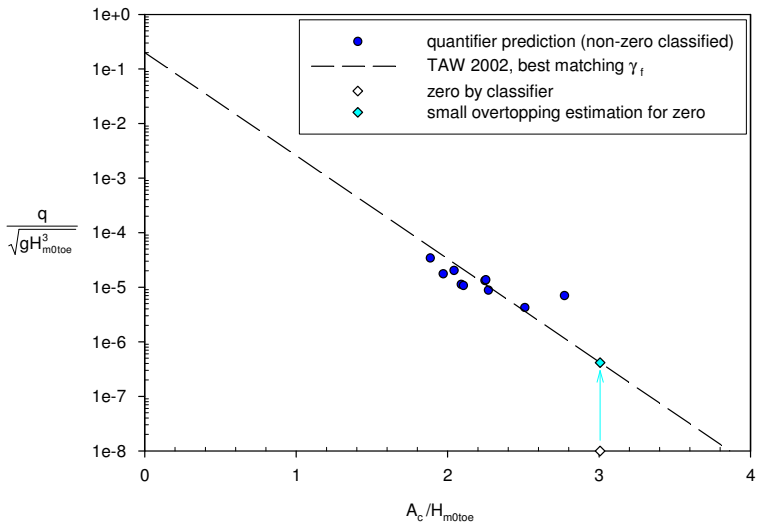

Figure 4.46 Non-zero estimation of zero classified Zeebrugge measurement based on quantifier predictions of non-zero classified Zeebrugge measurements

The best matching TAW prediction line (TAW, 2002, eq. (2.5b) in chapter 2) corresponds to a value of γ_f = 0.60. The obtained small non-zero estimation for the zero-classified data point, q_{ss_est}, is used to determine the corresponding prototype prediction with the same scaling factor f_{scale_wind} as used in section 4.6.9.1.3.

The outcome of the combined classifier-quantifier network can be summarised as follows, see figure 4.47:

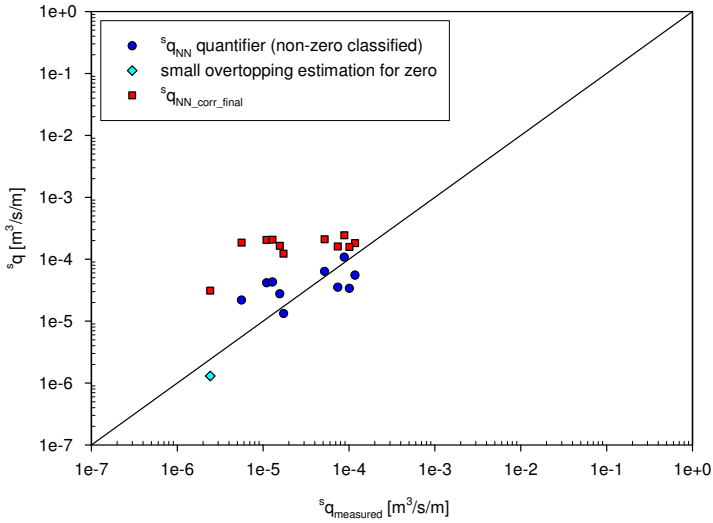

Figure 4.47 Combined classifier-quantifier prediction of Zeebrugge measurements

- One of the 11 prototype data is assessed by the classifier as resulting in zero or negligible overtopping in small scale tests. The same methodology as described for test series 381 is applied to estimate a small non-zero value for the zero prediction by the classifier, resulting in a value of ${}^{s}q_{ss\_est} = 1.30*10^{-6}$ m^3/s/m.
- Applying a scaling factor f_{scale_wind} to the single converted zero prediction q_{ss_est} combined with the previously obtained values of ${}^{s}q_{NN\_corr}$ for the remaining 10 data, results in values of ${}^{s}q_{NN\_corr\_final}$ as represented in figure 4.47. The rms-error of the final corrected network prediction ${}^{s}q_{NN\_corr\_final}$ is found to be 0.9113 (versus an rms-error of 0.8893 for ${}^{s}q_{NN\_corr}$ in section 4.6.9.1.3).

4.7.6.1.4 Conclusion

In the previous sections the performance of the combined classifier-quantifier prediction method in combination with the CLASH scaling procedure has been studied for the available CLASH prototype measurements.

In a few cases, the classifier leads to zero predictions where significant overtopping was measured in prototype. The expected model and scale effects, resulting in small scale overtopping discharges which are negligible, can be mentioned as reason for this. The scaling procedure established within CLASH (see section 4.4.2.1), allowing to determine non-zero prototype discharges in case of non-zero predictions as well as in case of zero predictions in small scale tests,

was applied to determine prototype discharges for all obtained classifier-quantifier predictions.
Compared to the single quantifier prediction, the combined classifier-quantifier prediction leads to the following:

- for the Samphire Hoe case:
  Three of the 23 data with a measured overtopping discharge > 0 $m^3/s/m$ can be assessed extra by the classifier as significant overtopping. However, no quantification of the overtopping discharge is possible. The final rms-error is the same as obtained with the single quantifier, i.e. 0.6050.
- for the Ostia case:
  The final rms-error is 0.5249 whereas for the simulation of the same 77 data by the quantifier only, an rms-error of 0.5258 was obtained. As both values may be considered as equivalent, one can conclude that the single quantifier prediction was quite good.
- for the Zeebrugge case:
  One extra overtopping prediction could be performed by the combination classifier-quantifier, resulting in an rms-error of 0.9113 for 11 data instead of an rms-error of 0.8893 for the prediction of 10 data by the quantifier only. The former rms-error is slightly higher compared to the latter, implicating that the prediction of the extra point is on average worse than the previously obtained predictions. However, the combination classifier-quantifier allows to obtain this extra prediction.

As all prototype overtopping measurements concern non-zero overtopping data, it is quite logic that the combined classifier-quantifier result has approximately the same outcome as the single quantifier result. It may be concluded that the classifier performs very well for the considered prototype data.

One could remark that the 90% percentile intervals have not been given anymore in this section. For the quantifier simulations, these are the same as obtained in section 4.6.9.1, whereas for the overtopping estimations (for the zero classified data), no percentile intervals are available anymore.

4.7.6.2 Simulation of synthetic datasets

In this section the four synthetic datasets which were generated in section 4.6.9.3 are studied. As the limits of application of the classifier are less restricted than those of the quantifier, the classifier simulations are performed up to larger values of ${}^{s}R_c$ (factor 1.5, see section 4.7.5). The four test series consider overtopping at a smooth dike, a rubble mound structure with rocks, a vertical wall and a recurve

wave wall. More detailed information on the generated test series was given in section 4.6.9.3.

For the smooth dike a classifier simulation for 0m ≤ ${}^{s}R_c$ ≤ 6m is performed (see table 4.28). The outcome of this simulation is a consistent significant overtopping prediction.
Figure 4.48 represents the final combined classifier-quantifier prediction. It concerns the same graph as figure 4.33 which was previously set up, where the classifier information is added.

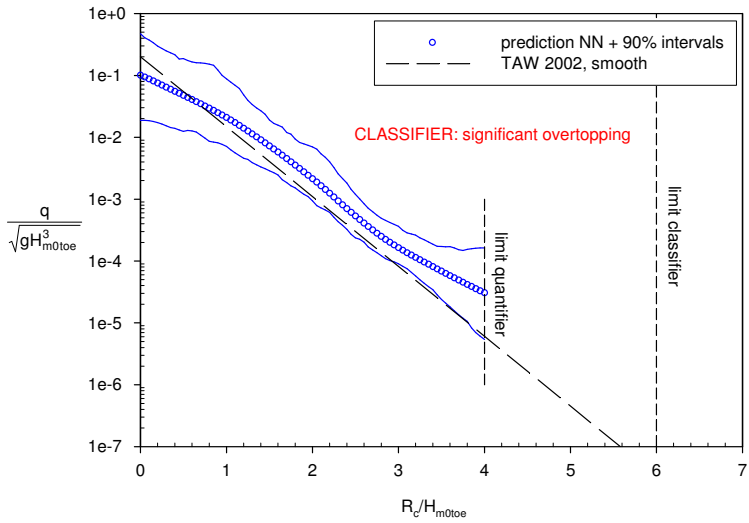

Figure 4.48 Combined classifier-quantifier prediction of overtopping at dike

The results can be summarised as follows:

- Overtopping at the considered dike under previously specified wave attack may be expected at least for values of ${}^{s}R_c$ up to 6m. For higher values of ${}^{s}R_c$ the classifier is not able to make a reliable classification.
- The developed quantifier predicts overtopping discharges for values of 0m ≤ ${}^{s}R_c$ ≤ 4m which can be seen in figure 4.48. For values of 4m < ${}^{s}R_c$ ≤ 6m, it is only known that overtopping may be expected, but no reliable discharges can be quantified with the developed model.

The second dataset is related to a rubble mound structure armoured with rocks. The classifier simulation is performed for values of 0.25m ≤ ${}^{s}R_c$ ≤ 4.2m (see table 4.28).

The result consists of a classifier prediction of negligible overtopping for values of ${}^{s}R_c > 2$m. For values of ${}^{s}R_c \leq 2$m consistent significant overtopping is predicted.
In figure 4.49 the final combined classifier-quantifier prediction is shown. It concerns the same figure as figure 4.34, where the classifier information is added.

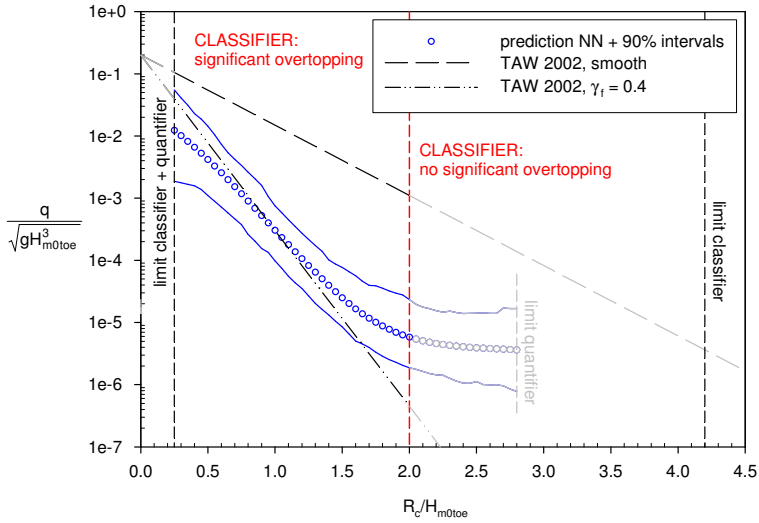

Figure 4.49 Combined classifier-quantifier prediction of overtopping at rubble mound structure with rocks

The previously obtained overtopping predictions for values of ${}^{s}R_c > 2$m are represented in figure 4.49 in light grey. As the classifier predicts zero or insignificant overtopping for these crest heights, the corresponding quantifier predictions should not be considered. The outcome of the combined classifier-quantifier network can thus be summarised as follows:

- The classifier only predicts significant overtopping at the considered rubble mound structure under previously specified wave attack for values of $0.25\text{m} \leq {}^{s}R_c \leq 2\text{m}$. For values of $2\text{m} < {}^{s}R_c \leq 4.2\text{m}$ no significant overtopping is expected. For values of ${}^{s}R_c > 4.2$m and values of ${}^{s}R_c < 0.25$m the classifier is not able to make a reliable classification.
- For values of $0.25\text{m} \leq {}^{s}R_c \leq 2\text{m}$ the quantifier can be used to predict values for the overtopping discharges. The results are represented in blue in figure 4.49.

It is clear from figure 4.49 that the obtained result with the combination classifier-quantifier is a significant improvement over the original result obtained by the quantifier only.

The third synthetic dataset is related to overtopping at a vertical wall. Analogously to the smooth dike, a simulation by the classifier is performed for 0m ≤ ${}^{s}R_c$ ≤ 6m (see table 4.28), resulting in a consistent significant overtopping classification.
Figure 4.50 shows the combined classifier-quantifier prediction. It concerns the same figure as figure 4.35, where the classifier information is added.

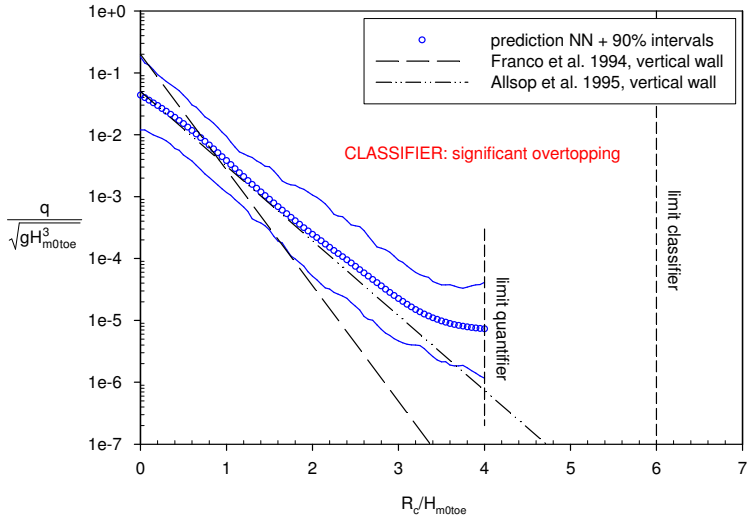

Figure 4.50 Combined classifier-quantifier prediction of overtopping at vertical wall

Analogously to the results obtained for the dike, it can be stated that:

- Overtopping at the considered vertical wall under previously specified wave attack may be expected at least for values of ${}^{s}R_c$ up to 6m. For higher values of ${}^{s}R_c$ the classifier is not able to make a reliable classification.
- The predictions obtained with the quantifier for values of 0m ≤ ${}^{s}R_c$ ≤ 4m are shown in figure 4.50. For values of 4m < ${}^{s}R_c$ ≤ 6m, it is only known that overtopping may be expected, but no reliable discharges can be quantified with the developed model.

Finally, the fourth dataset is related to overtopping at a recurve wave wall. The classifier simulation is performed for values of ${}^{s}R_c$ up to 4.2m (see table 4.28). As the classifier has the same ranges of applicability as the quantifier for values of γ_f, also for the classifier no reliable simulation is possible for values of 0.5m < ${}^{s}R_c$ < 0.5833m (see section 4.6.9.3).

For values of ${}^{s}R_c$ < 3.5m (and ≤ 0.5m or ≥ 0.5833m), the classifier predicts significant overtopping. For simulated values of ${}^{s}R_c$ > 3.5m, consistent negligible overtopping discharges are predicted.
The combined classifier-quantifier prediction is shown in figure 4.51. It concerns the same figure as figure 4.36, where classifier information is added.

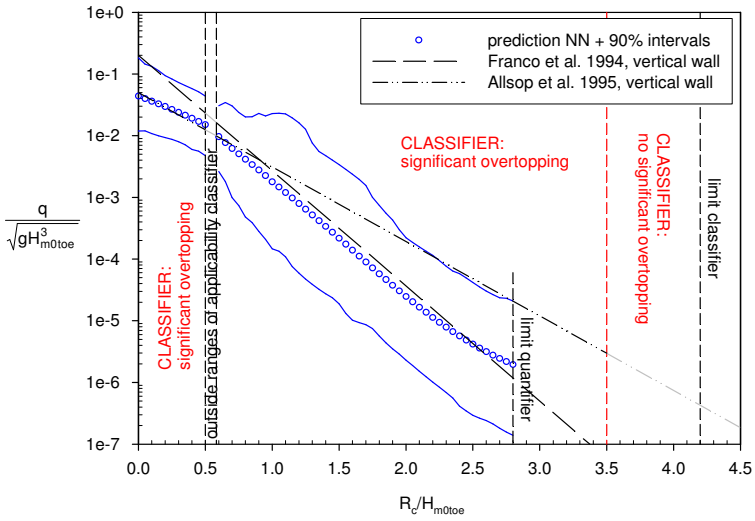

Figure 4.51 Combined classifier-quantifier prediction of overtopping at recurved wall

The results can be summarised as follows:

- Overtopping at the considered recurve wall under previously specified wave attack is expected for values of 0m ≤ ${}^{s}R_c$ ≤ 0.5m and 0.5833m ≤ ${}^{s}R_c$ ≤ 3.5m. For values of 3.5m < ${}^{s}R_c$ ≤ 4.20m, no significant overtopping is expected. For values of 0.5m < ${}^{s}R_c$ < 0.5833m and for values of ${}^{s}R_c$ > 4.20m the classifier is not able to make a reliable classification.
- The developed quantifier predicts corresponding overtopping discharges as represented in figure 4.51. A prediction is only available for values of 0m ≤ ${}^{s}R_c$ ≤ 0.5m and 0.5833m ≤ ${}^{s}R_c$ ≤ 2.8m. For values of 2.8m < ${}^{s}R_c$ ≤ 3.5m, it is only known that overtopping may be expected, but no discharges can be quantified.

The combined classifier-quantifier prediction of the 4 considered datasets shows that by adding the classifier as filter for the network, large overpredictions by the

quantifier may be avoided. In section 4.6.9.3 it was concluded that the quantifier prediction resulted especially for the rubble mound structure armoured with rocks in overpredictions of the overtopping discharges for larger values of ${}^{s}R_{c}$. This section shows that the classifier avoids these overpredictions by filtering the input for the quantifier up to values of ${}^{s}R_{c} \leq 2$m. The classifier offers a solution here for the fact that the quantifier seems to have difficulties predicting low overtopping discharges.

As the selection criterion of the classifier is very strict for zero overtopping predictions (i.e. only if more than 55 bootstrap models predict zero or negligible overtopping, a data point is assigned to class -1), the classifier is inclined to predict non-zero overtopping at the zero border. However, the choice of this 'safe' selection criterion avoids that large overtopping measurements are classified as zero.

CHAPTER 5
GENERAL CONCLUSIONS AND RECOMMENDATIONS FOR FURTHER RESEARCH

5.1 General conclusions

5.1.1 Problem formulation and approach

Wave overtopping is a critical factor in crest level design of coastal structures. Reliable and robust prediction methods are indispensable to provide safety of densely populated coastal regions in the near future.

Nowadays, empirical models developed based on small scale laboratory experiments, are most frequently used for overtopping predictions at coastal structures. A drawback of these models is that they are only valid for specific structure types, and within a restricted range.

In this thesis this problem is dealt with by developing a prediction method able to predict wave overtopping at a variety of structure types, with an extensive range of applicability.

The lack of reliable, generally applicable prediction methods, as well as the presumption that small scale overtopping measurements might be subject to model and scale effects, were on the basis of the set-up of the EC project CLASH (January 2002 - December 2004, www.clash-eu.org, see De Rouck et al., 2005). The intention of CLASH was to improve the knowledge on the phenomenon of wave overtopping. One of the objectives enclosed the set-up of an extensive database on wave overtopping. The set-up of this database was the first aim of this thesis and has been described in detail in chapter 3 of this work. The development of the generally applicable overtopping prediction method described in chapter 4 of this thesis is performed separately from CLASH.

5.1.2 Results and conclusions

Conclusions have been formulated in each chapter for specific parts of this thesis. In order to obtain an overall view of the outcome of the performed research, in this final chapter the most important results and conclusions are compiled. It will be shown that the objectives as formulated in chapter 1 are met.
The two main results of this thesis are emphasised:

- an extensive, screened overtopping database composed of overtopping measurements at a variety of coastal structures, and
- a generally applicable prediction method for wave overtopping, based on the extensive database and composed of 2 subsequent neural models

The objectives as formulated in chapter 1 are repeated one by one, with corresponding results and conclusions.

5.1.2.1 objective 1

→ *to carry out a literature survey on existing models for wave overtopping, with the specific goal to investigate the parameters influencing the phenomenon of wave overtopping*

A concise summary of the research performed on the phenomenon of wave overtopping since halfway the previous century is given in chapter 2 of this work.
The most important existing models predicting mean overtopping discharges, q in $m^3/s/m$, are described. Empirical models, of which the simple regression models are most frequently applied, were distinguished from numerical models. In view of setting up a database describing overtopping tests by means of a restricted number of parameters, special attention was given to parameters which were found to influence the overtopping phenomenon. This resulted in a list of wave parameters, structural parameters and an environmental parameter. The obtained knowledge contributed to the set-up of the schematisation procedure in chapter 3.
In addition, chapter 2 describes the more recent research performed on the distribution of individual overtopping waves.
Finally, chapter 2 treats existing knowledge on tolerable overtopping limits, set up for mean overtopping discharges as well as for individual overtopping volumes. These limits were further used in this thesis to assess overtopping measurement accuracies and the prediction capacity of neural models.

5.1.2.2 objective 2

→ *to gather as much existing data as possible on overtopping measurements, and to screen these data on consistency, in order to get a homogeneous collection of data on overtopping measurements*

The gathering of existing overtopping data is performed in the framework of the CLASH project, and is described in chapter 3 of this work.
Within the 3 year duration of CLASH, over 10000 overtopping tests were gathered. Many data originate from CLASH partners, but also data from non-CLASH institutes within Europe as well as from outside Europe contribute to this huge dataset. Both publicly available data, often related to basic research and already described in literature, and confidential reports, in most cases related to overtopping tests performed for specific sites and practical situations, were considered. Visits to the involved authorities were performed during this period to get the information needed. The comprehensive task of studying and screening all these data resulted in a homogeneous, large dataset, available as basis for the overtopping database.

5.1.2.3 objective 3

→ *to set up a database on wave overtopping by schematising each single overtopping test of the gathered data by means of a fixed number of parameters, where information on the wave characteristics, the structure geometry, as well as the reliability of the test is included*

The compilation of the final CLASH database is described in chapter 3 of this work. For each overtopping test a fixed number of parameters was included in the database, summarising the most important information of the test. The main difficulty consisted of choosing adequate parameters to describe the overtopping tests. Although various schematisation methodologies were tried, only the final schematisation procedure where each overtopping test is included in the database by means of 31 parameters is incorporated in this work. Besides structural parameters and wave parameters, also some general parameters were assigned to each test. A first general parameter accounts for the reliability of the test, a second one for the complexity of the overtopping structure. Both parameters were further used for the development of the neural models. In addition, an overall view of the lay-out and the contents of the finalised database is given in chapter 3.

The final overtopping database, consisting of 10532 parameterised overtopping tests from 163 independent test series, is the first of the two main results of this thesis. The database is available in spreadsheet format on the enclosed CD-ROM. The intention of this extensive database on wave overtopping entries is dual:

- The database provides a wealth of data to researchers, especially to those studying the phenomenon of wave overtopping, and gives an inventory of the many reliable overtopping tests ever performed, independent of any place or time. It concerns a unique compilation of data, never before such effort was made to gather and screen so many overtopping data.
- The database is used as basis for the development of two generic prediction methods for overtopping: the CLASH prediction method (see Pozueta et al., 2004a and 2004b) and the prediction method composed of 2 subsequent neural models developed as a part of this thesis (see chapter 4 of this work).

Although the more fundamental goal of the CLASH database was to serve as input for a neural prediction method for overtopping, the importance of the database as a stand-alone tool should be stressed. The database creates e.g. the possibility to extract data, related to specific structures or groups of structures, to function as validation data for new analytical or numerical research on overtopping. However, the database may also be useful for non-overtopping related research. The possibility to compare deep water wave characteristics with wave characteristics at the toe of the structure is only an example.

5.1.2.4 objective 4

→ *to develop a generally applicable prediction method for wave overtopping in small scale tests, by training neural models with data from the overtopping database*

The development of a neural prediction method for wave overtopping at coastal structures, based on the extensive database, is described in chapter 4 of this work. A final neural prediction method composed of 2 subsequent neural models is proposed:

- The 'classifier' predicts whether overtopping occurs or not, i.e. $q = 0$ $m^3/s/m$ or $q > 0$ $m^3/s/m$.
- *If* the classifier predicts overtopping $q > 0$ $m^3/s/m$, *then* the 'quantifier' is used to determine the mean overtopping discharge, expressed as q in $m^3/s/m$, i.e. the classifier serves as filter for the application of the quantifier.

Not all of the information included in the database was used for the set-up of the neural prediction method. Prototype measurements were excluded from the training process of the models, resulting in a prediction method for overtopping in small scale tests. In addition, only 17 of the 31 parameters included in the CLASH database were used for the development of the final neural prediction method, i.e.:

- 13 input parameters, consisting of wave parameters as well as structural parameters,
- 1 output parameter, q in $m^3/s/m$, which is preprocessed for the quantifier and replaced by 2 discrete values for the classifier,
- 1 scaling parameter used to scale the input parameters, and for the quantifier also the output parameter, according to the Froude model law (to $H_{m0\ toe} = 1m$),
- 2 general parameters, i.e. the reliability factor RF and the complexity factor CF, combined into 1 weight factor, used to force the classifier and quantifier to draw more attention to overall more reliable data.

The gathered information within CLASH regarding model and scale effects affecting small scale overtopping measurements (see Kortenhaus et al., 2005), may be used to estimate prototype overtopping discharges corresponding to the small scale neural predictions.

Chapter 4 describes in detail the successive steps undertaken to obtain the final neural prediction method. For both neural models, the classifier and the quantifier, a multilayer perception with 1 hidden layer was proposed. After the determination of an optimal network lay-out for both models, the bootstrap technique was applied, allowing an optimal use of the available data. In addition, the bootstrap method resulted in percentile intervals for the quantifier, providing a certain probability around the point prediction. For the classifier an optimised decision boundary, which is inclined to predict non-zero overtopping in case of doubt (prediction on the safe side), was determined with the bootstrap method. Application ranges for both classifier and quantifier were set up, which avoids the use of the models outside their ranges of applicability with possibly pointless results.

It was found that the additional use of the classifier in the prediction method results in a significant improvement over the use of the single quantifier. Due to the filter-effect of the classifier, which is able to distinguish situations where no or negligible overtopping occurs from significant overtopping situations, large overpredictions by the quantifier are avoided.

The final neural prediction method is the second of the two main results of this thesis. Given the necessary 14 input parameters (transposed by the neural prediction method to 13 scaled input parameters to $H_{m0\ toe} = 1m$), the prediction method provides a prediction of the mean overtopping discharge to be expected in a small scale test, as well as an indication of the reliability of this prediction.

5.1.2.5 objective 5

→ *objective 5: to check the performance of the developed prediction method based on*

- *the available CLASH prototype measurements and the CLASH scaling procedure accounting for model and scale effects,*
- *synthetic datasets considering overtopping at specific structure types for which the overtopping performance is known.*

The developed neural prediction method has been validated in chapter 4 for some specific test series.
The first test series concern the CLASH prototype measurements. The combined classifier-quantifier results obtained for the CLASH prototype data were corrected according to expected model and scale effects (see CLASH scaling procedure, Kortenhaus et al., 2005).
For the Samphire Hoe case no corrections for model and scale effects were applied to the combined classifier - quantifier outcome. The obtained results were found to correspond reasonably well with the prototype measurements.
For the Ostia and Zeebrugge case, both rough sloping structure types, the combination neural prediction method - CLASH scaling procedure was found to generally overpredict the smallest measured overtopping discharges. For the Ostia case the overpredictions are rather small and are suggested to originate from the vicinity of the limit of applicability of the quantifier. It may be concluded that a good result is obtained for the Ostia case.
For the Zeebrugge case rather large overpredictions were found. It is not clear whether these overpredictions originate from the quantifier prediction or from the scaling factors included in the CLASH scaling map. Further research on both, the Zeebrugge quantifier predictions and the scaling factors, is therefore advised.

Additional test series concern some synthetic datasets. Overtopping at a smooth dike, a rough sloping structure, a vertical wall and a recurve wall were studied for a varying dimensionless crest height. Comparison of the combined classifier - quantifier predictions with overtopping discharges proposed by existing empirical models for these synthetic datasets showed that the neural prediction method performs very well for the considered structure types. In addition, as expected, the percentile intervals were found to be wider in sparsely occupied parts of the input space.
Although it was found that the classifier predicts rather ‘safe’ overtopping, which was exactly the intention of the decision criterion, it was shown that the combined classifier-quantifier result clearly improves the single quantifier result.

5.2 Recommendations for further research

In the previous section it has been shown that the proposed objectives are met. However, further research on specific parts of the work performed is advised. This section gives some recommendations for further research.

The final neural prediction method was found to perform well for the considered test series. However, the performance of the developed method should be checked in more detail, especially with newly available overtopping measurements. It is expected that the results of such research will lead to minor adaptations of the developed network. The ranges of applicability may for example be further restricted or extended for specific parameters or parameter combinations. It is the aim to treat this subject in future research.

The specific influence of an input parameter of the neural prediction method on overtopping at specific structure types can be derived by simulating synthetic datasets in which this single input parameter is altered. The obtained results may be compared to existing empirical formulae describing the influence of the considered input parameter. Also new small scale overtopping measurements performed with regard to this specific parameter influence may provide additional validation information.

Based on the available CLASH prototype measurements it was concluded that the combination neural prediction method - CLASH scaling procedure results in prototype predictions which are sometimes too high. There may be a contribution to this overprediction from both the neural prediction method and the scaling procedure. Especially for small overtopping discharges a contribution of the neural prediction method in these overpredictions is suspected. It is therefore recommended to look in more detail to the performance of the neural prediction method for small overtopping discharges, i.e. ‘Does the prediction method indeed predict too high overtopping discharges in some cases?’ and ‘Is there a possible way to deal with this problem?’. As the present CLASH scaling procedure is based on a limited number of prototype measurements, and as the validation time of the procedure within CLASH was rather restricted, it is advisable to perform additional research on this subject. Prototype overtopping measurements in combination with model tests are needed in this context.

The overtopping database is composed of data from 163 independent test series. It has not been studied to which extent data from one series are dependent of each other. All 10532 tests were assumed to be independent of each other. However, it may be expected that this assumption is not completely correct. How big the impact is of this interdependency on the final outcome of the neural prediction method is a topic which should be investigated.

The overtopping database contains a restricted number of small scale model tests with artificial wind generation. These tests were not considered in this work, as at this moment little is known about the correct scaling procedure for wind in laboratory. Future research on this specific subject could lead to an additional influencing parameter in the neural prediction method, i.e. wind.

An important benefit of the developed overtopping prediction method concerns its overall applicability, i.e. overtopping at any coastal structure (included in the training process) may be predicted.
However, as previous studies to the overtopping phenomenon have shown, the physics related to overtopping at a sloping structure differ from those related to overtopping at a vertical wall. In the literature survey in chapter 2 it was found that this results in different parameters influencing the overtopping phenomenon. In addition, vertical structures are less represented in the database than sloping structures, which may result in a worse performance for the former structures.
Therefore, it might be advantageous to split up the developed overtopping prediction method in two separate prediction models: one model to predict wave overtopping at sloping structures versus another model to predict wave overtopping at vertical walls. Both models might consist of different input parameters, leading to two more simple models. It would be interesting to check the performance of both separate structure types.
A drawback of the proposed approach is the difficulty of assessing e.g. composite structures to one of both structure types. The behaviour of such structures is not easy to determine and moreover may be dependent on the (even slightly) varying water level.

Finally, it should be mentioned that the CLASH database which was set up contains a wealth of information for researchers in several research areas. Keeping this dataset up to date, i.e. adding new overtopping information in the future, would be very interesting for future research.

ANNEX
MATRIX PLOT

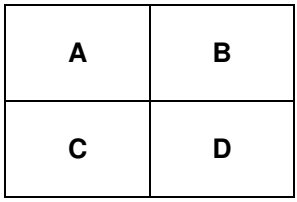

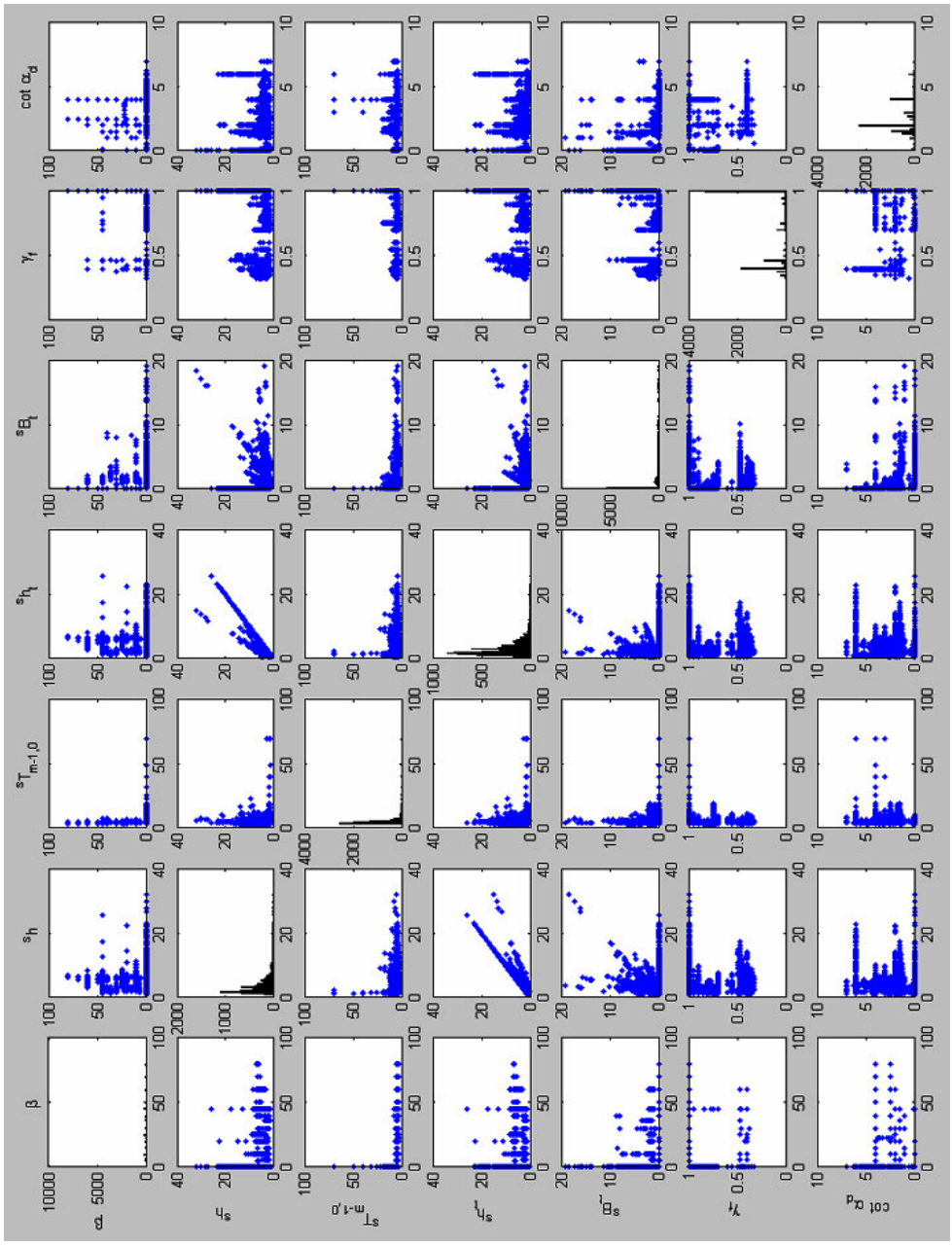
A

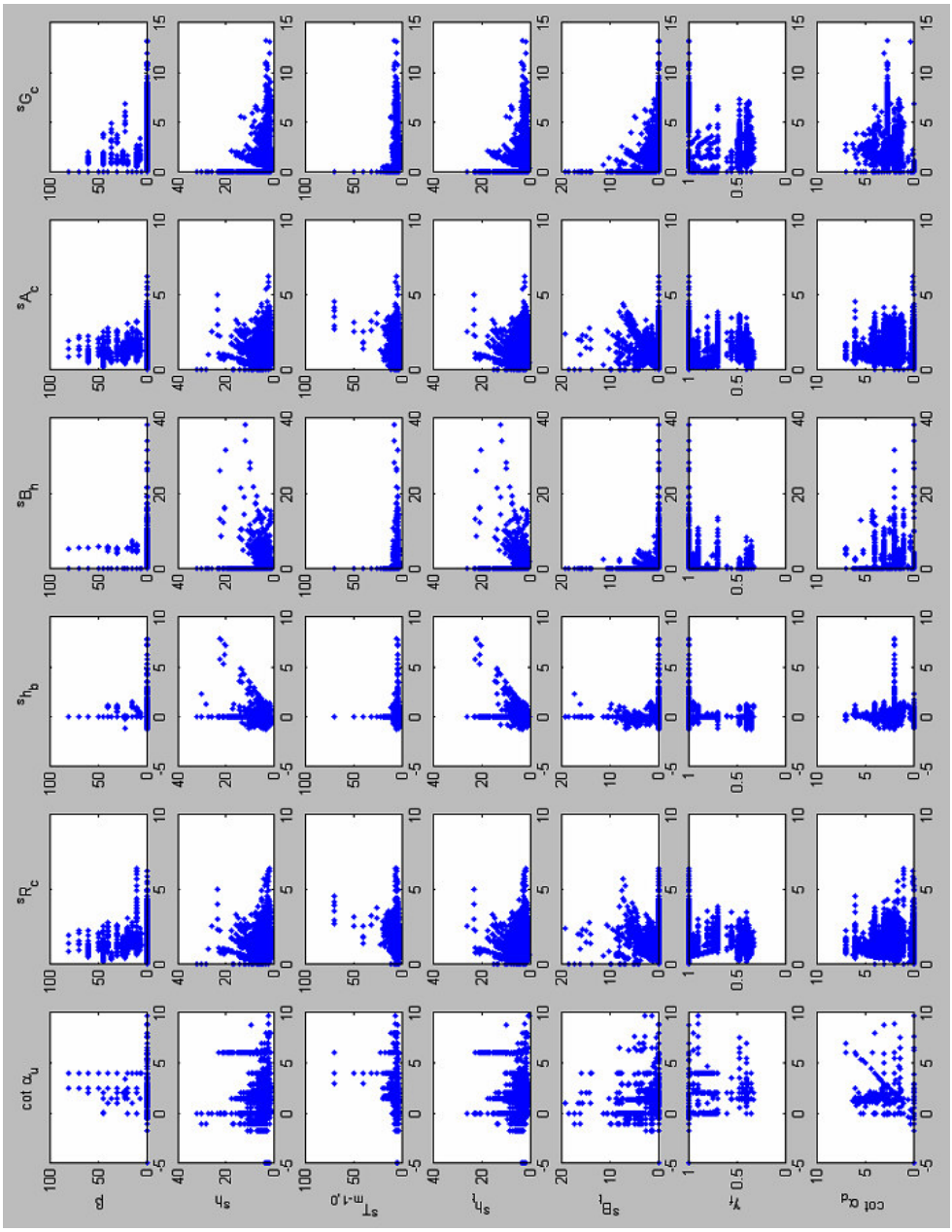
B

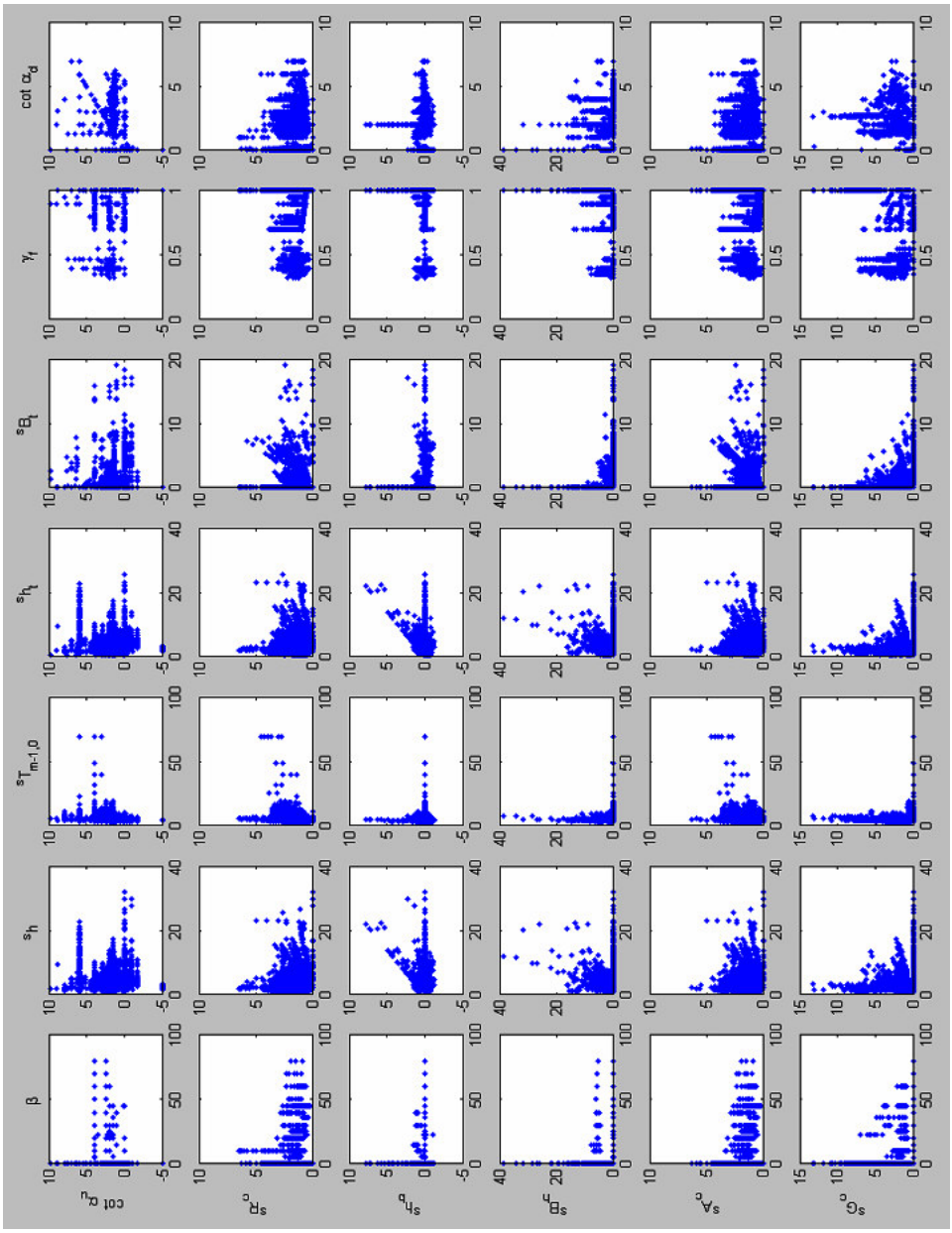
β
s_h
$s_{T_{m-1,0}}$
s_{h_t}
s_{B_t}
γ_f
cot α_d
cot α_u
s_{R_c}
s_{h_b}
s_{B_c}
s_{A_c}
s_{G_c}

C

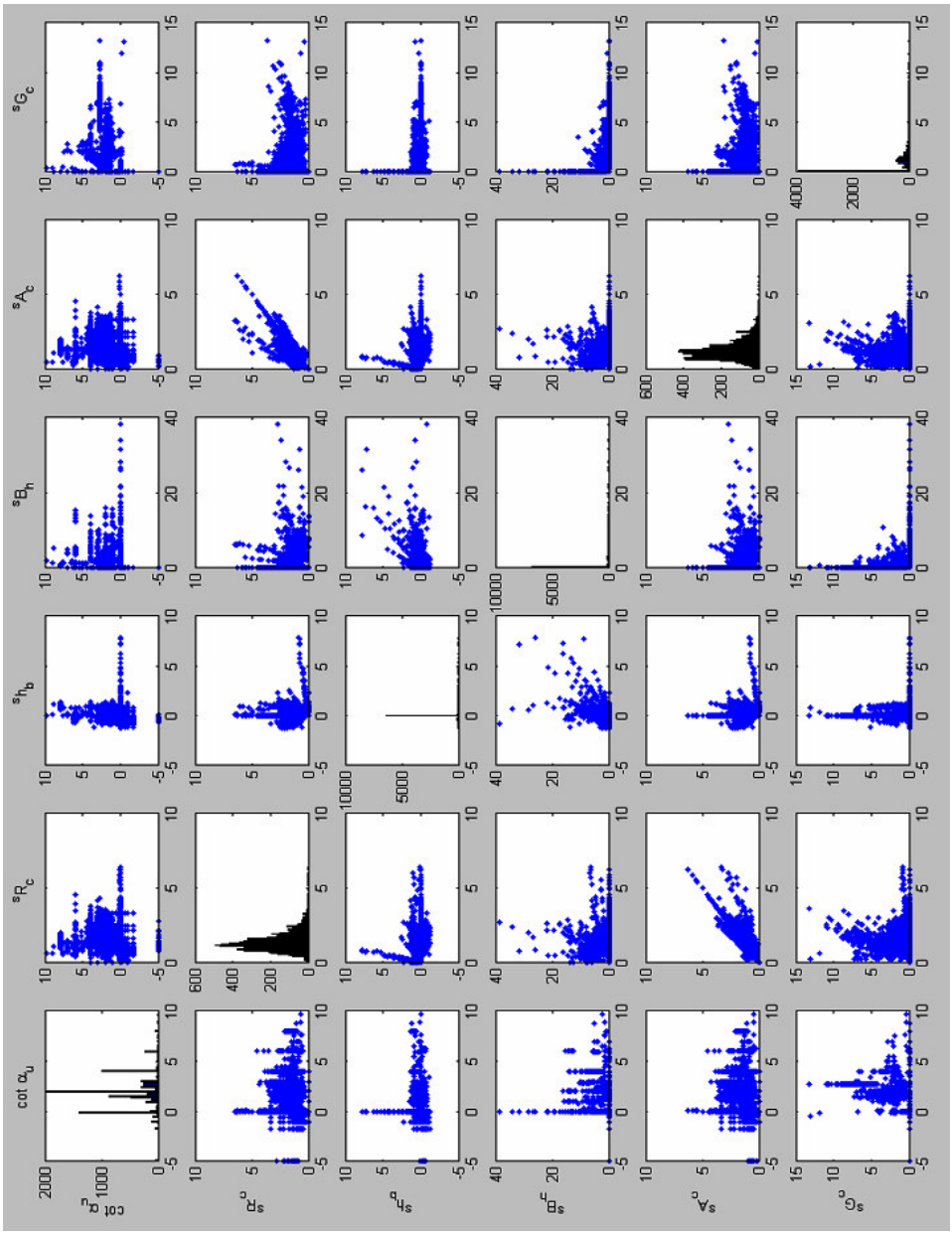

D

REFERENCES

Abramowitz, M., Stegun, I.A., 1964. Handbook of Mathematical Functions. Dover Publications, New York, USA.

Ahrens, J., 1977. Prediction of irregular wave overtopping, US Army Corps of Engineers CETA 77-7, Coastal Engineering Research Center, Fort Belvoir, Virginia, USA.

Ahrens, J.P., Heimbaugh, M.S., Davidson, D.D., 1986. Irregular wave overtopping of seawall/revetment configurations, Roughans Point, Massachusetts, USA, final report of experimental model investigation, Coastal Engineering Research Centre, Department of the Army, Mississippi.

Ahrens, J. P., Heimbaugh, M. S., 1988. Seawall Overtopping Model, Proceedings of the 21st International Conference on Coastal Engineering, Malaga, Spain, ASCE, pp. 795-806.

Allsop, N.W.H., Besley, P., Madurini, L., 1995. Overtopping performance of vertical and composite breakwaters, seawalls and low reflection alternatives, Paper to the final MCS Project Workshop, Alderney, United Kingdom.

Allsop, N.W.H., 2005. Report on hazard analysis, CLASH WP6 report, HR Wallingford, United Kingdom.

Aminti, P., Franco, L., 1988. Wave overtopping on rubble mound breakwaters, Proceedings of the 21st International Conference on Coastal Engineering, Malaga, Spain, ASCE, pp. 770-781.

Banyard, L., Herbert, D.M., 1995. The effect of wave angle on the overtopping of seawalls, Report SR396, HR Wallingford, United Kingdom.

Barron, A.R., 1993. Universal approximations bounds for superposition of a sigmoidal function, Institute of Electrical and Electronics Engineers, Transactions on Information Theory, Vol. 39, No. 3, pp. 930-945.

Battjes, J.A., Groenendijk, H.W., 2000. Wave height distributions on shallow foreshores, Coastal Engineering, No. 40, pp. 161-182.

Beji, S., Battjes, J.A., 1993. Experimental investigation of wave propagation over a bar, Coastal Engineering, No. 19, pp. 151-162.

Besley, P., Stewart, T., Allsop, N.W.H., 1998. Overtopping of vertical structures: new prediction methods to account for shallow water conditions, Proceedings of the International Conference on Coastlines, structures and breakwaters, ICE, Thomas Telford, London, UK, pp. 46-57.

Besley, P., 1999. Overtopping of seawalls - design and assessment manual, R & D Technical Report W178, Environment Agency, Bristol, United Kingdom, ISBN 1 85705 069 X.

Bierens, R.W.P., 2002. Sedimentation in the Maasmond, dredging prediction by neural networks, PIANC Bulletin, No. 109.

Bishop, C.M., 1995. Neural networks for pattern recognition, Oxford University Press, Oxford, United Kingdom.

Booij, N., Ris, R.C., Holthuijsen, L.H., 1999. A third-generation wave model for coastal regions, Part I, Model description and validation, Journal of Geophysical Research, No. 104, C4, pp. 7649-7666.

Bouma, J.J., Schram, A., François, D., 2004. Report on socio-economic impacts, CLASH WP6 report, Ghent University, Belgium.

Bradbury, A.P., Allsop, N.W.H., Stephens, R.V., 1988. Hydraulic performance of breakwater crown walls, Report No. SR146, HR Wallingford, United Kingdom.

Bruce, T., Allsop, N.W.H., Pearson, J., 2001. Violent overtopping of seawalls - extended prediction methods, Proceedings of the International Conference on Breakwaters, coastal structures and coastlines, ICE, Thomas Telford, London, pp. 245-255.

Bruce, T., Allsop, N.W.H., Pearson, J., 2002. Hazards at coast and harbour seawalls - velocities and trajectories of violent overtopping jets, Proceedings of the 28th International Conference on Coastal Engineering, Cardiff, United Kingdom, ASCE, pp. 2216-2226.

Carter, D.J.T., Draper, L., 1988. Has the Northeast Atlantic become rougher ?, Nature, No. 332 (6164), p. 494.

Causon, D.M., Ingram, D.M., Mingham, C.G., Yang G., Pearson R.V., 2000. Calculation of Shallow Water Flows Using a Cartesian Cut Cell Approach, Advances in Water Resources, Vol. 23, pp. 545-562.

Cornett, A., Li, Y., Budvietas, A., 1999. Wave overtopping at chamfered and overhanging vertical structures, Proceedings of the International Workshop on Natural Disasters by Storm Waves and Their Reproduction in Experimental Basins, Kyoto, Japan, 14 pp.

De Gerloni, M., Cris, E., Franco, L., Passoni, G., 1991. The Safety of Breakwaters Against Wave Overtopping, Proceedings of the International Conference on Coastal structures and breakwaters, ICE, Thomas Telford, London, United Kingdom, pp. 335-342.

Deo, M.C., Gondane, D.S., Sanil Kumar, V., 2002. Analysis of wave directional spreading using neural networks, Journal of Waterway, Port, Coastal and Ocean Engineering, No. 128, pp. 30-37.

Deo, M.C., Jagdale, S.S., 2003. Prediction of breaking waves with neural networks, Ocean Engineering, No. 30, pp. 1163-1178.

De Rouck, J., Boone, C., Van de Walle, B., 2001. Detailed scientific and technical report, OPTICREST MAS03/1031 Final report, Ghent University, Belgium.

De Rouck, J., Geeraerts, J., 2005. CLASH Final Report, Full Scientific and Technical Report, Ghent University, Belgium.

De Waal, J. P., Van der Meer, J. W., 1992. Wave Run-Up and Overtopping on Coastal Structures, Proceedings of the 23rd International Conference on Coastal Engineering, Venice, Italy, ASCE, pp. 1758-1771.

De Waal, J.P., Tönjes, P., Van der Meer, J.W., 1996. Wave overtopping of vertical structures including wind effect, Proceedings of the 25th International Conference on Coastal Engineering, Orlando, USA, ASCE, pp. 2216-2229.

Dodd, N., 1998. A numerical model of wave run-up, overtopping and regeneration, Journal of Waterway, Port, Coastal and Ocean Eng., Vol. 124, No. 2, pp. 73-81.

Douglass, S. L., 1985. Review and comparison of methods for estimating irregular wave overtopping rates, Technical Report CERC-85, Waterways Experiment Station, Vicksburg, USA.

Efron, B., 1982. The Jackknife, the Bootstrap and Other Resampling Plans, Society for Industrial and Applied Mathematics, Philadelphia, USA.

Efron, B., Tibshirani, R.J., 1993. An Introduction to the Bootstrap, Chapman & Hall, New York, USA.

Eldeberky, Y., 1996. Nonlinear transformation of wave spectra in the nearshore zone, Ph.D. thesis, Delft University of Technology, Department of Civil Engineering, The Netherlands.

Endoh, K., Takahashi, S., 1994. Numerically Modelling Personnel Danger on a Promenade Breakwater Due to Overtopping Waves, Proceedings of the 24th International Conference on Coastal Engineering, Kobe, Japan, ASCE, pp. 1016-1029.

Foresee, F. D., Hagan, M. T., 1997. Gauss-Newton Approximation to Bayesian Learning, Proceedings of the International Joint Conference on Neural Networks.

Franco, C., Franco, L., Restano, C., Van der Meer, J.W., 1995. The effect of wave obliquity and shortcrestedness on the overtopping rate and volume distribution on caisson breakwaters, Paper 4.9, MAST2-MCS Project Final Proceedings, University of Hannover, Germany.

Franco, C., 1996. Wave overtopping and loads on caisson breakwater under three-dimensional sea-states, LIP-MAST-TAW Full Final Report, DIIAR, Politecnico di Milano, Milan, Italy.

Franco, C., Franco, L., 1999. Overtopping Formulas for Caisson Breakwaters with Nonbreaking 3D Waves, Journal of Waterway, Port, Coastal, and Ocean Engineering, Vol. 125, No. 2, pp. 98-108.

Franco, L., 1993. Overtopping of vertical breakwaters: results of model tests and admissible overtopping rates, MAST2-MCS, 1st workshop, Madrid, Spain.

Franco, L., 1994. Further results of hydraulic model tests on wave overtopping, MAST2-MCS, 2nd workshop, Politecnico di Milano, Milan, Italy.

Franco, L., De Gerloni, M., Van der Meer, J. W., 1994. Wave Overtopping on Vertical and Composite Breakwaters, Proceedings of the 24th International Conference on Coastal Engineering, Kobe, Japan, ASCE, pp. 1030-1045.

Franco, L., Briganti, R., Bellotti, G., 2004. Report on full scale measurements, Ostia, 2nd full winter season, CLASH WP3 report, Modimar, Rome, Italy.

Führböter, A., Sparboom, U., Witte, H.H., 1989. Groβer Wellenkanal Hannover: Versuchsergebnisse über den Wellenauflauf auf glatten und rauhen Deichböschungen met der Neigung 1:6, Die Küβte, Archive for Research and Technology on the North Sea and Baltic Coast. (in German)

Fukuda, N., Uno, T., Irie, I., 1974. Field Observations of Wave Overtopping of Wave Absorbing Revetment, Coastal Engineering in Japan, Vol. 17, pp. 117-128.

Geeraerts, J., Boone, C., 2004a. Report on full scale measurements Zeebrugge, 2nd full winter season, CLASH WP3 report, Ghent University, Belgium.

Geeraerts, J., De Rouck, J., 2004b. Report on additional tests, part C, CLASH WP4 report, Ghent University, Belgium.

Geeraerts J., Willems, M., 2004c. Final report on laboratory measurements, Ostia, CLASH WP4 report, Ghent University, Belgium.

Goda, Y., 1970. Estimation of the Rate of Irregular Overtopping of Seawalls, Report of Port and Harbor Research Institute, Vol. 9, No. 4. (in Japanese)

Goda, Y., Nagai, K., 1974. Investigations of the statistical properties of sea waves with field and simulation data, Report of Port and Harbour Research Institute, Vol. 13 (1), pp. 3-37. (in Japanese)

Goda, Y., Kishira, Y., Kamiyama, Y., 1975. Laboratory investigation on the overtopping rate of seawalls by irregular waves, Report of the Port and Harbour Research Institute, Vol. 14(4), pp. 3-44. (in Japanese)

Goda, Y., 1985. Random Seas and Design of Maritime Structures, University of Tokyo Press, Japan. ISBN 0-86008-369-1.

González-Escrivá, J.A., Medina, J.R., 1999. Wave and wind tunnel testing for analysis of run-up and overtopping, Proceedings of the International Conference on Coastal Structures, Santander, Spain, pp. 413-420.

González-Escrivá, J. A., Medina, J. R., Garrido, J., De Rouck, J., 2002. Wind Effects on Runup and Overtopping: Influence on breakwater crest design, Proceedings of the 28th International Conference on Coastal Engineering, Cardiff, United Kingdom, ASCE, pp. 2251-2263.

Goutte, C., 1997. Note on free lunches and cross-validation, Neural Computation, Vol. 9, pp. 1211-1215.

Hasselmann, K., 1974. On the spectral dissipation of ocean waves due to whitecapping, Boundary-Layer Meteorology, Vol. 6, 1-2, pp. 107-127.

Hasselmann, S., Hasselmann, K., Allender, J.H., Barnett, T.P., 1985. Computations and parameterizations of the nonlinear energy transfer in a gravity wave spectrum, Part II, Parameterizations of the nonlinear transfer for application in wave models, Journal of Physical Oceanography, Vol. 15(11), pp. 1378-1391.

Hebsgaard, M., Sloth, P., Juhl, J., 1998. Wave overtopping of rubble mound breakwaters, Proceedings of the 26th International Conference on Coastal Engineering, Copenhagen, Denmark, ASCE, pp. 2235-2248.

Hedges, T.S., Reis, M.T., 1998. Random wave overtopping of simple sea walls: a new regression model, Water, Maritime and Energy Journal, Proceedings of ICE, Vol. 130, pp. 1-10.

Herbert, D.M., 1993. Wave overtopping of vertical walls, Report SR 316, HR Wallingford, United Kingdom.

Herbert, D.M., Owen, M.W., 1995. Wave overtopping of sea walls - further research, Advances in Coastal structures and breakwaters, ICE, Thomas Telford, London, United Kingdom, pp. 81-92.

Herbert, D.M., 1996. The overtopping of seawalls, a comparison between prototype and physical model data, Report TR22, HR Wallingford, United Kingdom.

Hirt, C.W., Nichols, B.D., 1981. Volume of Fluid (VoF) methods for dynamics of free boundaries, Journal of Computational Physics, Vol. 39, pp. 201-225.

Holthuijsen, L.H., de Boer, S., 1988. Wave forecasting for moving and stationary targets, Computer modelling in Ocean Engineering, pp. 231-234.

Hornik, K., Stinchcombe, M., White, H., 1989. Multilayer feedforward networks are universal approximators, Neural networks, Vol. 2, pp. 359-366.

IAHR Working Group on Wave Generation and Analysis, 1989. List of sea-state parameters, Journal of Waterway, Port, Coastal, and Ocean Engineering, Vol. 115(6), pp. 793-808.

Ingram, D., 2005. Guidance on the use of Numerical Models of Wave Overtopping, CLASH internal report, Manchester Metropolitan University, United Kingdom.

Jain, A., Mao, J., Mohiuddin, K., 1996. Artificial neural networks: a tutorial, Computer, Institute of Electrical and Electronics Engineers, Vol. 29, No. 3, pp. 31-44.

Jensen, O.J., Sorensen, T., 1979. Overspilling/Overtopping of Rubble Mound Breakwaters, Results of Studies, Useful in Design Procedures, Coastal Engineering, Vol. 3, pp. 51-65.

Jensen, O.J., 1984. A Monograph on Rubble Mound Breakwaters, Danish Hydraulic Institute, Denmark.

Juhl, J., 1992. Investigations on the effect of structural measures on wave impact forces and overtopping, Proceedings 3rd Project Workshop, MAST I, G6-S/Project 2: Wave impact loading on vertical structures, Hannover, Germany, 18 pp.

Juhl, J., Sloth, P., 1994. Wave overtopping of breakwaters under oblique waves. Proceedings of the 24th International Conference on Coastal Engineering, Kobe, Japan, ASCE, pp. 1182-1196.

Kelecy, F.J., Pletcher, R.H., 1997. The Development of a Free Surface Capturing Approach for Multidimensional Free Surface Flows in Closed Containers, Journal of Computational Physics, Vol. 138, pp. 939-980.

Kikkawa, H., Shi-igai, H., Kono, T., 1968. Fundamental study of wave overtopping on levees, Coastal Engineering in Japan, Vol. 11, pp. 107-115.

Kortenhaus, A., Haupt, R., Oumeraci, H., 2001. Design aspects of vertical walls with steep foreland slopes, Proceedings of the International Conference on Breakwaters, coastal structures and coastlines, ICE, Thomas Telford, London, United Kingdom, pp. 221-232.

Kortenhaus, A., Pearson, J., Bruce, T., Allsop, N.W.H., Van der Meer, J.W., 2003. Influence of parapets and recurves on wave overtopping and wave loading of complex vertical walls, Proceedings of the International Conference on Coastal Structures, Portland, USA, pp. 369-381.

Kortenhaus, A., Medina, J., González-Escrivá, J., Garrido, J., 2004. Final report on laboratory measurements, Zeebrugge, CLASH WP4 report, Leichtweiβ Institute for Hydraulics, Technical University of Braunschweig, Germany.

Kortenhaus, A., Van der Meer, J.W., Burcharth, H.F., Geeraerts, J., Pullen, T., Ingram, D., Troch, P., 2005. Quantification of measurement errors, model and scale effects related to wave overtopping, CLASH WP7 report, Leichtweiβ Institute for Hydraulics, Technical University of Braunschweig, Germany.

Li, T., Troch, P., De Rouck, J., 2004. Wave Overtopping of a Sea Dike, Journal of Computational Physics, No. 198, pp. 686-726.

Liriano, S.L., Day, R.A., 2001. Prediction of scour depth at culvert outlets using neural networks, Journal of Hydroinformatics, Vol. 3 (4), pp. 231-238.

Longuet-Higgins, M.S., 1952. On the statistical distributions of heights of sea waves, Journal of Marine Research, No. 11 (3), pp. 245-266.

Lykke Andersen, T., Burcharth, H.F., 2004a. Report on additional tests, part A, CLASH WP4 report, Aalborg University, Aalborg, Denmark.

Lykke Andersen, T., Burcharth, H.F., 2004b. Report on additional tests, part D, CLASH WP4 report, Aalborg University, Aalborg, Denmark.

MacKay, D.J.C., 1992a. Bayesian interpolation, Neural Computation, No. 4(3), pp. 415-447.

MacKay, D.J.C., 1992b. A practical Bayesian framework for backpropagation networks, Neural Computation, No. 4(3), pp. 448-472.

Mase, H., Sakamoto, M., Sakai, T., 1995. Neural network for stability analysis of rubble mound breakwaters, Journal of Waterway, Port, Coastal, and Ocean Engineering, Vol.121 (6), pp.294-299.

Mase, H., Kitano, T., 1999. Prediction model for occurrence of impact wave force, Ocean Engineering, Vol. 26, pp. 949-961.

Medina, J.R., 1998. Wind effects on run-up and breakwater crest design, Proceedings of the 26th International Conference on Coastal Engineering, Copenhagen, Denmark, ASCE, pp. 1068-1081.

Medina, J.R., 1999. Neural network modelling of runup and overtopping, Proceedings of the International Conference on Coastal Structures, Santander, Spain, pp. 421-429.

Medina, J.R., González-Escrivá, J.A., Garrido, J., 2001. Zeebrugge model tests performed in the UPV, OPTICREST report, Universidad Politécnica de Valencia, Spain.

Medina, J.R., Gonzalez-Escriva, J.A., Garrido, J., De Rouck, J., 2002. Overtopping analysis using neural networks, Proceedings of the 28th International Conference on Coastal Engineering, Cardiff, United Kingdom, ASCE, pp. 2165-2177.

Medina, J.R., Garrido, J., Gómez-Martín, E., Vidal, C., 2003. Armor damage analysis using neural networks, Proceedings of the International Conference on Coastal Structures, Portland, USA, pp. 236-248.

Mingham, C., Causon, D., 1998. High-resolution finite-volume method for shallow water flows, Journal of Hydraulic Engineering, June, pp. 605-614.

Moody, J., 1994. Prediction Risk and Architecture Selection for Neural Networks, in: V. Cherkassky, J.H. Friedman, and H. Wechsler (eds.), From statistics to Neural Networks: Theory and Pattern Recognition Applications, Springer-Verlag NATO ASI Series F, Berlin, Vol. 136.

Oumeraci, H., 1999a. Physical modelling, field measurements and numerical modelling in coastal engineering: synergy or competition?, 2nd German-Chinese Joint Seminar on Recent Developments in Coastal Engineering - Sustainable Development in the Coastal Zone, Tainan, Taiwan, pp. 513-537.

Oumeraci, H., 1999b. Strengths and limitations of physical modelling in coastal engineering - synergy effects with numerical modelling and field measurements. Proceedings Hydralab Workshop on Experimental Research and Synergy Effects with Mathematical Models, Hannover, Germany, pp. 7-38.

Owen, M.W., 1980. Design of seawalls allowing for wave overtopping, Report No. EX 924, HR Wallingford, United Kingdom.

Owen, M. W., Steele, A. A. J., 1991. Effectiveness of recurved wave return walls, Report SR 261, HR Wallingford, United Kingdom.

Panizzo, A., Briganti, R., Van der Meer, J.W., Franco, L., 2003. Analysis of wave transmission behind low-crested structures using neural networks, Proceedings of the International Conference on Coastal Structures, Portland, USA, pp. 555-566.

Pearson, J., Bruce, T., Allsop, W., Kortenhaus, A., Van der Meer, J.W., 2004a. Effectiveness of recurve wave walls in reducing wave overtopping on seawalls and breakwaters, Book of Abstracts of the 29th International Conference on Coastal Engineering, Lisbon, Portugal, ASCE, Paper No 319.

Pearson, J., Bruce, T., Franco, L., Van der Meer, J.W., 2004b. Report on additional tests, part B, CLASH WP4 report, University of Edinburgh, United Kingdom.

Pedersen, J., Burcharth, H.F., 1992. Wave forces on crown walls, Proceedings of the 23rd International Conference on Coastal Engineering, Venice, Italy, ASCE, pp. 1489-1502.

Pedersen, J., 1996. Experimental Study of Wave Forces and Wave Overtopping on Breakwater Crown Walls, Series paper 12, Hydraulics & Coastal Engineering Laboratory, Aalborg University, Denmark.

Pilarczyk, K., Zeidler, R., 1996. Offshore breakwaters and shore evolution control A. Balkema, Rotterdam, The Netherlands, pp. 96-117.

Pozueta, B., Van Gent, M.R.A., Van den Boogaard, H.F.P., 2004a. Neural Network prediction method, CLASH WP8 Neural Network, Delft Hydraulics, The Netherlands.

Pozueta, B., Van Gent, M.R.A., Van den Boogaard, H.F.P., Medina, J.R., 2004b. Final report on generic prediction method, CLASH WP8 report, Delft Hydraulics, The Netherlands.

Pullen, T., 2004a. Report on full scale measurements, Samphire Hoe, TR133, CLASH WP3 report, HR Wallingford, United Kindom.

Pullen, T., 2004b. Final report on laboratory measurements, Samphire Hoe, CLASH WP4 report, HR Wallingford, United Kingdom.

Qian, L., Causon, D.M., Ingram, D.M., Mingham, C.G., 2003. A Cartesian Cut Cell Two-Fluid Method for Hydraulic Flow Problems, Journal of Hydraulic Engineering, No. 129(9), pp. 688-696.

Rice, S.O., 1944. Mathematical analysis of random noise, Reprinted in: Selected Papers on Noise and Stochastic Processes, Dover Publications, New York, USA, 1954, pp.132-294.

Rojas, R., 1996. Neural networks - A systematic introduction, Springer Verlag, Berlin, New York.

Rumelhart, D.E., Hinton, G.E., Williams, R.J., 1986. Learning representations by back-propagation errors, Nature, Vol. 323, pp. 533-536.

RWS, 1993. Het ontwerpen van een bekleding voor een zeedijk, Rijkswaterstaat, Dienst Weg-en Waterbouwkunde, The Netherlands. (in Dutch)

Sakakiyama, T., Kajima, R., 1996. Wave overtopping and stability of armor units under multidirectional waves, Proceedings of the 25th International Conference on Coastal Engineering, Orlando, USA, ASCE, pp. 1862-1875.

Saville, T., Jr., 1955. Laboratory data on wave run-up and overtopping on shore structures, TM-64, Beach Erosion Board, US Army Corps of Engineers, USA.

Schüttrumpf, H., 2001. Wellenüberlaufströmung bei Seedeichen - Experimentelle und Theoretische Untersuchungen, Ph.D. Thesis, Leichtweiβ Institute for Hydraulics, Technical University of Braunschweig, Germany.

Smidth, W.G., Kobayashi, N., Kaku, S., 1992. Profile changes of rock slopes by irregular waves, Proceedings of the 23rd International Conference on Coastal Engineering, Venice, Italy, ASCE, pp. 1559-1572.

Smith, G.M., Seijffert, J.W., Van der Meer, J. W., 1994. Erosion and Overtopping of a Grass Dike: Large Scale Model Tests, Proceedings of the 24th International Conference on Coastal Engineering, Kobe, Japan, ASCE, pp. 2639-2652.

Smith, G.M., 1999. Oploop- en overslagmetingen op een ondiep voorland, Report H3471, Delft Hydraulics, September 1999, Delft. (in Dutch)

Suykens, J., 2001. Data mining and neural networks, syllabus of course HJ70 & HJ71, academic year 2001-2002, Katholieke Universiteit Leuven, Belgium.

TAW, 1985. Leidraad voor het ontwerpen van rivierdijken. Deel 1 - Bovenrivierengebied, Technical Advisory Committee on Flood Defence, The Netherlands. (in Dutch)

TAW, 1989. Leidraad voor het ontwerpen van rivierdijken. Deel 2 - Benedenrivierengebied, Technical Advisory Committee on Flood Defence, The Netherlands. (in Dutch)

TAW, 1997. Golfoploop en golfoverslag bij dijken, Technical Advisory Committee on Flood Defence, The Netherlands. (in Dutch)

TAW, 2002. Technical report wave run-up and wave overtopping at dikes, Technical Advisory Committee on Flood Defence, The Netherlands.

TAW, 2003. Leidraad Kunstwerken, B2 Kerende hoogte, Technical Advisary Committee on Water Defences, The Netherlands. (in Dutch)

Troch, P., De Rouck, J., Van Damme, L., 1998. Instrumentation and prototype measurements at the Zeebrugge rubble mound breakwater, Coastal Engineering, Vol. 35, pp. 141-166.

Troch, P., Li, T., De Rouck, J., Ingram, D.M., 2003. Wave Interaction with a Sea Dike using a VOF Finite-Volume Method, Proceedings of the 13th International Offshore and Polar Engineering Conference, Honolulu, USA, pp. 325-332.

Tsai, C.-P., Lee, T.L., 1999. Back-propagation neural network in tidal level forecasting, Journal of Waterway, Port, Coastal and Ocean Engineering, Vol 125 (4), pp. 195-202.

Tsai, C.-P., Hsu, J.R.-C., Pan, K.-L., 2000. Prediction of storm-built beach profile parameters using neural networks, Proceedings of the 27th International Conference on Coastal Engineering, Sydney, Australia, ASCE, pp. 3048-3061.

Tsuruta, S., Goda, Y., 1968. Expected Discharge of Irregular Wave Overtopping, Proceedings of the 11th International Conference on Coastal Engineering, London, United Kingdom, ASCE, pp 833-852.

U.S. Army Corps of Engineers, 1978. Shore Protection Manual, Coastal Engineering Research Centre, Washington DC, USA. (periodically revised edition of 1978).

U.S. Army Corps of Engineers, 2002. Coastal Engineering Manual, Engineer Manual 1110-2-1100, Washington D.C., USA. (in 6 volumes)

Van der Meer, J.W., 1988. Rock slopes and gravel beaches under wave attack, Ph.D. Thesis, Delft University of Technology, Delft, The Netherlands.

Van der Meer, J.W., Petit, H.A.H., Van den Bosch, P., Klopman, G., Broekens, R.D., 1992. Numerical simulation of wave motion on and in coastal structures, Proceedings of the 23rd International Conference on Coastal Engineering, Venice, Italy, ASCE, pp. 1772 -1784.

Van der Meer, J.W., 1993. Conceptual design of rubble mound breakwaters, Report No. 483, Delft Hydraulics, The Netherlands.

Van der Meer, J. W., Janssen, W. 1995. Wave Run-Up and Wave Overtopping at Dikes, Wave Forces on Inclined and Vertical Wall Structures, ed. Kobayashi N. & Demirbilek Z., ASCE, New York, USA, ISBN 0-7844-0080-6.

Van der Meer, J.W., Tönjes, P., De Waal, H., 1998. A code for dike height design and examination, Proceedings of the International Conference on Coastlines, structures and breakwaters, ICE, Thomas Telford, London, United Kingdom, pp. 5-19.

Van der Meer, J.W., Verhaeghe, H., Steendam, G.J., 2005a. Database on wave overtopping at coastal structures, CLASH WP2 database, Infram, Marknesse, The Netherlands.

Van der Meer, J.W., Verhaeghe, H., Steendam, G.J., 2005b. Final report on wave overtopping at coastal structures, CLASH WP2 report, Infram, Marknesse, The Netherlands.

Van Gent, M.R.A., 1994. The modelling of wave action on and in coastal structures, Coastal Engineering, Vol. 22, pp. 311-339.

Van Gent, M.R.A., van den Boogaard, H.F.P., 1998. Neural network modelling of forces on vertical structures, Proceedings of the 26th International Conference Coastal Engineering, Copenhagen, Denmark, ASCE, pp. 2096-2109.

Van Gent, M.R.A., 1999. Physical model investigations on coastal structures with shallow foreshores; 2D model tests with single and double-peaked wave energy spectra, Report H3608, Delft Hydraulics, Delft, The Netherlands.

Van Gent, M.R.A., 2001. Wave runup on dikes with shallow foreshores, Journal of Waterway, Port, Coastal and Ocean Engineering, Vol.127(5), pp. 254-262.

Van Gent, M.R.A., Doorn, N., 2001. Numerical model simulations of wave propagation and wave run-up on dikes with shallow foreshores, Proceedings of the 4th Conference on Coastal Dynamics, Lund, Sweden.

Verhaeghe, H., Van der Meer, J.W., Steendam, G.J., 2003a. Database on wave overtopping at coastal structures, CLASH WP2 internal report, Ghent University, Belgium.

Verhaeghe, H., Van der Meer, J.W., Steendam, G.J., Besley, P., Franco, L., van Gent, M.R.A., 2003b. Wave overtopping database as the starting point for a neural network prediction method, Proceedings of the International Conference on Coastal Structures, Portland, USA, pp. 418-430.

WAMDI group, 1988. The WAM model - a third generation ocean wave prediction model, Journal of Physical Oceanography, No. 18, pp. 1775-1810.
Ward, D. L., Wibner, C. G., Zhang, J., Edge, B., 1994. Wind effects on run-up and overtopping, Proceedings of the 24th International Conference on Coastal Engineering, Kobe, Japan, ASCE, pp. 1687-1699.

Ward, D. L., Zhang, J., Wibner, C. G. and Cinoto, C. M., 1996. Wind Effects on Runup and Overtopping of Coastal Structures, Proceedings of the 25th International Conference on Coastal Engineering, Orlando, USA, ASCE, pp. 2206-2215.

Weggel, J.R., 1976. Wave overtopping equation, Proceedings of the 15th International Conference on Coastal Engineering, Honolulu, USA, ASCE, pp. 2737-755.

Westra, M.R., Van Vledder, G.Ph., Van Banning, G.K.F.M., Hurdle, D.P., 2002. Predicting water levels using artificial neural networks, Proceedings of the 28th International Conference on Coastal Engineering, Cardiff, United Kingdom, ASCE, pp. 1292-1302.

Zhu, H., Rohwer, R., 1996. No free lunch for cross-validation, Neural Computation, Vol. 8, pp.1421-1426.